Progress in Polymer Science 36 (2011) 1326–1414

Contents lists available at ScienceDirect

Progress in Polymer Science

journal homepage: www.elsevier.com/locate/ppolysci

How the structural deviations on the backbone of conjugated polymers influence their optoelectronic properties and photovoltaic performance

Christos L. Chochos*, Stelios A. Choulis

Molecular Electronics and Photonics Research Unit, Department of Mechanical Engineering and Materials Science and Engineering, Cyprus University of Technology, 3603 Limassol, Cyprus

ARTICLE INFO

Article history:
Received 5 October 2010
Received in revised form 23 February 2011
Accepted 7 April 2011
Available online 17 April 2011

Keywords:
Conjugated polymers
Polymer:fullerene blends
Organic solar cells
HOMO and LUMO levels
Optical band gap

ABSTRACT

The design of novel conjugated polymers with appropriate frontier orbital energy levels, low band gap (LBG) and suitable carrier transport properties are needed to improve the power conversion efficiency (PCE) of organic photovoltaic devices. In this review, a detailed structure–property relationship study is presented, by identifying those chemical entities in the backbone of conjugated polymers that are responsible for the modification of optoelectronic properties towards high photovoltaic performance.

Contents

* Corresponding author. Tel.: +357 25002335.
E-mail address: christos.chochos@cut.ac.cy (C.L. Chochos).

0079-6700/$ – see front matter © 2011 Elsevier Ltd. All rights reserved.
doi:10.1016/j.progpolymsci.2011.04.003

Nomenclature

A	acceptor
AFM	atomic force microscopy
B_{1245}DT	benzo[1,2-*b*:4,5-*b*′]dithiophene
B_{2134}DT	benzo[2,1-*b*:3,4-*b*′]dithiophene
BHJ	bulk heterojunction
BTz	bithiazole
CB	chlorobenzene
CF	chloroform
CN	chloronaphthalene
CN-PPV	cyano-substituted poly(*p*-phenylenevinylene)
CPDT	cyclopenta[2,1-*b*:3,4-*b*′]dithiophene
CPP	4*H*-cyclopenta[*def*]phenanthrene
CS	charge separation
CT	charge transfer
CTC	charge-transfer complex
CV	cyclic voltammetry
D	donor
DAD	donor–acceptor–donor
DCPTCz	dicyclopentathienocarbazole
DPBz	4,7-diphenyl-2,1,3-benzothiadiazole
DPV	differential pulse voltammetry
DSC	differential scanning calorimetry
DTPy	dithieno[3,2-*b*:2′,3′-*e*]pyridine
DTP	dithieno[3,2-*b*:2′,3′-*d*]pyrrole
DTS	dithieno[3,2-*b*:2′,3′-*d*]silole
DTT	dithieno[3,2-*b*:2′,3′-*d*]thiophene
E	electric field
E_{BLA}	bond length alternation
E_{CT}	charge transfer energy
E_{inter}	intermolecular interactions
E_g	optical band gap
E_{Res}	aromatic resonance energy
E_{sub}	substituents
E_T	triplet energy
E_θ	planarity
ECL	effective conjugation length
EDOT	ethylenedioxythiophene
EQE	external quantum efficiency
FET	field-effect transistor
FF	fill factor
FT-IR	Fourier transform infrared
GIXS	grazing incidence X-ray scattering
GRIM	Grignard metathesis
HOMO	highest occupied molecular orbital
I_{sc}	short circuit current
IC	indolo[3,2-*b*]carbazole
ICT	intramolecular charge transfer
IF	indeno[1,2-*b*]fluorene
IQE	internal quantum efficiency
IPCE	incident photon to current efficiency
J_{sc}	short-circuit current density
j_{sc}	injection current
kT	thermal energy
LBG	low band gap
LUMO	lowest unoccupied molecular orbital
λ	incident photon wavelength
MDMO-PPV	poly[2-methoxy-5-(3′,7′-dimethyloctyloxy)-1,4-phenylene vinylene]
MEH-PPV	poly[2-methoxy-5-(2-ethylhexyloxy)-1,4-phenylene vinylene]
M_n	number average molecular weight
M_w	weight average molecular weight
NDT	naphtho[2,1-*b*:3,4-*b*′]dithiophene
NMR	nuclear magnetic resonance
NREL	national renewable energy laboratory
ODCB	ortho-dichlorobenzene
OPVs	organic photovoltaics
PBzP	proDOT-[2,1,3]-benzothiadiazole-proDOT
$PC_{61}BM$	[6,6]-phenyl-C_{61}-butyric acid methyl ester
$PC_{71}BM$	[6,6]-phenyl-C_{71}-butyric acid methyl ester
PCE	power conversion efficiency
PEDOT:PSS	poly(3,4-ethylenedioxythiophene): poly(styrenesulfonate)
PF	polyfluorene
PFN	poly[(9,9-dioctyl-2,7-fluorene)-*alt*-(9,9-bis(3′-(*N*,*N*-dimethylamino)propyl)-2,7 fluorene)]
photo-CELIV	photoinduced charge carrier extraction in a linearly increasing voltage regime
PIF	poly(indeno[1,2-*b*]fluorene)
PII	poly(indeno[2,1-*a*]indene)s
PM	2-pyran-4-ylidenemalononitrile
PP	pyrido[3,4-*b*]pyrazine
PPV	poly(*p*-phenylenevinylene)
ProDOT	propylenedioxythiophene
PTV	poly(thienylenevinylene)
q	elementary charge
QDT	dithieno[3,2-*f*:2′,3′-*h*]quinoxaline
QTN	quadrathienonaphtalene

rrP3ATs	regioregular poly(3-alkylthiophenes)
rrP3HS	regioregular poly(3-hexylselenophene)
rrP3HT	regioregular poly(3-hexylthiophene)
R_s	series resistances
R_{SH}	shunt resistances
SAED	selected area electron diffraction
SBzS	selenophene-[2,1,3]-benzothiadiazole-selenophene
SCLC	space charge limited current measurements
SEM	scanning electron microscopy
SiIDT	silaindacenodithiophene
T_1	triplet state
TBseT	thiophene-2,1,3-benzoselenadiazole-thiophene
TBzT	thiophene-2,1,3-benzothiadiazole-thiophene
TDPPT	thiophene-diketopyrrolo[3,4-*c*]pyrrole-thiophene
TDTQT	thiophene-6,7-dihexyl[1,2,5]thiadiazolo[3,4-*g*]quinoxaline-thiophene
TEM	transmission electron microscopy
TP	thieno[3,4-*b*]pyrazine
TPD	thieno[3,4-*c*]pyrrole-4,6-dione
TPT	thiophene–phenylene–thiophene
TPyT	thiophene–thiadiazolo[3,4-*c*]pyridine–thiophene
TQT	thiophene–quinoxaline–thiophene
TTPT	thiophene-thieno[3,4-*b*]pyrazine-thiophene
TVM	bithiophenevinyl-2-pyran-4-ylidenemalononitrile
UV–vis	ultraviolet–visible spectroscopy
V_{oc}	open-circuit voltage
VPV	vinylene–phenylene–vinylene
VTV	vinylene–terthiophene–vinylene
XRD	X-ray diffraction

1. Introduction

Organic and polymer photovoltaic cells are an extremely active area of research, in order to meet the urgent need for clean and renewable sources of energy. During the last decade the field of polymer photovoltaics has shown a continuous improvement in both device efficiency and understanding of the underlying physical processes. Despite exhibiting lower power conversion efficiency (PCE) in comparison to conventional inorganic technologies, polymer photovoltaic cells have attracted particular attention due to their potential applications as flexible, low-cost and solution processible energy sources [1]. At present the so-called bulk heterojunction (BHJ) structure based on blends of conjugated polymers as electron donors and soluble fullerene derivatives (especially [6,6]-phenyl-C_{61}-butyric acid methyl ester ($PC_{61}BM$) or [6,6]-phenyl-C_{71}-butyric acid methyl ester ($PC_{71}BM$)) as electron acceptors represent one of the most extensively studied type of organic photovoltaics (OPVs) [2,3] with PCEs in the range of 6–7.5% [4]. On the OPV technology roadmap towards higher PCEs, studies on existing materials have identified parameters limiting the PCE in organic BHJ solar cells. These include the charge mobility, the optical band gap (E_g), the ionization potential (HOMO level) and electron affinity (LUMO level) from the part of the conjugated polymer [5,6], the elimination of rotational barriers and the recently reported charge transfer (CT) state of both components [7]. Hence, in order to further enhance the PCE and to obtain the desired performances with polymeric semiconductors, different parameters at the molecular and supramolecular levels (such as electronic structure, regioregularity, purity, solubility, molecular weight, thermal transitions, crystallinity and morphology within the blend) should be carefully controlled. For example, the good solubility of polymers in common organic solvents is an essential parameter for the utilization of low-cost solution processing techniques. The polymer solubility as well as the miscibility with fullerene derivatives is usually controlled by the choice of the side chain, its structure (linear or branched), and its position along the backbone. However, it is not easy to predict how such structural modifications at the molecular level affect many of the above-mentioned parameters. Even though several reviews have been published highlighting the major classes of conjugated polymers applied as donors in solar cells [8–13], an in-depth conjugated polymers structure–property relationship study for OPVs is not presented in the literature.

This review is based on how minor structural modifications in the main chain for the different classes of conjugated polymers affecting their optoelectronic properties and photovoltaic performance. Published results will be discussed, showing the effect of the nature (alkyl or alkoxy), the type (linear or branched), the positioning and the density of the solubilizing side chains on their optical band gap (E_g^{opt}), HOMO and LUMO levels, charge carrier mobility, morphology and photovoltaic performance when blended with fullerene derivatives. The review is organised as follows. In the first part, the basic principles of OPV operation and characterization are discussed and the design principles for novel electron donor conjugated polymers are presented. In the second part, we categorize and analyze how the structural parameters of the various classes of conjugated polymers influencing their optoelectronic properties and photovoltaic performance. The review focus initially on poly(*p*-phenylenevinylene)-substituted derivatives and polythiophene derivatives and later presents details for more complex (fused) structures such as bridged bithiophenes with 5- and 6-member fused aromatic rings in the central core, bridged biphenylenes with 5-member fused aromatic rings in the central core, polycyclic aromatics bridged with fused aromatic rings and LBG conjugated polymers based on various electron-deficient units. The review is completed by concluding some of the main observations.

2. Basic principles and characterization of solar cells

The active region of BHJ solar cells consists of a bicontinuous interpenetrating network of an electron donor

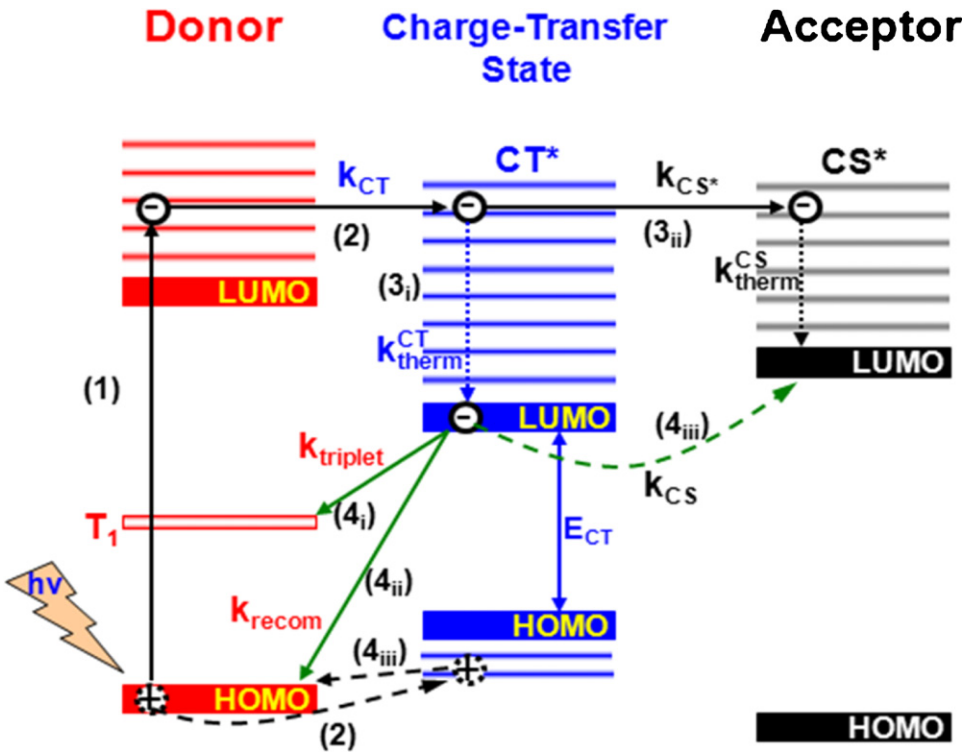

Fig. 1. Schematic of charge dissociation at the polymer (donor):PCBM (acceptor) interface, where k_{CT}: exciton dissociation to form the hot charge-transfer (CT) state, k_{CT}^{therm}: thermal relaxation of the CT state, k_{CS^*}: dissociation of the hot CT state into a fully charge-separated (CS) state, k_{CS}^{therm}: thermal relaxation of the CS state, $k_{triplet}$: geminate recombination of the CT to the triplet exciton (T_1), k_{recom}: geminate recombination to the ground state and k_{CS}: dissociation of the thermally relaxed CT state into the CS state [7,14,15].

(polymer) and acceptor materials (fullerene). Fig. 1 summarises the energy level diagram of the main processes involved within the charge photogeneration process within the polymer:fullerene active layer. When photoexcitation occurs (step 1), an electron from the donor's HOMO into the LUMO is promoted resulting in exciton formation. The singlet exciton can diffuse to the donor (D)–acceptor (A) heterojunction, where it can dissociate by energy transfer (step 2) to the charge transfer (CT) state, if the optical band gap (E_g) is higher than the energy of the CT state (E_{CT}) [7]. Since that CT state initially is formed with excess thermal energy, then the possible pathways are either the thermal relaxation of the CT state (step 3i), or the dissociation of the hot CT state into a fully charge-separated (CS) state and migration away from the D/A interface (step 3ii) [14–16]. Then, the bound polaron pair formed upon thermal relaxation of the CT state can undergo geminate recombination: (i) into a triplet state T_1 on the donor by electron back transfer (step 4i), if the triplet energy E_T is smaller than E_{CT}, or (ii) to the ground state (step 4ii). Alternatively, it can be separated (step 4iii), in case the Coulomb binding energy of this geminate pair is overcome, to form dissociated charge carriers [7,14–16]. It should be noted that other relaxation processes (not shown in Fig. 1) that compete with charge photogeneration include excited-state relaxation of Frenkel excitons and bimolecular recombination of separated charge carriers.

Important key points are: (i) the competition between the thermal relaxation of the CT state and the dissociation of the hot CT state into a fully CS state determines the efficiency of charge photogeneration in organic solar cells. Because the dynamics of the electronic and vibronic coordinates are highly coupled, diabatic descriptions of the charge separation reaction are needed to properly describe charge photogeneration on this process for these types of materials [16]. (ii) Knowing the energy of the CT state, it is observed that a minimal driving force of $E_g - E_{CT} \geq \sim 0.1$ eV is sufficient to effectively populate the CT state in D/A blends from the lowest energy singlet excited state of D or A [17]. (iii) Recombination of CT states into the lowest T_1 state occurs if $E_{CT} - E_T \geq \sim 0.1$ eV. Hence, triplet state energies should be considered when designing materials for organic solar cells with minimal $E_g - E_{CT}$ [17,18]. As a matter of fact, Nelson et al. observed recently that triplet formation occurs when the offset between the HOMO of the D and the LUMO of the A is larger than 1.6 eV by studying a series of polyfluorene:fullerene blends [19]. More information about the formation of triplet states in organic semiconductors and triplet state values of various conjugated polymers can be found elsewhere [20]. Additionally, this CT state depends on the HOMO of the D [21] and finally, carrier recombination through the CT excitons is mainly controlled by the intrachain conformation of the polymer (D) and to a limited extent by the mesoscopic morphology of the blend [22].

The PCE of a solar cell is determined by the open-circuit voltage (V_{oc}) value multiplied by the short-circuit current density (J_{sc}) and the fill factor (FF) values and divided by the incident-light intensity as shown by the formula given in

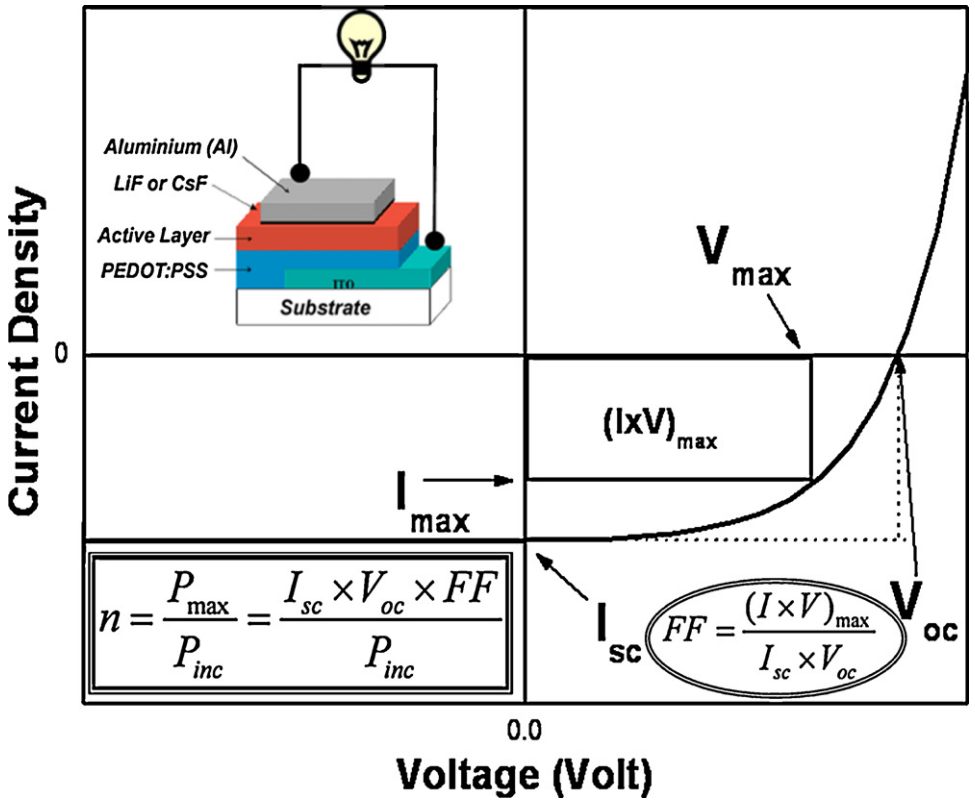

Fig. 2. *I–V* curve and the characteristic parameters for the calculation of the power conversion efficiency of the organic photovoltaics.

the inset of Fig. 2. The open-circuit voltage of a conjugated polymer:fullerene solar cell can be estimated by [23]:

$$V_{oc} = \frac{kT}{q} \ln\left(\frac{j_{sc}}{j_0} + 1\right)$$

where kT is the thermal energy, q is the elementary charge, j_{sc} is the injection current driving the CT electroluminescence and j_0 is the dark saturation current that can be calculated from the experimental electroluminescence and photoconversion experiments according to: $j_0\ \mathrm{EQE_{EL}}(E) = q\mathrm{EQE_{PV}}(E)\ \Phi_{BB}(E)$. Owing to the logarithmic dependence of V_{oc} on j_0, V_{oc} depends linearly on the spectral position of the charge transfer state. This model provides good correlation of V_{oc} with the onset of the CT state [24] or the peak of CT emission [25,26]. A more simplified expression for V_{oc} has also been proposed by Janssen et al. predicting that for organic BHJ solar cell the maximum attainable V_{oc} is ultimately set by the lowest optical band gap energy of either D or A material via $V_{oc} = E_g - 0.6\,\mathrm{eV}$ [17]. Moreover, the short circuit current (I_{sc}) can be estimated from: $I_{sc} = ne\mu E$ (ideal situation; loss free contacts), where n is the density of charge carriers, e is the elementary charge, μ is the mobility and E is the electric field, or can be determined by the amount of absorbed light and the internal conversion efficiency. Experimentally accessible is the external quantum efficiency or incident photon to current efficiency [IPCE(%)], describing the relation of the numbers of electrons generated by the cell under short circuit conditions to the number of the incident photons and is defined from:

$$\mathrm{IPCE}(\%) = \frac{1240 \times I_{sc}(\mu\mathrm{A\,cm^{-2}})}{\lambda(\mathrm{nm}) \times P_{in}(\mathrm{W\,m^{-2}})}$$

where λ (nm) is the incident photon wavelength, I_{sc} ($\mu\mathrm{A\,cm^{-2}}$) is the photocurrent of the device and P_{in} ($\mathrm{W\,m^{-2}}$) is the incident power. The fill factor (FF) is defined by the equation shown in the inset of Fig. 2 and describes the quality of the diode in the 4th quadrant. The FF for a simplified equivalent circuit for a photovoltaic device is given from:

$$I = I_0\left(\exp\left(\frac{q}{nkT}(U - IR_s)\right) - 1\right) + \frac{U - IR_s}{R_{SH}} - I_{PH}$$

and is mainly influenced by the series R_s and shunt resistances R_{SH}. To achieve high FF values the series resistances should be minimized while the shunt resistances should be maximized. Finally, P_{in} is the incident light power and is standardized for solar cell testing at AM 1.5 (air mass 1.5) spectrum. This is the solar irradiation (diffuse and direct) on sea level on a 37° tilted, sun facing surface and attenuated by the earth atmosphere [27].

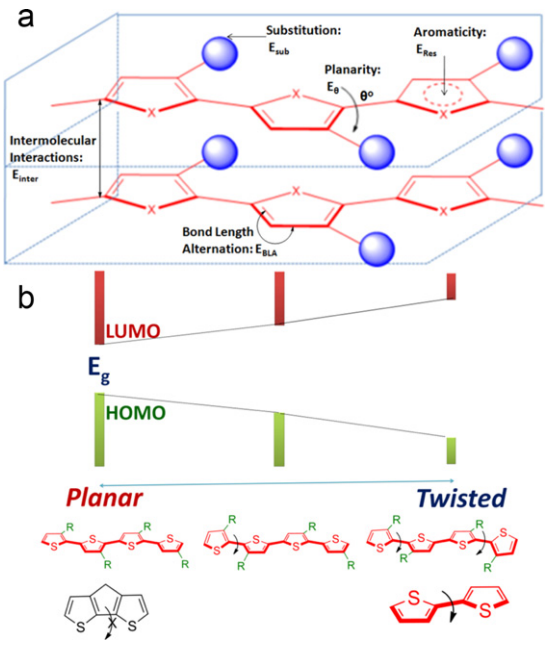

Fig. 3. (a) Structural factors affecting the band gap of π-conjugated polymers [11,30,31] and (b) influence of the side chain positioning and rigidity of the individual monomer on the band gap variation [33].

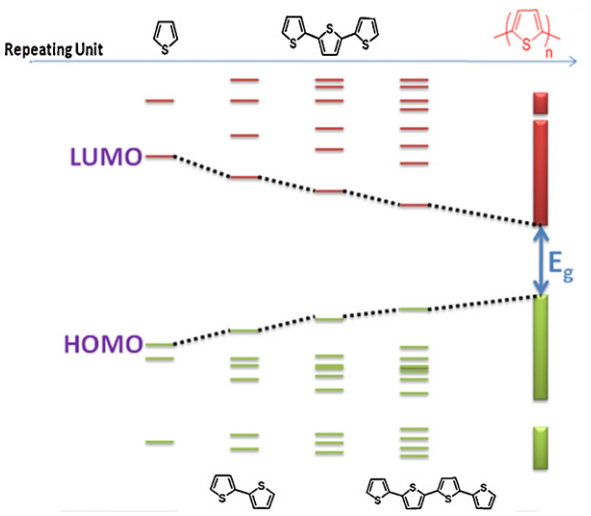

Fig. 4. Development of the band gap structure of polythiophene from energy levels of corresponding monomer during polymerization [34].

3. Conjugated polymers as electron donors components

3.1. Design considerations for new electron donor polymers

At present it is possible to calculate the theoretical PCE of a BHJ solar cell consisting of an electron D polymer blended with PCBM based on the E_g of the D along with the difference between the LUMO level of the D with the LUMO level of the A and experimental predicted values for the device external quantum efficiency (EQE) and FF [28,29]. Therefore, conjugated polymer control over the HOMO–LUMO energy gap it is one of the most important parameters for high PCE and has been extensive studied from the view of synthetic chemistry. The tuning and modification of the band gap of a conjugated polymer is a multiparameter effect involving six factors: molecular weight, bond length alternation (E_{BLA}), planarity (E_θ), aromatic resonance energy (E_{Res}), substituents (E_{sub}) and intermolecular interactions (E_{inter}) (Fig. 3a) [30,31], thus, the design and synthesis of most of the low band gap (LBG) polymers reported in literature, is rationally based on these parameters. However the exact control of individually the HOMO and LUMO energy levels is not a very simple process because despite the fact that all the above mentioned six parameters have an influence on the band gap, they also related to each other, affecting other important chemical, mechanical, and physical properties. For example, even though the solubility of conjugated polymers is increased by the use of large alkyl or alkoxy chains, this is also influences the E_{sub}, the tendency for supramolecular arrangement E_{inter} and finally the increment of the torsion angle (E_θ). Therefore, any external stimulus that will modify the planarity of the backbone and the degree of π-orbital overlap, will alter E_g and as a sequence the relative position of the HOMO and LUMO levels [32]. Thus, by synthesizing LBG conjugated polymers for solar cells the positioning as well as the nature of the substituents must be carefully designed and selected properly. When substituents are employed, it is important to arrange them in a regioregular way to avoid steric effects that would cause twisting of the main chain (Fig. 3b). Another way to insure greater conjugation is to rigidify the individual monomer units by employing additional rings that serve to enforce planarity and this also minimizes or eliminates steric crowding (Fig. 3b) [33]. More details relevant to the influence of the above six parameters on the E_g can be found elsewhere [11,12]. On the other hand, there is no theoretical model up to now predicting the density, the appropriate length and the type of the substituents that should be inserted in the main chain of conjugated polymers in order to obtain a soluble high molecular weight polymer (at least $M_n > 20{,}000$ g/mol) with high charge carrier mobility, properly aligned energy levels and optimum segregation when blended with fullerene derivatives to achieve simultaneously maximum EQE, J_{sc} and V_{oc}.

The onset of the optical absorption spectrum of a conjugated polymer is a measure by the E_g value of the polymer. Therefore, in order to achieve a low E_g, it is necessary to design polymers that absorb in the near infrared wavelength region. However, in the case of conjugated polymers the optical absorption reaches the maximum value after a certain conjugation length, which is referred to as the effective conjugation length (ECL) (Fig. 4) [34]. Currently, two are the more preferable strategies for improving the ECL of conjugated polymers to a considerable extent, and thus efficiently reducing their E_g. The first one includes the conversion of a polyaromatic chain into a conjugated system with an enhanced quinoid character and the second one is based on the synthesis of the so-called "D–A" alternat-

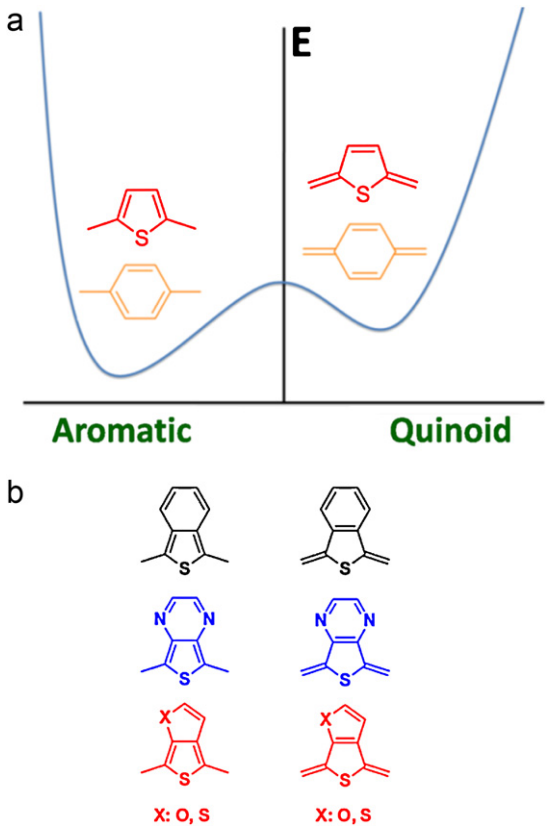

Fig. 5. (a) Schematic presentation of the non-degenerate fundamental energy for the aromatic and quinoid resonance forms. (b) Typical heterocyclic moieties used for the stabilization of the quinoid form.

ing copolymers containing alternating electron-rich and electron-deficient building blocks.

The principal of the first approach is based on the stabilization of the quinoid form, which is actually lying higher in energy than the aromatic form (Fig. 5a) [31,35]. Stabilization of the quinoid form can be achieved by the fusion of a heterocycle ring (usually phenyl or thiophene) with an aromatic or another heterocycle system with higher resonance energy (E_{Res}) (Fig. 5b). This results in the reduction of E_{BLA}, thereby narrowing of E_g. However, this approach usually requires multiple and complex synthetic steps which is a major drawback.

The second approach is based on the creation of an intramolecular charge transfer (ICT) through association of alternative donor and acceptor groups leading to a broadening of the valence and conduction bands, thereby increasing the double bond character between repeating units, which lead to the reducing of E_{BLA} and E_g (Fig. 6) [36,37]. Despite the fact that this is the preferred approach for the synthesis of a plethora of new LBG conjugated polymers for solar cell applications, many issues remain to be addressed including the relative strength, the placement and the ratio of the donor and acceptor moieties in the polymer backbone.

Another important issue that should be considered when designing new LBG conjugated polymers is their hole mobilities. In general, low charge mobilities in conjugated polymers negatively influence the OPV performance by allowing bimolecular charge recombination to compete with charge collection, thereby reducing the photocurrent by limiting the optimum thickness values of the photoactive layer. In addition, the FF decreases by the high resistivity of the semiconductor layers and finally the local charge mobility (influenced by the order of molecular packing) appears to influence the efficiency of charge pair separation following exciton dissociation. Therefore, it is essential the synthesis of high charge carrier mobility conjugated polymers. Recently, conjugated polymers with hole mobilities up to 1 $cm^2/V\,s$ have been reported [38]. On the other hand, one should always keep in mind that since the bimolecular recombination is related to the mobilities of the charge carriers in the two phases, achieve balanced transport within the blend is also a parameter of high importance for efficient OPV performance. For example, when hole and electron transport within the polymer:fullerene blend are unbalanced a build up of space charge results to recombination losses limiting the FF values [28]. In order to determine the hole charge carrier mobility in a D conjugated polymer, several types of experimental techniques have been employed including the field-effect transistor (FET) [39], space charge limited current measurements (SCLC) [40,41], photoinduced charge carrier extraction in a linearly increasing voltage regime (photo-CELIV) [42], and time-of-flight photocurrent measurements [43].

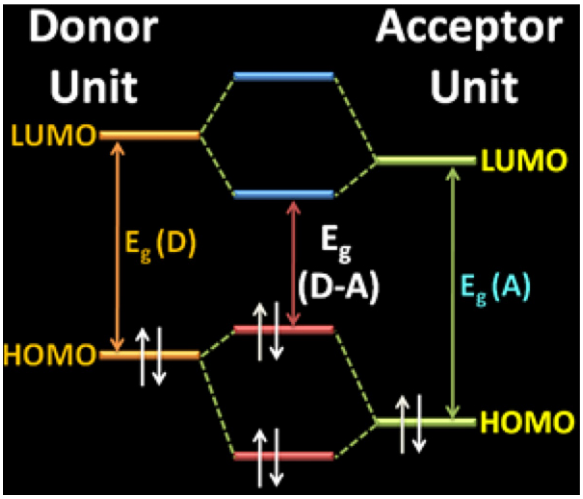

Fig. 6. Orbital interaction between donor and acceptor units lowers the band gap of conjugated polymers by the creation of an intramolecular charge transfer (ICT) [8,12].

In parallel to the above requirements based on optical and electrical properties, other important factors of π-conjugated polymers suitable for solar cell applications including solubility issues, easy processing, simple and high purity large scale synthetic quantities and importantly environmental and photochemical stability. Therefore, it is evident that the chemistry of functional conjugated polymers is facing major challenges and suitable materials have to achieve a broad range of specifications in order to be established a suitable choice for high photovoltaic performance.

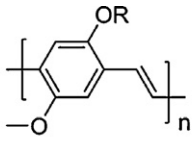

1 R: 2-ethylhexyl (MEH-PPV)
2 R: 3,7-dimethyloctyl (MDMO-PPV)

Chart 1. Chemical structures of MEH-PPV and MDMO-PPV.

In the following paragraphs the recent developments on the main classes of conjugated polymer donors with particular emphasis on the influence of chemical modification in their optoelectronic properties and photovoltaic performance are reviewed.

3.2. Categories of electron donor polymers

3.2.1. Poly(p-phenylenevinylene)-substituted derivatives

Two are the most extensive studied poly(*p*-phenylenevinylene) (PPV) derivatives, processable in common organic solvents, used as electron donor in organic photovoltaics. The chemical structures of **1** and **2** (the so-called poly[2-methoxy-5-(2-ethylhexyloxy)-1,4-phenylene vinylene]; MEH-PPV and the poly[2-methoxy-5-(3′,7′-dimethyloctyloxy)-1,4-phenylene vinylene]; MDMO-PPV) are shown in Chart 1. The photovoltaic performance of MEH-PPV and MDMO-PPV in blends with $PC_{61}BM$ (1:4, w/w) is 1.1–1.3% [44] and 2.5% [45], respectively. As reported by Shaheen et al. the PCE of the MDMO-PPV:$PC_{61}BM$ is dependent from the casting solvent used to deposit the active layer. When chlorobenzene was used as solvent an optimal morphology with finer phase segregation and enhanced microstructure was obtained which provided a PCE of 2.5% instead of the 0.1% PCE achieved when toluene was used as solvent. Further improvement in the efficiency of MDMO-PPV:$PC_{61}BM$ was achieved by two different approaches. The one way is by increasing the regioregularity of the MDMO-PPV which leads to a PCE of 3.1% [46] due to the increased crystallinity of the polymer, resulting to higher hole mobility due to better mixing (morphology) with the $PC_{61}BM$. The other way to improve PCE performance is by using an isomeric mixture of C_{70} ($PC_{71}BM$) instead of $PC_{61}BM$. It has be shown that in some cases the replacement of the C_{60} moiety of $PC_{61}BM$ by C_{70} fullerene derivative makes the HOMO–LUMO transitions slightly more allowed and increases the light absorption properties [47,48].

One very interesting observation of this system is the increase of the hole mobility of the MDMO-PPV by increasing the $PC_{61}BM$ concentration within the polymer:fullerene blend [49,50]. Initially this phenomenon was attributed to the fact that the addition of the $PC_{61}BM$ (up to 67 wt%) favors the uncoiling of the polymer chains, despite the dissolution of the polymer [51]. However in a very recently report it has been demonstrated that the hole mobility of the MDMO-PPV increases upon addition of the fullerenes, because the fullerenes intercalate between the side-chains of the MDMO-PPV affecting the intermolecular packing of the polymer [52]. Nevertheless, the main limitations preventing this system for higher PCE are the high band gap of the polymer and the unbalanced charge carrier mobilities between MDMO-PPV and $PC_{61}BM$ [53,54].

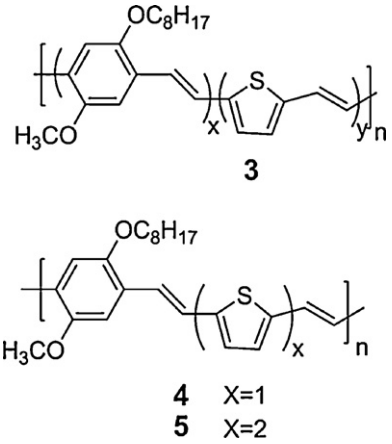

Chart 2. Chemical structures of the thienylenevinylene-based poly(*p*-phenylenevinylene) derivatives **3–5**.

3.2.2. Substituted poly(p-phenylenevinylene)-based copolymers

The need for lowering the band gap of the poly(*p*-phenylenevinylene)-based derivatives has lead to the synthesis of a variety of poly(*p*-phenylenevinylene) random copolymers incorporating various percentages of thienylene groups (**3**) [55] or alternative copolymers with one or two thiophene rings in the main chain (**4**–**5**) [55,56] (Chart 2). The random copolymers were synthesized by Gilch method and the alternative copolymers by Hornor–Emmons reaction. The Horner–Emmons coupling reaction seems to be the most appropriate method to synthesize well-defined polymers because it provides strict regioselectivity and an all-trans configuration, in contrast to Wittig's reaction, which generally gives molecules having a mixture of *cis* and *trans* isomers. The optical band gap of the polymers decreased slightly from 2.2 eV to 1.8 eV (**5**) as the thienylene vinylene content was increased and demonstrate enhanced hole mobility in comparison to MEH-PPV.

Since the band gap of **3**–**5** was slightly decreased (up to 1.8 eV) by the insertion of the thienylene or dithienylene vinylene segments in the main chain, new cyano-substituted poly(*p*-phenylenevinylene) copolymers with either unsubstituted (**6**) [57] or alkyl substituted thiophenes (**7** and **8**) [57,58] or ethylenedioxythiophene (EDOT) rings (**9** and **10**) [57] were synthesized by oxidative polymerization using $FeCl_3$ (**6**, **7**, **9** and **10**) or Knoevenagel polycondensation (**8**) (Chart 3). In an analogous approach, some more cyano-substituted poly(*p*-phenylenevinylene) copolymers based on propylenedioxythiophene rings (ProDOT) [58,59] were also synthesized (Chart 3) using either the Knoevenagel polycondensation (**11**–**15**) or the oxidative polymerization (**16**) or the Yamamoto cross-coupling polymerization (**17**).

The optical band gaps, the energy levels and the photovoltaic performance of the cyano-substituted poly(*p*-

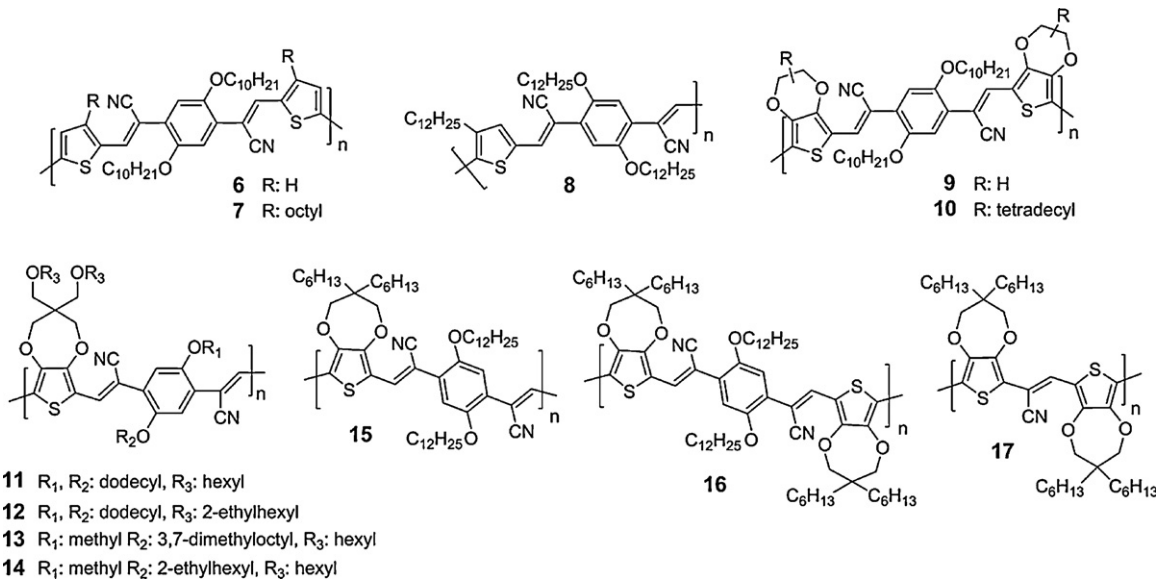

Chart 3. Chemical structures of the cyano-substituted poly(*p*-phenylenevinylene) derivatives **6**–**17**.

Table 1
Optical, electrochemical and photovoltaic properties of the copolymers **6**–**17**.

Polymers	E_g^{opt} (eV)	LUMO (eV)	HOMO (eV)	PCE (%)
6	1.77	3.42	5.73	–
7	1.72	3.35	5.48	0.14
8	1.80	3.5	6.0	0.01
9	1.59	3.27	4.82	0.19
10	1.72	3.30	5.34	–
11	1.70	3.5	5.9	0.10
12	1.75	3.6	5.9	0.27
13	1.75	3.6	5.8	0.13
14	1.70	3.6	5.7	0.36
15	1.7	3.5	5.8	0.15
16	1.6	3.4	5.4	–
17	1.5	3.6	5.4	0.21

phenylenevinylene) derivatives (**6**–**17**) are presented in Table 1. Polymer **8** has the highest band gap (1.8 eV), but is lower than the similar analogue cyano-substituted poly(*p*-phenylenevinylene) (CN-PPV) which has a band gap of 2.1 eV [58], as expected since that thiophene is a stronger electron donor compared to the phenylene. Further reduction of the band gap was achieved by introducing one more thiophene ring in the polymer backbone of **8**, providing the copolymers **6** and **7**. One can notice that the band gap of **7** is lower than **6**. This behaviour is a result of the electron-releasing effect of the octyl chains. Apparently, the electronic substituent effect created by the introduction of the alkyl side chains is larger than the possible effect of reduced electronic interchain interactions as well as the increased disorder in the conjugated system due to steric hindrance imparted by the octyl side chains. The effect of steric hindrance can be seen more clearly in **9** and **10**. When the bulky tetradecyl group is used on **10** the band gap is 1.72 eV in comparison to 1.59 eV for the unsubstituted EDOT derivative **9**. Moreover, comparing the band gaps of **6** with **9**, the band gap of **9** is 0.18 eV lower than **6** due to the stronger electron-donating EDOT rings incorporated in polymer **9**. In addition, polymer **11** with the linear alkyl chains on the phenylene and ProDOT rings has lower band gap than the structural analogue **12**, with the branched alkyl chains on the ProDOT, due to the better π–π stacking of the polymer chains. Meanwhile, when unsymmetrical branching is introduced on the phenylene ring induces a large influence on the polymer disorder and conjugation by shifting the absorption to the blue region and as the branching becomes bulkier (**13**) in comparison to **14**, the band gap is higher (Table 1). Replacing the hexyloxy substituents from the ProDOT of **11** with hexyl side chains in **15** the band gap remain unaltered, whereas adding one more ProDOT ring in the polymer backbone of **15**, the band gap of **16** lowers by 0.1 eV and finally removing the phenylene ring from **16**, the band gap of **17** is further reduced by 0.1 eV due to the stronger D–A interactions.

Concerning the energy levels, it is clearly observed that the LUMO levels of **6** and **7** are not altered significantly by the incorporation of EDOT rings in **9** and **10**. This suggests that the LUMO levels are localized on the cyanovinylene linkages and that for these polymers the decrease of 0.7 eV in the electrochemical band gap, by replacing the thiophene rings of **6** with EDOT rings in **9**, is mainly due to alteration of the HOMO levels of the polymers [57]. More-

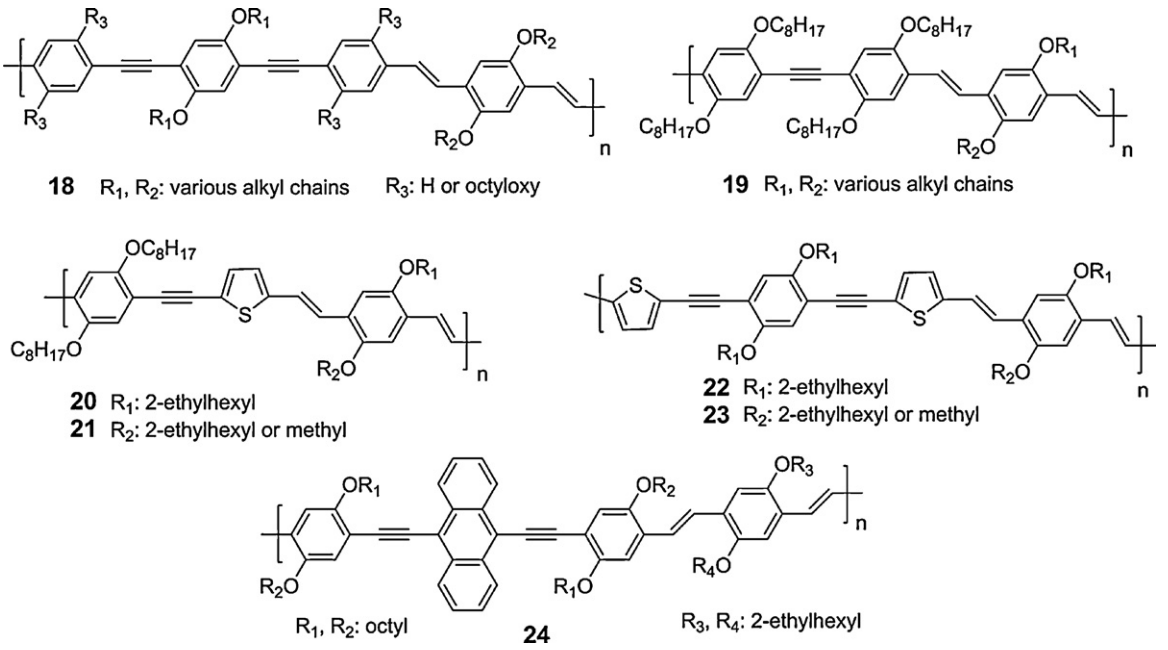

Chart 4. Chemical structures of the acetylene-based poly(*p*-phenylenevinylene) derivatives **18**–**24**.

over, two different effects are observed in relation to the role of the alkyl substitution on the HOMO levels of the polymers. The octyl substitution in **7** elevates the HOMO level as compared with the non-substituted analogue **6**, however the tetradecyl substitution in **10** shifts the HOMO to a deeper level compared to the non-substituted analogue **9** [57].

In general, analogous results are obtained by exploring the energy levels of ProDOT-based poly(*p*-phenylenevinylene) derivatives **11**–**17**. The LUMO levels are relatively constant in the range of 3.4–3.6 eV. The HOMO levels of the polymers with one ProDOT ring in the main chain (**11**–**15**) have relatively low lying HOMO levels varying between 5.7 and 5.9 eV and the polymers with two ProDOT rings in the main chain (**16** and **17**) have upshifted HOMO levels of 5.4 eV. It is interesting to note that comparing **11** with **8**, the HOMO level is raised from 6.0 eV to 5.7 eV upon replacing the alkyl thiophene with the more electron-rich ProDOT. An even more pronounced change is observed by passing from **11** to **16**, in which the HOMO level further raises from 5.7 eV to 5.4 eV upon introducing one more ProDOT ring in the polymer chain. The fact that the HOMO level of **16** is the same with **17**, points out that the HOMO level values appears to be determined by the ProDOT in either case. Finally, replacing the ProDOT rings of **16** with the EDOT rings in **10** the HOMO level is slightly raised (0.06 eV) indicating that the HOMO level of these polymers raise by increasing the donor strength and more precisely by passing from EDOT as the strongest donor to the ProDOT and then to thiophene.

The photovoltaic performance of the poly(*p*-phenylenevinylene) copolymers **3**–**5** without the cyano groups in the main chain is at least 3 times higher, 1.13% the PCE of **3**:C_{60} in 1:2 (w/w) with V_{oc} = 0.66 V, J_{sc} = 2.68 mA and FF = 0.43 [55] as compared to the polymers having the cyano groups (**6**–**17**; 0.36% the highest PCE for **14**) [59]. The reasons for this result is that probably the cyano groups act as trapping sites for the electrons [59] and the severe macrophase separation that atomic force microscopy (AFM) clearly demonstrates which is not improved even after thermal annealing [57,60].

3.2.3. *Poly(p-phenylenevinylene) derivatives containing acetylene segments*

Another very interesting class of poly(*p*-phenylenevinylene) copolymers that has been extensively studied in OPVs is the one consisting of alternating arylene-ethylene units. Alkyl-substituted phenyl moieties (**18** and **19**) [61], thiophene (**20**–**23**) [62] and anthracene **24** [63,64] units (Chart 4) have been introduced in the main chain of these copolymers in order to alter their optical and electrochemical band gaps while the rigid and coplanar nature of the acetylene bond allow the strong π–π stacking which can be beneficial for transport properties providing enhanced PCE.

The highest PCE of ~3.8% was observed for the copolymers incorporating the anthracene unit in the main chain [64]. Egbe et al. has synthesized and extensively characterized eight anthracene–ethylene poly(*p*-phenylenevinylene) derivatives which are varied on the length and the type (linear versus branched) of the side alkyl chains [63]. Polymer **24**, consisting of segments of linear octyloxy and segments of branched 2-ethylhexyloxy side chains that are evenly distributed along the conjugated backbone in a random manner, in blends with $PC_{61}BM$ (1:1, w/w) provides the maximum PCE with J_{sc} = 8.49 mA/cm^2, V_{oc} = 0.83 V and FF = 0.53. Morphological studies on a series of these alternating anthracene–ethylene copolymers in blends with $PC_{61}BM$ (1:1, w/w) presented more coarse scale morphologies for the copolymers with linear alkyl

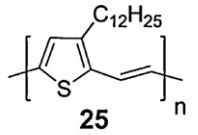

25

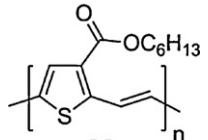

26

Chart 5. Chemical structures of the poly(thienylenevinylene) derivatives **25** and **26**.

chains close to the anthracene, indicating the formation of polymeric aggregates. On the other hand, those copolymers consisting of branched alkyl chains close to anthracene showed finer scale morphologies [63]. The more coarse grained film morphologies demonstrating higher PCEs probably due to the formation of more percolation paths, enhancing the charge transport properties. Another interesting point to note is that asymmetrically copolymers exhibit a 2-fold increase (1.9%) in the PCE when casted from solvent mixtures [chlorobenzene (CB):chloroform (CF) 1:1 volume ratio] compared to CB (1%) showing that the use of solvent mixtures is a possible way for optimizing the PCE for this class of polymers. Finally, comparing the PCE of the alternating alkyl-substituted phenyl-ethylene (**18** and **19**) and the thiophene-ethylene poly(*p*-phenylenevinylene) copolymers (**20**–**23**) when blended in 1:3 (w/w) with $PC_{61}BM$, it is observed that the copolymers incorporating the thiophene unit demonstrating higher PCE (1.2–1.7%).

3.2.4. Poly(thienylenevinylene)-substituted derivatives

Poly(thienylenevinylene)s (PTVs) are considered as an interesting class of materials as alternative to poly(*p*-phenylenevinylene) derivatives because the replacement of the phenyl ring by a thiophene unit result to a lower band gap material (~1.7 eV) combined with higher hole mobility [65]. The main disadvantage of the non-alkyl substituted polymers is their pure solubility, hence a dodecyl substituted PTV derivative **25** (Chart 5) has been initially synthesized resulting in an easier processable polymer with band gap of 1.72 eV and absorption maximum at 580 nm [66]. Photovoltaic devices fabricated using a mixture of **25** with $PC_{61}BM$ in various compositions (from 1:1 to 1:20, w/w) exhibit a maximum PCE of 0.24% (for the 1:10, w/w composition) [66]. It was shown that the composition of the mixture plays crucial role on the topography and morphology, with the appearance of a rough surface active layer for the 1:10 composition while large phase separation is detected in all the other compositions studied, parameters negative affecting the PCE of this material system [66]. Another important factor contributing to the poor performance is that PTVs are non-luminescent because the lifetime of the singlet excited state are extremely short due to the fast thermal decay.

A breakthrough in the improvement of the PCE of PTV derivatives has been achieved by the synthesis of the poly(3-carboxylated thienylenevinylene) **26** [67]. The insertion of the electron-deficient carboxylate group in the 3-position of the PTVs results to the lowering of the HOMO level and to the stronger photoluminescent emission as compared with the 3-alkyl PTV derivatives. The initial PCE of the **26**:$PC_{61}BM$ (1:2, w/w) is 1.59%, while the PCE increases to 2.01% with V_{oc} = 0.86 V, J_{sc} = 5.47 mA and FF = 0.43, upon annealing at 110 °C for 5 min. The 2.01% PCE of **26** results to 10 times higher PCE compared to the 3-alkyl PTV derivatives.

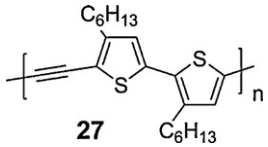

27

Chart 6. Chemical structure of the alternate ethynylene and bithiophene copolymer **27**.

3.2.5. Acetylene-based polymers

Analogous structure to poly(thienylenevinylene)s is polymer **27** consisting of alternative ethynylene and 4,3′-dihexyl-2,2′-bithien-5,5′-diyl unit along the chain (Chart 6), presenting a HOMO energy level of 0.3 eV lower compared to regioregular poly(3-hexylthiophene) [68]. When **27** implemented in BHJ devices with $PC_{61}BM$ in 1:4 (w/w), a PCE of 1.1% was exhibited.

As reported above, many poly(*p*-phenylenevinylene) derivatives containing acetylene segments have been synthesized and examined in OPVs showing PCEs as high as ~3.8% [64]. These copolymers consisting of electron-rich moieties, like thiophene and anthracene in their main chain, however no aryleneethylene copolymers consisting of electron deficient units have been largely explored for OPVs. As the matter of fact, only few examples have been reported in the literature including dialkoxy-substituted phenylene diacetylenes and thiophene diacetylenes with electron-deficient moieties like 2,1,3-benzothiadiazole and thieno[3,4-*b*]pyrazine (TP) (Chart 7) that have been synthesized through Sonogashira cross-coupling reaction and exhibit optical band gap of 1.94 eV (**28**) [69] and 1.57 eV (**29** and **30**) [70]. The fact that **29** and **30** have the same band gaps indicates that **29** has higher interchain interactions in the solid state, possibly due to a higher degree of planarization of the phenyl rings and result to an increase of the conjugation length for the resulting polymer [70]. On the other hand, the electrochemical band gaps of **29** and **30** as estimated by cyclic voltammetry are not the same for the two polymers. **29** has an electrochemical band gap of 1.99 eV with HOMO and LUMO levels at 5.29 eV and 3.30 eV, respectively, whereas the electrochemical band gap of **30** is 1.86 eV and its HOMO and LUMO levels are situated at 5.22 eV and 3.36 eV, respectively. It is therefore evident that the replacement of the dialkoxy phenylene ring of **29** with the dialkyl thiophene in **30**, lowers the LUMO level and raise the HOMO level by similar value.

Comparing the influence of the electron-deficient unit between **28** (having the 2,1,3-benzothiadiazole unit) and **29** (having the thienopyrazine unit) one can observe that **29** displays higher PCE (1.36%) in blends with $PC_{61}BM$ (1:2, w/w) [70] than **28** (0.022%) in 1:4 (w/w) blend with $PC_{61}BM$

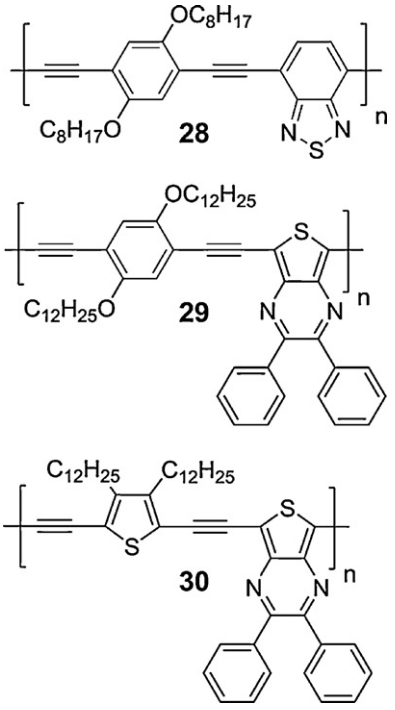

Chart 7. Chemical structures of the copolymers **28**–**30** composed of aryleneethylene and different electron-deficient units.

[69]. Furthermore, the PCE can be increased to 2.37% by replacing the dialkoxy-substituted phenylene with a dialkyl-substituted thiophene in **30** when blended with $PC_{61}BM$ (1:1, w/w) with J_{sc} = 10.72 mA/cm^2, V_{oc} = 0.67 V and FF = 0.33 [70].

3.2.6. Vinylene-linked donor–acceptor based polymers

Conjugated polymers consisting of vinylene-linked D–A segments are currently still largely unexplored in contrast to the classic D–A conjugated polymers that will be reported in details later within this text. Some of the polymers that have been reported consisting of vinylene-linked 2,1,3-benzothiadiazole-various donor moieties, including: dialkoxy-substituted phenylenes (**31** and **32**) [71,72], diphenylamine (**33**) [72], triphenylamine (**34**) [72] and dialkylthiophene (**35**) [73] (Chart 8).

31–**34** have been synthesized using the Heck cross-coupling reaction while **35** with Suzuki cross-coupling reaction. The optical band gap of these polymers varies from 1.94 eV for **31** to 1.5 eV for **35**. It is interesting to note the almost 0.2 eV difference on the optical band gap of **31** compared to **32** (1.76 eV) which differ only to the side alkyl chains (symmetrical versus non symmetrical), while no significant difference on the optical band gap is observed between **33** (1.87 eV) and **34** (1.86 eV). The energy levels are in the range of 3.08–3.61 eV for the LUMO and 5.02–5.31 eV for the HOMO, respectively. The photovoltaic performance was examined in blends with $PC_{61}BM$ (1:4, w/w for **31** [71]; 1:2, w/w for **32**–**34** [72] and 10% weight ratio of polymer for **35** [73]) and the PCE was varied between 0.2% and 0.52% (for **34** with J_{sc} = 2.85 mA/cm^2, V_{oc} = 0.57 V and FF = 0.33). These unsatisfactory PCEs are attributed to the low V_{oc} and to the low hole mobilities (10^{-5}–10^{-6} cm^2/V s) that **32**–**34** are demonstrating as measured by the SCLC method. It was also shown that an important factor limiting the PCE of **35** is the blend film morphologies as presented by measurements of tapping mode AFM as a function of polymer concentration [73]. By increasing the percentage of the polymer in the blend with $PC_{61}BM$, formation of small, round pits that became deeper and coalesce and small valleys are observed indicating that the polymer was concentrating close to the anode surface, effect that negatively affect the IPCE and PCE values.

3.2.7. Poly(3-alkyl)thiophene and poly(3-hexylselenophene) derivatives

3.2.7.1. Poly(3-alkyl)thiophenes and their analogues. One of the most extensively studied material for solar cell applications is the regioregular poly(3-hexylthiophene) (rrP3HT) (**36**; Chart 9) achieving efficiency of around 5% in blends with $PC_{61}BM$ (1:1, w/w) [74–78]. The molecular weight [79,80] and the regioregularity [81,82] (defined as the per-

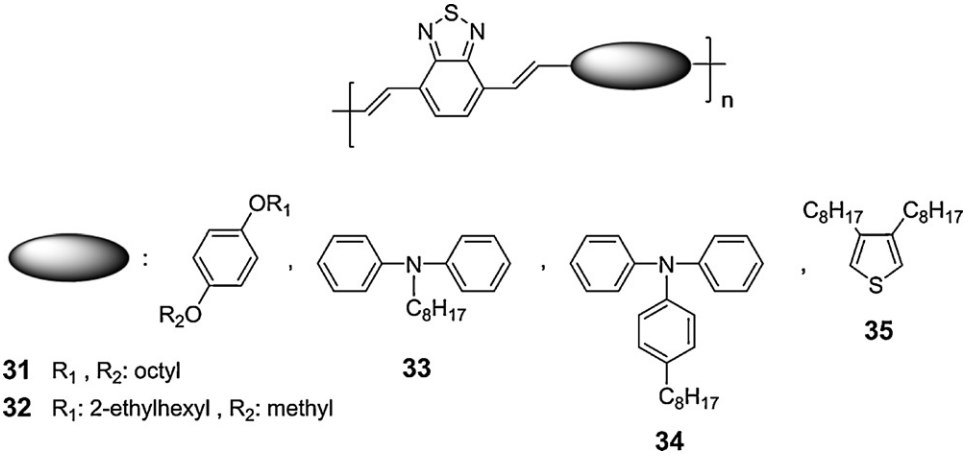

Chart 8. Chemical structures of the copolymers **31**–**35** consisting of vinylene-linked 2,1,3-benzothiadiazole with various electron-rich moieties.

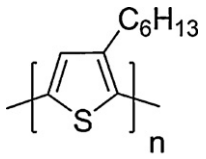

36
rrP3HT

Chart 9. Chemical structure of the regioregular poly(3-hexylthiophene) **36**.

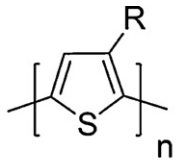

37 R: butyl
38 R: pentyl

Chart 10. Chemical structure of the regioregular poly(3-butylthiophene) **37** and poly(3-pentylthiophene) **38**.

centage of head-to-tail linkages in the polymer) of rrP3HT have been determined to play a crucial role on the light absorption and hole mobility within the blend and as a consequence to the overall OPV efficiency. While it was shown that when the molecular weight of rrP3HT ranged between $30{,}000 < M_n < 75{,}000$ higher efficiencies are exhibited due to the ideal morphology formed, the role of regioregularity has been shown to be critical in order to achieve the rrP3HT crystallinity during the annealing processing step within the blend [77,81,82]. Moreover, the optical band gap of rrP3HT is ~2.0 eV while the energy levels are situated at 2.8–3.0 eV for the LUMO level and ~5.0 eV for the HOMO level.

The first report in the realization of an efficient device based on rrP3HT:$PC_{61}BM$ was based on the work of Padinger et al. reporting PCE of 3.5% upon post-annealing and annealing with an external bias [83]. After this report, extensive efforts from many groups all over the world towards the understanding and optimizing the rrP3HT chemical properties and processing of the active layer have been published, demonstrating PCE values of around 5% [28,84]. It was manifested that the favourable morphology, for balanced hole and electron mobilities resulting in high external quantum efficiencies, is based on fibrillar-like rrP3HT crystals embedded in a matrix that is probably contain $PC_{61}BM$ nanocrystals and amorphous regions of rrP3HT [76]. However, in recent studies it is raising the number of works pointing out that the primary role of thermal annealing in increasing the PCE of the rrP3HT:$PC_{61}BM$ might be the reduced geminate recombination of the dissociated exciton at the D/A interface [85–87]. As an alternative to the thermal annealing, other methods of controlling the morphology have been proposed [29,88], such as the slow drying of solvent, the use of additives or selective solvents and slow cooling of the rrP3HT solution, as well as various deposition techniques (doctor blading [89], inkjet printing [82,90], brush painting [91] and spraying coating [92]) have been used for indicating that this material system can be suitable for large scale OPV production towards the first OPV products.

Very recently, a series of regioregular poly(3-alkylthiophenes) (rrP3ATs) with butyl (**37**) or pentyl (**38**) alkyl side chains (Chart 10) were synthesized and their optoelectronic and morphological properties were compared with those of rrP3HT [93]. All the rrP3ATs were synthesized based on the Rieke method. The weight-average molecular weights of **37**, **38** and rrP3HT are 33,400 g/mol, 34,100 g/mol and 46,000 g/mol, respectively, whereas the regioregularities of **37**, **38** and rrP3HT are 92%, 93.8% and 94%, respectively, as determined by ^1H NMR spectroscopy.

In general, the rrP3ATs have the potential to deliver comparably high PCE in solar cells irrespective of their side-chain length. However, the variation of their morphology with side chain length is the main source of differences in solar cell performance. Transmission electron microscopy (TEM) images show an increase in the degree of phase separation with increasing rrP3AT alkyl side chain length. The **37**:$PC_{61}BM$ displays relatively insignificant phase separation, while **38**:$PC_{61}BM$ has moderate phase separation. Therefore, by passing from **37** to rrP3HT, the increasing alkyl side-chain length facilitates the diffusion of $PC_{61}BM$ through the blend during film drying and/or thermal annealing, resulting in increasing degrees of $PC_{61}BM$ clustering. The photovoltaic parameters of the studied rrP3ATs are presented in Table 2. According to the values of Table 2, the photovoltaic parameter that is mainly affected by comparing **37** with rrP3HT is the FF. In the reported study, the shunts and series resistances values of all the devices under studied were low limiting the measured FF values. Charge transport properties of the rrP3ATs reveal that, the hole mobility of **37**:$PC_{61}BM$ is about two orders of magnitude larger than its electron mobility under all treatment conditions applied. The hole and electron mobilities of **38**:$PC_{61}BM$ also have large differences in the non-annealed samples. However, these differences are reduced significantly upon annealing the films. On the other hand, in the rrP3HT:$PC_{61}BM$ the holes and electrons exhibit well-balanced mobilities for both thermally annealed and non-annealed blends [93]. The variation of bipolar transport characteristics with side chain length can be attributed to local morphology variations as observed with TEM.

It should be noted that in a parallel study, blends of **37** with $PC_{61}BM$, where **37** was in the form of nanowires, compared with blends consisting of conventional phase separated **37**:$PC_{61}BM$ [94]. It was observed that the interpenetrating two-phase morphology enabled by the **37** nanowires provides improved hole transport properties than the blend containing the conventional phase separated polymer **37**. Thus the PCE of **37** nanowires-based devices (2.2%) is more than double higher compare to the phase separated **37**:$PC_{61}BM$ devices (1.0%) and when $PC_{61}BM$ was replaced with $PC_{71}BM$, PCEs of 3.0% were reported [94].

Table 2
Photovoltaic parameters of the rr poly(3-alkylthiophenes):$PC_{61}BM$ devices.

Blends	J_{sc} (mA/cm^2)	V_{oc} (V)	FF	PCE (%)
37:$PC_{61}BM$ (1:0.8, w/w)	11.2	0.54	0.53	3.2
38:$PC_{61}BM$ (1:1, w/w)	12.5	0.55	0.62	4.3
rrP3HT:$PC_{61}BM$ (1:1, w/w)	12.0	0.57	0.68	4.6

As mentioned before, a thermal annealing step, usually above the glass transition temperature (T_g) of the rrP3HT, is necessary so as both the rrP3HT and the $PC_{61}BM$ crystallize to form a nanoscale interpenetrating network. But thermal annealing also drives the phase segregation of rrP3HT and $PC_{61}BM$ since this morphology might not be thermally stable. In fact, it was reported that a prolonged thermal treatment during the processing step induces the formation of large aggregations of $PC_{61}BM$ in the films, negative affecting the device performance [95]. A possible explanation is that the high driving force for crystallization of the rrP3HT initiates the phase segregation of the BHJ by the exclusion of $PC_{61}BM$ from the ordered P3HT domains [76,95]. Therefore, in order to stabilize the morphology upon annealing, two polythiophene derivatives (Chart 11) were synthesized and employed as alternative candidates of rrP3HT that were proved to be very effective in preventing the phase segregation of the active layer components.

The first approach is based on the fact to slightly reduce the regioregularity of P3HT, since the high regioregularity is responsible for the high degree of crystallinity, without provoking its superior optoelectronic properties. **39** has been synthesized using the Grignard metathesis polymerization (GRIM method) by randomly incorporating a thiophene monomer with hexyl side chains at both the 3 and 4 positions [96]. A control sample of rrP3HT has been synthesized using the same methodology and the molecular weights of the polymers were similar (22,000 g/mol (**39**), 28,000 g/mol (rrP3HT)). Photovoltaic devices based on the control rrP3HT and **39** with $PC_{61}BM$ in 1:1 (w/w) were fabricated and tested with respect to their thermal stability. It was shown that initial PCEs of 4.3–4.4%, for both polymers, were obtained upon annealing for 30 min. However the continued annealing of rrP3HT devices causes a decrease in performance (the average PCE fell to 2.6% after 300 min at 150 °C), whereas the devices with **39**:$PC_{61}BM$ showing better thermal stability with the appearance of a slightly lowering performance (3.5% after 300 min at 150 °C) [96]. These results indicating that the annealing time and the degree of regioregularity are critical to achieve stable photovoltaics.

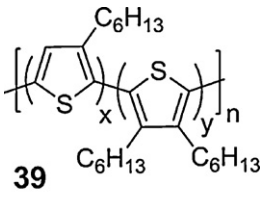

39

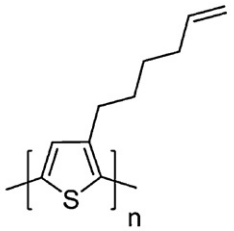

40

Chart 11. Chemical structures of the polythiophene derivatives **39** and **40**.

The second approach is based on the synthesis of a cross-linkable regioregular polythiophene (**40**) having a vinyl group at the end of the side chain which will act as the cross-linkable site [97]. Two are the main reasons for this choice: (1) to maintain the high crystallinity of the polymer because the use of large functionalities to the side chain can prevent the π–π stacking and thereby decrease the crystallinity and the hole mobility and (2) **40** is expected to crystallize and generate nanoscale phase-separated structures in a manner similar to rrP3HT:$PC_{61}BM$ films due to their structural similarity, while simultaneously the thermal treatment can induced a cross-linking reaction of the vinyl group at the side chains. Therefore, **40** and a control rrP3HT have been synthesized using the GRIM method. The regioregularities of the polymers are the same (97%) while their molecular weights (M_n) are 42,600 g/mol (rrP3HT) and 32,000 g/mol (**40**), respectively. BHJ devices comprising rrP3HT and **40** blended with $PC_{61}BM$, were fabricated and subsequent annealed at 150 °C. During this thermal process **40** was cross-linked in the films as confirmed by various spectroscopic techniques such as FT-IR and observation of insolubility of the films in chloroform. Initially, both rrP3HT and **40** based devices showed similar averaged PCEs of ~3.0%. During thermal annealing for 600 min all the PCE parameters of rrP3HT:$PC_{61}BM$ were decreased: V_{oc} from 0.54 V to 0.46 V, FF from 0.65 to 0.51 and J_{sc} from 8.93 mA/cm^2 to 4.22 mA/cm^2. As a result the PCE of rrP3HT decreased from 3.11% to 1.0%. In the case of **40**:$PC_{61}BM$, the V_{oc} increased slightly from 0.64 V to 0.69 V, FF decreased from 0.63 to 0.43 and J_{sc} was decreased from 7.55 mA/cm^2 to 5.83 mA/cm^2. This leads to a reduction of the PCE of **40** from 3.03% to 1.74%, indicating that the drop of PCE was suppressed by using the **40** polymer donor as an alternative to rrP3HT. The more stable PCE of **40**:$PC_{61}BM$ during the thermal annealing process was attributed to the suppression of the formation of large $PC_{61}BM$ aggregations that were present upon thermal treatment of the rrP3HT:$PC_{61}BM$ blends [97].

The considerably high optical band gap of rrP3HT, which prevents devices for obtaining higher J_{sc}, and its relatively high-lying HOMO level at 5.0 eV, which leads to rather low V_{oc} are two of the major drawbacks concerning the optoelectronic properties of the rrP3HT that needs major adjustments for improved PCE. While in the first case many LBG polythiophene derivatives were synthesized and will be presented in detail within the next paragraphs, for the latter only few examples (**41**–**44**) have been presented

Table 3
Optical, electrochemical, charge transporting and photovoltaic properties of **41–44**.

Polymers	E_g^{opt} (eV)	LUMO (eV)	HOMO (eV)	FET (cm^2/V s)	SCLC (cm^2/V s)	V_{oc} (V)	PCE (%)
41	1.9	3.05	5.25	0.03	–	0.75	0.60
42	–	3.39	5.35	0.01	2.7×10^{-4}	0.59	0.54
43	–	3.41	5.45	0.001	2.8×10^{-4}	0.68	1.84
44	1.9	–	5.30	–	–	0.82	3.40

towards lowering the HOMO level with the aim to increase the V_{oc}. These examples include a series of terthiophene (**41** [98], **44** [99]), quaterthiophene (**42**) [100,101] and randomly distributed bithiophene (**43**) [101] polymers (Chart 12) consisting of 3-alkylthiophenes (having various alkyl side chains) combined with unsubstituted thiophene rings in the polymer main chain that were synthesized using either by the Stille cross-coupling polymerization (**41**, **42**, and **44**) or by the Rieke method (**43**). The design concepts behind the synthesis of polythiophene analogues **41–44** are (i) that the introduction of unsubstituted thiophene units in the polymer chain twist slightly out of plane, perturbing the planarity of the backbone and lowering the HOMO level as compared with rrP3HT and (ii) since alkyl is still an electron donating group, one of the simplest ways to reduce the electron donating effect of the side chains would be to reduce the number of alkyl side chains. In addition, based on these polythiophene derivatives (Chart 12), the effect of substituent sequence distribution as well as the influence of the type and length of various alkyl side chains on the crystallinity and PCE in polythiophene derivatives:$PC_{61}BM$ based BHJ OPVs is examined.

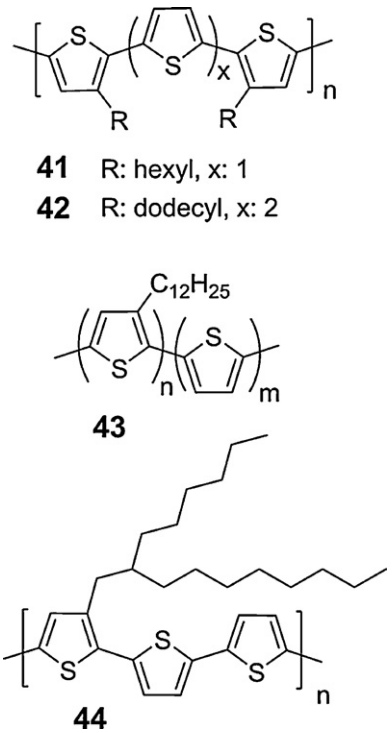

Chart 12. Chemical structures of the polythiophene derivatives **41–44**.

The optical band gaps, the energy levels and the PCE (along with the V_{oc}) of the polythiophene derivatives **41–44** are included in Table 3. It is observed that all the HOMO levels of **41–44** are lying deeper than rrP3HT proving that the above approaches efficiently lower the HOMO level. Unexpectedly though, the order of the HOMO level lowering is not in agreement with the amount of the V_{oc} improvement. For example, since that the HOMO level of **43** is 5.45 eV it is expected to exhibit higher V_{oc}, but this is not observed on the V_{oc} values of Table 3. According to Table 3, **44** with HOMO at 5.30 eV exhibits the highest V_{oc} (0.82 V) and **41** with HOMO at 5.25 eV demonstrates the second highest V_{oc} (0.75 V). Nevertheless, the reported V_{oc} values of **41–44** are higher than the V_{oc} of rrP3HT except from **42**. Furthermore, the crystallinity of the polymers as examined by X-ray diffraction (XRD) measurements showed that **41** and **42** were significantly more crystalline than **43**. This can be due to the perfectly alternating structure of **41** and **42** relative to the more random structure of **43**. The higher degree of crystallinity for **41** and **42** in contrast to **43** was also verified to affect hole transport properties. While the hole mobilities of **41** and **42** in FETs are 0.03 cm^2/V s and 0.01 cm^2/V s, respectively, the hole mobility of **43** in FET is 0.001 cm^2/V s, one order of magnitude lower than **41** and **42**. However, the hole mobilities of **42** and **43** as measured with the SCLC method are not in agreement with the hole mobilities measured by using FETs measurements (Table 3). The difference between these two techniques (SCLC and FETs) is that SCLC measures the mobility perpendicular to the electrodes rather than parallel to the substrate and not under the influence of a gate bias, as in FETs. Possible explanation of the discrepancy of **42** and **43** mobilities values measured by FET and SCLC methods can be that despite the lack of observed long range order in **43**, locally ordered domains should exist and can be a factor for the above mentioned bulk mobility discrepancy [101].

The photovoltaic performance of **41–44** in blends with $PC_{61}BM$ was examined and a promising PCE of 3.4% was recorded for **44**:$PC_{61}BM$ system in 1:1 (w/w) with J_{sc} = 6.33 mA/cm^2, V_{oc} = 0.82 V and FF = 0.66 [99]. It is obvious that the combination of one alkyl side chain (in this case the branched 2-hexyldecyl in order to provide good solubility) for three thiophene units leads to lower HOMO level, leading to improved V_{oc} and surprisingly high FF that is very close to the best FF of the rrP3HT:$PC_{61}BM$ based OPVs. The limiting factor preventing this polymer for higher efficiencies is the rather high optical band gap that limits the J_{sc} of the device. Moreover, comparing the PCEs of **41–43**, it is illustrated that the polymers with the higher crystallinity (**41**, **42**) exhibit lower PCEs than the amorphous **43**. Especially for the two polythiophenes **42** and **43**, which are compositionally and electronically equiv-

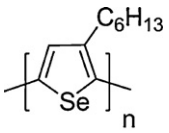

45

rrP3HS

Chart 13. Chemical structure of the regioregular poly(3-hexylselenophene) **45**.

alent and differ only in the sequence distribution of the alkyl side chains, the polymer with the random structure is superior to the polymer with the precisely defined structure, in the context of solar cell performance. For all weight ratios investigated, the random and amorphous **43** outperformed its highly ordered analogue **42** with the best PCEs recorded for a 30:70 (w/w) blend of **43**:$PC_{61}BM$ (1.84%) and for a 25:75 (w/w) blend of **42**:$PC_{61}BM$ (0.54%), respectively [101]. Slightly higher is the PCE of **41** (0.60%) as compared to that of **42**. It is assumed that the reason for the higher PCE of **43** is the higher miscibility with $PC_{61}BM$ and thereby the ability to form a bicontinuous structure in contrast to the suboptimal mixing of **41** and **42** with the $PC_{61}BM$ [101]. In general, this is the first example, and more will be reported later in the text, showing that the PCE of conjugated polymers with similar chemical structures and electronic properties influenced not only by the light absorption and matching of energy levels but also from the placement and choice of alkyl side chains affecting polymer crystallinity and miscibility with $PC_{61}BM$.

3.2.7.2. Poly(3-hexylselenophene). Despite the high PCEs of the rrP3HT:$PC_{61}BM$ solar cells, the high band gap of rrP3HT (1.9 eV) is the major disadvantage preventing this system to achieve higher efficiencies. An efficient approach for lowering the band gap of rrP3HT by reducing the LUMO level and keeping the HOMO level constant is the switching from the sulphur containing polymers to selenium containing polymers. This approach was demonstrated by the synthesis of a new class of LBG (1.6 eV) polymer, the regioregular poly(3-hexylselenophene) (rrP3HS (**45**); Chart 13) [102,103]. rrP3HS was synthesized based on the GRIM method and the energy levels are situated at 4.8 eV for the HOMO energy level and 3.2 eV for the LUMO energy level.

The photovoltaic performance of rrP3HS:$PC_{61}BM$ blend films showed PCE of 2.7%, with J_{sc} = 6.5 mA/cm^2, V_{oc} = 0.52 V and FF = 0.40. This OPV performance was achieved with 52 wt% $PC_{61}BM$ after annealing at 150 °C. This PCE is lower compared to rrP3HT:$PC_{61}BM$ system (PCE of 3.0%) measured under the same conditions, due to lower charge separation efficiency and limited charge transport properties [102,104]. It is observed that replacing the rrP3HT with rrP3HS in the blend with $PC_{61}BM$ the J_{sc} is higher (as expected from the lower band gap) and the V_{oc} is similar (as expected from the similar HOMO level). However the external quantum efficiency (EQE) was much lower for the P3HS-based devices. Despite the larger photocurrent the FF parameter was also reduced. The results revealed that, despite the high crystallinity of rrP3HS

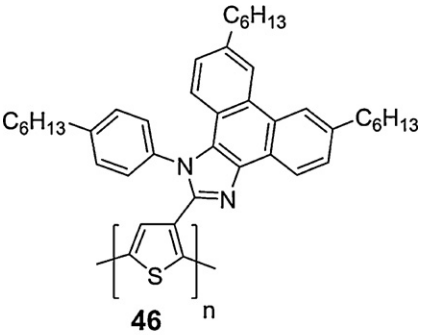

46

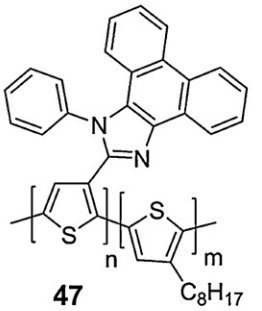

47

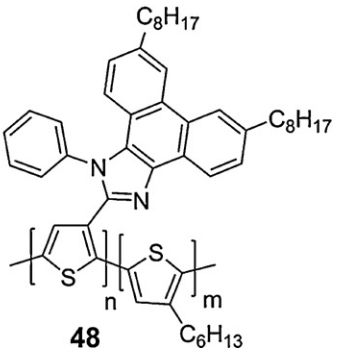

48

Chart 14. Chemical structures of the imidazole-substituted polythiophene derivatives **46**–**48**.

[as indicated by differential scanning calorimetry (DSC)], XRD measurements for the rrP3HS:$PC_{61}BM$ blends show a lower degree of crystallinity than the rrP3HT:$PC_{61}BM$ blends [104]. Thus the low degree of phase segregation is likely to contribute to the faster recombination kinetics observed in rrP3HS:$PC_{61}BM$ compared to rrP3HT:$PC_{61}BM$ blends, and this is likely due to the lower hole mobility in rrP3HS compared to that of rrP3HT [104]. These results further indicating the importance of controlling the polymer:fullerene blend microstructure through the self-organizing properties of the component materials.

3.2.7.3. Imidazole-substituted polythiophene derivatives. Based on the intramolecular D–A concept, a regioregular polythiophene homopolymer (**46**) and a series of copolymers (**47** and **48**) were prepared by covalently binding the electron-withdrawing and conjugated phenanthrenylimidazole moiety, either unsubstituted (**47**) [105] or alkyl functionalized (**46** [106], **48** [107]), as side chains onto the polythiophene backbone (Chart 14). The GRIM method was employed for the synthesis of the homopolymer **46** and

Table 4
Molecular composition, optical–electrochemical properties and photovoltaic performance of **46**–**48**.

Polymers	*n*	*m*	E_g^{opt} (eV)	LUMO (eV)	HOMO (eV)	PCE (%)
46	–	–	1.85	2.90	4.70	4.10
47a	10	90	–	3.57	5.35	–
47b	20	80	–	3.60	5.30	–
47c	30	70	–	3.64	5.25	–
47d	50	50	1.82	3.66	5.21	1.68
47e	70	30	1.81	3.70	5.20	2.15
47f	80	20	1.77	3.75	5.15	2.80
48a	20	80	1.88	2.80	4.70	–
48b	40	60	1.86	2.87	4.70	2.42
48c	60	40	1.85	2.95	4.65	2.63
48d	80	20	1.83	3.02	4.65	2.85
48e	90	10	1.80	3.05	4.65	3.45

the copolymers **47** and **48** that contain different contents from the phenanthrenyl-imidazole moieties along with 3-alkyl substituted thiophene monomers. Some of the possible advantages of such a molecular architecture are: (i) by incorporating the electron-withdrawing moieties as side chains it is expected that the charge separation and transportation through sequential transfer of electrons from the main chain to the side chains will be facilitated and (ii) multiple absorption can be occurred especially if the electron withdrawing unit absorbs at a different wavelength than the polymer main chain, an approach that can be used to expand polymer absorption properties.

The optical band gaps and the energy levels of the synthesized phenanthrenyl-imidazole-based polythiophene derivatives **46**–**48** are included in Table 4. It is observed that the band gap of **47** and **48** derivatives is reduced upon increasing the content of incorporated phenanthrenyl-imidazole moieties in the copolymers. Moreover, the presence of the phenanthrenyl-imidazole moieties altered the HOMO and LUMO levels of **47** and **48** derivatives. For example, the HOMO energy levels of **47** raised from 5.35 eV to 5.15 eV, while those of **48** from 4.70 eV to 4.65 eV. It should be noted, that even though the HOMO levels of both **47** and **48** are elevated upon increasing the content of the phenanthrenyl-imidazole, the HOMO level of **47** is subsequent rising while the HOMO levels of **48a**, **48b** and **48c**–**e** remain constant at 4.70 eV and 4.65 eV, respectively. Similar with the HOMO levels, the LUMO levels upon increasing the content of the phenanthrenyl-imidazole are subsequent lower, from 3.57 eV to 3.75 eV for **47** and from 2.80 eV to 3.05 eV for **48**. To conclude, the general trend is that the optical band gaps of the unsubstituted phenanthrenyl-imidazole polythiophene derivatives **47** are lower compared to **46** and **48** most probably due to the better π–π stacking between the polymer chains, whereas both the energy levels of **47** are lying lower than **48**.

BHJ solar cells were fabricated based on the polymers **46**–**48** blended with $PC_{61}BM$ and promising PCEs above 2% have been achieved. The maximum PCE of 4.1% was reported for the **46**:$PC_{61}BM$ blend in 1:1 (w/w) ratio after thermal annealing at 120 °C for 30 min. The PCE parameters reported have the following values J_{sc} = 11.3 mA/cm^2, V_{oc} = 0.61 V and FF = 0.60 [106]. **46** comprised of ~20 repeating units and the HOMO level of **46** is around 4.7 eV, this indicated sensitivity to air oxidation. The combination of lower band gap with high and balanced charge transport (1.9×10^{-5} cm^2/V s for holes and 4.2×10^{-5} cm^2/V s for electrons as measured based on the SCLC method) resulted to higher external quantum efficiencies, thus much higher short-circuit current densities for the **46**:$PC_{61}BM$ BHJ OPVs compared to reference solar cells of rrP3HT:$PC_{61}BM$ processed under the same conditions [106]. Finally, a rather unexpected outcome is observed by examining the photovoltaic parameters of the devices based on **47** and **48** copolymers. By increasing the phenanthrenyl-imidazole moiety in the polymer backbone, the HOMO values of both **47** and **48** derivatives are affected (Table 4). Despite the subsequent differences on their HOMO levels, all V_{oc}s reported ranged between 0.6 and 0.69 V, even if the HOMO values of **47** are at least 0.5–0.6 eV higher than that of **48**.

3.2.7.4. Polythiophene derivatives with vinylene groups as side chains. Based on the consideration that extension of the conjugation degree of conjugated polymers leads to enhanced and red-shifted of the absorption spectra of conjugated polymers [108], a series of polythiophene derivatives with different ratios of conjugated thiophenevinylene side chains have been synthesized (**49** [109] and **50** [110]) and applied as electron donor polymers in OPVs (Chart 15). The bi(thienylenevinylene) substituted polythiophene **49** and the branched (terthiophenevinylene) substituted polythiophene **50** were synthesized using the Stille cross-coupling polymerization.

The absorption spectra, the energy levels and the photovoltaic properties of **49** and **50** are influenced by the content of the conjugated vinylene side chains as shown in Table 5. The optical band gap in the series of copolymer **49** increases from 1.80 eV to 1.82 eV, by decreasing the content of the conjugated side chains. In contrast, increase on the content of the conjugated side chains in the series of copolymer **50**, showed that the absorption peak of the branched polythiophenes was enhanced and blue-shifted, thus the optical band gap was decreased. Regarding the energy levels of **49**, the HOMO level slightly decreases and the LUMO level remains almost constant by decreasing the content of the bithienylenevinylene side chain. On the other hand, the HOMO level of **50** remains almost constant but the LUMO level is subsequent rising upon increasing the content of the terthiophenevinylene side chains. Furthermore, comparing the energy levels between the two copolymers **49** and **50**, it is observed that the LUMO lev-

Table 5
Molecular composition, optical–electrochemical properties and photovoltaic performance of **49**–**50**.

Polymers	*n*	*m*	E_g^{opt} (eV)	LUMO (eV)	HOMO (eV)	PCE (%)
49a	0	1	1.80	2.97	4.96	1.71
49b	0.01	0.99	1.81	2.95	4.94	2.57
49c	0.41	0.59	1.82	2.96	4.93	3.18
50a	1	0	–	–	–	0.87
50b	0.9	0.1	–	2.72	5.07	1.47
50c	0.8	0.2	–	2.75	5.07	1.91
50d	0.7	0.3	–	2.79	5.09	1.65
50e	0.6	0.4	–	2.84	5.09	1.47

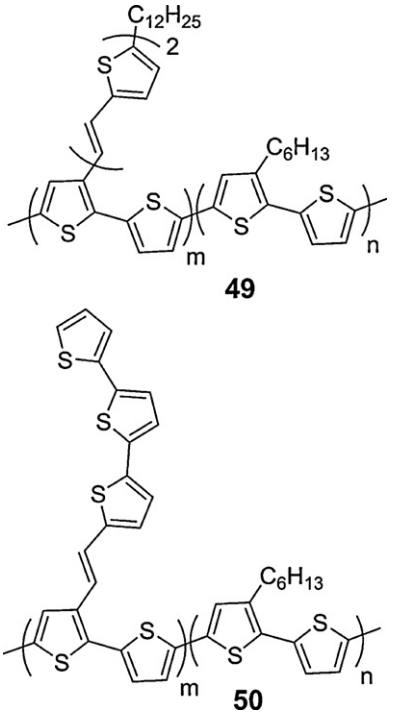

Chart 15. Chemical structures of the polythiophene derivatives **49**–**50** with vinylene groups as side chains.

els of **49** derivatives are lower than those of **50**, while the electrochemical band gaps of the branched copolymers **50** are higher than that of the **49** derivatives. This is an indication that bithienylenevinylene side chains can be used to decrease more effectively the band gap of the side chain conjugated polythiophenes than terthiophenevinylene side chains [109].

The photovoltaic properties of polymers **49** and **50** in blends with $PC_{61}BM$ were investigated and PCEs as high as 3.18% were recorded for polymer **49c**:$PC_{61}BM$ in 1:1 (w/w) ratio with J_{sc} = 11.3 mA/cm^2, V_{oc} = 0.61 V and FF = 0.60. In general, the PCE of **49** derivatives increases as the content of the bithienylenevinylene side chain decreases [109]. However, the PCE of the **50**:$PC_{61}BM$ derivatives increases as the content of the conjugated side chains of **50** reach up to 20% and then the PCE subsequent decreases for contents above 20%. The maximum PCE for the **50**:$PC_{61}BM$ derivatives was recorded for **50c**:$PC_{61}BM$ (1.91%) when blended with $PC_{61}BM$ in 1:1 (w/w) ratio with J_{sc} = 6.85 mA/cm^2, V_{oc} = 0.73 V and FF = 0.38 [110].

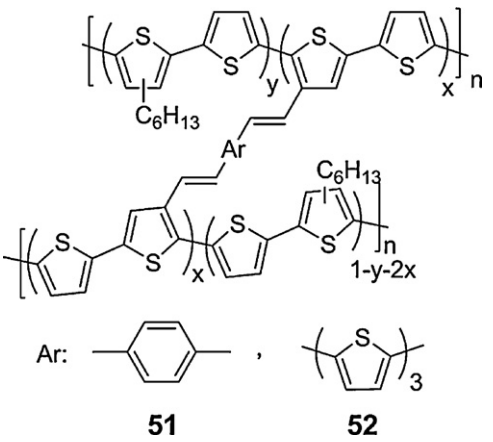

Chart 16. Chemical structures of the cross-linked polythiophene derivatives **51** and **52**.

3.2.7.5. Cross-linked polythiophene derivatives through conjugated bridges. One of the approaches for increasing the charge transport properties of conjugated polymers is the use of a network structure, like a cross-linked conjugated polymer due to their ability to better facilitate the carrier interchain hopping [111]. On the basis of this approach, several crosslinked polythiophene derivatives with various percentages of conjugated bridges, such as vinylene–phenylene–vinylene (VPV) (**51**) [112] or vinylene–terthiophene–vinylene (VTV) (**52**) [113] were synthesized (Chart 16) through the Stille cross-coupling polymerization.

The absorption spectra, the energy levels and the photovoltaic properties of **51** and **52** are influenced by the content of the conjugated bridges as shown in Table 6. Despite, that no absolute values for the optical band gaps of **51** and **52** is provided within the literature, both copolymers exhibit blue shifted absorption spectra as the content of the conjugated bridge increases. The increase of conjugated bridges, might result to a more pronounced distortion of the polymer backbone that effectively reduce the conjugation length of the polymer [112,113]. Comparing the absorption spectra of **51** and **52**, it is revealed that the presence of the longer VTV bridge of **52a**–**d** blue shifts their absorption spectra to a lower extent compared to that of **51a**–**d**. This is an indication that the distortion of the main chains should be less for the polymers with the VTV bridges compared to that with VPV bridges [113]. Regarding the energy levels of the polymers, the HOMO level of **51** is subsequent getting deeper as the VPV bridge increases but has

Table 6
Various percentages of conjugated bridges, electrochemical properties and photovoltaic performance of **51** and **52**.

Polymers	*x*	LUMO (eV)	HOMO (eV)	PCE (%)
51a	0	2.77	5.06	0.37
51b	0.02	2.76	5.07	1.05
51c	0.05	2.74	5.13	1.26
51d	0.1	2.73	5.23	0.78
52a	0	2.77	5.06	0.87
52b	0.02	2.77	5.06	1.72
52c	0.04	2.75	5.06	1.47
52d	0.08	2.74	5.11	1.21

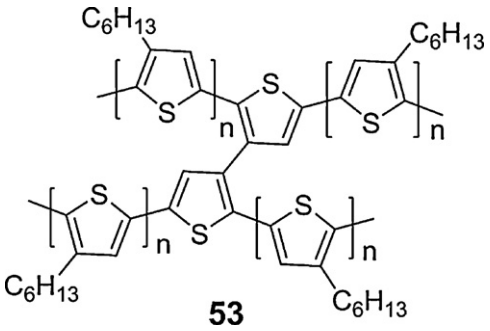

53

Chart 17. Chemical structure of the cross-linked polythiophene **53**.

only slight influence on their LUMO levels. It is interesting that the HOMO and LUMO levels of **52b** are the same as those of **52a**, indication that small amount of VTV bridges (2%) have minor influence on the electrochemical properties of the polymers. By increasing further the VTV bridges, both the HOMO and LUMO level up-shifted to some extent. Finally, an interesting point is that the energy levels of both **51** and **52** are similar regardless of the type of conjugated bridged chains (Table 6).

BHJ solar cells based on polymers **51** and **52**, in blends with $PC_{61}BM$ in 1:1 (w/w) ratio, were fabricated and PCEs as high as 1.26% for **51c** with $J_{sc} = 4.06\,mA/cm^2$, $V_{oc} = 0.72\,V$ and FF = 0.35 [112] and 1.72% for **52b** with $J_{sc} = 6.82\,mA/cm^2$, $V_{oc} = 0.67\,V$ and FF = 0.38 [113], have been reported. One possible reason for the improved PCE for the polymer:fullerene BHJ solar cells based on **51b** and **51c**, compared to that of **51a** and **51d** electron donors can be the higher hole mobilities, which are $1.28 \times 10^{-4}\,cm^2/V\,s$ (**51b**) and $7.01 \times 10^{-3}\,cm^2/V\,s$ (**51c**) compared to $5.23 \times 10^{-6}\,cm^2/V\,s$ (**51a**) and $2.34 \times 10^{-5}\,cm^2/V\,s$ (**51d**), respectively as measured by SCLC method. Except of the different hole mobilities, the large number of conjugated bridges in **51d** result in main chain distortion and poor solubility of the polymer. Similar to polymer:fullerene BHJ solar cells based on **51b** and **51d** electron donors, the higher PCE of **52b**:$PC_{61}BM$ can be attributed to its higher hole mobility $4.70 \times 10^{-3}\,cm^2/V\,s$ compared to $5.23 \times 10^{-6}\,cm^2/V\,s$ for **52a**, $2.58 \times 10^{-3}\,cm^2/V\,s$ for **52c** and $9.48 \times 10^{-4}\,cm^2/V\,s$ for **52d**, also measured by the SCLC method.

In another example, regioregular poly(3-hexylthiophene) copolymers (**53**; Chart 17) having different degree of branching through simple bonds were synthesized and employed in photovoltaic cells as electron donors in blends with $PC_{61}BM$ [114]. However, a distinctly decreased hole mobility and a reduced solar cell PCE with increasing amount of interchain branching was observed, compared to rrP3HT:$PC_{61}BM$ material system, because the formation of ordered poly(3-hexylthiophene) domains is suppressed.

3.2.7.6. Polythiophene derivatives with thiophene rings as side chains. In an attempt to obtain LBG polythiophene derivatives with broad absorption and high hole mobility, a bithiophene unit, functionalized with alkylthiophenes as side chain pendants, was copolymerized with either an electron rich thiophene ring (**54** and **55**) [115] or an electron withdrawing 2,1,3-benzothiadiazole unit (**56**) [116] or various DAD segments with thiophene rings as the constant donor and different acceptor moieties including: 2,1,3-benzothiadiazole (TBzT) segment (**57**) [116] or alkoxyphenyl-functionalized quinoxaline (TQT) segment (**58**) [116] or finally diketopyrrolo[3,4-*c*]pyrrole (TDPPT) segment (**59**) [116] through Stille cross-coupling polymerization (Chart 18). The design and synthesis of these copolymers was based on the fact that the incorporation of conjugated side chains, such as bi(thienylenevinylene), into polythiophene significantly broadened the absorption spectrum, while the cross-linked polythiophene derivatives with conjugated bridges were shown to have high charge carrier mobility, as also discussed in more details above.

The optical band gaps, the energy levels and the PCEs of the two-dimensional polythiophene copolymers **54**–**59** are presented in Table 7. The optical band gap of **55** is lower than **54** because of the longer length of its conjugated side chains [115]. Furthermore, the band gaps of the D–A polythiophene derivatives **56**–**59** are tuned by copolymerizing with different conjugated electron-accepting units. For example the band gap values of **56**–**59** follows the order: **56** > **58** > **57** > **59** but are significantly lower than that of **54**. Regarding the energy levels of the copolymers, it is revealed that the HOMO level of **55** is deeper than that of **54**, pointing out that despite the fact of the lower optical band gap of **55**, the electron donating ability of **54** is higher. Furthermore, according to the energy level values of **56**–**59**, it is observed that the HOMO level of **57** is raised to a value of 0.48 eV upon the addition of one more thiophene ring next to the 2,1,3-benzothiadiazole compared to **56**, whereas the LUMO level of **57** is lower by only 0.14 eV. Among the studied copolymers, **59** exhibits the lower LUMO level and optical band gap. This can be an indication that the combination of the higher electron affinity and the planarity of the diketopyrrolo[3,4-*c*]pyrrole unit, can

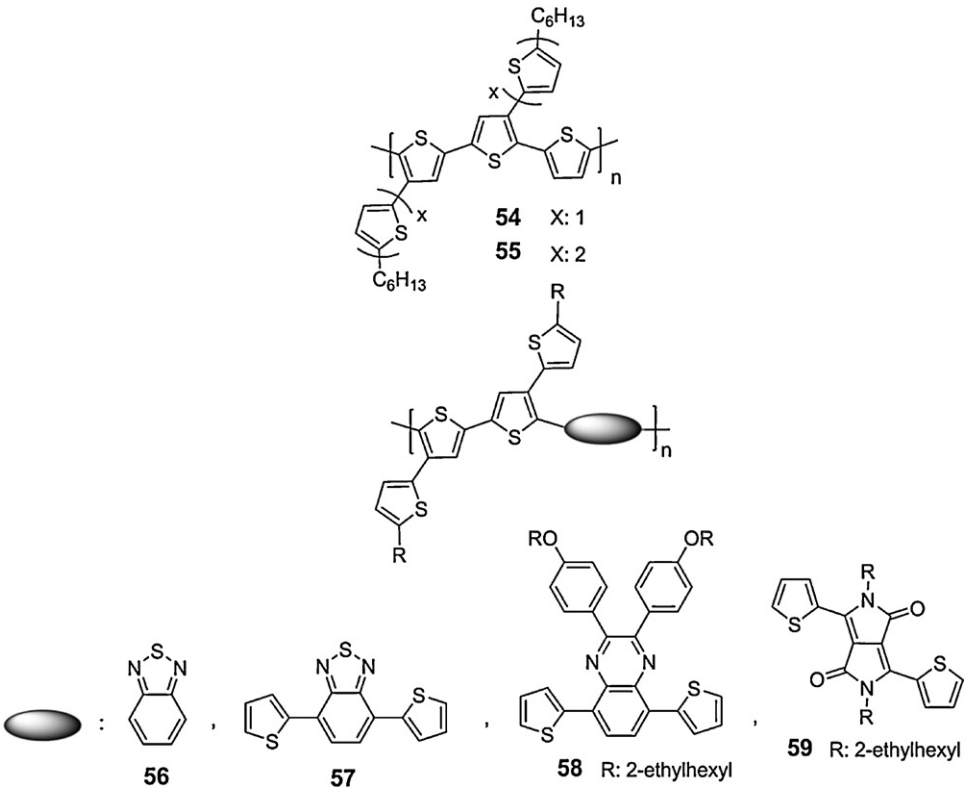

Chart 18. Chemical structures of the polythiophene derivatives **54**–**59** with thiophene rings as side chains.

Table 7
Optical band gaps, electrochemical properties and photovoltaic performance of **54**–**59** with $PC_{71}BM$ in [a] 1:3 (w/w) and [b] 1:2 (w/w).

Polymers	E_g^{opt} (eV)	LUMO (eV)	HOMO (eV)	PCE (%)
54	1.98	–	5.46	2.50
55	1.77	–	5.62	1.30
56	1.88	3.24	5.52	1.39
57	1.60	3.38	5.04	1.28
58	1.83	3.22	5.28	1.29
59	1.29	3.62	5.17	1.67[a]/2.43[b]

provide stronger π–π interactions between the polymer chains [116].

The photovoltaic performances of the synthesized copolymers were evaluated in blends with $PC_{71}BM$ using different composition ratios. The highest PCE (2.5%) was obtained from **54**:$PC_{71}BM$ system in 1:3 (w/w) with J_{sc} = 6.4 mA/cm^2, V_{oc} = 0.91 V and FF = 0.43 upon annealing at 140 °C for 20 min [115]. Comparing the photovoltaic characteristics of **54** with those of **55** (J_{sc} = 6.3 mA/cm^2, V_{oc} = 0.60 V and FF = 0.35), one can clearly notice that the V_{oc} of **55** is significant lower than that of **54** despite its higher HOMO level. Furthermore, the PCEs of the D–A polythiophene derivatives **56**–**59** in blends with $PC_{71}BM$ in 1:3 (w/w) ratio are in the range 1.28–1.67%. The PCE was increased up to 2.43% for the **59**:$PC_{71}BM$ in 1:2 (w/w) because of the balanced hole (4.20×10^{-4} cm^2/V s) and electron (2.83×10^{-4} cm^2/V s) mobilities values measured by FETs [116].

3.2.7.7. Oligothiophene copolymers incorporating 2,1,3-benzothiadiazole unit. A small library of D–A conjugated polymers (**60**–**70**) composed of oligothiophenes (as donor) and 2,1,3-benzothiadiazole (as acceptor) were synthesized from various research groups by Stille cross-coupling polymerization [117–119] and are included in Chart 19. The number of the thiophene rings vary from 1 to 8, the alkyl chains differs relating to the position on the thiophene ring, the number of the carbon atoms and the type; linear versus branched.

As can been seen in Table 8, the optical band gap variation presents an interesting trend. By increasing the number of the thiophene units is expected that the optical band gap should be decreased [117]. However, the optical band gap seems to be a function of not only the number of the thiophene rings around the 2,1,3-benzothiadiazole core but also to the density and the relative position of the side alkyl chains attached on the thiophene rings. For example, the band gaps of **60** [117] and **61** [117] are the same despite the addition of the one more thiophene ring in the polymer backbone of **61**. However, the band gap of **62** [118] is 0.13 eV lower than that of **61**, consisting of the same number of thiophene units. This means that the

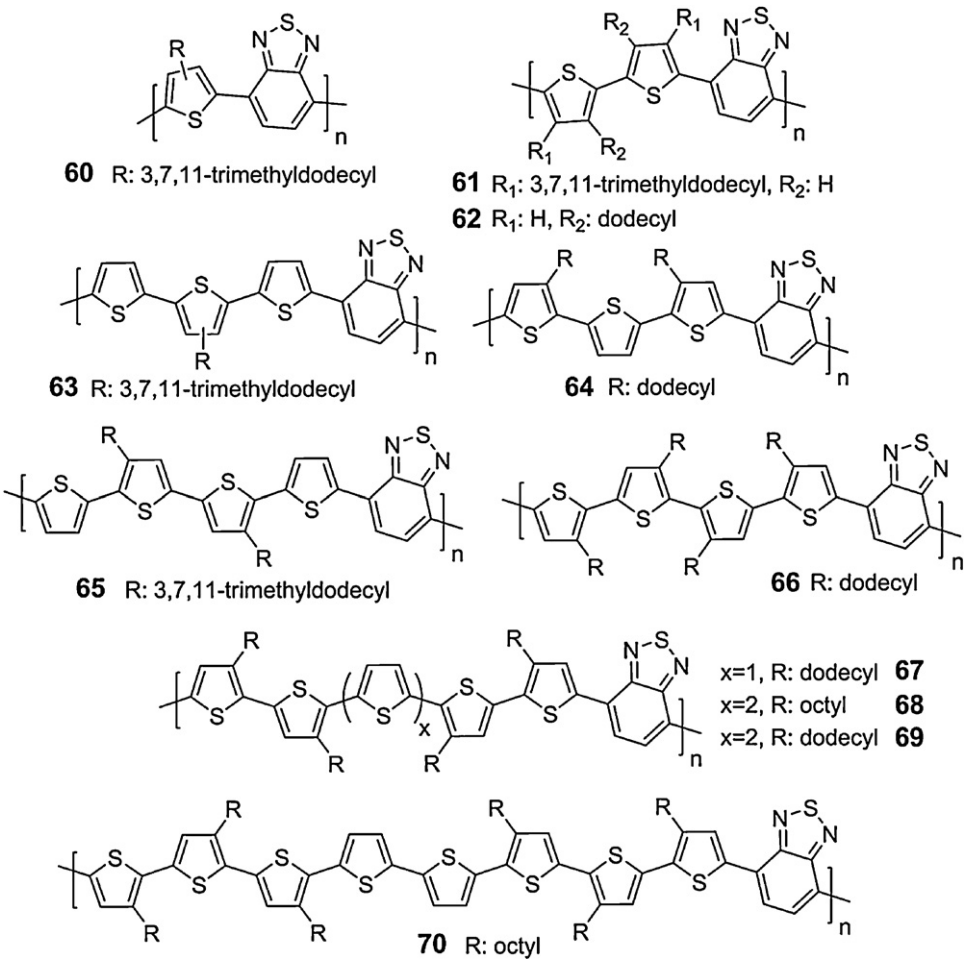

Chart 19. Chemical structures of the oligothiophene copolymers **60**–**70** consisting of 2,1,3-benzothiadiazole.

introduction of the alkyl side chain on the thiophene unit in the β position in relation to the 2,1,3-benzothiadiazole results to lower band gap values most likely due to the less steric hindrance. Similar observations will be reported to other chemical structures with more details later within the text (see polymers **175** and **176**). Moreover, the addition of one more thiophene ring in the polymer backbone (**63** [117] and **64** [118]) results to further band gap reduction. The decrease of the band gap related to the position of the side alkyl chains on the thiophene rings. When there are no alkyl side chains on the thiophene rings next to the 2,1,3-benzothiadiazole and a branched dodecyl side chain on the thiophene unit between the two thiophenes (**63**) the band gap is 1.82 eV. While the band gap of **64**, consisting of two dodecyl side chains on the thiophene units in the β position regarding to the 2,1,3-benzothiadiazole and no alkyl chain on the thiophene between the other two thiophenes, is 1.59 eV. This indicates that the polymer chains of **64** adopt a more planar geometry and closely packing in solid state. Furthermore, the band gaps of **65** [117] (1.65 eV) and **66** [118] (1.72 eV) are lower than **63** but higher when compared to **64**. This suggests that the increase of the thiophene units next to the 2,1,3-benzothiadiazole in the polymer backbone is not leading always to band gap reduction. This might be due to the steric repulsion between the β-alkyl chains in 3,3′-dialkyl-2,2′-bithiophene units, which prohibits the polymers from forming more planar chains in the solid state [118].

Table 8
Optical band gaps and electrochemical properties of **60**–**70**.

Polymers	E_g^{opt} (eV)	LUMO (eV)	HOMO (eV)
60	2.10	3.30	5.40
61	2.10	2.82	4.92
62	1.97	3.23	5.59
63	1.82	4.02	5.84
64	1.59	3.17	5.03
65	1.65	3.02	4.67
66	1.72	3.18	5.20
67	1.56	3.10	4.88
68	1.78	3.37	5.26
69	1.52	3.18	4.94
70	1.82	3.30	5.23

Additionally, the further increase of the thiophene number to 5, 6 and 8 units next to the 2,1,3-benzothiadiazole reveal a controversially trend as presented by two inde-

Table 9
Electrochemical properties of **71**–**73**.

Polymers	Cyclic voltammetry LUMO–HOMO (eV)		Differential pulse voltammetry LUMO–HOMO (eV)	
71	3.53	5.35	3.59	5.35
72	3.50	5.60	3.63	5.53
73	3.47	5.28	3.62	5.24

pendent research groups. Yue et al. [118] show that the band gaps of **67** and **69** are 1.56 eV and 1.52 eV respectively, while Liang et al. [119] reported that **68** and **70** exhibit band gaps of 1.78 eV and 1.82 eV, respectively. These results are rather unexpected especially if someone compares **68** and **69**. Although, these two polymers have similar molecular weights (M_n = 8200 g/mol (**68**) and 7200 g/mol (**69**)), the difference on their band gap is 0.26 eV and cannot be explained by the different alkyl side chains within their polymer backbones. Furthermore, as Yue et al. reported the band gap decreases when passing from the 5 thiophene rings (**67**) to 6 thiophene rings (**69**) [118]. On the contrary, comparing **68** and **70**, the band gap of **68** is lower than **70**, even though the polymer backbone of **70** has two more thiophene units than **68** [119].

Concerning the HOMO–LUMO energy levels direct comparison between the polymers cannot be provided since different experimental techniques (cyclic voltammetry and ultraviolet photoelectron spectroscopy) have been used for HOMO–LUMO energy levels calculation [117–119]. The PCE of these polymers in blends with $PC_{61}BM$ are ranged from 0.93% to 2.23%. The highest PCE (2.23%) is observed for the **69** when is blended with $PC_{61}BM$ in 1:3 (w/w) ratio with J_{sc} = 5.62 mA/cm^2, V_{oc} = 0.85 V and FF = 0.47 [118]. It should be noted that no difference on the PCE values is observed when thermal treatment is applied.

3.2.7.8. Alkoxy-substituted oligothiophene copolymers with 2,1,3-benzothiadiazole unit. Another series of D–A conjugated polymers (**71**–**73**) comprised of electron-rich 3,4-dioxythiophenes and 2,1,3-benzothiadiazole have also been synthesized (Chart 20) and their photovoltaic properties were extensively investigated [120,121].

All polymers have been synthesized by oxidative polymerization using the mild oxidizing agent $FeCl_3$ [120]. **71** has been also synthesized from another research group using the nickel-catalyzed Yamamoto polycondensation procedure [121]. The optical band gaps of the polymers are 1.6 eV (**71**), 1.65 eV (**72**) and 1.55 eV (**73**). The HOMO and LUMO energy levels of the polymers are presented in Table 9 and were determined using two different experimental techniques [cyclic voltammetry (CV) and differential pulse voltammetry (DPV)]. All the electrochemical band gaps were found to be slightly larger than the optically estimated values but the electrochemical band gaps obtained using the DPV method are closer to the optically estimated values than that obtained using the CV method [120].

The PCE of the unsubstituted bithiophene **72** in blends with $PC_{61}BM$ (1:8, w/w) is 1.90% (J_{sc} = 5.56 mA/cm^2, V_{oc} = 0.77 V and FF = 0.44) two times higher than that of **71** (0.88%) and **73** (0.70%) [120]. The reason for the low PCE of **71** and **73** is their low hole mobility and their unfavourable

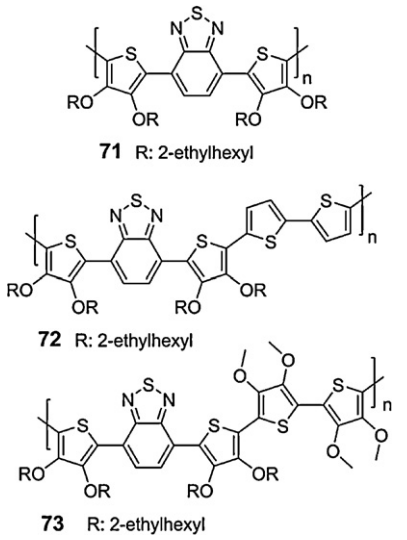

Chart 20. Chemical structures of the alkoxy-substituted oligothiophene copolymers **71**–**73** consisting of 2,1,3-benzothiadiazole.

thin film morphologies. The thin film morphology of the polymers in blends with $PC_{61}BM$ was examined with AFM [120]. For the **71**:$PC_{61}BM$ (1:4, w/w) the AFM images show a particularly coarse morphology with the formation of very large $PC_{61}BM$ clusters and without the appearance of any interpenetrating network. The **72**:$PC_{61}BM$ (1:8, w/w) demonstrates a more heterogeneous morphology with dispersed large $PC_{61}BM$ domains in the active layer. Finally, the **73**:$PC_{61}BM$ (1:5, w/w) exhibits a more homogeneous morphology suggesting no obvious phase separation which is necessary for the formation of bicontinuous transport network. Further optimization on the solar cell device configuration for the **72**:$PC_{61}BM$ has been achieved by replacing the PEDOT:PSS with molybdenum oxide (MoO_3) (2.12%) and finally a PCE of 2.71% (J_{sc} = 5.96 mA/cm^2, V_{oc} = 0.80 V and FF = 0.57) has been demonstrated replacing both the $PC_{61}BM$ with $PC_{71}BM$ and PEDOT:PSS with MoO_3 [120].

3.2.7.9. Oligothiophene copolymers incorporating alkoxy-substituted 2,1,3-benzothiadiazole unit. Three new D–A oligothiophene copolymers containing alkoxysubstituted 2,1,3-benzothiadiazoles and one (**74**), two (**75**) or three (**76**) thiophene rings in the polymer backbone have been synthesized using both Stille and Yamamoto cross-coupling polymerization reactions (Chart 21) [122].

The optical band gap of **74** is 1.74 eV, for **75** is 1.73 eV and for **76** is 1.75 eV with the appearance of a fine vibronic feature centered at 625 nm for **74** and **76**. The PCE of the polymers in blends with $PC_{61}BM$ (1:2, w/w) are 2.22% (**74**), 0.62% (**75**) and 1.78% (**76**) [122]. The photovoltaic charac-

Table 10
Optical band gaps, electrochemical properties and photovoltaic efficiency of **77**–**80**.

Polymers	E_g^{opt} (eV)	E_{red} (V)/LUMO (eV)	E_{ox} (V)/HOMO (eV)	PCE (%)
77	1.01	–/3.59	–/4.71	0.11
78	1.38	–1.52/–	0.01/–	0.72
79	1.28	–1.18/–	0.15/–	0.24
80	1.64	–/3.60	–/5.20	1.92

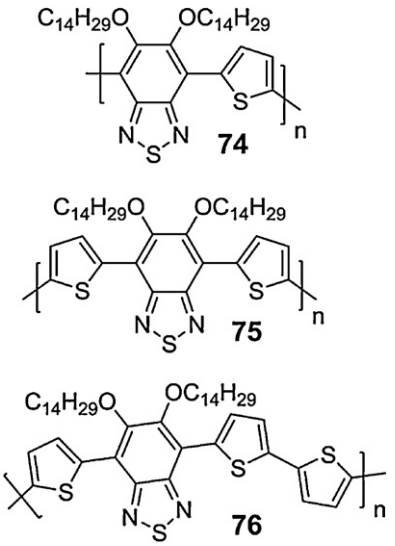

Chart 21. Chemical structures of the alkoxy-substituted 2,1,3-benzothiadiazole-based oligothiophene copolymers **74**–**76**.

teristics of the best cell are J_{sc} = 5.18 mA/cm^2, V_{oc} = 0.93 V and FF = 0.46. As reported, the possible reason for the lower PCE of **75** compared to **74** and **76** is the different polymerization procedure followed (Yamamoto instead of Stille coupling) where excess of nickel(0) was used instead of palladium [122].

3.2.7.10. Other polythiophene derivatives with various electron-deficient groups. As also mentioned above, the most common D–A polythiophene derivatives consisting of 2,1,3-benzothiadiazole (unsubstituted or alkoxy functionalized) as the electron deficient units. However, other electron-withdrawing groups have been also incorporated into a polythiophene matrix and these are thieno[3,4-*c*][1,2,5]thiadiazole (**77**) [123], pyrazino[2,3-*g*]quinoxaline (**78**, **79**) [124] and *N*-(dodecyl)-phthalimide (**80**) [125] (Chart 22). These polymers have been synthesized using either the Stille cross-coupling (**77**, **80**) or Yamamoto cross-coupling (**78**, **79**) polymerization reactions.

The optical band gap of the polymers follows the order **80** > **78** > **79** > **77** according to the values shown in Table 10. The fact that the band gap of **78** is higher than **79** indicates the influence of the substituents on the optical properties, similar with previous examples reported previously. The alkyl chains reduce the electron deficiency of the pyrazino[2,3-*g*]quinoxaline resulting to a larger band gap for **78** [124]. It should be noted that aggregate formation, even in solution, is detected for **78** due to the linear octyl side chains that were introduced in order to enhance the

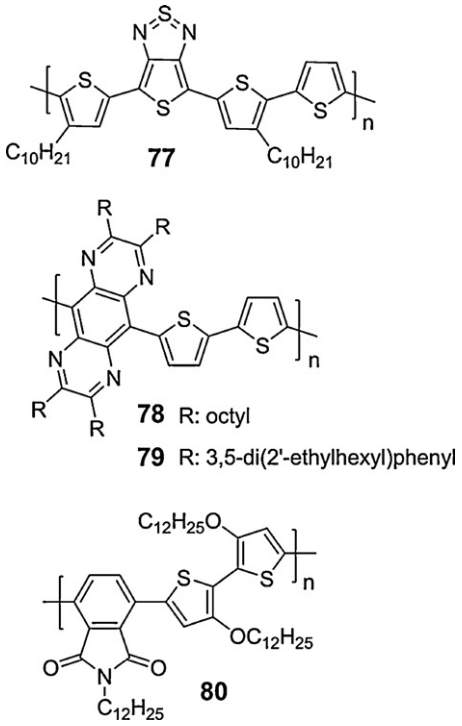

Chart 22. Chemical structures of the polythiophene derivatives **77**–**80** consisting of various electron-withdrawing moieties.

aggregate formation through the closer packing of the polymer chains. Furthermore, **78** exhibits a red shift of the absorption maxima passing from solution to the solid state while **79** absorption shows a blue shift probably due to the presence of the bulky substituents that prevent the formation of a planar structure and inhibit the aggregation of polymer chains that usually causes the bathochromic shift in a conjugated polymer film.

Concerning the energy levels of the polymers, it is observed that **77** and **80** have similar electron affinities. However, the HOMO level of **77** is significantly up-shifted as compared to **80**. This result indicates that the presence of the thiophene ring of thieno[3,4-*c*][1,2,5]thiadiazole in **77**, which is more electron rich than the phenyl ring of the phthalimide, has stronger effect on HOMO level than the dodecyloxy side chains in the bithiophene unit of **80**, which also elevate the HOMO level through their strong electron donating effect. Moreover, comparing the effect of the substituents on the energy levels of **78** and **79** it is observed that the electron affinity of **78** is lower than **79** because the existence of the linear octyl side chains reduces the electron deficiency of the pyrazino[2,3-*g*]quinoxaline via an inductive effect. This effect can be explained if you take

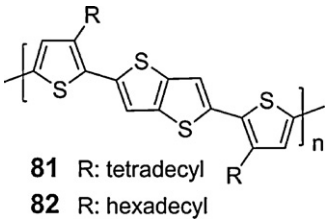

Chart 23. Chemical structures of the polythiophene derivatives **81**–**82** consisting of thieno[3,2-*b*]thiophene unit.

into consideration that the sterically less demanding octyl chains facilitate to the more planar conformation of the polymer chain [124].

BHJ solar cells based on blends consisting of **77**–**80** with fullerene derivatives were fabricated and investigated. The most promising PCE of 1.92% originates from **80** in combination with $PC_{71}BM$ (1:1, w/w) with $J_{sc} = 6.15\,mA/cm^2$, $V_{oc} = 0.56\,V$ and FF = 0.55 [125]. One of the reasons of the higher PCE of **80** as compared with **77**–**79** is the crystalline nanoscale morphology of **80**:$PC_{71}BM$ with the appearance of a hole mobility as high as $4.0 \times 10^{-4}\,cm^2/V\,s$, as measured by the SCLC method. Attempts to improve the PCE of **80**:$PC_{71}BM$ with thermal treatment were not successful due to the severe phase separation of the films [125]. The limited PCEs of **78**, **79** are caused due to low current densities, a consequence of the reduced electron transfer to the fullerene which can be attributed to their very high electron affinity values [124]. On the other hand, the limiting factor preventing **77** for higher PCE is the low V_{oc} (0.35 V) due to raised HOMO level [123].

3.2.8. Thieno[3,2-b]thiophene-based polymers

3.2.8.1. Polythiophene derivatives with thieno[3,2-b]thiophene. Poly(2,5-bis(3-alkylthiophen-2-yl)thieno[3,2-*b*]thiophene) derivatives (**81**, **82**; Chart 23) are very promising electron donor materials for BHJ solar cells due to their high reported hole mobility, $0.6\,cm^2/V\,s$ in FETs [126] as a result of their ability of forming large crystals. The formation of large crystals is attributed to the incorporation of the thieno[3,2-*b*]thiophene fused ring into the polythiophene backbone which enhance the crystallization [127]. Extensive studies in blends of **82** with $PC_{71}BM$ and bisadduct $bisPC_{71}BM$ demonstrate that the intercalation of the fullerene derivatives between the side chains of **82** can be controlled by adjusting the fullerene size [128]. By specular X-ray diffraction it was shown that the addition of the $PC_{71}BM$ leads to the intercalation of **82**, while by the addition of $bisPC_{71}BM$, **82** shows no intercalation. The maximum PCE of the intercalated **82**:$PC_{71}BM$ (1:4, w/w) is 2.51% with $J_{sc} = 7.99\,mA/cm^2$, $V_{oc} = 0.57\,V$ and FF = 0.55 [128]. The observation of the optimum performance at 1:4 (w/w) ratio is in agreement with the intercalated blends of the MDMO-PPV:$PC_{61}BM$ (maximum PCE at 1:4, w/w) [52]. On the contrary, the nonintercalated **82**:$bisPC_{71}BM$ outperforms at 1:1 (w/w) ratio with maximum PCE of 1.94% and $J_{sc} = 5.35\,mA/cm^2$, $V_{oc} = 0.65\,V$ and FF = 0.56.

However, the high bandgap (~2.0 eV) with HOMO and LUMO levels at 5.1 eV and 3.1 eV, respectively and a hole mobility of $3.8 \times 10^{-4}\,cm^2/V\,s$ in **81**:$PC_{71}BM$ [129], as measured by the SCLC method are the major drawbacks preventing higher efficiencies. The recorded hole mobility of **81** in the blend is one order of magnitude less than the typical reported out-of-plane mobility of $PC_{61}BM$ [129].

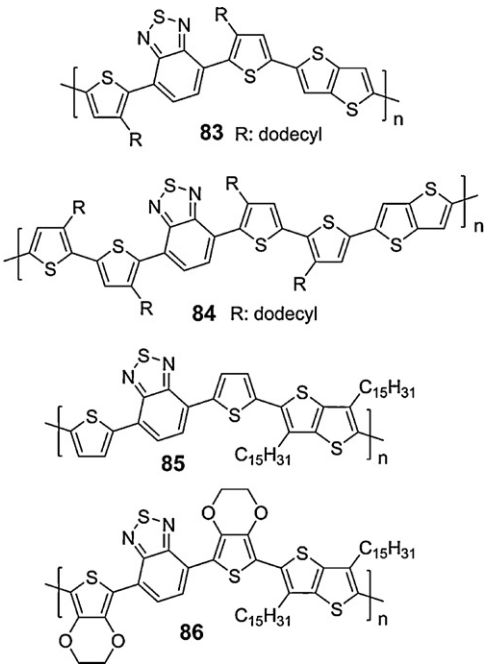

Chart 24. Chemical structures of polythiophene derivatives **83**–**86** consisting of both thieno[3,2-*b*]thiophene and 2,1,3-benzothiadiazole units.

3.2.8.2. Oligothiophene copolymers with both thieno[3,2-b]thiophene and 2,1,3-benzothiadiazole. Attempts to obtain thieno[3,2-*b*]thiophene-based polymers with lower band gaps than **81**, **82** led to the synthesis of **83**–**86** (Chart 24) by Stille cross-coupling polymerization [130–132]. The incorporation of the electron-deficient 2,1,3-benzothiadiazole in the polymer backbone proved to be an efficient approach for lowering the band gap. Other structural modifications, including the increase of the conjugation length by the introduction of two more thiophene rings in the polymer backbone (**84**) [131] or changing the positioning of the alkyl side chains from the thiophene rings to the thieno[3,2-*b*]thiophene unit (**85**) [132] or replacing the thiophene rings with 3,4-ethylenedioxythiophene (EDOT) units (**86**) [132], were also explored with respect on the modification of the band gap and energy levels.

The optical band gaps, the energy levels and the PCE of the synthesized copolymers are included in Table 11. The optical band gap of **83**, consisting of a TBzT segment with dodecyl side chains at the 3-positions of the thiophene rings alternate with thieno[3,2-*b*]thiophene unit, is 1.88 eV. Further lowering of the band gap at 1.80 eV is achieved by the addition of two more 3-dodecylthiophene rings around the 2,1,3-benzothiadiazole in **84** [130,131]. However, the lowering of the band gap is not accompanied by the lowering of the electrochemical band gap (Table 11). Instead an increase of the electrochemical band gap is observed

Table 11
Optical band gaps, energy levels and photovoltaic efficiency of **83**–**86**.

Polymers	E_g^{opt} (eV)	LUMO (eV)	HOMO (eV)	PCE (%)
83	1.88	3.18	5.34	1.00
84	1.80	3.16	5.43	1.80
85	1.62	3.66	5.17	1.72
86	1.48	3.48	5.00	0.045

by the additional lowering of the HOMO level of **84**. On the other hand, the LUMO levels of **83** and **84** are almost similar (Table 11) showing that the LUMO level is localized on the 2,1,3-benzothiadiazole. Usually, the HOMO level is raised upon increasing the number of the unsubstituted electron rich compounds, for example thiophene rings, in the polymer backbone (Fig. 4). However, the presence of two more dodecyl side chains at the 3-position of the thiophene rings in **84**, enhance the steric hindrance through the twisting of the bonds between the adjacent units, disrupting the effective conjugation length, and as a consequence the HOMO level is further lowering instead of raising.

Moreover, changing the position of the alkyl side chains from the thiophene rings of the TBzT segment in **83** to the thieno[3,2-*b*]thiophene unit in **85**, the band gap of **85** significantly lowers by 0.26 eV (Table 11). It seems that stronger π–π stacking between the polymer chains of **85** is obtained when the alkyl side chains are attached on the thieno[3,2-*b*]thiophene unit. Based on this result, it can be concluded that the positioning of the dodecyl side chains at the 3-position on the TBzT segment of **83** is causing severe steric hindrance between the thiophene rings and the 2,1,3-benzothiadiazole. This prevents **83** for providing lower band gap. Regarding the influence of the different positioning of the alkyl side chains on the energy levels of **83** and **85**, the HOMO level of **85** is elevated by 0.17 eV, whereas the LUMO level significantly lowers by 0.48 eV. Finally, replacing the thiophene rings of **85** with the more electron rich EDOT units, the optical band gap of **86** is 1.48 eV, slightly lower than that of **85**, whereas both the energy levels of **86** are upshifted by ~0.17 eV.

BHJ solar cells based on blends of **83**–**86** with fullerene derivatives were prepared and PCE of 1.80% was obtained from **84**:$PC_{71}BM$ in 1:4 (w/w) ratio with J_{sc} = 8.5 mA/cm^2, V_{oc} = 0.54 V and FF = 0.39 upon annealing at 150 °C for 30 min [131]. In addition, the PCE of **84**:$PC_{61}BM$ in 1:4 (w/w) ratio is 1.1% with J_{sc} = 4.0 mA/cm^2, V_{oc} = 0.79 V and FF = 0.34 upon annealing at 110 °C for 15 min. By replacing the $PC_{61}BM$ with $PC_{71}BM$ the current density of the **84**:$PC_{71}BM$ system is more than doubled in the optimized devices. This increase in J_{sc} reflects the improved photon harvesting ability of the active layer. On the other hand, the V_{oc} in **84**:$PC_{71}BM$ devices is lower than that of **84**:$PC_{61}BM$ devices (0.54 V compared to 0.79 V) [131]. The origin of this drop in V_{oc} is rather unclear and is in contrast with what is generally observed in other polymer systems that will be presented next in the text. Finally, comparing the photovoltaic parameters of the optimized **85**:$PC_{71}BM$ system in 1:3 (w/w) ratio (J_{sc} = 6.86 mA/cm^2, V_{oc} = 0.67 V and FF = 0.37) [132] with those of **84**:$PC_{71}BM$, it is obvious that the V_{oc} of **85** is higher than that of **84** despite the elevated HOMO level. On the contrary, the J_{sc} of **84** is higher than that of **85** despite its higher optical band gap.

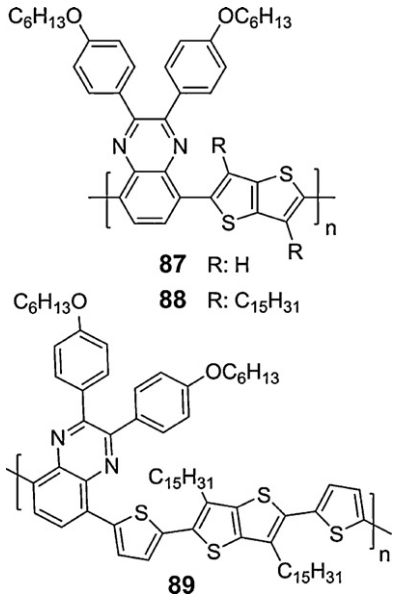

Chart 25. Chemical structures of the polythiophene derivatives **87**–**89** consisting of both thieno[3,2-*b*]thiophene and quinoxaline units.

3.2.8.3. Oligothiophene copolymers with both thieno[3,2-b]thiophene and quinoxaline. Three new D–A conjugated polymers consisting of unsubstituted (**87**) or substituted with dipentadecyl side chains thieno[3,2-*b*]thiophene (**88**, **89**) as the donor and quinoxaline as the acceptor have been synthesized by the Stille cross-coupling polymerization reaction (Chart 25) [133].

The optical band gaps of the polymers **87**–**89** are shown in Table 12. The large difference on the optical band gaps between **87** and **88** is attributed to the increased steric effects that thieno[3,2-*b*]thiophene is affecting when it is substituted with long alkyl side chains. Moreover, comparing the HOMO and LUMO energy levels of **87** and **88**, the steric effect that alkyl chains are producing, significantly influence the HOMO levels while the LUMO levels remain unaltered (~0.1 eV difference). In addition, the insertion of the two thiophene rings between the quinoxaline and the substituted thieno[3,2-*b*]thiophene influence more the HOMO level. The presence of two electron-rich units in the polymer chain elevates the HOMO level by 0.48 eV. On the contrary, the LUMO level is less affected and is lowered by 0.15 eV.

The photovoltaic performance of the polymers was examined in blends with $PC_{61}BM$ or $PC_{71}BM$. The highest

Table 12
Optical band gaps and energy levels of **87**–**89**.

Polymers	E_g^{opt} (eV)	LUMO (eV)	HOMO (eV)
87	1.65	3.61	4.96
88	2.30	3.53	5.60
89	1.70	3.68	5.12

PCE of 2.27% was recorded for **89**:$PC_{71}BM$ in 1:3 (w/w) ratio (J_{sc} = 8.8 mA/cm^2, V_{oc} = 0.71 V and FF = 0.36). In addition, **87** and **88** in blends with $PC_{71}BM$ (1:3, w/w) exhibited PCEs of 1.39% and 0.30%, respectively [133]. The limiting factor preventing the polymer:fullerene systems for achieving higher PCE is the FF that most likely is attributed to the poor morphology (incomplete channels between polymers and fullerene derivatives) as the AFM images revealed. Finally, it is rather unexpected the very low V_{oc} of **88** (0.36–0.37 V) despite the higher HOMO level between all the polymers.

3.2.9. Thieno[3,4-b]thiophene-based polymers

Other examples of fused thiophene-based polymers are those consisting of the thieno[3,4-*b*]thiophene unit, which vary from the thieno[3,2-*b*]thiophene analogue regarding the location of the sulphur atom in the peripheral thiophene. The UV–vis absorption spectrum of thieno[3,4-*b*]thiophene unit is red shifted compared to the thieno[3,2-*b*]thiophene [134] and the poly(thieno[3,4-*b*]thiophene) has a very low band gap of 0.84 eV. This is due to the fact that thieno[3,4-*b*]thiophene is capable of stabilizing the quinoid form of the main chain [135].

Very recently, a soluble copolymer **90**, consisting of an alternating ester-substituted thieno[3,4-*b*]thiophene and a thiophene, was synthesized by Stille cross coupling polymerization reaction [136] (Chart 26) and exhibited high external quantum efficiency in the near-IR region. However, a PCE below 1% was obtained probably due to the unfavourable position of the energy levels [136]. Thus a series of regio random copolymers based on the same ester-substituted thieno[3,4-*b*]thiophene, but with dodecyl side chain, and thiophene units (**91**) [137] were synthesized in an attempt to control the band gap of the polymers and as a consequence the energy levels (Chart 26). It is shown that by increasing the content of the 3-hexylthiophene unit the band gap is increasing and the hole mobility is decreasing. This observation was attributed to the irregular insertion of the 3-hexylthiophene unit in the polymer backbone that is causing the twisting of the main chain [137]. The optimum ratio between the thieno[3,4-*b*]thiophene and 3-hexylthiophene is 1:3.7 leading to a band gap of 1.45 eV and more suitable energy levels relative to $PC_{61}BM$. The PCE of the optimum copolymer:$PC_{61}BM$ (1:1, w/w) is 1.93%.

Furthermore, **92** was synthesized in order to examine the influence of the regioregularity of the oligothiophene units on the properties of the thieno[3,4-*b*]thiophene-based copolymers (Chart 26). In this case, a perfluorohexyl-substituted thieno[3,4-*b*]thiophene was used instead of the ester analogue. The reason is that the proton at the 4-position of the alkylthiophene which is next to the thieno[3,4-*b*]thiophene is more prone to bromination, preventing the synthesis of the desired polymer [138]. **92** exhibits an optical band gap of 1.62 eV and a HOMO level

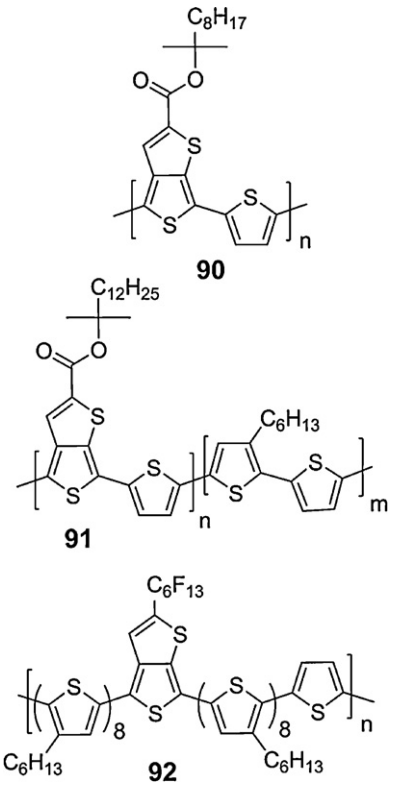

Chart 26. Chemical structures of the thieno[3,4-*b*]thiophene-based polythiophene derivatives **90**–**92**.

of 4.92 eV. The introduction of regioregularity between the alkyl thiophene units results with higher hole mobility (1.9×10^{-4} cm^2/V s by the SCLC method) as compared to the optimum **91** (4.8×10^{-5} cm^2/V s). The enhanced hole mobility of **92** improved also the PCE of **92**:$PC_{61}BM$ (1:1, w/w) blend to 2.38% with J_{sc} = 10.22 mA/cm^2, V_{oc} = 0.59 V and FF = 0.40 [138]. The thin film morphology of the system revealed the formation of nanofibers with diameter ranging from 15 to 20 nm.

3.2.10. Isothianaphthene-based polymers

One of the first LBG conjugated polymer synthesized is poly(isothianaphthene) [139]. This polymer exhibits a very low optical band gap of 1.1 eV and thus an absorption spectrum extending until the near-infrared. The lowering of the band gap is attributed to the increased quinoidal structure of the polymer backbone. However, poly(isothianaphthene) is not soluble in organic solvents and thus not processable. Introduction of dithioctyl side chains on poly(isothianaphthene) provided **93** [140] (Chart 27) which is more soluble compared to poly(isothianaphthene) but its molecular weight (7000 g/mol) is still low. Accordingly, the PCE of **93** in blends with $PC_{61}BM$ was extremely poor (0.008%) with solar cell characteristics of J_{sc} = 45 μA/cm^2, V_{oc} = 550 mV and FF = 0.30 [141]. In another example, a poly(bisthienylene dithiooctyl isothianaphthene) **94** (Chart 27) was synthesized by oxidative polymerization with $FeCl_3$ [142] and the molecular weight (M_w) obtained

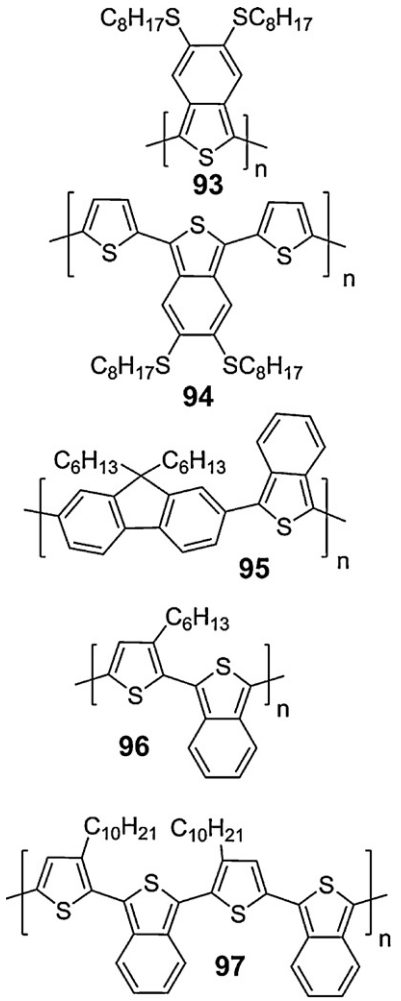

Chart 27. Chemical structures of the isothianaphthene-based conjugated polymers **93**–**97**.

is 10,000 g/mol. The optical band gap is 1.4 eV and the PCE of **94** in blends with $PC_{61}BM$ is 0.4% with J_{sc} = 2.4 mA/cm^2, V_{oc} = 0.37 V and FF = 0.28 [143]. The low molecular weight significantly limited the film-forming ability of **94** and thus the PCE of the solar cells. As a matter of fact, poly(methyl methacrylate) had to be employed as a host matrix material for casting thin films of **94**.

In another example, three isothianaphthene-containing copolymers **95**–**97** (Chart 27), the properties of which, such as solubility, band gap and HOMO/LUMO levels, can be fine-tuned through the careful selection of proper co-monomers, were synthesized and their photovoltaic performances in blends with $PC_{61}BM$ were examined [144]. A new distannylated isothianaphthene monomer is served as a versatile building block for the synthesis of **95**–**97** by Stille cross-coupling reactions. The molecular weights (M_n) of **95**–**97** were in the range of 3600 and 11,000 g/mol, while their optical band gaps and energy levels are presented in Table 13. The band gaps of the polymers are depending on the chemical nature of the different co-monomers (fluorene and thiophene structures) used, but surprisingly the band gaps of **96** and **97** are the same. This points out

Table 13
Optical band gaps and energy levels of **95**–**97**.

Polymers	E_g^{opt} (eV)	LUMO (eV)	HOMO (eV)
95	2.34	2.70	5.26
96	1.66	3.56	5.22
97	1.66	3.41	5.07

that the relative position of the alkyl chains attached on the thiophene rings has no impact on the optical band gap but significantly influences the energy levels of the polymers. The HOMO levels of the thiophene derivatives (5.07 and 5.22 eV) are elevated compared to that of the fluorene derivative (5.26 eV), due to the stronger electron rich thiophene ring, while the LUMO levels are situated between 2.70 and 3.56 eV. As reported above, the relative position of the second alkyl chain for the copolymers **96** and **97** influence both the HOMO and the LUMO levels (Table 13). When the second alkyl chain of copolymer **97** is introduced on the left side of the thiophene, close to the first alkyl side chain, both HOMO and LUMO levels are upshifted by exactly 0.15 eV as compared to copolymer **96**. The PCEs of **95**–**97** in blends with $PC_{61}BM$ in 1:4 (w/w) ratio are ranged between 0.12% and 0.43%. Despite the lower molecular weight and the higher optical band gap, **95** exhibits the higher PCE with J_{sc} = 1.37 mA/cm^2, V_{oc} = 0.63 V and FF = 0.50 [144].

3.2.11. Bridged bithiophenes with 5-member fused aromatic rings in the central core

3.2.11.1. Cyclopenta[2,1-b:3,4-b′]dithiophene-based polymers. One of the most well studied heteroaromatic electron-rich unit which serves as efficient electron donor building block in LBG polymers is cyclopenta[2,1-*b*:3,4-*b*′]dithiophene (CPDT), where a 2,2′-bithiophene is covalently bridged and rigidified at the 3,3′-position by a carbon atom. Because of the fully coplanar structure, the intrinsic properties based on bithiophene can be altered, leading to more extended conjugation, lower band gaps and stronger intermolecular interactions [145]. CPDT has been copolymerized with either electron-rich or electron-withdrawing groups in order to obtain LBG polymers.

3.2.11.1.1. Poly(cyclopenta[2,1-b:3,4-b′]dithiophene) derivatives with electron-rich units. CPDT homopolymers have been synthesized by Suzuki or nickel-catalyzed Yamamoto cross-coupling polymerization [145,146], and their absorption maxima are extended to longer wavelengths compared to that of the rrP3HT by exhibiting an optical band gap of ~1.8 eV. However, despite the lower band gap achieved compared to that of rrP3HT, the photovoltaic performance of the CPDT homopolymers is very poor. For example, the PCE of **98**:$PC_{61}BM$ in 1:2 (w/w) ratio is 0.016% [146]. In order to improve the PCE of the CPDT-based polymers, the synthesis of CPDT copolymers incorporating electron-rich units like carbazole (**99**) [146], bithiophenes (**100**) [147] and biselenophenes (**101**–**103**) [147] (Chart 28) was achieved. The percentage of the carbazole unit incorporated in **99** does not alter significantly the optical band gap (1.83 eV) and the energy levels (HOMO at 4.98 eV and LUMO at 2.48 eV) as compared to **98** (band gap of 1.82 eV and HOMO at 4.92 eV and LUMO

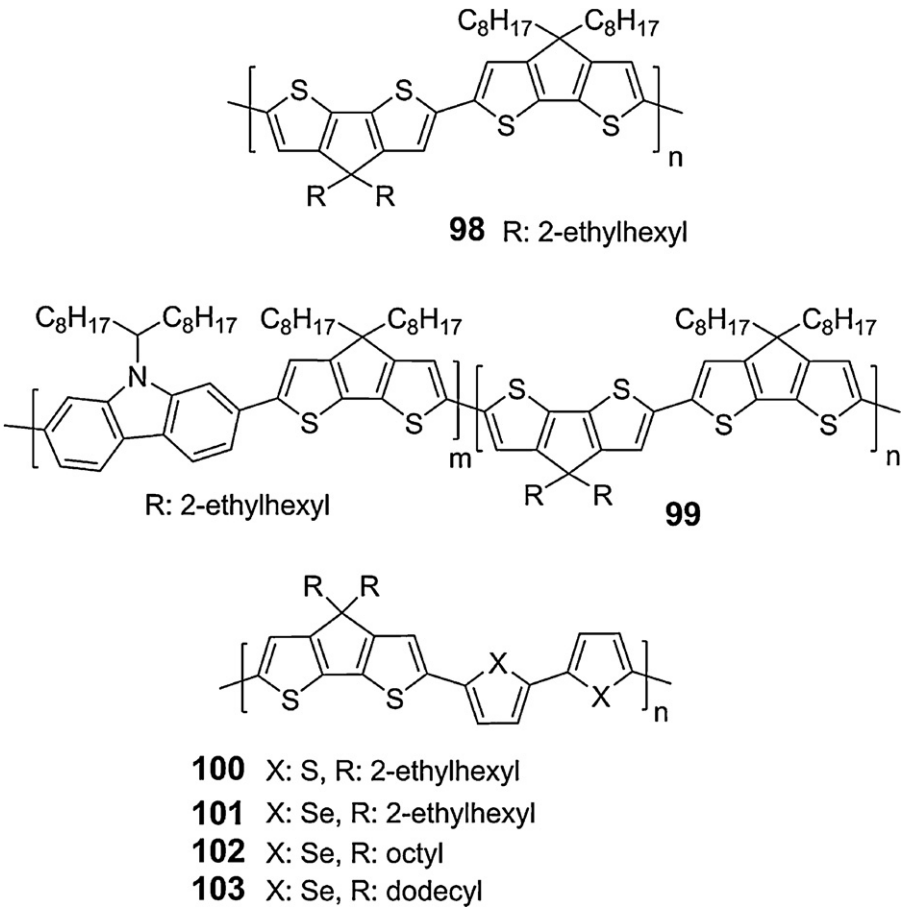

Chart 28. Chemical structures of the poly(cyclopenta[2,1-*b*:3,4-*b*′]dithiophene) derivatives **98**–**103** consisting of electron-rich moieties.

at 2.49 eV). Hence, the PCE of **99**:$PC_{61}BM$ in 1:4 (w/w) (0.013%) is similar to **98** [146].

100 and **101**–**103** were synthesized by Stille cross-coupling polymerization reaction and their optical band gaps and energy levels are summarized in Table 14. The band gap of the CPDT-based copolymer incorporating the bithiophene unit (**100**) is 1.88 eV, whereas lower band gaps of 1.71–1.77 eV were revealed for the related biselenophene derivatives (**101**–**103**). In detail, a decrease of 0.1 eV is observed comparing the band gaps of **100** and **101**, which is explained by the higher π-electron delocalization and bandwidth of selenophene unit than that of thiophene [147]. Examining, the band gaps of the selenophene-based CPDT copolymers (**101**–**103**), it is shown that the linear alkyl side chain derivatives (**102**, **103**) have lower band gaps than that of **101** due to the improved packing of the polymer chains.

By replacing the bithiophene unit in **100** with the biselenophene (**101**), the influence on the energy levels is presented in Table 14, where the HOMO of **101** is slightly raised and the LUMO is lowered by 0.1 eV. The change of the type of the side alkyl chains between **101** and **102**, influence only the LUMO (**102** with the linear alkyl chain has lower LUMO than **101**), whereas the HOMO remains constant (Table 14). The photovoltaic performance of copolymers **100**–**103** has been examined in blends with $PC_{71}BM$ [147]. The PCE of the copolymer with the bithiophene unit (**100**) is higher than those consisting of the selenophene unit (**101–103**). In addition, the PCE of the selenophene derivatives with the different type of side alkyl chains is higher for the copolymer with the branched alkyl side chain (**101**). For **102** and **103**, as the length increases, the PCE is decreasing (Table 14). The copolymers show moderate hole mobilities in the range of 10^{-3} to 10^{-4} $cm^2/V\,s$ in FET measurements, with **100** exhibiting the highest (1.9×10^{-3} $cm^2/V\,s$). For the selenophene-based CPDT derivatives, **102** consisting of the octyl side chain exhibits the highest hole mobility (1.3×10^{-3} $cm^2/V\,s$) due to the improved packing of the polymer chains and this value is comparable to the corresponding bithiophene-based **100**.

Furthermore, three new CPDT-based copolymers (**104**–**106**) were synthesized by Suzuki cross-coupling polymerization (Chart 29), consisting of two modified bithiophene units with one of them planarized by bridging intrinsically different π system to bithiophene moiety like benzo (**104**), naphtha (**105**) or quinoxalino (**106**) segments, respectively [148].

The energy levels and the optical band gaps are included in Table 14. The band gap of **104** is 2.00 eV while lower band gaps are presented for **105** (1.91 eV) and **106** (1.94 eV).

Table 14
Optical band gaps, energy levels and photovoltaic efficiency of **100**–**106**.

Polymers	E_g^{opt} (eV)	LUMO (eV)	HOMO (eV)	PCE (%)
100	1.88	2.89	5.38	2.22
101	1.77	2.99	5.31	1.86
102	1.71	3.03	5.30	1.50
103	1.72	3.04	5.31	0.70
104	2.00	2.83	5.04	0.38
105	1.91	2.94	5.04	0.55
106	1.94	3.05	5.15	1.14

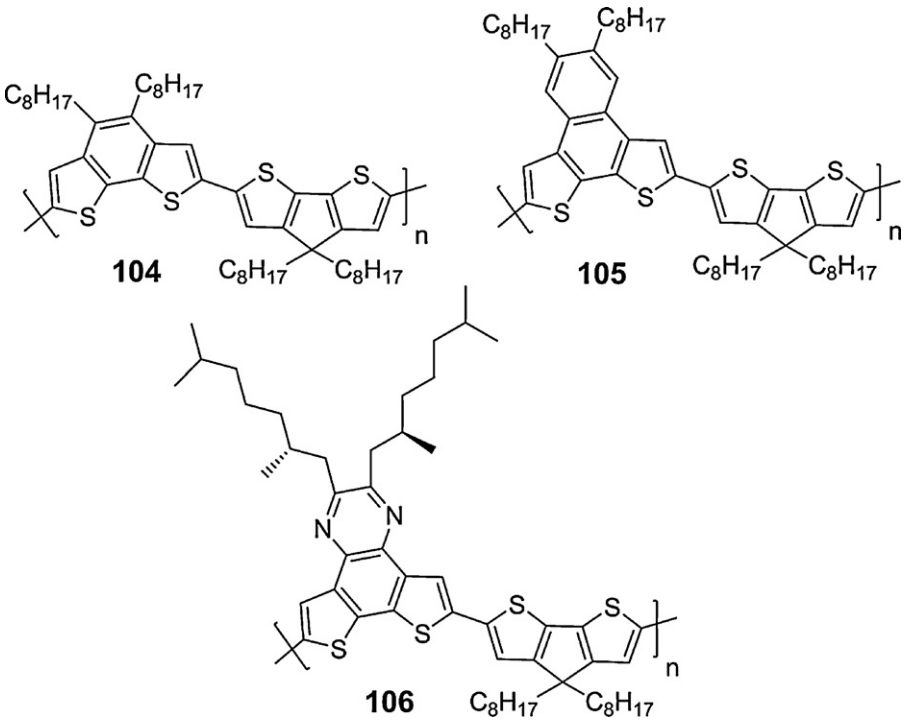

Chart 29. Chemical structures of the poly(cyclopenta[2,1-*b*:3,4-*b*′]dithiophene) derivatives **104**–**106** consisting of various electron-rich moieties.

Such a decrease in the band gap can be explained due to the stronger π–π stacking interactions of the naphthalene and quinoxaline units as compared to the benzene ring when incorporated into the bithiophene unit. However, the band gaps of **104**–**106** are higher than those of **100**–**103** indicating that the packing of the polymer chains is more effective in the unbridged and less rigidified bithiophene and selenophene based CPDT copolymers. Furthermore, by passing from the phenyl ring of **104** to the naphthalene in **105**, the HOMO levels remain unchanged while the LUMO is lowering by ~0.1 eV (Table 14). On the contrary, both HOMO and LUMO are lowering by 0.11 eV, when the naphthalene unit of **105** is replaced by the quinoxaline in **106**. The hole mobilities of **104**–**106** are relative low with the maximum reach 5.15×10^{-5} $cm^2/V\,s$ (for **106**) in FETs measurements. The recorded hole mobilities of **104–106** is one and two order of magnitude lower than those of **100**–**103**, supporting the less effective packing of **104**–**106** chains [148]. For these reasons, polymers **104**–**106** exhibit moderate PCEs with the maximum of 1.14% for the **106**:$PC_{61}BM$ in 1:1.6 (w/w) ratio with J_{sc} = 4.56 mA/cm^2, V_{oc} = 0.53 V and FF = 0.47.

3.2.11.1.2. Poly(cyclopenta[2,1-b:3,4-b′]dithiophene) derivatives with electron-deficient units. The alternating copolymer **107**, consisting of CPDT with 2-ethylhexyl side chains and 2,1,3-benzothiadiazole has been proven to be one of the most efficient LBG electron donor polymer with PCE of 5.5% [149–156]. **107** has been synthesized by Stille or Suzuki cross-coupling polymerization [149,152–155]. Improvement in the synthetic procedure has been presented by Bazan et al. very recently [156] with the use of microwave-assisted Stille cross-coupling polymerization in combination with the screening of comonomer reactant ratios affording high molecular weight polymers and in high yields. The high PCE of **107** has stimulated extensive research efforts towards related structural polymers like **108**–**116** which are shown in Chart 30, and have been synthesized by Suzuki and Stille cross-coupling polymerizations [152–155].

The optical band gaps, the electrochemical properties and the PCE of the polymers are presented in Table 15. For the majority of the polymers, the oxidation and reduction potentials presented in Table 15 were estimated in ODCB solution rather as thin films. Nevertheless, a general con-

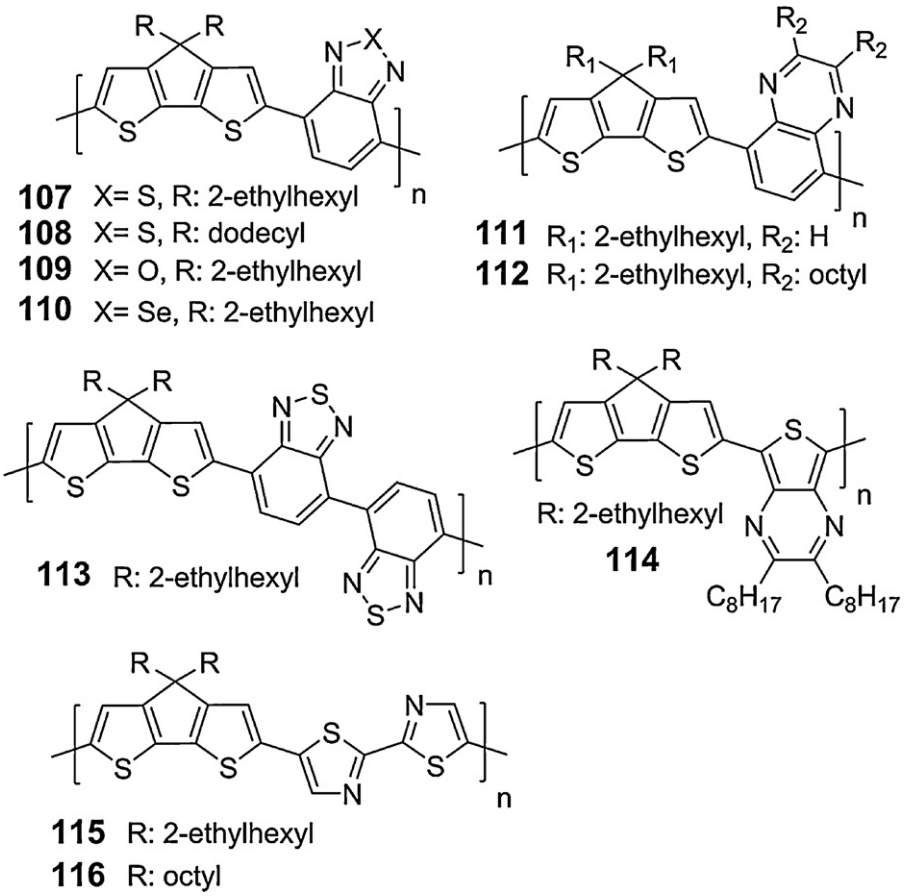

Chart 30. Chemical structures of the poly(cyclopenta[2,1-*b*:3,4-*b*′]dithiophene) derivatives **107**–**116** consisting of different electron-deficient units.

Table 15
Optical band gaps, electrochemical properties and photovoltaic efficiency of **107**–**116**.

Polymers	E_{red} (V)/LUMO (eV)	E_{ox} (V)/HOMO (eV)	E_g^{opt} (eV)	PCE (%)
107	−1.67/3.55	−0.07/5.30	1.40	3.6[a]/5.5[b]
108	–/3.50	–/5.12	1.25	2.70
109	−1.52/–	+0.16/–	1.47	2.50
110	–/3.34	–/5.10	1.35	0.89
111	−1.80/–	−0.06/–	1.54	1.10
112	–	–	–	0.74
113	−1.60/–	+0.22/–	1.53	2.00
114	−1.73/–	−0.39/–	1.18	0.10
115	–/3.44	–/5.20	1.89	1.12
116	–/3.43	–/5.24	1.86	0.59

[a] Without.
[b] With the use of 1,8-diiodooctane as surfactant.

clusion is that the selection of the electron-withdrawing unit can have an equally large effect both on the HOMO and the LUMO level of the polymers as derived from the study of the electrochemical properties of **107**–**116**. Regarding the optical band gap of the polymers, it is shown that the bithiazole based CPDT copolymers (**115** and **116**) [155] exhibit the highest band gap among all the copolymers, while quinoxaline (**111** and **112**) [152] and bis(benzothiadiazole) (**113**) [152]-based CPDT copolymers have slightly higher band gaps than the thieno[3,4-*b*]pyrazine (TP) (**114**) [152], 2,1,3-benzooxadiazole (**109**) [152], 2,1,3-benzoselenadiazole (**110**) [153,154] and 2,1,3-benzothiadiazole (**107** and **108**) [149,152,153,156]-based CPDT copolymers. The influence of the type of the alkyl side chains (linear versus branched) on the band gap is clearly observed comparing **107**, **108** and **115**, **116**. The band gaps of **107** and **115**, with the branched alkyl side chains, are 1.40 eV and 1.89 eV, respectively. However, by replacing the branched alkyl side chains of **107** and **115** with the linear dodecyl side chains in **108** or with the linear octyl side chains in **116**, a significant reduction of 0.15 eV in the band gap of **107** and **108** and a less significant reduction of

0.03 eV for **115** and **116**, is presented (Table 15). Two of the reasons for the significant red shift is (i) the increased order of **108** as compared to **107**, with the close π–π stacking distance as TEM and selected area electron diffraction (SAED) images are demonstrating, and (ii) the higher molecular weight of **108** (the M_n of **108** is 44,000 g/mol and **107** is 35,000 g/mol). Furthermore, the fact that the band gap of **113** with the bis(benzothiadiazole) unit is higher than that of **107**, which has a single benzothiadiazole, is attributed to unfavourable steric interactions between the neighboring benzothiadiazole units in the bis(benzothiadiazole) that lead to twisting around their interring bonds, causing reduced conjugation [152].

Initially, the PCE of **107** in blends with $PC_{71}BM$ (1:3.3, w/w) was 3.2% with J_{sc} = 11 mA/cm^2, V_{oc} = 0.70 V and FF = 0.47 [150]. Despite the high hole mobility (1×10^{-3} cm^2/V s) of **107** in FETs measurements [149], the inefficient nanomorphology of the bulk composite with a non-optimized phase structure between the $PC_{61}BM$ or $PC_{71}BM$ and **107** limits the efficiency of the solar cell due to the low FF, short carrier lifetime and high rate of charge recombination [150]. Even though annealing was the suitable process to control the morphology in the rrP3HT:$PC_{61}BM$ solar cells, only slightly improvement (PCE of 3.6%) in the case of **107** was observed upon extensive studies of the thermal treatment on **107**:fullerenes blends [157]. A breakthrough was achieved by the use of small concentrations alkanedithiols in the solution from which the BHJ films are cast [151]. Thus, several 1,8-di(R)octanes with various functional groups (R) as processing additives have been investigated [158] and certified PCEs of 5.21% with maximum PCEs values of 5.5% were obtained when iodine was used as the R functional group without the use of any thermal treatment. It was shown that 1,8-diiodooctane is a selective solvent for the fullerene than the polymer, resulting in three separate phases in solution: (i) a fullerene-di(R)octane phase, (ii) a polymer aggregate phase, and (iii) a polymer–fullerene phase [158]. This effect dramatically increases the aggregation and order within the polymer domains while avoiding excessive crystallization of the fullerene in the solid state. In addition, a very important observation has been demonstrated recently by Janssen et al. It is suggested that the increase in the yield of photoinduced free carrier formation by the use of processing additive on the **107**:$PC_{61}BM$ system can be also attributed to the suppression of the photogenerated carriers recombination into the lowest triplet excited state of the polymer, parameter which enhanced the formation of free charge carriers out of the CT state [159].

Each of the other polymers also exhibit promising PCEs (above 2.00%), especially **109** with the benzooxadiazole and **113** with the bis(benzothiadiazole) in blends with $PC_{61}BM$ in 1:3 (w/w) ratio (Table 15). The V_{oc} of the devices with **109** and **113** is higher than that of **107** while the FF of the **109**:$PC_{61}BM$ device is particularly high (0.60), indicating that neither charge transport nor electron–hole pair lifetime seem to limit the performance [152]. The lower performance of the TP, 2,1,3-benzoselenadiazole, quinoxaline and bithiazole-based CPDT copolymers is attributed to a loss in J_{sc} (**111**), the low EQE (**114**), the weak absorbance and the unbalance hole and electron transporting properties of **110** and the very low hole mobility of 2.0×10^{-6} cm^2/V s for **115** and **116** in FET measurements.

Finally, a series of conjugated copolymers containing the coplanar CPDT unit [incorporated with arylcyanovinyl and keto groups in different molar ratios (**117**)] were synthesized (Chart 31) and employed in solar cells [160]. The optical band gap and HOMO and LUMO levels of **117** were varying depending on the molar ratio. For example, the optical band gaps were in the range of 1.38–1.70 eV, while the HOMO and LUMO levels at 4.90–5.25 eV and ~3.6 eV, respectively. In addition, by increasing the molar ratio of the cyclopentadithiophenone the HOMO level is expected to remain constant and the LUMO lowering. In contrast, the LUMO level remains almost constant and the HOMO level is elevated. Preliminary results on the photovoltaic properties of **117** in blends with $PC_{61}BM$ in 1:4 (w/w) ratio were recorded providing a V_{oc} of 0.84 V, a J_{sc} of 2.36 mA/cm^2, and a FF of 0.38, providing a PCE of 0.77% for the polymer derivative without the cyclopentadithiophenone unit [160].

3.2.11.1.3. Poly(cyclopenta[2,1-b:3,4-b′]dithiophene) derivatives with both electron-rich and electron-deficient units. As reported in the previous paragraph, the alternating copolymer **107** represents one of the most promising LBG polymer for use in OPVs due to its very high PCE,. Although such a structurally well-defined alternating D–A copolymer can effectively shift its absorption spectrum to longer wavelengths in the near-infrared region (ca. 600–800 nm), significantly decreases the localized π–π* transitions and weakens the absorption ability in the visible region from 450 to 600 nm. To address this issue, the alternating copolymers **118**, **119** consisting of the CPDT with either the TBzT segment (**118**) [161] or the thiophene-benzoselenadiazole-thiophene (TBseT) segment (**119**) [154] were synthesized by Stille cross-coupling polymerization reaction (Chart 32). Moreover, the random copolymers **120**–**123** [162] where the CPDT with either the 2,1,3-benzothiadiazole (**120**) or the quinoxaline (**121**) or the TQT segment (**122**) or the TP (**123**) are dispersed and separated by the unsubstituted thiophene spacers in the conjugated backbone, were also synthesized by Stille cross-coupling polymerization reaction (Chart 32).

The optical band gaps, the energy levels and the PCEs of the copolymers are presented in Table 16. Comparing the band gaps of the alternating copolymers with those of the random copolymers, it is shown that the alternating copolymers reveal lower band gaps, except from **123** that demonstrates the lowest band gap (1.20 eV) of all the polymers presented in this category. This is due to the fact that TP tend to favorably adopt the quinoid form through π-electron delocalization, because pyrazine has larger aromatic resonance energy than thiophene, in order to selectively preserve the pyrazine's aromaticity [162]. This in turn decreases the bond length alternation and greatly reduces the band gap. In addition, the insertion of a thiophene ring between the CPDT and 2,1,3-benzothiadiazole in **118** or CPDT and 2,1,3-benzoselenadiazole in **119** results with an increase in the band gap of 0.17 eV or 0.11 eV, respectively, as compared with the structural analogue polymers **107** and **110**. It seems that the two additional thiophene rings attached at the 2,1,3-benzothiadiazole or

Table 16
Optical band gaps, energy levels and photovoltaic efficiency of **118–123**.

Polymers	E_g^{opt} (eV)	LUMO (eV)	HOMO (eV)	PCE (%)
118	1.57	–	–	2.10
119	1.46	3.25	5.09	1.34
120	1.59	3.58	5.17	2.00
121	1.77	3.28	5.05	0.30
122	1.82	3.31	5.13	0.70
123	1.20	3.82	5.02	0.60

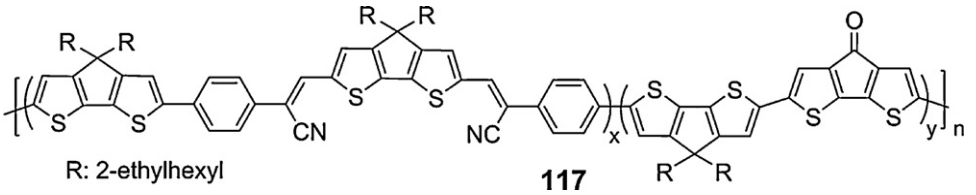

Chart 31. Chemical structures of the conjugated polymer **117**.

2,1,3-benzoselenadiazole can effectively reduce the degree of the ICT. Moreover, the alternating copolymer **118** and the similar random copolymer **120** present similar band gaps and PCEs in blends with fullerenes, showing that the different polymeric architecture does not influence drastically the optoelectronic properties of these polymers. Furthermore, by replacing the 2,1,3-benzothiadiazole unit in the random copolymer **120** with quinoxaline in **121**, the band gap is increased by 0.16 eV. Whereas, the two additional thiophene rings attached at the quinoxaline in **122** resulting to the further increase of the band gap as compared to **121**, similar with the case of **107** and **118**.

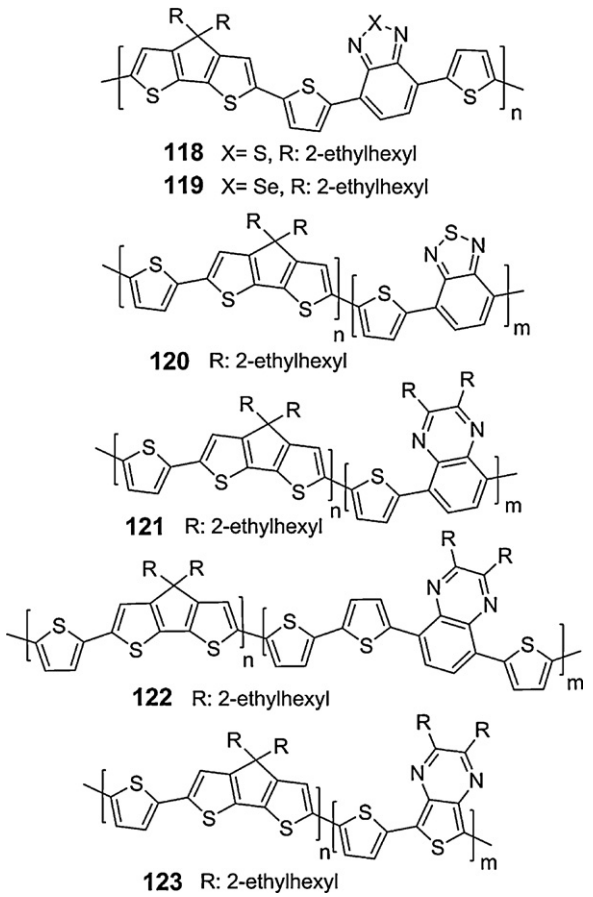

Chart 32. Chemical structures of the poly(cyclopenta[2,1-*b*:3,4-*b*′]dithiophene) derivatives **118–123** consisting of both electron-rich and deficient units.

The HOMO energy levels of the polymers are between 5.17 eV and 5.02 eV with small variation, showing that the HOMO level is more dependent on the electron-rich CPDT and thiophene units in the polymer backbone, while their LUMO levels are determined by the electron-deficient units. For example, the LUMO levels of the quinoxaline-based random copolymers are 3.28 eV (**121**) and 3.31 eV (**122**) and those of the 2,1,3-benzothiadiazole (**120**) and TP (**123**) are 3.58 eV and 3.82 eV, respectively. Finally, the 2,1,3-benzoselenadiazole-based alternate copolymer **119** exhibits the higher-lying LUMO level (3.25 eV).

The PCE of **118** in blends with 75 wt% $PC_{61}BM$ is 2.1%, which is lower than **107** and the very promising analogous polymers **171**, **198**, **248** and **259** as will be shown in the following. Two are the main factors limiting the performance of **118**, (i) the low hole mobility (2×10^{-4} $cm^2/V\,s$ in FETs) and (ii) the improper morphology of the blend. Studies on devices prepared from mixtures of **118** and $PC_{61}BM$ using many casting solvents showed a very large phase separation. The use of a 19:1 (v/v) mixture of CB and anisole exhibit the best performance. This has been achieved because the addition of anisole to the CB resulted in the formation of two distinct domains from the two components and also in the formation of an intermediate mixed concentration domain that had improved electrical properties leading to better FF and PCE [161]. On the other hand, the PCEs of the quinoxaline based copolymers **121** and **122** are lower as compared to the 2,1,3-benzothiadiazole counterparts due to the lower hole mobilities (9.5×10^{-5} $cm^2/V\,s$ for **121** and 1.8×10^{-4} $cm^2/V\,s$ for **122**, as determined by the SCLC method) which resulted lower J_{sc}. However, although **123** has the lower band gap and exhibits the higher hole mobility (7.7×10^{-4} $cm^2/V\,s$ as measured by

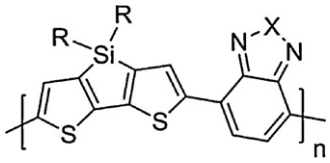

124 X= S, R: 2-ethylhexyl
125 X= S, R: dodecyl
126 X= O, R: dodecyl

Chart 33. Chemical structures of the poly(dithieno[3,2-*b*:2′,3′-*d*]silole) derivatives **124**–**126** consisting of 2,1,3-benzothiadiazole or 2,1,3-benzooxadiazole units.

SCLC), the PCE in blends with $PC_{71}BM$ in 1:1 (w/w) ratio is low (0.6%). The reason for the low PCE is the improper alignment of the energy levels between **123** and $PC_{71}BM$ [162].

Finally, an improvement in the PCE (2.5%) has been achieved through a BHJ device with an active layer containing the ternary blend **118** and **120** as the electron donors with $PC_{71}BM$ in 1:1:4 (w/w) ratio with J_{sc} = 11.1 mA/cm^2, V_{oc} = 0.64 V and FF = 0.36. This is the first example of using two *p*-type conjugated polymers with complementary absorption ability within a single active layer to improve the solar cell performance [162].

3.2.11.2. Dithieno[3,2-b:2′,3′-d]silole-based polymers.

Dithieno[3,2-*b*:2′,3′-*d*]silole (DTS)-containing polymers have attracted attention as novel systems[163] in which the silicon–carbon σ*-orbital effectively mixes with the π*-orbital of the butadiene fragment to afford a low-lying LUMO and a relatively low band gap [164,165]. In addition, silicon introduction stabilizes the diene HOMO level compared to the carbon counterparts [166], which should enhance the ambient stability of silole polymers. For these reasons, the silole polymer **124** [167–170], an analogue of the carbon-bridged **107**, along with **125** [156,171], which varies regarding the type of the side alkyl chains and **126** [172] where the 2,1,3-benzothiadiazole has been replaced by the 2,1,3-benzooxadiazole (Chart 33), have been synthesized by the Stille cross-coupling polymerization either by thermal heating (**124**) or by microwave heating (**125**, **126**). Moreover, their optoelectronic as well as their photovoltaic properties have been extensively analyzed in some very recently reported papers.

The optical band gaps and the energy levels of copolymers **124**–**126** are presented in Table 17. The optical band gap of the silicon bridged **124** is similar to the carbon bridged **107**. However, from the absorption profiles of **124** and **107** it is revealed that **124** is more crystalline than that of **107** due to the fine vibronic feature of the absorption spectrum. On the contrary, **107** exhibits a broad featureless absorption spectrum in the solid state [167–170]. These conclusions are in agreement with results obtained from grazing incidence X-ray studies [168,170]. The transition from the amorphous phase in **107** to a more crystalline phase in **124** by just replacing the carbon atom with silicon can be attributed to the longer C–Si bond as compared with the C–C bond, based on simulation results, which reduces

Table 17
Optical band gaps and energy levels of **124**–**131**.

Polymers	E_g^{opt} (eV)	LUMO (eV)	HOMO (eV)
124	1.45	3.60	5.30
125	1.37	3.55	5.36
126	–	3.70	5.50
127	1.40	3.23	5.13
128	1.51	3.19	5.02
129	1.53	3.17	4.99
130	1.57	3.58	5.15
131	1.79	3.28	5.07

the steric hindrance from the branched alkyl side groups. Moreover by replacing the branched alkyl side chains of **124** with the linear dodecyl side chains in **125**, the band gap decreases due to the more efficient π–π stacking. On the contrary, the band gap value of **125** is 0.12 eV higher than that of the related analogue **108** (both consisting of dodecyl side chains) most likely due to the higher molecular weight of **108** [156,171].

Concerning the modification on the energy levels, it was revealed that changing the carbon-bridged atom of **107** with silicon, the HOMO level of **124** remains unchanged while the LUMO level is slightly decreased (∼0.05 eV). Comparing the energy levels of **124** with those of **125**, the HOMO and LUMO levels of **125** are shifted by ∼0.05 or 0.06 eV but on the opposite way (LUMO is raised and HOMO is lowering). On the other hand, comparing the structural related polymers **108** and **125** another trend is revealed. The LUMO levels of both **108** and **125** are almost similar, but the HOMO level of **125** is lower than that of **108** by 0.24 eV. Summarizing, the LUMO level remains almost constant regardless the bridging atom and the type of the alkyl chain while the HOMO level is mostly a function of the type of the alkyl chain and not of the bridging atom. Finally, further lowering of both the HOMO and LUMO levels by ∼0.15 eV can be achieved by replacing the 2,1,3-benzothiadiazole of **125** with 2,1,3-benzooxadiazole in **126**.

The photovoltaic performance of **124** has been examined in blends with $PC_{71}BM$. Initially, a PCE of 3.8% has been recorded for **124**:$PC_{71}BM$ in 1:1.5 (w/w) without any special treatment [167,168] which was further improved to 5.6% upon thermal annealing (140 °C for 5 min) [168]. The increased hole mobility of **124** upon annealing (3×10^{-3} cm^2/V s as determined in FET measurements), which is approximately five times higher than that before annealing ($\sim 6 \times 10^{-4}$ cm^2/V s), is likely one of the reasons for the increased PCE. Moreover, since that the crystallinity of **124** is improved by replacing the carbon atom in **107** with silicon, as mentioned above, the recorded hole mobilities both as pristine films and in blends with $PC_{71}BM$ are exceeding those of **107** in all cases. Consequently, the PCE of **124** is slightly higher than that of **107** which has been achieved upon addition of additive (1,8-diiodooctane) and a higher loading of $PC_{71}BM$ (1:3, w/w).

In order to further explore the higher photogeneration achieved in **124**:$PC_{71}BM$ blends, extensive morphological and fluorescence spectroscopy studies have been performed and the obtained results were compared with those of **107**:$PC_{71}BM$ films [170]. The major difference between the two blend films is that the introduction of the sili-

con bridge induces a larger phase separation between the polymer and the fullerene, compared to that of the carbon counterpart. As a consequence the fullerene separates from **124** matrix, and is found to partially arrange in crystallites, providing an efficient transport for electrons as confirmed by bright-field TEM [170]. Moreover, the enhanced aggregation of **124** significantly reduces the formation of the charge-transfer states [the so-called charge-transfer complexes (CTC)] and increases the formation of free charge carriers, an outcome that was also confirmed by steady state fluorescence spectroscopy studies [170]. On the other hand, CTC are present in **107**:$PC_{71}BM$ films and show dependence on the polymer–fullerene composition ratio, but upon addition of 1,8-diiodooctane, a partial suppression of CTC was detected [157,170].

PCE of 5.9%, which is even higher from that of **124**, was obtained by fabricating **125**:$PC_{71}BM$ films (1:1, w/w) from solvent mixture of 4% chloronaphthalene (CN) in CB with J_{sc} = 17.3 mA/cm^2, V_{oc} = 0.57 V and FF = 0.61 [156]. The photovoltaic performance of this system is dependent from the molecular weight of **125** [156,171]. By increasing the molecular weight, a slight decrease in V_{oc} is observed from 0.64 V at M_n = 7000 g/mol to 0.57 V at M_n = 34,000 g/mol; however, there is a more significant increase in J_{sc} from 4.2 to 17.3 mA/cm^2, which is accompanied by a similarly large increase in FF from 0.35 to 0.61 [156]. By changing the 2,1,3-benzothiadiazole unit in **125** with 2,1,3-benzooxadiazole in **126**, a slightly lower PCE was obtained (5.4%) from **126**:$PC_{71}BM$ films (1:2, w/w) fabricated from a solvent mixture of 2% by volume CN relative to CB with J_{sc} = 13.7 mA/cm^2, V_{oc} = 0.68 V and FF = 0.58 [172].

In both cases (**125** and **126**) CN (having a boiling point of 250 °C) was selected based on the fact that a solvent additive which could slow down the drying of the film and at the same time would not induce further aggregation in **125** or **126** is necessary, since that the pristine **125** or **126**:$PC_{71}BM$ films present a complex morphology that is not optimal for high performance solar cells due to the strong aggregation tendency of the **125** and **126** polymer chains. The addition of CN leads to smoother films (the surface of the active layer was planarized), less heterogeneous surface features and improved PCEs. These results open the way for the wider selection of solvent additives as an effective tool towards to the desired manipulation of the active layer [156,172].

All the above results inspired the further exploitation of new silole containing derivatives such as **127**–**131** as alternative electron donor candidates for OPVs (Chart 34). Thus, three new alternating copolymers consisting of different alkyl substituted DTS and TBzT segment (**127**–**129**) [173] have been synthesized by Stille cross-coupling polymerization reaction. In addition, the random copolymers (**130** and **131**) [162] where the DTS with either the 2,1,3-benzothiadiazole (**130**) or the quinoxaline (**131**) are dispersed and separated by the unsubstituted thiophene spacers in the conjugated backbone, were also synthesized by Stille cross-coupling polymerization reaction similarly as the CPDT derivatives **118**, **120** and **121** reported above.

The optical band gaps and the energy levels of the copolymers are presented in Table 17. For the alternating polymers **127**–**129**, the optical band gaps of the polymers

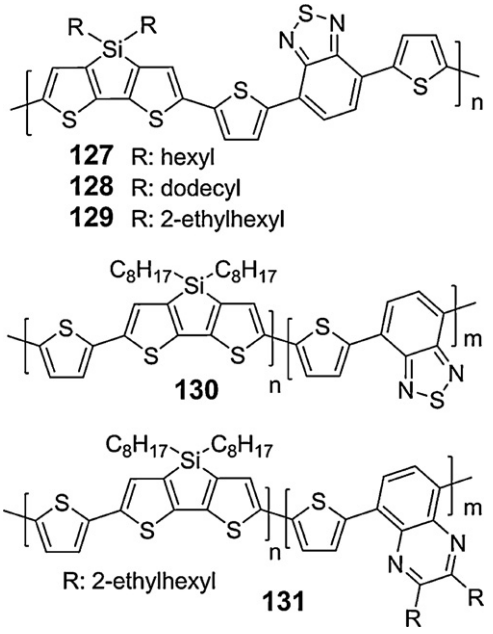

Chart 34. Chemical structures of the poly(dithieno[3,2-*b*:2′,3′-*d*]silole) derivatives **127**–**131** consisting of both electron rich and deficient units.

containing the linear alkyl chains (**127**, **128**) are lower than that of **129** (having the branched alkyl side chain) due to the better π–π stacking. In addition, comparing the band gaps of **127** and **128** it is shown that the shorter the alkyl chain the lower the band gap is. Regarding the energy levels of **127**–**129**, both the HOMO and LUMO levels are raised by passing from the polymer **127** (shorter linear alkyl chain) to **128** (longer alkyl side chain) and then to **129** (branched alkyl side chain). On the other hand, the band gaps of both the random copolymers **130** and **131** are higher than that of the alternating copolymers **127**–**129**, but are similar with the structural related random copolymers **120**, **121** (Table 16). Furthermore, by replacing the 2,1,3-benzothiadiazole in random copolymer **130** with quinoxaline, although both the HOMO and LUMO levels are raised, the LUMO level is being shifted in greater extent than HOMO level.

The photovoltaic performance of the copolymers **127**–**131** was examined in blends with $PC_{71}BM$ and was found that the PCE of the alternating copolymers were superior to those of random copolymers. In detail, the PCE of the alternating copolymers **127**–**129** are influenced from the type of the alkyl side chains [173]. **128** bearing the dodecyl side chains in blends with $PC_{71}BM$, in 1:1 (w/w) ratio exhibits the highest PCE (3.43%) with J_{sc} = 10.67 mA/cm^2, V_{oc} = 0.62 V and FF = 0.52 and is almost 16% improved by that of the 2-ethylhexyl counterpart **129** which exhibits a PCE of 2.95% in (1:1, w/w $PC_{71}BM$) with J_{sc} = 9.76 mA/cm^2, V_{oc} = 0.60 V and FF = 0.50. The PCE of **127** is very low 0.18% due to the lack of complete solubility in common organic solvents and easy processing [173,174]. On the other hand, the PCE of **130**:$PC_{71}BM$ in 1:2 (w/w) is lower (2.2%) than that of the alternating copolymers (**128**, **129**) with J_{sc} = 9.6 mA/cm^2, V_{oc} = 0.51 V and FF = 0.45 [162], while the PCE of **131**:$PC_{71}BM$ in 1:1 (w/w) is very low

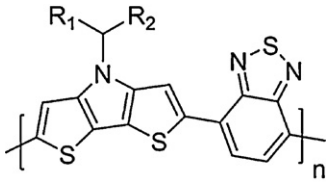

132 R_1, R_2: octyl
133 R_1, R_2: hexyl
134 R_1, R_2: pentyl
135 R_1: H, R_2: undecyl

Chart 35. Chemical structures of the poly(dithieno[3,2-*b*:2′,3′-*d*]pyrrole) derivatives **132**–**135** consisting of 2,1,3-benzothiadiazole.

(0.3%). It is shown that even though the HOMO level of **130** is higher than that of **128** and **129**, the V_{oc} of **130**:$PC_{71}BM$ is lower by ~0.1 V.

3.2.11.3. Dithieno[3,2-b:2′,3′-d]pyrrole-based polymers.

Structural related analogue of CPDT and DTS is dithieno[3,2-*b*:2′,3′-*d*]pyrrole (DTP) where a 2,2′-bithiophene is covalently bridged and rigidified at the 3,3′-position by a nitrogen atom. As reported above, two of the most promising LBG polymers for high performance OPVs are the alternating D–A copolymers **107** and **124** which demonstrate PCEs above 5%. According to this, four structurally related LBG alternating D–A copolymers consisting of *N*-alkyl DTP as the electron-rich unit and 2,1,3-benzothiadiazole as the electron-deficient unit were synthesized by Stille cross-coupling polymerization (Chart 35), containing different alkyl side chains, such as two octyl (**132**) [175], two hexyl (**133**) [175], two pentyl (**134**) [175] and a dodecyl (**135**) [176], in the periphery of the DTP.

The optical band gap of the polymers are 1.41 eV (**132**), 1.42 eV (**133**), 1.43 eV (**134**) and 1.2 eV (**135**) showing that the type of the alkyl side chain affects the band gap of the resulting polymers. The linear alkyl side chain of **135** allows the efficient π–π stacking of the polymer chains resulting to the lower band gap. Regarding the energy levels, the three polymers (**132**–**134**) have the same LUMO level at 3.08 eV, while their HOMO levels have minor difference in the range 4.81–4.89 eV. Moreover, the energy levels of **135** are situated at 4.65 eV (HOMO) and 3.13 eV (LUMO), respectively. It seems that by replacing the bulkier alkyl side chains of **132**–**134** with the linear alkyl side chain in **135**, the HOMO is upshifted by almost 0.25 eV, while the LUMO of **135** is somewhat lower as compared to that of **132**–**134**. In addition, the higher-lying HOMO levels of **132**–**135** as compared to the similar polymers **107**–**108** and **124**–**125** indicates that DTP is somehow stronger electron donor than CPDT and DTS units, respectively.

BHJ solar cells were prepared based on blends of **132**–**134** with $PC_{61}BM$ in 1:3 (w/w) ratio [175]. **134** with the shortest alkyl chain exhibits higher PCE (2.80%) as compared to **132**–**135** with J_{sc} = 11.9 mA/cm^2, V_{oc} = 0.54 V and FF = 0.44, whereas the PCEs of **132** and **133** are 1.23% and 2.06%, respectively. The unoptimized PCE of **134** is comparable with the unoptimized PCE of **107** (3.2%) and **124** (3.8%), showing the potential of this polymer towards higher PCE. Moreover, the PCE is drastically improved as the length of the side chain decreases, due to the enhanced film absorption coefficient and improved thin film morphology. It was reported that as the length decreases, the film becomes more uniform and the domain size decreases from 400–900 nm for **132** to 50 nm for **134** [175]. This result is supporting the fact that optimizing the structure of the side alkyl chain is crucial for the design and synthesis of conjugated polymer for high performance solar cells.

Furthermore, a series of D–A alternating copolymers (Chart 36) based on *N*-aryl and *N*-alkyl DTP donors linked through thienylene bridges to 2,1,3-benzothiadiazole-based acceptors have been synthesized by Stille cross-coupling polymerization and extensively characterized with respect to their optical and electrochemical properties and photovoltaic performances [177,178].

The optical band gaps and the energy levels of the synthesized copolymers **136**–**142** are presented in Table 18. In general, it is demonstrated that the LUMO levels and the optical band gaps are strongly influenced by the choice of the acceptor, in contrast to the HOMO levels that are only weakly dependent on the acceptor used. For example, the band gaps are lowering by passing from the 2,1,3-benzothiadiazole (**136**–**139**) to thiadiazolo[3,4-*g*]quinoxaline (**140**–**141**) and then to benzobisthiadiazole (**142**). Moreover, a rather controversial result is revealed about the influence of the type (alkyl versus aryl) of the side groups on the band gap of copolymers **136**–**141** containing different acceptor units. For example, comparing the band gaps of **136**–**139**, consisting of the same acceptor unit in the polymer backbone, the band gap of **139**, with three linear alkyl side chains linked one on the DTP and two on the 4-position of the thiophene rings of the TBzT segment, exhibits lower band gap than polymers **136**, **137** consisting of bulky alkyl side chains only on the DTP monomer. Similar observation with **136** and **137** is presented for **138**, having an alkoxy substituted phenyl ring attached in the nitrogen atom of the DTP. Thereby, the lower band gap of **139** is possibly attributed to the better π–π stacking of the polymer chains in the solid state [177]. Furthermore, **136** with *N*-alkyl and **138** with *N*-aryl substituents on the DTP demonstrating similar band gaps. On the contrary, comparing the band gaps of **140** and **141**, where both incorporate the thiadiazolo[3,4-*g*]quinoxaline as the acceptor unit in the main chain, is shown that the band gap of **141** is slightly lower than that of **140**.

The photovoltaic performance of the polymers was examined in blends with $PC_{61}BM$ and the PCEs are presented in Table 18. **137**:$PC_{61}BM$ in 1:1 (w/w) ratio exhibits the highest PCE (2.18%) with J_{sc} = 9.47 mA/cm^2, V_{oc} = 0.52 V and FF = 0.44 while **138**:$PC_{61}BM$ in 1:3 (w/w) ratio shows a moderate PCE of 1.3% with J_{sc} = 3.9 mA/cm^2, V_{oc} = 0.51 V and FF = 0.47 [178]. The limiting factors preventing the DTP-based copolymers **136**–**142** for obtaining higher PCEs is the low V_{oc} that is significantly lower than other D–A copolymers such as the copolymers **198** (V_{oc} ~ 1 V), **248** (V_{oc} ~ 0.9 V) and **259** (V_{oc} ~ 0.9 V) that will be reported next in the text, and in part to the reduced driving force for charge transfer to $PC_{61}BM$, especially for **140**–**142** [177]. However, one of the potential advantages of these

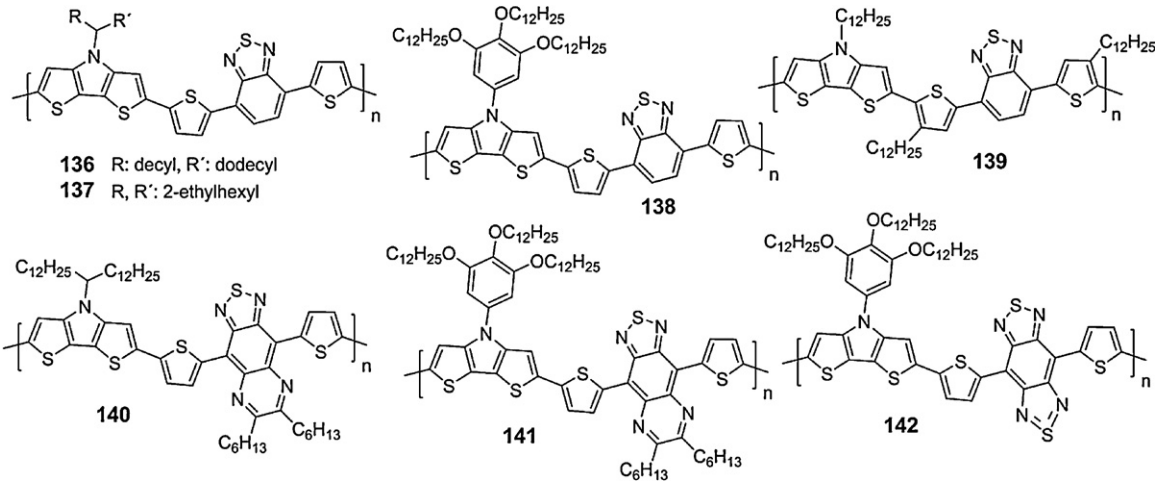

Chart 36. Chemical structures of the poly(dithieno[3,2-*b*:2′,3′-*d*]pyrrole) derivatives **136**–**142** consisting of both electron-rich and deficient units.

Table 18
Optical band gaps, energy levels and photovoltaic efficiency of **136**–**142**.

Polymers	E_g^{opt} (eV)	LUMO (eV)	HOMO (eV)	PCE (%)
136	1.41	3.40[a]	4.80[a]	0.17
137	1.46	3.43	5.00	2.18
138	1.41	3.20[a]	4.90[a]	1.30
139	1.30	3.13	5.07	0.43
140	0.92	3.70[a]	4.80[a]	–
141	0.87	3.70[a]	4.90[a]	0.22
142	0.56	4.00[a]	4.70[a]	0.007

[a] Values estimated by DPV technique.

polymers is that they might act as active components in tandem solar cells due to their broad absorbance in the near-IR, especially when mixed with stronger electron-withdrawing acceptors than $PC_{61}BM$.

3.2.11.4. Dithieno[3,2-b:2′,3′-d]thiophene-based polymers. Structural related analogue of CPDT, DTS and DTP is dithieno[3,2-*b*:2′,3′-*d*]thiophene (DTT) where a 2,2′-bithiophene is covalently bridged and rigidified at the 3,3′-position by a sulphur atom. Conjugated polymers consisting of unsubstituted (**143** [179], **144** [176]) or alkyl substituted DTT units (**145** [180], **146** [176]) with various electron-rich and electron-deficient units have been synthesized (Chart 37) by oxidative polymerization using $FeCl_3$ (**143**) or Stille cross-coupling polymerization (**144**–**146**).

The optical band gaps and the energy levels of the polymers are included in Table 19. From all the DTT-based conjugated polymers presented in this category, only **144** can be considered a LBG polymer since that its optical band gap is 1.5 eV, while those of **143**, **145–146** are between 2.0 eV (**145**, **146**) and 2.1 eV (**143**). It is demonstrated that the insertion of an electron-rich unit like thiophene or bithiophene in the backbone of the DTT-based conjugated polymers is not an effective approach for lowering the band gap. On the other hand, the incorporation of both the DTT moiety and the 2,1,3-benzothiadiazole into the same polymer chain, effectively lowers the band gap of **144**, but the band gap of **146** still remains high (Table 19). This result

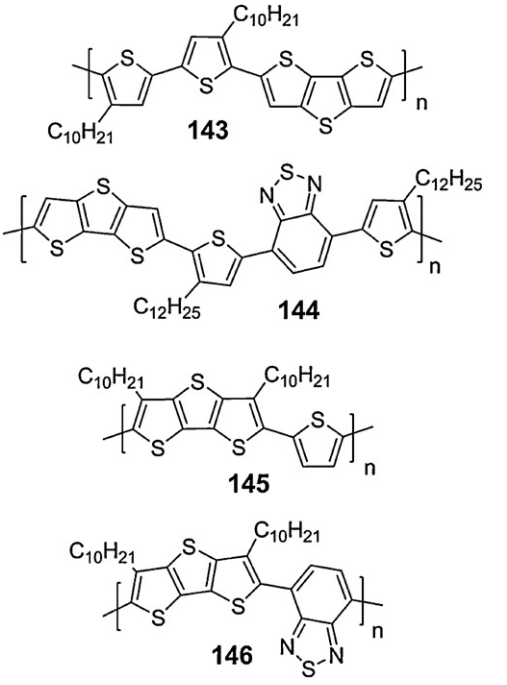

Chart 37. Chemical structures of the poly(dithieno[3,2-*b*:2′,3′-*d*]thiophene) derivatives **143**–**146** consisting of both electron-rich and deficient units.

Table 19
Optical band gaps, energy levels and photovoltaic efficiency of **143**–**146**.

Polymers	E_g^{opt} (eV)	LUMO (eV)	HOMO (eV)	PCE (%)
143	2.1	3.84	5.84	0.81
144	1.5	2.90	5.12	0.17
145	2.0	3.40	5.40	0.70
146	2.0	3.28	5.60	–

Table 20
Optical band gaps and energy levels of **147**–**154**.

Polymers	E_g^{opt} (eV)	LUMO (eV)	HOMO (eV)
147	2.13	2.67	5.16
148	2.03	2.86	5.07
149	2.06	3.69	5.05
150	1.97	2.66	4.56
151	1.63	3.28	4.78
152	1.70	3.19	5.10
153	1.52	3.33	4.88
154	1.05	3.46	4.65

indicates that the position of the alkyl side chains drastically affects the band gap, through the steric hindrance that favors the highly twisting conformation structure of the polymer chain and prevents the effective conjugation length [176].

The photovoltaic performance of the polymers was examined in blends with $PC_{61}BM$ and the PCEs are presented in Table 19. Blends of **143** with $PC_{61}BM$ in 1:3 (w/w) ratio showed the highest PCE (0.81%) with J_{sc} = 2.56 mA/cm^2, V_{oc} = 0.80 V and FF = 0.36 [179], even though it is low as compared to the other fused dithieno-based conjugated polymers reported above.

3.2.12. Bithiophenes with 6-member aromatic rings in the central core

3.2.12.1. Benzo[1,2-b:4,5-b′]dithiophene-based polymers. Benzo[1,2-*b*:4,5-*b*′]dithiophene ($B_{1245}DT$)-based LBG conjugated polymers present the highest PCE in plastic solar cells when blended with fullerene derivatives. The major advantage of conjugated polymers consisting of $B_{1245}DT$ is the demonstration of a high hole mobility (0.25 cm^2/V s in FETs) because $B_{1245}DT$ can easily form π–π stacking due to its large planar structure [181]. Taking this into account, Hou et al. designed and synthesized a series of $B_{1245}DT$-based conjugated polymers where the band gap and the energy levels were fine tuned through the copolymerization with different electron-rich or electron-deficient aromatic units (Chart 38) [182,183]. Since the band gap of conjugated polymers is generally very susceptible to steric hindrance, 4,9-bis-alkoxy-$B_{1245}DT$ having no substituent on 1, 3, 5, and 7 positions was used because the steric hindrance between adjacent units is very small.

The energy levels and the band gap of the synthesized polymers are summarized in Table 20 [182]. Only a slight decrease (~0.1–0.15 eV) in the band gap is observed when $B_{1245}DT$ unit is copolymerized with electron-rich units such as vinylene (**148**), thiophene (**149**) and EDOT (**150**) as compared to the homopolymer **147**. On the contrary, when $B_{1245}DT$ unit was copolymerized with electron-deficient units such as quinoxaline (**151**), 2,1,3-benzothiadiazole (**152**), 2,1,3-benzoselenadiazole (**153**) and thieno[3,4-*b*]pyrazine (TP) (**154**), the resulting alternating D–A conjugated polymers exhibit lower band gaps as compared to **147**–**150**. Regarding the modification of the energy levels, it is revealed that the $B_{1245}DT$-based polymers consisting of the EDOT (**150**) and TP (**154**) cannot be used as electron donor polymers in plastic solar cells because their HOMO levels are significantly raised after the incorporation of these units in their polymer backbones. Furthermore, the use of the 2,1,3-benzothiadiazole can lower the band gap of **152** by reducing only the LUMO level. Further lowering of the band gap of **153** can be achieved by the use of the 2,1,3-benzoselenadiazole unit, whereas both the HOMO and LUMO levels are shifted. Initially, **149** exhibited the maximum PCE (1.6%) in blends with $PC_{61}BM$ (1:1, w/w) with V_{oc} = 0.75 V, I_{sc} = 3.8 mA/cm^2, and FF = 0.56 [182]. However, it was shown very recently [184] that the bis(2-ethylhexyloxy) substituted **148** in blends with $PC_{71}BM$ (1/4, w/w ratio) provides a PCE of 2.63% with J_{sc} = 6.46 mA/cm^2, V_{oc} = 0.71 V and FF = 0.57.

As shown above, the band gap values of the $B_{1245}DT$-based conjugated polymers containing the electron-rich units are higher from what is reported to be the ideal band gap of a conjugated polymer for OPVs [28]. However, Yu et al. demonstrated very recently the synthesis

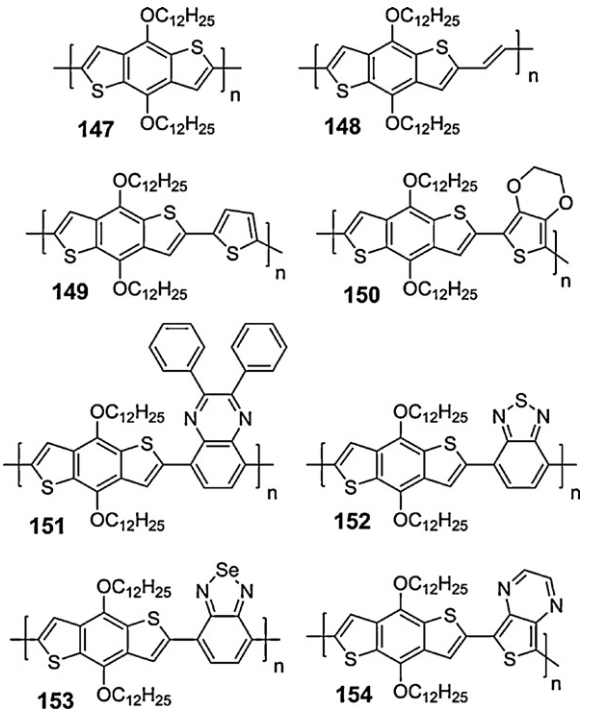

Chart 38. Chemical structures of the poly(benzo[1,2-*b*:4,5-*b*′]dithiophene) derivatives **147**–**154**.

Table 21
Energy levels and hole mobilities of **155**–**163**.

Polymers	LUMO (eV)	HOMO (eV)	Hole mobility ($\times 10^{-4}$ cm^2/V s)
155	3.20	4.90	4.7
156	3.22	4.94	4.0
157	3.29	5.04	7.0
158	3.31	5.12	7.7
159	3.24	5.01	4.0
160	3.17	5.01	2.6
161	3.31	5.15	5.8
162	3.35	5.12	2.0
163	3.45	5.22	7.0

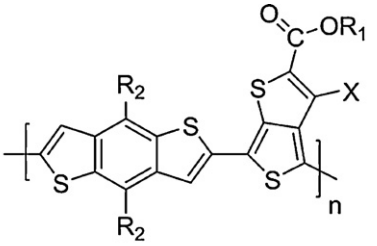

155 X = H, R_1 = $nC_{12}H_{25}$, R_2 = *n*-octyloxy
156 X = H, R_1 = 2-ethylhexyl, R_2 = *n*-octyloxy
157 X = H, R_1 = 2-ethylhexyl, R_2 = *n*-octyl
158 X = F, R_1 = *n*-octyl, R_2 = 2-ethylhexyloxy
159 X = H, R_1 = *n*-octyl, R_2 = 2-ethylhexyloxy
160 X = H, R_1 = 2-butyloctyl, R_2 = *n*-octyloxy
161 X = F, R_1 = 2-ethylhexyl, R_2 = 2-ethylhexyloxy

Chart 39. Chemical structures of the various alkyl substituted benzo[1,2-*b*:4,5-*b*′]dithiophene alternate thieno[3,4-*b*]thiophene copolymers **155**–**161**.

of a series (**155**–**161**) of LBG (~1.6 eV) B_{1245}DT-based conjugated polymers consisting of the highly electron-rich thieno[3,4-*b*]thiophene (Chart 39) which lowers the band gap through the stabilization of the quinoidal structure in the main chain [183,185,186]. The new polymers were synthesized via the Stille polycondensation between an ester functionalized 2,5-dibromothieno[3,4-*b*]thiophene and B_{1245}DT distannane monomers.

One of the highest PCEs in solar cells has been initially recorded using **155** as the electron donor and PC_{61}BM (4.76%) or PC_{71}BM (5.6%) in 1:1 (w/w) ratio with J_{sc} = 15.6 mA/cm^2, V_{oc} = 0.56 V and FF = 0.63 [183]. The combination of the band gap at 1.6 eV and the high hole mobility (4.7×10^{-4} cm^2/V s) as measured by the SCLC method resulted the impressive J_{sc} and FF values. However, the limiting factor preventing the **155**:PC_{71}BM system of achieving higher PCE is the low V_{oc} resulting from the HOMO level of the **155** (4.9 eV), while the LUMO is situated at 3.2 eV as estimated from the CV measurements (Table 21). Therefore, six related polymers (**156**–**161**) were further developed with the aim to adjust the HOMO–LUMO energy levels in order to further optimize their photovoltaic performance [185,186]. Various side chains (linear versus branched and alkoxy versus alkyl) have been used in both B_{1245}DT and thieno[3,4-*b*]thiophene in order to fine tune the physical properties of **156**–**161**. The electrochemical properties and their hole mobilities are presented in Table 21.

Since that all the side chains of **155** are linear, the general structural modification occurred on **155** was the combination of linear and branched side chains (**156**–**160**) or the use of all branched side chains (**161**) on the polymer backbone. The primary modifications include: (i) the replacement of the dodecyl chain on the thieno[3,4-*b*]thiophene with the shorten and branched 2-ethylhexyl (**156**) or the bulkier 2-butyloctyl (**160**) and (ii) the use of the 2-ethylhexyloxy side chain on the B_{1245}DT with the simultaneously shortening of the dodecyl chain on the thieno[3,4-*b*]thiophene with octyl (**159**). The steric hindrance that introduced in the main chain lowered the HOMO level (4.94 eV for **156** and 5.01 eV for **159** and **160**) and decreased the hole mobility. Moreover, as it is generally known alkoxy side chains are strong electron-donating groups leading to the raise of the HOMO level. Hence their replacement with the less electron-donating octyl groups in **157** lead to the slight lowering of the HOMO (5.04 eV) and simultaneously the hole mobility was increased (7.0×10^{-4} cm^2/V s).

However, no significant drop in the HOMO levels of the above mentioned polymers was obtained as compared to **155**. Therefore, another approach presented for modifying the energy levels of the alternating B_{1245}DT-thieno[3,4-*b*]thiophene copolymers was achieved by introducing an electron-withdrawing group onto thieno[3,4-*b*]thiophene. Based on this concept, fluorine was chosen due to its high electronegativity and small atom size and introduced in the 3-position of the thieno[3,4-*b*]thiophene (**158**, **161**). The resulting polymers exhibited relatively low-lying HOMO levels (5.12 eV for **158** and 5.15 for **161**) while their hole mobilities were maintained high (Table 21). These combined properties lead to further improvement on the initial photovoltaic performance of **155** and record PCEs of 6.1% and 7.4% were obtained for **158** and **161**, respectively. Therefore, **161** is one of the first polymers showing PCE over 7%. The photovoltaic parameters of the **158**:PC_{61}BM in 1:1 (w/w) are J_{sc} = 13.0 mA/cm^2, V_{oc} = 0.74 V and FF = 0.61 [185] while those of the **161**:PC_{71}BM in 1:1.5 (w/w) are J_{sc} = 14.50 mA/cm^2, V_{oc} = 0.74 V and FF = 0.69 [186]. The V_{oc} has been improved almost 28% over the **155** system without negative influence on the photocurrent value.

Morphological studies performed on blends of **155**–**161** with fullerenes by TEM indicated unoptimized morphologies for **157**–**161** with the appearance of large domains

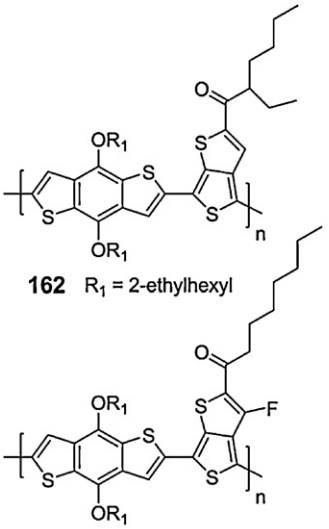

Chart 40. Chemical structures of the benzo[1,2-*b*:4,5-*b*′]dithiophene alternate thieno[3,4-*b*]thiophene copolymers **162** and **163**.

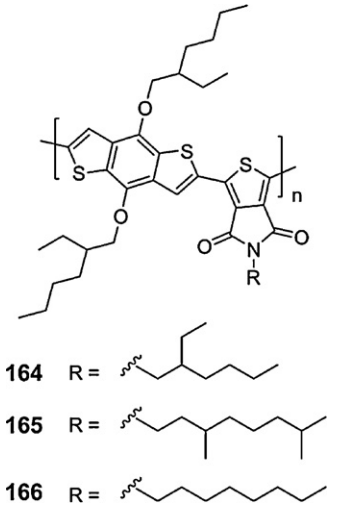

Chart 41. Chemical structures of the benzo[1,2-*b*:4,5-*b*′]dithiophene alternate *N*-alkylthieno[3,4-*c*]pyrrole-4,6-dione copolymers **164**–**166**.

when blends were prepared from CB or dichlorobenzene (DCB) as solvents, while **155** and **156** exhibit finer features [185]. The large domains observed on **157**–**161**-based blends suggest that diminish exciton migration to the D/A interface is the factor preventing efficient charge separation. Improvement on the morphology of the **157**–**161**:fullerene systems has been achieved by the use of processing additives. Addition of 3% by volume ratio of 1,8-diiodooctane on either CB or DCB resulted into uniform thin film morphologies without large phase separation and formation of appropriate interpenetrating networks. Especially for **161**, the exciton dissociation, the charge transport properties in donor and acceptor networks and the charge extraction properties in both organic/electrode interfaces are all very close to 100% implying that the morphology of the **161**:$PC_{71}BM$ is close to the ideal donor and acceptor nanometer-scale interpenetrating network [186]. Contrary to rrP3HT:$PC_{61}BM$ solar cells, annealing of **155**:$PC_{61}BM$ films decreased the PCE to 1.92% due to the reduced interfacial area between the electron donor and the acceptor [187].

Further attempts to modify the HOMO of the alternating B_{1245}DT-thieno[3,4-*b*]thiophene based polymers are presented by the addition of another electron-withdrawing group except ester in the 4 position of the thieno[3,4-*b*]thiophene (Chart 40). By changing the ester with a ketone group, the HOMO levels of **162** [188], **163** [189] were successfully lowered since that the alkyloxy group on the carbonyl of the thieno[3,4-*b*]thiophene is much stronger electron-donating than the alkyl side chain [188]. The energy levels of **162** and **163** are presented in Table 21. Comparing **159** with **162** and **158** with **163**, the HOMO and LUMO levels have been shifted by more than 0.1 eV. Solar cell devices prepared using **162** or **163** in blends with $PC_{71}BM$ in 1:1.5 (w/w) demonstrated PCEs as high as 6.58% (6.3% the average value based on 200 devices) for **162** with J_{sc} = 14.7 mA/cm^2, V_{oc} = 0.7 V and FF = 0.64 [188] and a record efficiency of 7.73% (7.4% the average value based on 200 devices) for **163** with J_{sc} = 15.2 mA/cm^2, V_{oc} = 0.76 V and FF = 0.67 [189]. However, there is a difference between the laboratory measured PCE of **163** with the PCE as certified by the National Renewable Energy Laboratory (NREL) (6.77%).

In light of these outstanding results, many research groups have focussed their research efforts towards alternative candidates of thieno[3,4-*b*]thiophene. Very recently, one symmetric and planar heterocycle unit that has attracted the interest of three research groups is the *N*-alkylthieno[3,4-*c*]pyrrole-4,6-dione (TPD), due to its ability to gain some stabilization energy by forming a quinoidal thiophene-maleimide structure in its excited state. Hence, when TPD is combined with B_{1245}DT, three B_{1245}DT-*alt*-TPD copolymers **164**–**166** (Chart 41) are provided through the Stille cross-coupling polymerization [190–192]. In **164**–**166**, the branched alkoxy side chains were maintained constant on the B_{1245}DT unit while three different alkyl side chains have been attached on the TPD in order to investigate the correlation between different alkyl substituents and optoelectronic properties, as well as photovoltaic performance. The M_n of **164** (42,000 g/mol) [192] and **165** (39,000 g/mol) [192], consisting of the branched alkyl chains, are higher than **166** [190–192] (having the octyl side chain) that ranges between 13,200 and 35,000 g/mol.

The optical band gaps, the energy levels and the photovoltaic parameters of the synthesized copolymers **164**–**166** are included in Table 22. The optical band gaps of **164**–**166** vary as a function of the type of the substituent used. The band gap of **164** is 1.75 eV, however by replacing the shorter and bulkier 2-ethylhexyl chain in **164** with the longer and less bulky octyl side chains in **165** and **166**, a reduction of the band gap (1.70 eV for **165** and 1.73 eV for **166**) is observed, combined with the appearance of broader and red-shifted absorption spectra with more defined vibronic structure [192]. However, that the optical band gap of **166** as reported from the other two research groups is slightly higher (1.80–1.82 eV) [190,191]. Moreover, the absorption of **166** in solution is very similar to that obtained in the

Table 22
Optical band gaps, energy levels and photovoltaic parameters of **164**–**166**.

Polymers	E_g (eV)	LUMO (eV)	HOMO (eV)	PCE (%)	J_{sc} (mA/cm^2)	V_{oc} (V)	FF
164	1.75	–	5.48	4.0	8.1	0.87	0.56
165	1.70	–	5.57	5.7	9.7	0.81	0.67
166[a]	1.73	–	5.40	6.8	11.5	0.85	0.68
166[b]	1.80	3.75	5.56	5.5	9.81	0.85	0.66
166[c]	1.82	3.40	5.43	4.1[d]–4.2[e]	9.8[d]–9.1[e]	0.84[d]–0.87[e]	0.50[d]–0.54[e]

[a] Values according to Ref. [192].
[b] Values according to Ref. [190].
[c] Values according to Ref. [191].
[d] Values for standard configuration device.
[e] Values of inverted structure device.

solid state, indicating a similar rigid-rod conformation for both states. Furthermore, the band gap of the B_{1245}DT-*alt*-TPD copolymer is higher by ~0.15 eV as compared to the B_{1245}DT-*alt*-thieno[3,4-*b*]thiophene copolymers. Regarding the energy levels, the HOMO level of **166** is close to 5.40 eV based on the results reported by two groups [191,192], whereas the third group estimated the HOMO level at 5.56 eV [190]. In addition, the HOMO levels of **164** and **165** are 5.48 eV and 5.57 eV, respectively. Similar with the HOMO level of **166**, two different values for the LUMO level of **166** were also reported, as shown in Table 22.

The photovoltaic performance of **164**–**166** copolymers was examined in blends with $PC_{71}BM$ [190–192]. The PCE of **166**:$PC_{71}BM$ without any treatment is 5.5% in 1:2 (w/w) [190] and 6.4% in 1:1.5 (w/w) [192], while upon optimization with the use of 1,8-diiodooctane (1% in volume) the PCE was increased to 6.8% [192] (the photovoltaic parameters are shown in Table 22). In the optimed devices of **164**:$PC_{71}BM$ (1:2, w/w with 2% by volume of 1,8-diiodooctane) and **165**:$PC_{71}BM$ (1:1.5, w/w with 1% by volume of 1,8-diiodooctane) the PCE increases from 4.0% for **164** to 5.7% for **165**, showing that the elimination of branching on the TPD enhances the photovoltaic performance [192]. Further studies on the morphology of the thin films were performed and the correlation between the structural modifications of **164**–**166** with their molecular organization as thin films was accomplished using the grazing incidence X-ray scattering (GIXS) technique [192]. It is revealed that most of the polymer backbones are oriented parallel to the substrates while their π-stacking distances are reduced by replacing the 2-ethylhexyl side chain of **164** with the dimethyloctyl and *n*-octyl analogues on **165** and **166**, respectively. In addition, **164**–**166** are still able to retain the same face-on orientation and π-stacking distances when blended with fullerenes [192]. The reduced π-stacking distances by passing from **164** to **165** and **166** correlates well with the increased device performance. Moreover, one of the research groups compared the PCE of **166** in both conventional and inverted device structure. Under the same experimental conditions the PCE of **166** in the inverted structure (4.2%) is slightly higher than in the conventional structure (4.1%) [191]. The configuration of the inverted device was based on ITO/ZnO/C_{70}-SAM/**166**:$PC_{71}BM$/PEDOT:PSS/Ag. The C_{70}-SAM is based on a carboxylic acid functionalized C_{70} molecule used to modify the ZnO surface and thus the properties of the bottom electrode for the inverted structure under study.

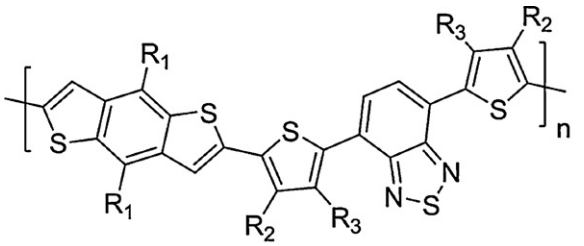

167 R_1: 3-hexylundecyl; R_2, R_3: H

168 R_1: 3-butylnonyl; R_2: hexyl; R_3: H

169 R_1: 2-ethylhexyloxy; R_2: H; R_3: hexyl

170 R_1: 2-ethylhexyloxy; R_2: H; R_3: hexyloxy

Chart 42. Chemical structures of poly(benzo[1,2-*b*:4,5-*b*′]dithiophene) derivatives **167**–**170** consisting of both electron-rich and electron-deficient units.

As shown above, a variety of heterocycle units have been copolymerized with B_{1245}DT moiety in order to fune tune the energy levels and the optical band gap of the resulting copolymers. Based on this concept, several B_{1245}DT-based copolymers consisting of the TBzT segment either unsubstituted or functionalized with hexyloxy and hexyl side chains at different positions (Chart 42) have been also synthesized by Stille cross-coupling polymerization, in order to investigate the influence of the side chains on the optoelectronic and photovoltaic properties of **167**–**170** [193,194].

The optical band gaps and the energy levels of **167**–**170** are presented in Table 23. The band gaps of **167** and **168** are the same, showing that the introduction of an alkyl chain at the 4-position on the TBzT segment does not alter significantly the optical properties of the resulting polymer as compared to the polymer consisting of the unsubstituted TBzT segment. A small difference on the optical properties of **167** and **168** is the profiles of the absorption spectra with the appearance of a more pronounced shoulder at ~650 nm for **167**, which can be attributed to a slightly increased π-stacking and extension of the conjugation [193]. On the other hand, when the hexyl side chains are placed on the 3-position of the TBzT segment, the band gap of **169** is 0.15 eV higher, indicating that between the thiophene and 2,1,3-benzothiadiazole of TBzT segment high steric hindrance is formed. Lowering of the band gap at 1.55 eV

Table 23
Optical band gaps, energy levels and photovoltaic efficiency of **167**–**170**.

Polymers	E_g (eV)	LUMO (eV)	HOMO (eV)	PCE (%)
167	1.70	3.17	5.33	3.85
168	1.70	2.96	5.26	4.31
169	1.85	–	5.23	1.95
170	1.55	–	4.80	1.28

was achieved for **170** though, by replacing the hexyl side chains at the 3-position with hexyloxy side chains due to the strong electron-donating effect of the alkoxy groups. Regarding the energy levels, the HOMO level of **169** is situated 0.4 eV lower than the HOMO level of **170**. The strong electron-donating effect of the alkoxy groups is the main reason for the raised HOMO level of **170**, which indicates that although alkoxy is a very effective functional group to reduce band gap, it is not a good choice for lowering the band gap, because a deeper HOMO level is crucial to obtain a high V_{oc}.

The photovoltaic performance of **167–170** was explored in blends with $PC_{61}BM$ [193,194]. Overall, the PCEs of **167** and **168** are higher than **169** and **170**, with **168**:$PC_{61}BM$ (1:1, w/w ratio) providing the highest PCE (4.31%) with J_{sc} = 9.70 mA/cm^2, V_{oc} = 0.81 V and FF = 0.55 [193]. Even though the HOMO of **168** is slightly raised as compared to **167**, the V_{oc}s of **167**:$PC_{61}BM$ and **168**:$PC_{61}BM$ devices are similar. One of the reasons for the higher PCE of **168** as compared to **167** is the improved solubility, which can lead to more homogeneous mixture with $PC_{61}BM$ and the higher molecular weight of the polymer. The PCE of **169** and **170** are 1.95% and 1.28%, respectively which is lower than **167** and **168** due to the severe steric hindrance between the two adjacent unit of the TBzT segment. Although some individual parameters of the **170**:$PC_{61}BM$ devices, such as the FF and the hole mobility (2.5×10^{-5} cm^2/V s based on the SCLC method) combined with the lower band gap of **170**, are better than the **169**:$PC_{61}BM$ system, the PCE of **169**:$PC_{61}BM$ is higher than **170**. This result shows that the very low V_{oc} (0.4 V) is the limiting factor preventing the **170**:$PC_{61}BM$ system for obtaining higher efficiencies [194].

Finally, by replacing the alkyl or alkoxy substituents from $B_{1245}DT$ unit with the symmetrically octyl-substituted thienylene groups, a new $B_{1245}DT$-based conjugated polymer **171** [195] was synthesized by Suzuki cross-coupling polycondensation (Chart 43). The optical band gap of **171** is 1.75 eV which is higher than that of the structural related analogue **167** indicating that the use of the bulkier and electron rich octyl substituted thiophene ring prevents the efficient π–π stacking between the polymer chains. Moreover, comparing the energy levels of **167** and **171** it is revealed that the HOMO levels of both polymers are similar (5.31 eV for **171** and 5.33 eV for **167**). By incorporating the thiophene rings as side pendants on the $B_{1245}DT$, the electron donating ability of **171** remains similar with **167**, albeit it consists of alkyl side chains on the $B_{1245}DT$ unit. On the other hand, the LUMO level of **171** is surprisingly lower than **167** pointing out that the electron affinity of **171** is higher than **167**. Furthermore, BHJ solar cells based on blends of **171** with $PC_{71}BM$ (1:2, w/w) exhibited a PCE of 5.66% with J_{sc} = 10.7 mA/cm^2, V_{oc} = 0.92 V and FF = 0.57 [195]. It is shown that the V_{oc} of **171** is almost 0.1 V higher than **167** despite their similar HOMO levels.

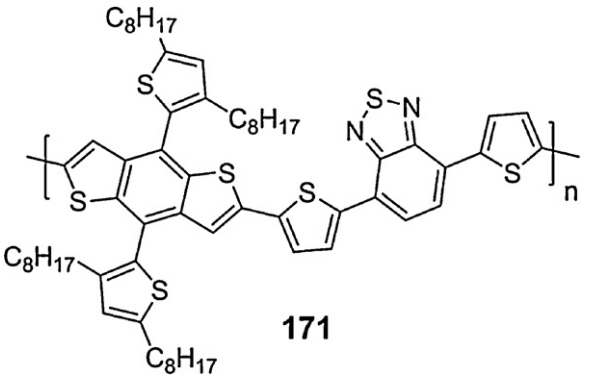

Chart 43. Chemical structure of the benzo[1,2-*b*:4,5-*b*′]dithiophene based copolymer **171**.

3.2.12.2. Benzo[2,1-b:3,4-b′]dithiophene-based polymers.

3.2.12.2.1. Poly(benzo[2,1-b:3,4-b′]dithiophene) homopolymers and copolymers with electron-deficient unit. Other examples of fused bithiophene-based polymers are those consisting of the benzo[2,1-*b*:3,4-*b*′]dithiophene ($B_{2134}DT$), which vary from the benzo[1,2-*b*:4,5-*b*′]dithiophene ($B_{1245}DT$) analogue regarding the relative position of the thiophene units incorporated next to the central phenyl core. The homopolymer **172** and the related alternating D–A copolymer **173** consisting of the $B_{2134}DT$, functionalized with alkylthiophene derivatives, and the electron-deficient 2,1,3-benzothiadiazole (Chart 44) were synthesized by the Stille cross-coupling polycondensation [196]. As compared with **147**, **172** demonstrates similar LUMO (2.65 eV), lower lying HOMO (5.7 eV) and higher optical band gap (2.31 eV). Moreover, the optical band gap of **173** is lower (1.78 eV) than that of **172**, but comparable to the analogue **152**, and the energy levels of **173** are situated at 3.16 eV (LUMO) and 5.34 eV (HOMO). Even though the LUMO level of **173** is similar to **152**, the HOMO level of **173** is situated 0.24 eV deeper than that of **152**.

The photovoltaic performances of **172** and **173** in blends with $PC_{61}BM$ (1:3, w/w) are 0.1% and 0.6%, respectively and their photovoltaic parameters are J_{sc} = 0.34 mA/cm^2, V_{oc} = 0.76 V and FF = 0.40 for **172** and J_{sc} = 2.06 mA/cm^2, V_{oc} = 0.72 V and FF = 0.42 for **173** [196]. The PCE of **173** is slightly lower than the structurally related **152** (0.90%), however the PCEs of both **172** and **173** are still low due to the unfavourable morphology of **172** (large phase separation is observed by AFM) and the low hole mobility of **173** (4.21×10^{-6} cm^2/V s as measured by the SCLC method) [196]. The hole mobility of **173** is two order of magnitude lower than that of **172** (1.58×10^{-4} cm^2/V s) showing that

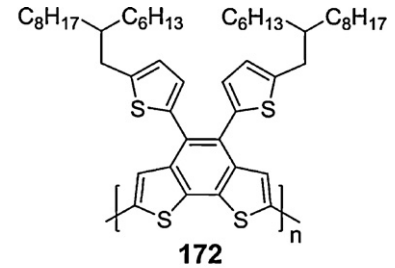

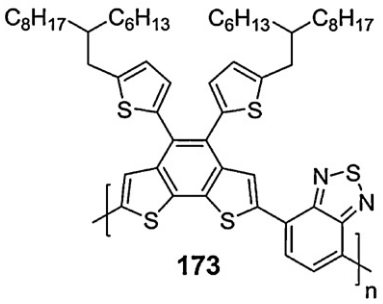

Chart 44. Chemical structures of the poly(benzo[2,1-*b*:3,4-*b*′]dithiophene) derivatives **172** and **173**.

even though the introduction of the 2,1,3-benzothiadiazole is beneficial for lowering the band gap and as a sequence to increase the J_{sc}, the thiophenes are twisted out of plane resulting to the low mobility and low PCE.

3.2.12.2.2. Poly(benzo[2,1-b:3,4-b′]dithiophene) derivatives with both electron-rich and electron-deficient units. As reported above the main limitation preventing **173** for achieving higher PCEs in OPVs is the combination of the moderate optical band gap (1.78 eV) and the low hole mobility (4.21×10^{-6} cm^2/V s). To further optimize the B_{2134}DT-based polymers, You et al. presented the synthesis of a series of alternating copolymers (**174**–**177**) [197] consisting of the B_{2134}DT with TBzT moiety in the polymer backbone by Stille cross-coupling polycondensation (Chart 45). The incorporation of the TBzT segment is expected to enhance the hole mobility of the polymers due to its tendency to form strong π–π stacking. Moreover, an extensive structure–property relationship studies have been achieved for **174**–**177** through the different positioning of the alkyl chains on TBzT [197].

Table 24
Optical band gaps and energy levels of **174**–**177**.

Polymers	E_g^{opt} (eV)	LUMO (eV)	HOMO (eV)
174	1.63	3.16	5.27
175	1.97	3.13	5.38
176	1.69	2.98	5.21
177	2.35	3.01	5.69

The optical band gaps and the energy levels of **174**–**177** are presented in Table 24. It is shown that the positioning of the alkyl chains on the TBzT has a strong influence on the optical and electrochemical properties of these polymers with identical polymer backbones. **174** and **176** exhibit almost identical optical band gaps (1.63 eV for **174** and 1.69 eV for **176**) and HOMO levels (5.27 eV for **174** and 5.21 eV for **176**) indicating slight steric hindrance within the polymer backbone by the anchoring of the alkyl side

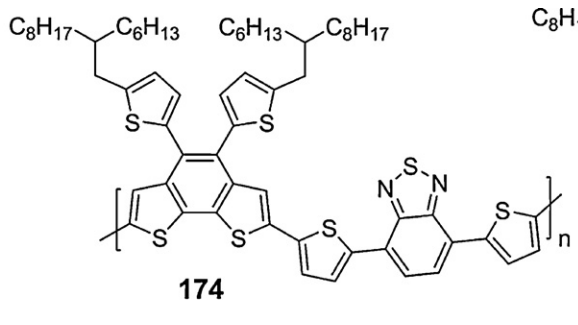

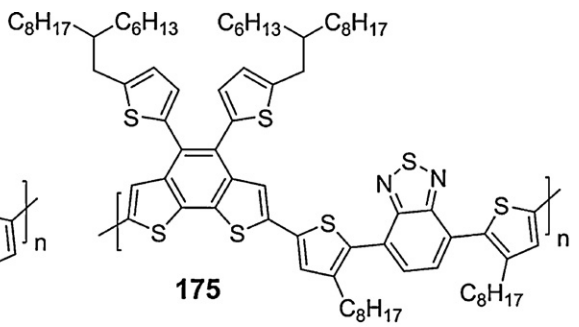

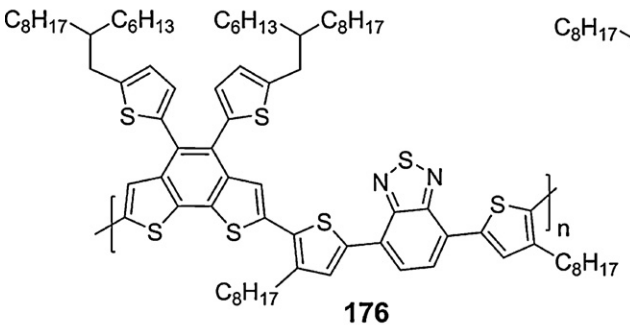

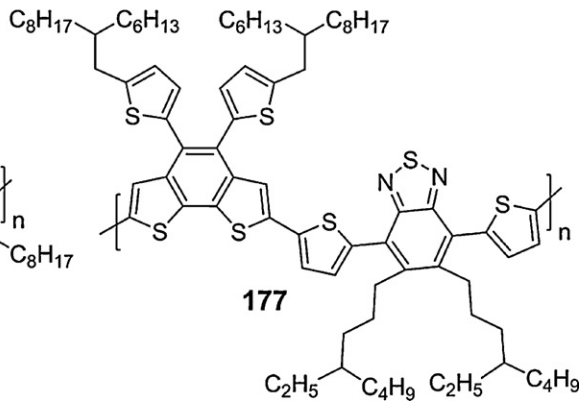

Chart 45. Chemical structures of the poly(benzo[2,1-*b*:3,4-*b*′]dithiophene) derivatives **174**–**176** consisting of TBzT segments.

chains at the 4-positions on the thiophene rings of the TBzT. Hence, the extended conjugation of the non-alkylated TBzT polymer derivative (**174**) is maintained [197]. Moreover, the introduction of the two thiophene rings around the 2,1,3-benzothiadiazole raise the HOMO level of **174** as compared to that of **173** (5.34 eV) due to the increased electron density in the polymer backbone. A small variation between **174** and **176** is observed on their LUMO levels (the LUMO of **176** is raised by 0.18 eV). On the contrary, when the alkyl side chains are located at either the 3-positions on the thiophene rings of the TBzT (**175**) or at the 5- and 6-positions of the 2,1,3-benzothiadiazole (**177**), severe steric hindrance is formed between the thiophene rings and the central 2,1,3-benzothiadiazole, resulting in the twisting of the polymer backbone at the D–A linkage. The increased steric hindrance of both **175** and **177** results in higher optical band gaps (1.97 eV for **175** and 2.35 eV for **177**) and lower lying HOMO levels (5.38 eV for **175** and 5.69 eV for **177**) due to the reduced electron delocalization.

The photovoltaic performance of **174**–**177** was examined in blends with $PC_{61}BM$ (1:1, w/w ratio) [197]. Interestingly, **176** exhibited higher PCE (1.83%) than **174** (0.72%) due to (i) the improved solubility and the higher molecular weight (M_n = 27,000 g/mol) of **176** than that of **174** (M_n = 9000 g/mol) as a result of the presence of the side alkyl chains at the 4-positions on the thiophene rings of TBzT and (ii) the higher hole mobility (9.20×10^{-6} $cm^2/V\,s$ as measured by the SCLC method) of the **176**:$PC_{61}BM$ system compared to that of **174**:$PC_{61}BM$ (3.94×10^{-6} $cm^2/V\,s$). The higher hole mobility of **176** is attributed to the higher molecular weight in contrast to the lower molecular weight of **174** that limits the interaction between different domains, due to the shorter chains and increased number of end groups, leading to an overall suppressed mobility [197]. Further enhancement of the PCE to 2.17% for the **176**:$PC_{61}BM$ has been achieved by the addition of 3% volume ratio of 1,8-diiodooctane in the CF solution with J_{sc} = 6.38 mA/cm^2, V_{oc} = 0.67 V and FF = 0.51. The addition of the 1,8-diiodooctane led to the improvement of the thin film morphology with increased ordering of the polymer domains and as a sequence to the enhanced hole mobility to 1.60×10^{-5} $cm^2/V\,s$. On the other hand, the PCEs of both **175** (0.21%) and **177** (0.01%) were very low due to their high optical band gaps and the conjugation interruption in the polymer backbone from the severe steric hindrance between the thiophene rings and the 2,1,3-benzothiadiazole [197].

3.2.12.3. Quadrathienonaphthalene-based polymers. Another class of polycyclic aromatic polymer is the one consisting of the quadrathienonaphthalene (QTN) moiety. QTN-based conjugated polymers have been developed through the extensive research efforts of You research group in an attempt to optimize the structurally related $B_{2134}DT$-based polymers reported above. More precisely, extensive theoretical studies, using computational modelling, performed on **173** showed that the two pendant substituted thiophene rings on $B_{2134}DT$ adopt an almost orthogonal configuration to the $B_{2134}DT$ main chain weakening the efficient π–π interaction between the polymer chains, leading to the observed low hole mobilities [198].

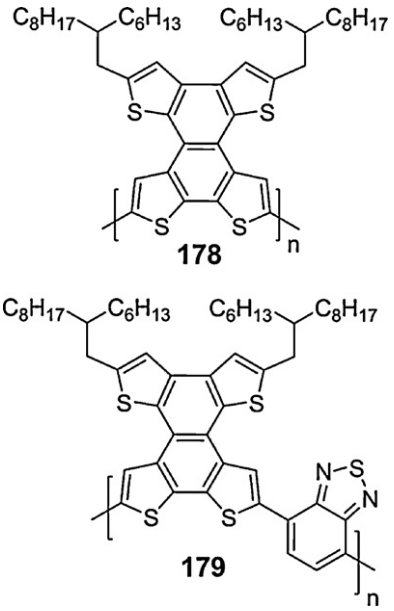

Chart 46. Chemical structures of the poly(quadrathienonaphtalene) derivatives **178** and **179**.

Thus, a simple oxidative photocyclization successfully converted the $B_{2134}DT$ with the two pendant thiophene rings into an enlarged planar polycyclic aromatic unit, the QTN. The QTN-based conjugated polymers **178** and **179** (Chart 46) have more planar structures with minimized steric hindrance as compared with the related structural analogue polymers **172** and **173**, thereby promoting the π–π interaction between the polymer chains. **178** and **179** were synthesized by Stille cross-coupling polymerization reaction and their M_n are 8000 g/mol and 6100 g/mol, respectively [198].

The optical band gaps of **178** (2.0 eV) and **179** (1.61 eV) are lower than that of the related structural homopolymer **172** and copolymer **173** by 0.3 eV and 0.17 eV, respectively. The energy levels of **178** are situated at 2.72 eV the LUMO and at 5.39 eV the HOMO, whereas those of **179** are 3.34 eV the LUMO and 5.38 eV the HOMO. It is shown that despite the incorporation of the 2,1,3-benzothiadiazole, **178** and **179** have identical HOMO levels which are similar to the HOMO of **173** (5.34 eV) and slightly raised from **172** (5.7 eV). On the contrary, the LUMO level of **179** decreases to 3.34 eV which is attributed to the intrinsic alternating D–A structure of its polymer backbone and is rather lower than that of **173** (3.16 eV). The energy levels of **178** and **179** indicate that the integration of the QTN moiety into the polymer backbone provided conjugated polymers with low lying stable HOMO levels and somewhat lower LUMO levels, especially for **179**.

The photovoltaic performance of either **178** or **179** in blends with $PC_{61}BM$ in 1:2 (w/w) ratio has been examined and PCEs of 2.03% for **178** and 2.06% for **179** have been recorded. The photovoltaic parameters of **178** are J_{sc} = 5.02 mA/cm^2, V_{oc} = 0.76 V and FF = 0.53 while those of **179** are J_{sc} = 5.69 mA/cm^2, V_{oc} = 0.72 V and FF = 0.50 [198]. The PCE of **178** is similar to **179** even though that the optical band gap of **178** is 0.4 eV higher than that of **179**. The higher

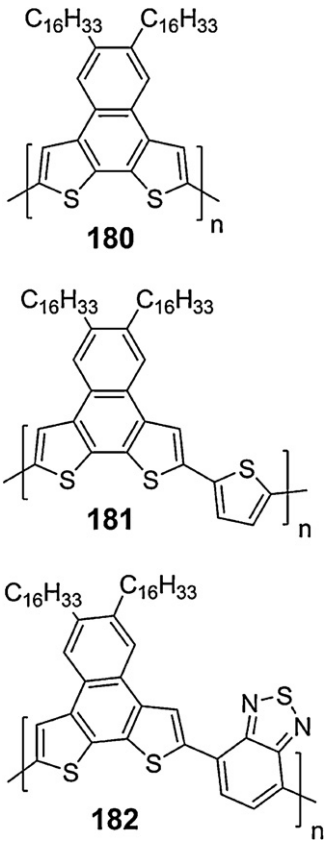

Chart 47. Chemical structures of the poly(naphtho[2,1-*b*:3,4-*b*′]dithiophene) derivatives **180**–**182**.

hole mobility of **178** (8.18×10^{-5} cm^2/V s, as measured by the SCLC method) as compared to **179** (1.28×10^{-5} cm^2/V s) is a possible reason for the similar PCE. Even though, the hole mobility of **178** is slightly lower than that of **172** (1.58×10^{-4} cm^2/V s), its PCE (2.03%) is significantly higher than that of **172** (0.1%) due to the efficiently lowering of the optical band gap. Moreover, the PCE of **179** is higher than that of **173** (0.6%) due to the simultaneously lowering of the band gap from 1.78 eV to 1.61 eV and the enhanced hole mobility. Finally, examination of the thin film morphologies of either **178** or **179** with $PC_{61}BM$ in 1:2 (w/w) by AFM, scanning electron microscopy (SEM) and TEM revealed (i) a phase segregation between $PC_{61}BM$ and **178** on the order of tens of nanometers but this phase separation is not uniform across the entire film and (ii) very homogenous microstructures with grain sizes averaging in the hundreds of nanometers for the **179**:$PC_{61}BM$ system [198].

3.2.12.4. Naphtho[2,1-b:3,4-b′]dithiophene-based polymers. Further attempts to alter the optical band gap and the energy levels of the QTN-based polymers led to the synthesis of the naphtho[2,1-*b*:3,4-*b*′]dithiophene-based homopolymer (**180**) and copolymers (**181**, **182**) consisting of the naphtho[2,1-*b*:3,4-*b*′]dithiophene alternate with a thiophene ring (**181**) or a 2,1,3-benzothiadiazole unit (**182**) (Chart 47), by Stille cross coupling polymerization [199]. Naphtho[2,1-*b*:3,4-*b*′]dithiophene (NDT) is the structural analogue of QTN moiety without the presence of the two pendant thiophene rings in the backbone.

The optical band gaps, the energy levels and the PCEs of the NDT-based polymers **180**–**182** are included in Table 25. It is shown that the optical band gap of **180** is 2.12 eV, 0.12 eV higher than that of **178**, while the band gap of **182** is 1.59 eV, almost similar to the structural related **179** (1.61 eV). The incorporation of the electron rich thiophene ring in **181** results with a slightly lower band gap (2.05 eV) as compared to **180**. Regarding the energy levels, it is shown that the HOMO levels of **180** and **182** are similar, while the LUMO level of **182** is significantly lower than that of **180** due to the insertion of the electron deficient 2,1,3-benzothiadiazole. Thus, the decrease of the band gap of **182** as compared to **180** is mostly attributed to the lowering of the LUMO level. Moreover, the insertion of the thiophene ring in the polymer backbone of **180** elevates the HOMO level of **181** in greater extent than the lowering of the LUMO level. Furthermore, comparing the energy levels between **178** and **180**, as well as between **179** and **182**, a general observation is that by switching from the QTN based polymers to the NDT based polymers both the HOMO and LUMO levels are raised, but the upshift of the LUMO level is more obvious than that of the HOMO level. In detail, the difference on the HOMO level of **182** (5.35 eV) with that of **179** (5.38 eV) is negligible (only 0.03 eV), while the difference between their LUMO levels are 0.24 eV. Considering that both copolymers consisting of the same electron deficient unit (2,1,3-benzothiadiazole), a possible explanation for the lower LUMO of **179** can be the higher electron affinity of the QTN as compared to NDT. This is rather unexpected, since that QTN has two pendant thiophene rings in the backbone. Strong evidence that verifies the above assumption is the lower LUMO level of **178** as compared to **180**.

Blends of all three polymers with $PC_{61}BM$ were prepared and their photovoltaic performance was examined by fabricating BHJ solar cells [199]. PCE of 1.27% was obtained for **182**:$PC_{61}BM$ in 1:4 (w/w) ratio with J_{sc} = 2.90 mA/cm^2, V_{oc} = 0.83 V and FF = 0.53. The PCE of **182** is lower compared to **179** (2.06%), however the V_{oc} is more than 0.1 V higher, despite the similar HOMO levels, and the FF is slightly improved. The limiting factor preventing **182** towards higher PCE is the low J_{sc} most likely due to the low hole mobility (6.23×10^{-6} cm^2/V s as measured by the SCLC method), which is almost one order of magnitude lower than **179** (1.28×10^{-5} cm^2/V s). In addition, the low M_n value of **182** (9000 g/mol) can be also one of the reasons for the low hole mobility.

3.2.12.5. Dithieno[3,2-b:2′,3′-e]pyridine-based polymers. Dithieno[3,2-*b*:2′,3′-*e*]pyridine (DTPy) is structurally similar to $B_{2134}DT$ having a central pyridine core instead of a benzene ring. Two alternating DTPy-based conjugated polymers (Chart 48) consisting either with electron-rich thiophene ring (**183**) or electron-deficient 2,1,3-benzothiadiazole (**184**) have been synthesized by Stille and Suzuki cross-coupling polycondensation reactions, respectively [200]. The measured molecular weights of **183** (M_n = 4300 g/mol) and **184** (M_n = 1500 g/mol) are very low, which is attributed to the lower solubility

Table 25
Optical band gaps, energy levels and photovoltaic efficiency of **180**–**182**.

Polymers	E_g^{opt} (eV)	LUMO (eV)	HOMO (eV)	PCE (%)
180	2.12	2.57	5.33	0.56
181	2.05	2.63	5.20	1.18
182	1.59	3.10	5.35	1.27

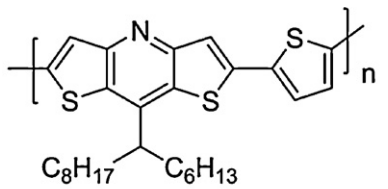

183

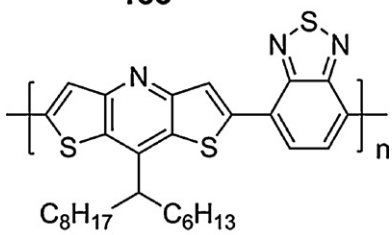

184

Chart 48. Chemical structures of poly(dithieno[3,2-*b*:2′,3′-*e*]pyridine) derivatives **183** and **184**.

during the polymerization reactions, and preventing the formation of high quality films.

The optical band gaps of **183** and **184** are 2.3 eV and 2.1 eV, respectively. The band gap of **183** is higher than that of **149** (2.06 eV), while similar behaviour is observed comparing the band gap of **184** with those of the related polymers **152** (1.70 eV) and **173** (1.78 eV). The higher band gaps of **183** and **184** are attributed to the presence of the more electron-deficient pyridine instead of the benzene ring into the bithiophene matrix, which weakens the electron donating ability of the DTPy moiety or diminishes the D–A interaction especially in **184** [200]. The energy levels of **183** are 2.97 eV (LUMO) and 5.43 eV (HOMO) and those of **184** are 3.33 eV (LUMO) and 5.56 eV (HOMO). The HOMO of **184** is lying deeper by 0.22 eV as compared to that of **173** due to the less electron donating ability of the DTPy unit.

The PCEs of **183**:$PC_{61}BM$ in 1:3 (w/w) ratio or **184**:$PC_{61}BM$ in 1:1 (w/w) ratio are 0.27% and 0.09%, respectively. The photovoltaic parameters of **183** are J_{sc} = 1.93 mA/cm^2, V_{oc} = 0.41 V and FF = 0.34 while those of **184** are J_{sc} = 0.75 mA/cm^2, V_{oc} = 0.31 V and FF = 0.37 [200]. The obtained V_{oc}s are significantly lower than the theoretically expected based on their low lying HOMO levels. Their poor photovoltaic performance can be attributed in part on the high optical band gaps as well as their low molecular weights which in combination with the bulky alkyl chains lead to very low hole mobilities (3.55×10^{-6} cm^2/V s for **183** and 2.55×10^{-6} cm^2/V s for **184** as measured by the SCLC method).

3.2.13. Bridged biphenylenes with 5-member fused aromatic rings in the central core

3.2.13.1. Fluorene-based polymers. It is envisioned that fluorene unit, which is a rigid and planar molecule with associated low HOMO energy levels, can emerge as an attractive building block for the design of new conjugated polymers acting as electron donors for photovoltaic applications due to the fact that the low-lying HOMO levels and the high hole mobilities of the polyfluorene (PF) derivatives are expected to provide higher V_{oc} and J_{sc}, respectively [201]. However, PFs exhibit optical band gaps in the range of 2.8–3.0 eV which are too high for efficient OPVs. Therefore, extensive research efforts towards the development of PF copolymers with lower optical band gaps were performed following two major approaches [202]. The first approach is based on the copolymerization of the fluorene unit with more electron rich compounds and the second approach is based on the incorporation of donor–acceptor–donor (DAD) segments in the PF chain in order to form a D–A alternating arrangement and hence narrowing the band gap.

3.2.13.1.1. Polyfluorene copolymers with electron-rich groups. Electron-rich compounds such as thiophene (**185**) [203], bithiophene (**186**–**187**) [204,205], thieno[3,2-*b*]thiophene (**188**–**190**) [206], substituted silole (**191**) [207], pentacene (**192**) [208] and anthradithiophene (**193**) [208] have been successfully copolymerized with the fluorene unit (Chart 49), providing LBG PF derivatives (Table 26). Comparing the optical band gaps of **185**, **186** and **188**, it is revealed that by switching the thiophene unit in **185** with the bithiophene unit in **186** the band gap remains unaltered (Table 26), while the band gap of **188** (2.54 eV) is higher than that of **186** (2.40 eV). Since the fused thieno[3,2-*b*]thiophene is more rigid and planar than bithiophene is expected the band gap of **188** to be lower than that of **186** due to closer π–π stacking of the polymer chains. However, the opposite happens. This result indicates a reduced electron delocalization in the presence of thieno[3,2-*b*]thiophene which may be related to the larger resonance energy of the fused thiophene ring, in comparison to bithiophene [131,206]. Moreover, the presence of the β-alkyl chain on thieno[3,2-*b*]thiophene in **189** and **190** results with higher optical band gaps (∼0.2 eV as compared to **188**) since that increased steric repulsion is formed between the pentyl or the undecyl side chains on thieno[3,2-*b*]thiophene with the hexyl side chains from fluorene unit. In addition, further decrease of the band gap of PF derivatives is achieved by incorporating a substituted silole unit between two thiophene rings in **191** (2.08 eV) or by introducing five-fused-ring acene systems such as pentacene (**192**) or anthradithiophene (**193**). **192** and **193** are the first examples of soluble acene-based PF copolymers with low band gaps (1.78 eV and 1.98 eV, respectively).

Table 26
Optical band gaps, energy levels and photovoltaic efficiency of **185–193**.

Polymers	E_g^{opt} (eV)	LUMO (eV)	HOMO (eV)	PCE (%)
185	2.43	2.51	5.20	0.62
186	2.41	2.52	5.41	2.70
187	2.40	3.10	5.50	2.14
188	2.54	2.58	5.27	–
189	2.74	2.42	5.12	–
190	2.78	2.35	5.15	–
191	2.08	3.60	5.71	2.01
192	1.78	3.56	5.20	–
193	1.98	3.31	5.22	0.68

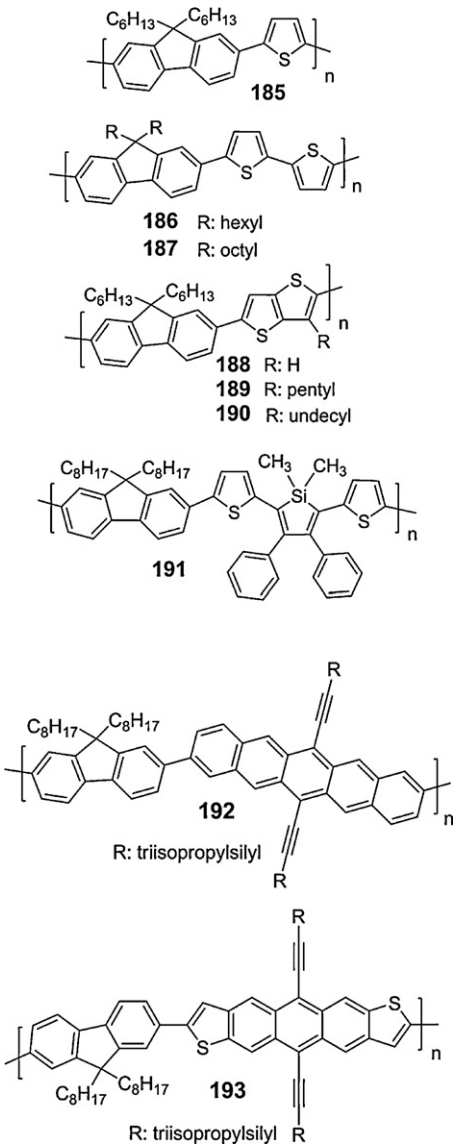

Chart 49. Chemical structures of the polyfluorene derivatives **185–193** consisting of electron-rich moieties.

Regarding the energy levels, it is shown that the addition of one more thiophene ring in **185** has no effect on the LUMO level of **186**, but the HOMO level of **186** unexpectedly presents a significant lowering of 0.21 eV (Table 26). On the other hand, by replacing the thiophene ring of **185** with the thieno[3,2-*b*]thiophene in **188** both the HOMO and LUMO levels are slightly lowering by 0.07 eV. This result points out that the presence of the unsubstituted bithiophene in **186**, which possess some rotational freedom, disrupts the π-conjugation to an extent that imparts sufficient oxidative stability to the system [204–206]. Moreover, the HOMO and the LUMO levels of **189** are upshifted by ~0.15 eV upon alkylation on the thieno[3,2-*b*]thiophene. On the contrary, upon increase the length of the alkyl side chain in **190** (undecyl side chain), the HOMO level remains unaltered as compared to **189** but the LUMO level is further raised by 0.07 eV. Although the alkylation on the thieno[3,2-*b*]thiophene disrupts the planarity between the fluorene and the thieno[3,2-*b*]thiophene unit as reported above, the upshift of the HOMO levels of **189** and **190** remains unclear. Furthermore, lowering of both HOMO and LUMO levels is observed by using the 3,4-diphenylsilole unit between the two thiophene rings in **191** (Table 26). The low-lying LUMO level of **191** is associated with the presence of the 3,4-diphenylsilole and more precisely with the σ^*–π^* conjugation along the polymer chain arising from the interaction between the σ^* orbital of two exocyclic σ bonds on the silicon atom and the π^* orbital of the butadiene moiety [207]. Finally, it is demonstrated that the anthradithiophene-based PF derivative **193** has lower electron affinity than the pentacene-based PF copolymer **192** since that the LUMO levels of **192** and **193** are 3.56 eV and 3.31 eV, respectively, whereas their HOMO levels are similar (Table 26).

BHJ solar cells were prepared based on blends of **185–193** with fullerene derivatives. PCE of 2.70% was obtained from the **186**:$PC_{61}BM$ system in 1:4 (w/w) ratio with J_{sc} = 4.96 mA/cm^2, V_{oc} = 1.03 V and FF = 0.53 [204], whereas the PCE of blends of the longer alkyl chain analogue **187**:$PC_{61}BM$ in 1:2 (w/w) ratio is lower (2.10%, upon annealing at 70 °C) with J_{sc} = 4.24 mA/cm^2, V_{oc} = 0.99 V and FF = 0.51 [205]. Even though the hole mobility of **187** is higher (10^{-7} cm^2/V s, based on the SCLC model) than that of **186** (3×10^{-8} cm^2/V s, based on SCLC model), the finer nanophase separated network for the **186**:$PC_{61}BM$ is responsible for the improved photovoltaic performance. Finally, PCE over 2.0% was presented for **191**:$PC_{61}BM$ in 1:4 (w/w) ratio with J_{sc} = 8.67 mA/cm^2, V_{oc} = 0.65 V and FF = 0.36 [207], while the anthradithiophene-based PF derivative **193** in blends with $PC_{61}BM$ in 1:3 (w/w) ratio exhibits a PCE of 0.68% with J_{sc} = 2.35 mA/cm^2, V_{oc} = 0.75 V and FF = 0.39 [208]. On the other hand, the devices based

on the pentacene copolymer **192** were shorted, hence extremely poor PCEs were attained.

3.2.13.1.2. Polyfluorene copolymers with donor–acceptor–donor (DAD) segments. PF copolymers incorporating a DAD segment are the most popular group of materials for solar cell applications because they can be synthesized easily since that the diboronic diakylated fluorene derivatives which provide the broad energy gap, the hole mobility and the high V_{oc} are commercially available in high quantities, while the DAD segment can be easily modified to provide the lowering of the band gap. Among the various PF derivatives, the most extensively studied is the one consisting of the TBzT segment as the DAD moiety (Chart 50). A plethora of TBzT-based PF copolymers have been synthesized by Suzuki cross-coupling polymerization, which the majority of them varied regarding the type (linear versus branched) and length of the alkyl side chains attached on the fluorene unit (**194**–**204**) [209–214] and less attention has been paid to the strength of the donor (**205**–**208**) [215–217].

The optical band gaps of **194**–**200** vary as a function of the length of the alkyl side chains. **194** and **200** reveal band gaps of 1.95 eV [209], **195** and **198**–**199** of 1.90 eV [209,211] and **197** of 1.87 eV [209]. Regarding the energy levels, the HOMO level of **195** and **198**–**199** is 5.5 eV [211,213], while the LUMO level of both **195** and **198** is 3.4 eV [202,211], showing that the different alkyl chains do not significantly affect the band gap and the energy levels of the polymers. However, the unsubstituted TBzT segment is a limiting factor preventing copolymers **194**–**200** of achieving high molecular weights and good solubilities, two very important parameters influencing the PCE of solar cells as reported above. Thus, two PF derivatives consisting of a dioctylfluorene and a functionalized TBzT segment with hexyl side chains at the 4-position (**201**) or octyloxy side chains at the 3-position (**202**) have been prepared [212–214], exhibiting very high molecular weights (M_n of 175,000 g/mol for **201**) and improved solubilities in common organic solvents. The anchoring of hexyl side chains at the 4-position of TBzT in **201** leads to a slight increase of the band gap at 1.97 eV as compared to **195**, while the band gap of **202** is 1.78 eV. The band gap of **202** is lower than that of **201**, despite the presence of substituents at the 3-position on the thiophene of the TBzT that is known to cause severe steric hindrance (see **175** and **176**). This is attributed to the stronger electron donating ability of the alkoxy side chains. Furthermore, the HOMO level of **201** is displayed at 5.6 eV, which is 0.1 eV lower than that of **195**, whereas the HOMO and LUMO levels of **202** are 5.14 eV and 3.36 eV, respectively. Comparing the HOMO and LUMO levels values of **202** with those of **195** is demonstrated that the HOMO level of **202** is raised by 0.36 eV upon substitution with the alkoxy side chains on the TBzT segment, as expected, while the LUMO levels are almost similar, indicating that the LUMO level is localized on the 2,1,3-benzothiadiazole. Finally, changing the position of the alkoxy side chains from the thiophene rings to the 2,1,3-benzothiadiazole and use two different linear alkyl side chains (methyl and octyl) on the fluorene unit (**203**–**204**) [213], the band gap of **204** is estimated at 2.01 eV, which is 0.23 eV higher than that of the structural related analogue **202**. It seems that the insertion of the electron donating octyloxy side chains on the 2,1,3-benzothiadiazole weaken the electron-withdrawing ability of the 2,1,3-benzothiadiazole and thereby facilitating the increase of the band gap. The use of the shorter alkyl side chains on the fluorene in **203** leads to lower band gap (1.96 eV), due to the more efficient π–π stacking between the polymer chains. Besides, the positioning of the octyloxy side chains on the 2,1,3-benzothiadiazole in **204** results to deeper HOMO value (5.5 eV) as compared to **202**, while the HOMO level of **203** is situated at 5.4 eV.

Up to now the most common electron rich unit used as donor along with 2,1,3-benzothiadiazole in the DAD sequence is thiophene ring. Except from thiophene, some other electron donor units such as diphenylamine with and without methyl group (**205**–**206**) [215], ProDOT (**207**) [216], and selenophene (**208**) [217] have also been employed. The band gaps of **205**–**206** are 1.99 eV and 1.98 eV, respectively while the band gaps of **207** and **208** are varying as a function of the content of the DAD segment. For example, the band gap of **207** gradually decreases from 1.88 eV to 1.73 eV by increasing the content of the ProDOT-[2,1,3]-benzothiadiazole-ProDOT (PBzP) segment up to 35%. Similar to **207**, the band gap of **208** decreases from 2.92 eV to 1.85 eV as the content of the selenophene-[2,1,3]-benzothiadiazole-selenophene (SBzS) increases up to 30%. Moreover, the HOMO levels of **205**–**206** are similar (5.04 eV and 5.03 eV, respectively), while the LUMO level of **205** is 2.74 eV, 0.04 eV lower than that of **206** (2.78 eV). Regarding the energy levels of **207** and **208**, the HOMO level of both copolymers is raised upon increase the content of PBzP and SBzS, respectively. For example, the HOMO level of **207** with 10% of PBzP is 5.39 eV while upon increasing the content of the PBzP segment to 35% the HOMO level is 5.16 eV. Similar to **207**, the HOMO level of **208** with 1% of SBzS is 5.70 eV and that with 30% of SBzS is 5.51 eV. On the other hand, the LUMO level of **208** with 1% of SBzS is 2.13 eV, while the LUMO of **208** with 30% of SBzS is 2.76 eV showing that upon increasing the content of the SBzS lowering of the LUMO level is detected.

In order to further alter the band gap and the energy levels of the D–A PF copolymers, the 2,1,3-benzothiadiazole has been replaced by various heterocycle units (Chart 51) including: thieno[3,4-*b*]pyrazine (TP) (**209**–**211**) [218–220], thieno[3,4-*c*][1,2,5]thiadiazole (**212**–**214**) [221], [1,2,5]thiadiazolo[3,4-*g*]quinoxaline (**215**–**217**) [222–225], quinoxaline (**218**–**222**) [219,226–229] and pyrazino[2,3-*g*]quinoxaline (**223**) [230]. All the polymers have been synthesized by the Suzuki cross-coupling polymerization and their optical, electrochemical and photovoltaic properties are presented in Table 27.

Generally, it is demonstrated that the optical band gap of the [1,2,5]thiadiazolo[3,4-*g*]quinoxaline (1.2–1.4 eV), thieno[3,4-*c*][1,2,5]thiadiazole (1.34–1.36 eV) and pyrazino[2,3-*g*]quinoxaline (1.4 eV) based PF derivatives are in the same range and lower than that of the TP (1.6 eV) and quinoxaline (1.9–1.96 eV) based PF derivatives. The band gaps of the TP, quinoxaline and thieno[3,4-*c*][1,2,5]thiadiazole based PF copolymers remain almost unaltered regardless the length and the position of the side alkyl chains in the polymer backbone while the band gaps of the PF derivatives with the [1,2,5]thiadiazolo[3,4-

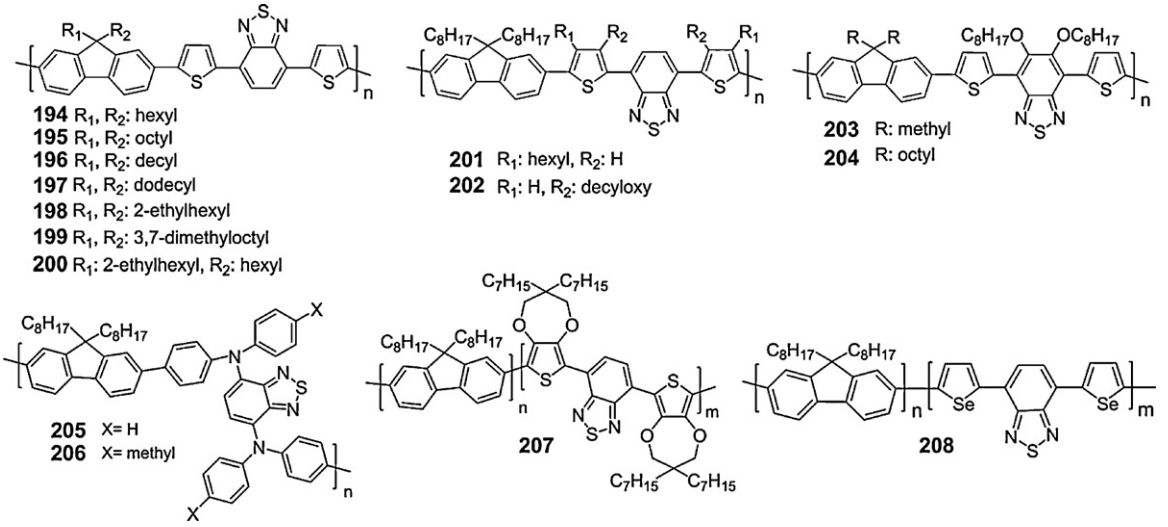

Chart 50. Chemical structures of the polyfluorene derivatives **194**–**208** consisting of various donor–[2,1,3]-benzothiadiazole–donor segments.

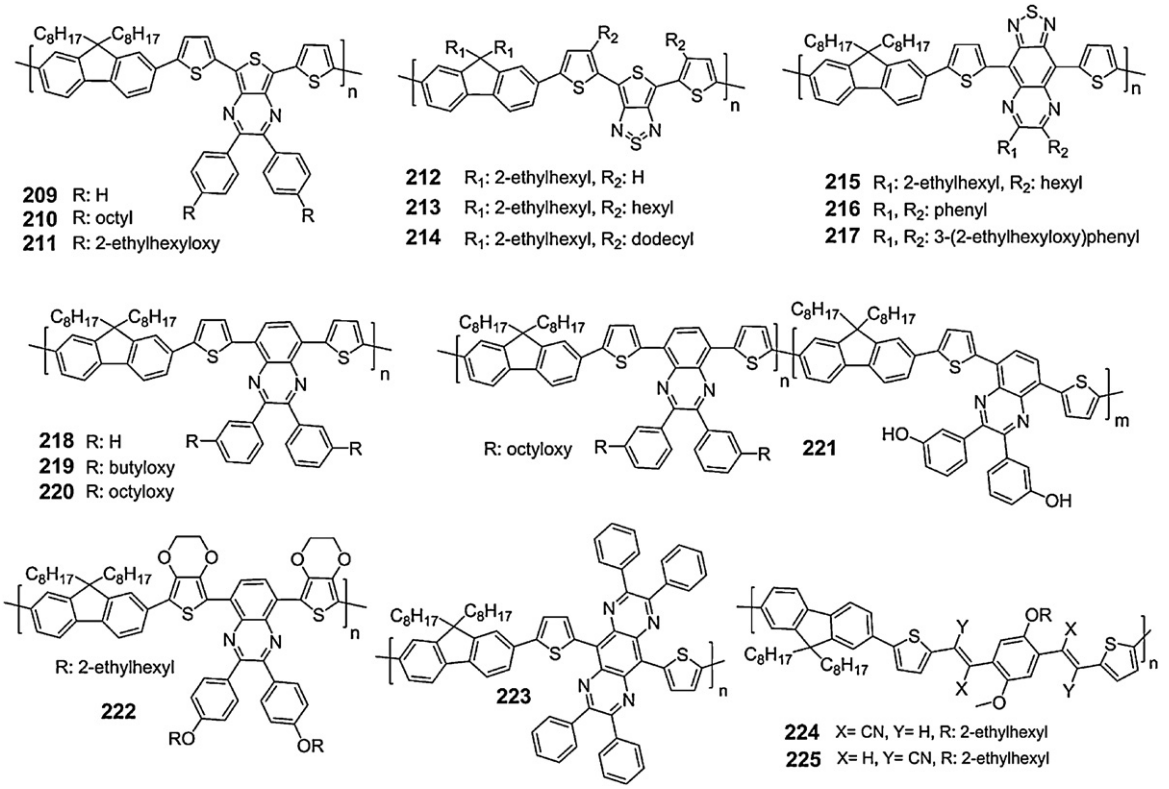

Chart 51. Chemical structures of the polyfluorene derivatives **209**–**225** consisting of various donor–acceptor–donor segments.

g]quinoxaline are varied based on the type of substituents (alkyl versus aryl) attached on the [1,2,5]thiadiazolo[3,4-*g*]quinoxaline unit (Table 27). Furthermore, comparing the band gap of **222** with those of **218**–**220** it is expected that the band gap of **222** being lower than that of **218**–**220** due to the stronger electron donor used (EDOT). However it seems that the position of the alkoxy chains on the phenyl rings of the quinoxaline unit affect the strength of the electron-deficient unit. For example, when the alkoxy groups are placed on the *para* position on the phenyl rings of the quinoxaline (**222**), weakening of the strength of the electron accepting unit will be performed through electron donation from the alkoxy groups into the quinoxaline. In contrast, the electron donation from the alkoxy group into the quinoxaline unit is avoided when the alkoxy groups are placed on the *meta* position of the phenyl

rings. Regarding the energy levels, it is shown that the LUMO levels of [1,2,5]thiadiazolo[3,4-*g*]quinoxaline and pyrazino[2,3-*g*]quinoxaline PF derivatives are lying lower (3.9–4.0 eV) than that of the other copolymers consisting of TP or thieno[3,4-*c*][1,2,5]thiadiazole (3.5–3.7 eV) and quinoxaline (3.3–3.45 eV).

Finally, two alternating D–A PF derivatives (**224**–**225**) consisting of cyano substituted phenylene vinylene segments inserted between two thiophene rings were synthesized and their optical band gaps were found to be depended on the relative position of the cyano groups [231]. When the cyano groups are located in the α-position (**225**), the band gap is lower (1.95 eV) than that of **224** (2.21 eV), where the cyano groups are located at the β-position because the aromatic subunits exhibit weaker torsion (Table 27). However, no significant variation on the HOMO levels of **224** and **225** is detected regarding the relative position of the cyano groups.

The photovoltaic performance of the DAD PF copolymers was evaluated in BHJ solar cells using various fullerene derivatives as the electron acceptors. The first and most extensively studied derivatives are those consisting of the TBzT as the DAD segment. The initial PCE of **200** with $PC_{61}BM$ in 1:4 (w/w) ratio was 2.4% [232] while upon optimization, a PCE of 4.5% was recorded from the **199**:$PC_{71}BM$ in 1:4 (w/w) with J_{sc} = 9.1 mA/cm^2, V_{oc} = 0.97 V and FF = 0.51 [211]. The balanced carrier transport in the active layer (electron and hole mobilities of 7×10^{-5} and 3×10^{-5} cm^2/V s, respectively based on the SCLC method) is one of the factors for this high efficiency. In addition, a PCE very close to 4.5% has been also recorded from **196** (4.2%) when blended with $PC_{61}BM$ in 1:4 (w/w), with J_{sc} = 7.7 mA/cm^2, V_{oc} = 0.99 V and FF = 0.54 [210]. Among the other TBzT based PF derivatives, **204** exhibits a PCE above 3% (3.1%) when blended with $PC_{71}BM$ in 1:3 (w/w) with J_{sc} = 6.7 mA/cm^2, V_{oc} = 0.97 V and FF = 0.47, using DCB as the solvent [213]. Changing the solvent from DCB to CF, the PCE of **204** decreases to 2.1%, as a result of the increased phase separation (about 200 nm domains) observed in the morphology of **204**:$PC_{71}BM$ by AFM.

Up to now, it is evident that the combination of the TBzT segment and fluorene provides copolymers that exhibit high PCEs when used as electron donors in BHJ solar cells. However, in recent studies the use of quinoxaline instead of the 2,1,3-benzothiadiazole as the electron withdrawing unit in the DAD sequence demonstrates even higher PCEs than the 2,1,3-benzothiadiazole based PF copolymers. For example, an impressive PCE of 5.5% has been recorded from devices based on **218**:$PC_{71}BM$ (1:4, w/w) as the active layer, that were processed from a solvent mixture of CB and CF, with J_{sc} = 9.72 mA/cm^2, V_{oc} = 0.99 V and FF = 0.57 [226]. On the contrary, **218**:$PC_{71}BM$ (1:4, w/w) devices prepared from CF solutions provided PCE as high as 2.90%. Except from the different solvent used for the deposition of the active layers, the M_n values of **218** were also different. The M_n of **218** that exhibits the higher PCE is 16,600 g/mol, while the batch of **218** with the lower PCE has a M_n of 8400 g/mol. Furthermore, the octyloxy substituted quinoxaline PF copolymer **220** exhibits also a promising PCE of 3.5% when blended with $PC_{61}BM$ (75 wt%) with J_{sc} = 6.0 mA/cm^2, V_{oc} = 1.00 V and FF = 0.63 [227,228]. The origin of the high V_{oc} and FF are the suitable mismatch of the energy levels and the balanced hole and electron transport in **220**:$PC_{61}BM$ films, respectively. From the rest of the electron-deficient units used in the DAD segment, the TP and pyrazino[2,3-*g*]quinoxaline based PF copolymers exhibit moderate PCEs (above 2%; Table 27). In details, the PCEs of **209**–**211** with $PC_{61}BM$ are varying between 0.9%, for **209**:$PC_{61}BM$ in 1:6 (w/w) [218], to 2.2%, for **211**:$PC_{61}BM$ in 1:3 (w/w) with J_{sc} = 8.8 mA/cm^2, V_{oc} = 0.59 V and FF = 0.42 [220]. The reason for this difference in PCE is that the hole mobility of **209** is $\sim 8 \times 10^{-6}$ cm^2/V s and that of **211** is $\sim 8 \times 10^{-4}$ cm^2/V s. This two orders of magnitude increase in the hole mobility of **211** has a significant effect on J_{sc} value and consequently on the PCE of the solar cells [218,220]. In addition, the PCE of **223**:$PC_{71}BM$ in 1:3 (w/w) is 2.3% with J_{sc} = 6.5 mA/cm^2, V_{oc} = 0.81 V and FF = 0.44 [230]. However, one of the advantages of **223** is that exhibits a remarkable high V_{oc}, especially for such low band gap polymer (1.4 eV), due to the optimized HOMO and LUMO levels. Based on these properties, **223** has already been used with great success in tandem solar cells, along with **195**, providing an extremely high V_{oc} of 1.8 eV [230,233].

On the contrary, the lower band gap PF copolymers consisting of the [1,2,5]thiadiazolo[3,4-*g*]quinoxaline as the electron-withdrawing unit (**215**–**217**) show very poor PCEs when combined with either the $PC_{61}BM$ or $PC_{71}BM$ [225]. Photoluminescence experiments between **215**–**217** and $PC_{61}BM$ indicate no quenching of photoluminescence, indication of inefficient charge separation at their interface. For this reason, a new C_{70} fullerene derivative was synthesized (Chart 52) that can absorbs light up to ~700 nm and when it is blended with **215**–**217**, efficient photoluminescence quenching is detected [224]. The proper

Table 27
Optical band gaps, energy levels and photovoltaic efficiency of **209**–**225**.

Polymers	E_g^{opt} (eV)	LUMO (eV)	HOMO (eV)	PCE (%)	Polymers	E_g^{opt} (eV)	LUMO (eV)	HOMO (eV)	PCE (%)
209	–	3.6	5.6	0.96	**218**	1.95	3.43	5.56 [227]/5.37 [226]	2.90 [227]/5.50 [226]
210	1.6	3.7	5.7	1.40	**219**	1.96	3.44	5.61	2.90
211	1.6	3.4	5.0	2.20	**220**	1.96	3.43	5.69 [227]/5.36 [226]	3.50
212	1.34	3.71	5.01	–	**221**	2.0	3.3	5.8	2.84
213	1.36	3.54	4.94	–	**222**	1.9	3.4	5.6	1.10
214	1.36	3.52	5.02	–	**223**	1.4	3.9	5.7	2.30
215	1.4	3.9	5.4	0.59	**224**	2.21	–	5.65	0.98
216	1.2	3.9	5.1	0.70	**225**	1.95	–	5.59	1.02
217	1.3	4.0	5.3	0.37					

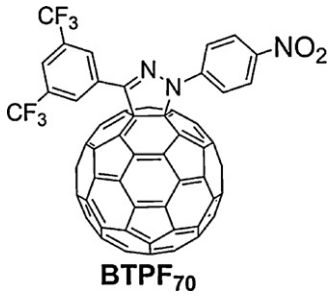

Chart 52. Chemical structure of the C_{70} derivative $BTPF_{70}$.

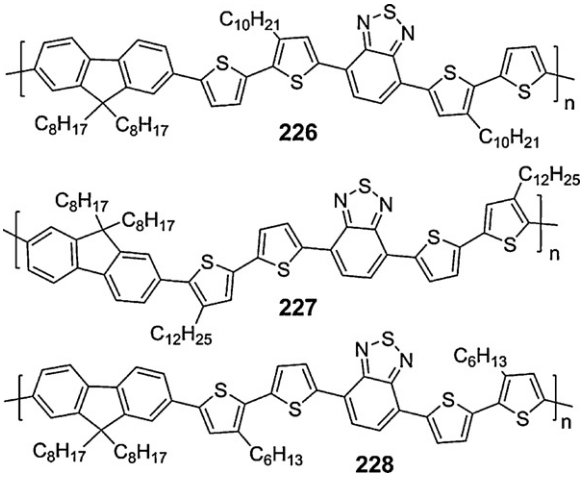

Chart 53. Chemical structures of the polyfluorene derivatives **226**–**228**.

alignment of the energy levels and the suitable morphology between **215**–**217** and $BTPF_{70}$ are two of the reasons for the enhanced driving force for charge separation. The highest PCE obtained from the blends of **215**–**217** and $BTPF_{70}$ is 0.7% for **216** [223,224] (in 1:4, w/w ratio), with J_{sc} = 3.4 mA/cm^2, V_{oc} = 0.58 V and FF = 0.35.

Finally, alternative attempts of further lowering the band gap of the TBzT based PF derivatives without replacing the 2,1,3-benzothiadiazole with another heterocycle unit led to the synthesis of three new PF copolymers (**226**–**228**) [234] consisting of 2,1,3-benzothiadiazole and four thiophene rings substituted with alkyl side chains at different positions (Chart 53). The polymers were synthesized by Suzuki cross-coupling polymerization and their optoelectronic properties and photovoltaic performance are summarized in Table 28.

As expected, the optical band gaps of **226**–**228** are lower than that of the TBzT based PFs (**194**–**202**) and are slightly influenced by the positioning of the side alkyl chains. In addition, the HOMO and LUMO levels of **226**–**228** are not varying remarkably by the different positioning of the alkyl side chains (Table 28). When the alkyl side chains are attached on the thiophene rings next to the 2,1,3-benzothiadiazole (**226**) the HOMO level is deeper than that of **227**–**228** where the alkyl side chains are inserted on the outer thiophene rings (next to the fluorene). Moreover, the HOMO level of **227** is 0.3 eV higher than **228**, indicating that when the dodecyl side chains on the thiophene rings are located next to the fluorene, the effective conjugation length is slightly lower as compared to **228**, where the hexyl side chains on the thiophene rings are attached closer to the 2,1,3-benzothiadiazole. On the other hand, the LUMO level of **228** is lying lower by 0.5 eV as compared to **227** pointing out that the positioning of the hexyl side chains on the thiophene rings close to the 2,1,3-benzothiadiazole enhance the electron affinity of the resulting polymer.

Even though, the different positioning of the alkyl side chains does not alter significantly the optical band gaps and the energy levels of **226**–**228**, the PCEs of the copolymers present vast variation (Table 28). **228** when blended with $PC_{61}BM$ in 1:2 (w/w) ratio exhibits the highest PCE of 2.63% with J_{sc} = 5.86 mA/cm^2, V_{oc} = 0.86 V and FF = 0.52 [234], while the similar analogue **227** blended with $PC_{61}BM$ in 1:2 displays a lower PCE of 0.7% with J_{sc} = 2.80 mA/cm^2, V_{oc} = 0.70 V and FF = 0.38. A possible reason for this variation in the PCE between **227** and **228** can be the different M_n. **227** has a M_n of 9000 g/mol, while **228** has a M_n of 62,000 g/mol [234].

3.2.13.1.3. Polyfluorene copolymers with donor–πbridge–acceptor side chains. As shown in the previous paragraph, the optical band gap of various PF copolymers with alternating electron-rich and -deficient units along their backbones can be readily tuned by controlling the ICT from the donors to the acceptors. However, in order to ensure efficient processability and charge transporting properties in this linear D–A polymers, the molecular interactions and packing orientation of the conjugated moieties need to be designed properly. On the other hand, one possible strategy for improving the properties of the active materials is the use of two-dimensional conjugated polymers, in which the electron-deficient units are located at the ends of the side chains and connected with donors on the electron-rich PF backbone through a π-bridge like in a D–πbridged–A architecture type [203,235–237].

Based on this approach, initially two alternating copolymers consisting of thiophene–fluorene (**229**) [203] and terthiophene–fluorene (**230**) [203] with oxadiazole unit as side chains and two triphenylamine–fluorene alternating copolymers possessing pendant monocyano (**231**) [235] and dicyano (**232**) [235] acceptor groups (Chart 54) were effectively synthesized. The optical and electrochemical properties as well as the photovoltaic performance of **229**–**232** are presented in Table 29.

Comparing the optical band gap of **229** with that of **185** it is shown that **229** has higher band gap due to the steric hindrance of the bulky oxadiazole side chain, which resulted in distortion of the polymer backbone and a decrease in the effective conjugation length. However, extending the thiophene units in the conjugated main chain in **230**, significant lowering of the band gap is achieved through the increase of the effective conjugation length. The increase of the effective conjugation length is a result of the reduced steric hindrance from the oxadiazole side chain. Moreover, the band gap of **231** is 2.46 eV whereas that of **232** is slightly lower, indicating that as the strength of the acceptor increases the band gap decreases. Regarding the energy levels (Table 29), it is revealed that both the HOMO and LUMO levels of **229** are lower than that of **185**, as

Table 28
Optical band gaps, energy levels and photovoltaic efficiency of **226**–**228**.

Polymers	E_g^{opt} (eV)	LUMO (eV)	HOMO (eV)	PCE (%)
226	1.79	3.13	5.40	1.82
227	1.81	3.17	5.37	0.74
228	1.77	3.22	5.34	2.63

Table 29
Optical band gaps, energy levels and photovoltaic efficiency of **229**–**236**.

Polymers	E_g^{opt} (eV)	LUMO (eV)	HOMO (eV)	PCE (%)
229	2.62	2.60	5.34	0.03
230	2.24	2.78	5.24	1.49
231	2.46	–	5.51	0.22
232	2.39	–	5.54	0.11
233	1.87	3.43	5.30	4.74
234	1.83	3.49	5.32	2.50
235	1.76	3.50	5.26	4.37
236	1.74	3.61	5.35	3.15

expected since that the electron-withdrawing oxadiazole side chain effectively lowers the LUMO level. Additionally the disruption of the conjugation along the polymer chain weakens the electron donating ability of **229**, thereby the HOMO level lowers. Besides, the introduction of π-excessive thiophene rings in **230** resulted the raising of the HOMO level, as compared to **229** as well as to the further lowering of the LUMO level. In the case of **231** and **232**, the HOMO levels are similar indicating that the HOMO level is independent from the strength of the acceptor. Moreover, the electron coupling between the alternating triphenylamine-fluorene backbone and the different electron acceptor groups does not affect the hole generation in the bulk of the resultant polymer to a significant extent [235].

Photovoltaic cells were prepared based on blends of **229**–**232** with $PC_{61}BM$ and PCE of 1.49% was obtained from **230**:$PC_{61}BM$ in 1:1 (w/w) ratio with J_{sc} = 6.27 mA/cm^2, V_{oc} = 0.73 V and FF = 0.32 [203]. The other copolymers exhibited low PCEs most likely due to the relatively high optical band gaps (above 2.0 eV), despite the fact that all the copolymers reveal high V_{oc}s due to the low-lying HOMO levels. Moreover, the PCE of **231** is higher than that of **232**, although the band gap of **232** is lower, which can be attributed to the finer phase separation of the **231**:$PC_{61}BM$ as compared with that of **232**:$PC_{61}BM$. The significant morphological difference between the two composite polymer films suggests that chemical similarity of the carboxylic ester functionality attached to **231** and $PC_{61}BM$ can improve the miscibility between them in the composite film, thereby efficiently suppressing the tendency of the $PC_{61}BM$ molecules to phase segregate [235].

In order to further lower the optical band gap of the D–πbridged–A type copolymers, an efficient approach seems to be the increase of the conjugation length of the side chain of **232**. This is verified by the addition of the styrylthiophene, affording copolymer **233** [236] (Chart 55) which exhibits an optical band gap of 1.87 eV (Table 29). The use of the styrylthiophene strengthens the ICT character of the polymer, thereby facilitates the lowering of the band gap. In addition, by replacing the bridged carbon atom from the fluorene unit of **233** with silicon, a dibenzosilole containing copolymer **234** was obtained which displays a slightly lower band gap (1.83 eV) than that of **233**, due to the better π–π stacking between the polymer chains [237]. Furthermore, by switching from the pendant dicyano acceptor group in **233** and **234** to the stronger acceptor diethylthiobarbituric acid moiety in **235** [236] and **236** [237], the band gap further lowers at 1.76 eV and 1.74 eV, respectively. Regarding the energy levels, it is observed that the HOMO level of **233** is raised upon insertion of the electron-rich styrylthiophene segment in the side chain as compared to **232**, while the silicon substitution in **234** does not influence the HOMO level (Table 29), but lowers the LUMO level by 0.06 eV. On the other hand, both the HOMO and LUMO levels of **235** are lowered by ~0.1 eV upon substituting the bridged carbon atom of fluorene unit with silicon in **236**. In general, comparing the energy levels of **233** with **235** and **234** with **236** it is concluded that the HOMO levels remain unaltered due to their similar donor main chain, while their LUMO levels are dictated by the acceptors on the side chains.

The photovoltaic properties of **233**–**236** were studied in BHJ solar cells using $PC_{71}BM$ and it is shown that the PCEs of the fluorene-based **233** [236] and **235** [236] are higher than the dibenzosilole-based **234** and **236** (Table 29). A possible reason for the higher PCEs of **233** and **235** than those of **234** and **236** is their higher hole mobilities which are 5.27×10^{-4} cm^2/V s for **233** and 1.16×10^{-3} cm^2/V s for **235** as compared to that of **234** (1.77×10^{-4} cm^2/V s) and **236** (2.11×10^{-4} cm^2/V s), measured by the SCLC method. However, this result is different from the general view that the mobility of the silicon bridging conjugated polymers are higher than their carbon analogues, which is widely observed in linear conjugated polymers, as reported above. Moreover, **233**:$PC_{71}BM$ in 1:4 (w/w) ratio reaches a PCE of 4.74% with J_{sc} = 9.62 mA/cm^2, V_{oc} = 0.99 V and FF = 0.50 [236], which is comparable to that of the linear narrow band gap D–A PF and polydibenzosilole derivatives (will be reported next in the text). Therefore, these initial results indicate that by the further structural and device optimization for this class of materials, higher PCEs can be anticipated in the future.

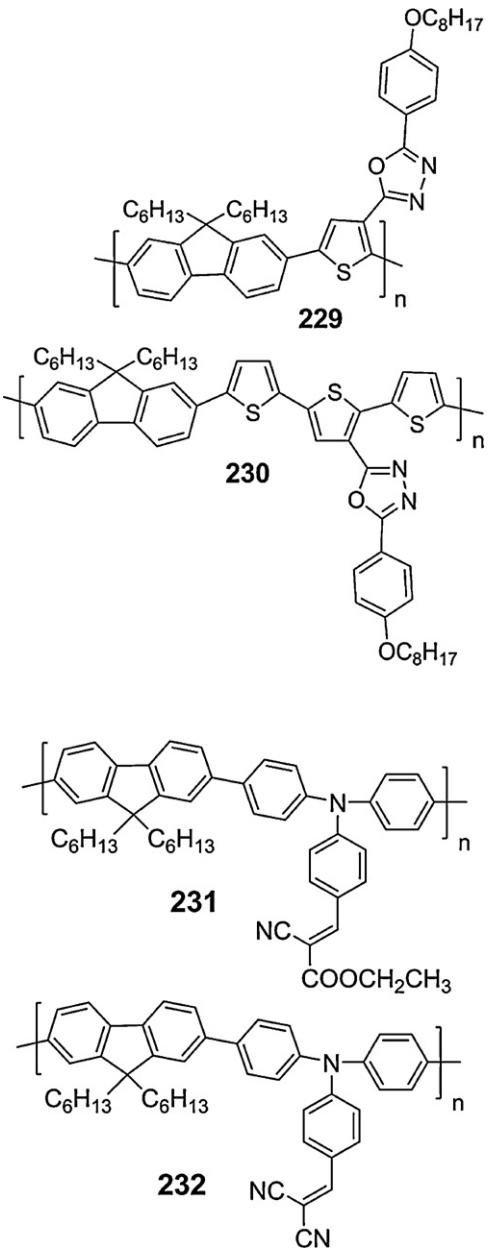

Chart 54. Chemical structures of the polyfluorene derivatives **229**–**232** consisting of donor–π bridged–acceptor side chains.

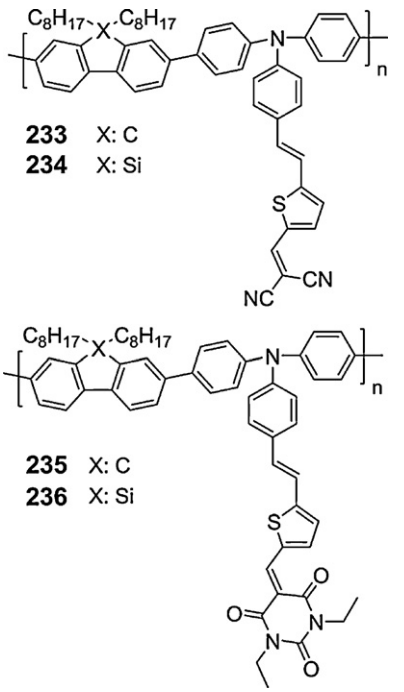

Chart 55. Chemical structures of the polyfluorene and polydibenzosilole derivatives **233**–**236** consisting of donor–π bridged–acceptor side chains.

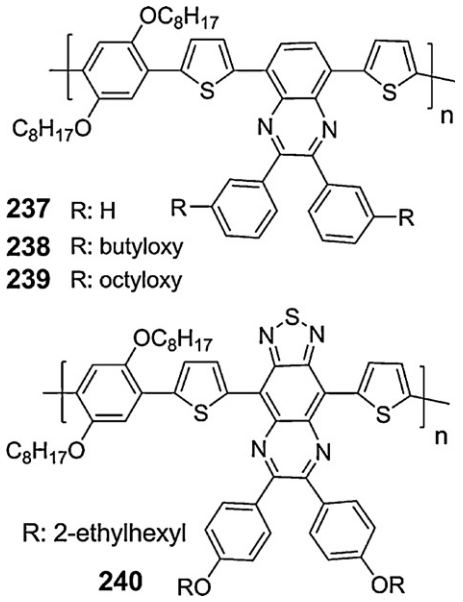

Chart 56. Chemical structures of the poly(phenylene) derivatives **237**–**240** consisting of various thiophene–electron deficient–thiophene segments.

3.2.13.2. Phenylene-based low band gap polymers. A simple structural analogue of fluorene unit is phenylene and even though it does not belong to the category of bridged biphenylenes with 5-member fused aromatic ring in the central core, the properties of some LBG conjugated polymers based on dialkoxy-phenylenes will be presented at this point and compared with the corresponding fluorene analogues before proceed to the other examples of bridged biphenylenes. The chemical structures of the copolymers **237**–**240** are presented in Chart 56, consisting of a dioctyloxy-phenylene unit alternate with various DAD segments containing thiophene rings as the donor and substituted quinoxaline (**237**–**239**) [227] or [1,2,5]thiadiazolo[3,4-g]quinoxaline (**240**) [238] as the electron deficient units and have been synthesized by Suzuki cross-coupling polymerization.

The optical band gaps and the energy levels of the polymers are presented in Table 30. The optical band gaps of **237**–**239** are 1.80 eV, which is 0.2 eV lower than that of the

Table 30
Optical band gaps, energy levels and photovoltaic efficiency of **237**–**240**.

Polymers	E_g^{opt} (eV)	LUMO (eV)	HOMO (eV)	PCE (%)
237	~1.80	3.37	5.22	0.38[a]/1.01[b]
238	1.80	3.37	5.28	1.68[a]/2.82[b]
239	1.80	3.37	5.32	2.04[a]/2.47[b]
240	1.00	3.90	5.30	0.38

[a] Using $PC_{61}BM$.
[b] Using $PC_{71}BM$.

structural related PF copolymers (**218**–**220**), and in combination with their raised HOMO levels as compared to **218**–**220**, it can be concluded that the dialkoxy-phenylene unit is more electron-rich compared to fluorene. Moreover, it is observed that regardless the length of the alkoxy substituents in the outer phenyl rings of quinoxaline, the LUMO levels of **237**–**239** remain unaltered. In addition, as the length of the alkoxy side chains increases, the HOMO level drops, indicating a decrease in the electron donating ability. Furthermore, the band gap of **240** is 1.00 eV, well below of **237**–**239**, as well as the similar PF analogue **217**. Similar with the observations on the band gaps of the **237**–**239** and **218**–**220**, the band gap of **240** is more than 0.2 eV lower than that of **217** due to the more electron-rich alkoxy-phenylene. Regarding the energy levels, the LUMO levels of **240** and **217** are the same, while the HOMO of **240** is raised by 0.1 eV as a result of the presence of the alkoxy-phenylene unit. Finally, the fact that the LUMO levels of the quinoxaline-based PF and polyphenylene copolymers are the same, indicates that the LUMO is localized on the electron-withdrawing unit. This is also verified comparing the LUMO levels of the [1,2,5]thiadiazolo[3,4-*g*]quinoxaline-based PF and polyphenylene copolymers.

BHJ solar cells using **237**–**240** and fullerene derivatives have been prepared and PCEs of 2.82% were obtained for **238**:$PC_{71}BM$ in 1:4 (w/w) ratio with J_{sc} = 6.54 mA/cm^2, V_{oc} = 0.71 V and FF = 0.60 [227]. Within the series of polymers, the length of the alkoxy substituents in the outer phenyl rings of quinoxaline play an important role in phase separation on a micrometer scale, which in turn has a large impact on device performance. The phase separation behaviour is observed in the devices with the $PC_{71}BM$ where the best performing devices are obtained using the polymers with the short alkoxy groups [227]. On the other hand when $PC_{61}BM$ is used, interestingly the PCE of **239** with the longer alkoxy side chains is higher than that of **238**.

3.2.13.3. Carbazole-based polymers.

3.2.13.3.1. Poly(2,7-carbazolenevinylene) derivatives. The optoelectronic properties of the polycarbazole derivatives, which are structurally related with PF but the two phenylene rings are bridged with a nitrogen atom instead of a carbon atom, can be fine tuned through copolymerization with various DAD segments for better mismatch with the absorption spectrum. Two approaches have been reported for lowering the band gap of polycarbazole derivatives [239]. Initially, conjugated copolymers consisting of alternating 2,7-carbazole and different oligothiophene moieties linked by vinylene groups (**241**–**245**) have been synthesized by Horner–Emmons reactions between dialdehyde and diphosphonate derivatives (Chart 57) [240].

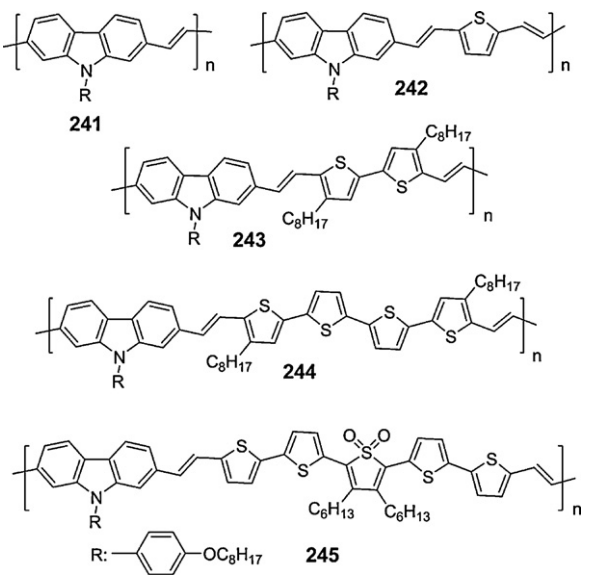

Chart 57. Chemical structures of the poly(2,7-carbazolenevinylene) derivatives **241**–**245**.

The optical band gaps and the energy levels of the polymers are presented in Table 31. The band gap of the polymers is decreasing as the number of the thiophene units increases, while the insertion of the *S*,*S*-dioxide thiophene in **245** induces a further lowering of the band gap below 2.0 eV. Moreover, all polymers are showing relatively low lying HOMO levels (5.4–5.6 eV) which decrease proportionally with the increase of the thiophene units in the main chain, except in the case of **245**. In addition, the introduction of the *S*,*S*-dioxide thiophene in **245** leads to an increase in the electron affinity as observed by its lower LUMO level. However, unoptimized PCEs of BHJ photovoltaic cells consisting of either **241**–**245** with $PC_{61}BM$ in 1:4 (w/w) ratio were relatively low. The maximum PCE obtained is 0.8% for **245** with J_{sc} = 1.56 mA/cm^2, V_{oc} = 0.80 V and FF = 0.55, due to the lack of high solubility and desired organization in the solid state [240]. Meanwhile, all the J_{sc} values of the polymers, except **245**, were in the same range indicating that the number of the thiophene units is not influencing the solar-cell performance. This shows that the mobility of the charge carriers for these copolymers is more important than that of the relatively small-variations in the fraction of the absorbed light [240].

3.2.13.3.2. Poly(2,7-carbazoles) with both electron-rich and electron-deficient units. Since that the interesting

Table 31
Optical band gaps and energy levels of **241**–**245**.

Polymers	E_g^{opt} (eV)	LUMO (eV)	HOMO (eV)
241	2.30	2.83	5.61
242	2.20	2.92	5.52
243	2.10	3.02	5.49
244	2.00	2.96	5.40
245	1.70	3.50	5.50

optoelectronic properties of polycarbazole derivatives can be easily modulated, new polycarbazole derivatives based on the D–A approach (Chart 58) were effectively designed based on theoretical models and synthesized by Suzuki cross-coupling polycondensation (**246**–**254**) [241,242]. A diboronic ester carbazole derivative containing a secondary alkyl side chain was copolymerized with nine DAD segments with thiophene ring as the fixed donor and different heterocycles as the acceptor units such as 2,1,3-benzooxadiazole (**246**) [241], [1,2,5]oxadiazolo[3,4-*d*]pyridazine (**247**) [242], 2,1,3-benzothiadiazole (**248**) [241], [1,2,5]oxadiazolo[3,4-*c*]pyridine (**249**) [241], [1,2,5]thiadiazolo[3,4-*c*]pyridine (**250**) [241], quinoxaline (**251**) [241], pyrido[3,4-*b*]pyrazine (**252**) [241], pyrazino[2,3-*d*]pyridazine (**253**) [242] and 2,3-dioctylpyrazino[2,3-*d*]pyridazine (**254**) [242].

The optical band gaps and the energy levels of the synthesized polycarbazole derivatives **246**–**254** are included in Table 32. The polymers according to their optical band gaps (starting from higher to lower), excluding the 2,3-dioctylpyrazino[2,3-*d*]pyridazine due to the fact that the band gap is also influenced by the presence of the alkyl side chains are presented. As can be seen, the band gaps follow the order: **251** > **252** > **248** > **246** > **253** > **250** > **249** > **247**. This demonstrates that the electron-withdrawing unit in the polymer backbone that efficiently lower the band gap of the studied polycarbazoles (**246**–**253**) follows the order: [1,2,5]oxadiazolo[3,4-*d*]pyridazine > [1,2,5]oxadiazolo[3,4-*c*]pyridine > [1,2,5]thiadiazolo[3,4-*c*]pyridine > pyrazino[2,3-*d*]pyridazine > 2,1,3-benzooxadiazole > 2,1,3-benzothiadiazole > pyrido[3,4-*b*]pyrazine > quinoxaline (Fig. 7a).

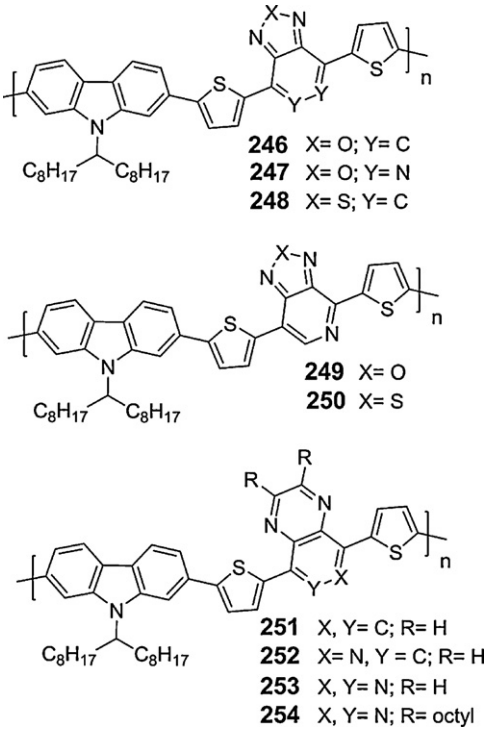

Chart 58. Chemical structures of the polycarbazole derivatives **246**–**254** consisting of various thiophene–electron deficient–thiophene segments.

On the other hand, a very interesting trend can be observed as derived from the results of the energy levels of the polycarbazole derivatives (**246**–**253**). Based on the LUMO level values presented in Table 32, the acceptor strength of the different heterocycles incorporated in the polycarbazole backbones follows the order: [1,2,5]oxadiazolo[3,4-*d*]pyridazine > pyrazino[2,3-*d*]pyridazine > [1,2,5]oxadiazolo[3,4-*c*]pyridine > [1,2,5]

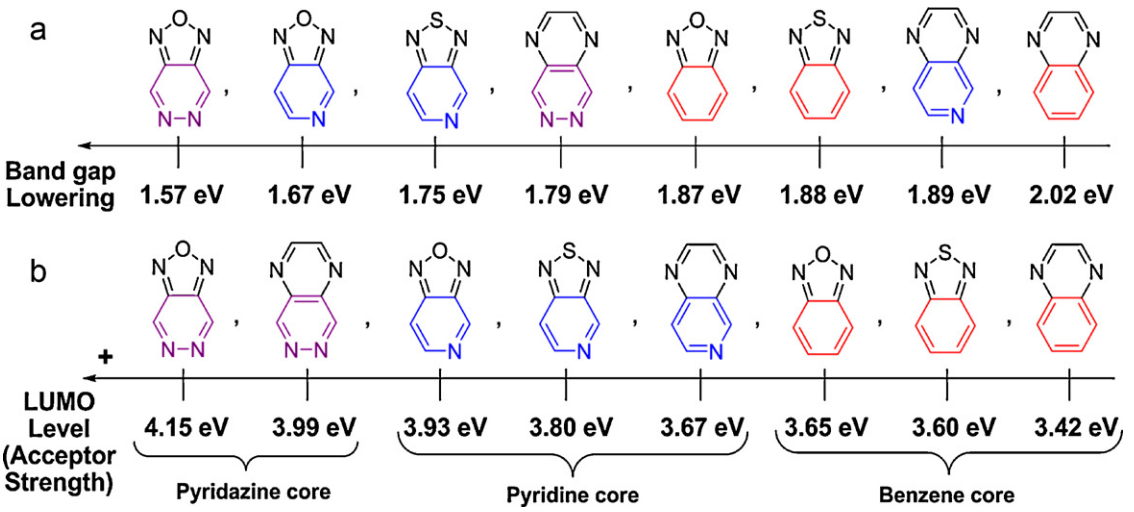

Fig. 7. Influence of the various heterocycles used as electron-deficient units on (a) the band gap lowering and (b) LUMO level ordering of the polycarbazole derivatives **246**–**253**.

Table 32
Optical band gaps, energy levels, hole mobility and photovoltaic efficiency of **246–254**.

Polymers	E_g^{opt} (eV)	LUMO (eV)	HOMO (eV)	Hole mobility (cm^2/V s)	PCE (%)
246	1.87	3.65	5.47	1×10^{-4}	2.4
247	1.57	4.15	5.70	–	0.47
248	1.88	3.60	5.45	1×10^{-3}	3.6[a]/6.1[b]
249	1.67	3.93	5.55	5×10^{-4}	0.8
250	1.75	3.80	5.53	4×10^{-5}	0.7
251	2.02	3.42	5.46	3×10^{-4}	1.8
252	1.89	3.67	5.52	2×10^{-5}	1.1
253	1.79	3.99	5.76	–	0.37
254	1.91	3.88	5.73	–	0.13

[a] Using $PC_{61}BM$.
[b] Using $PC_{71}BM$.

thiadiazolo[3,4-*c*]pyridine > pyrido[3,4-*b*]pyrazine > 2,1,3-benzooxadiazole > 2,1,3-benzothiadiazole > quinoxaline (Fig. 7b). This result demonstrates that the electron affinity increases by the transition from the benzene core-based polycarbazoles (**246**, **248**, **251**; lower electron affinity) to the pyridine-based polycarbazoles (**249**, **250**, and **252**) and finally to the pyridazine-based polycarbazoles (**247**, **253**; higher electron affinity). More importantly though, it is revealed that the order of the acceptor strength is not in agreement with the order of the band gap reduction ability of the different heterocycle as shown in Fig. 7. This clearly verifies that reduction of the band gap of the polymers through the incorporation of various electron-withdrawing units in a DAD segment is not a parameter related only to the electron affinity (strength) of the acceptor moiety but also other important factors should be taken into account such as the energy resonance of the monomer and the intermolecular interactions between the polymeric chains.

Although the HOMO levels of these polymers seem to be fixed by the carbazole moiety [241,242], the nature of the heterocycle acceptor unit also contributes to the overall HOMO value. For example, the HOMO levels are increased by passing from the three polymers (**246**, **248**, and **251**) with the benzene core-based acceptor units in the main chain (HOMO ca. 5.46 eV) to the three polymers (**249**, **250**, and **252**) with the pyridine core-based acceptor units in the main chain (HOMO ca. 5.53 eV) and finally to the two polymers (**247**, **253**) with the pyridazine core-based acceptor units (HOMO ca 5.73 eV). At the same time, these values confirm that all the polymers show good air stability.

Despite the higher LUMO level values of some polymers (**247**, **249**, **250**, **252**, and **253**), the better structural organization in copolymers (**246**, **248**, and **251**) and the slightly higher molecular weight obtained, leads to better hole mobilities of about 1×10^{-3} cm^2/V s for **248** and as a sequence an initially PCE of 3.6% for the **248**:$PC_{61}BM$ in 1:4 (w/w) ratio with J_{sc} = 6.8 mA/cm^2, V_{oc} = 0.86 V and FF = 0.56 is recorded [241,243]. The fact that **247** with the higher LUMO value and the lowest band gap exhibits a PCE of 0.47% can be attributed to the fact that the LUMO level is too low to expect efficient charge transfer to the $PC_{61}BM$ [242], while the structural related analogue **250**, with the more suitable energy levels for use with $PC_{61}BM$ exhibits also a low PCE of 0.7% mainly due to its lower hole mobility which is almost 2 orders of magnitude lower than that of **248** [241].

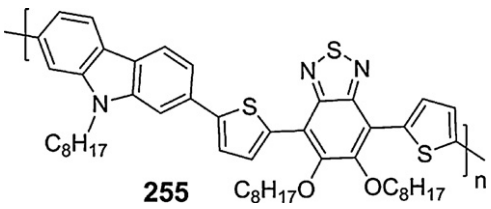

255

Chart 59. Chemical structure of the polycarbazole derivative **255**.

By further optimizing the molecular weight of **248** (M_n = 20,000 g/mol, PDI = 2.2) [244], the blending ratio between **248** and $PC_{61}BM$ (1:2, w/w) and the active layer thickness (60 nm), an improvement of the PCE (4.35%) was obtained with J_{sc} = 9.42 mA/cm^2, V_{oc} = 0.90 V and FF = 0.51 [244]. Then, replacing the $PC_{61}BM$ with $PC_{71}BM$ an enhanced PCE (4.6%) was recorded for the **248**:$PC_{71}BM$ in 1:2 (w/w) and an active layer thickness of 70 nm with J_{sc} = 10.22 mA/cm^2, V_{oc} = 0.89 V and FF = 0.51 [244]. Finally, by the addition of a titanium oxide layer (TiO_x) between the **248**:$PC_{71}BM$ thin film and the aluminium electrode, modifying the blending ratio to 1:4 (w/w) and changing the deposition solvent from CF to DCB, a very high PCE of 6.1% was recorded with J_{sc} = 10.6 mA/cm^2, V_{oc} = 0.88 V and FF = 0.66. This high efficiency is accompanied also with an impressive internal quantum efficiency (IQE) close to 100% implying that essentially every absorbed photon results in a separated pair of charge carriers and that all the photogenerated carriers are collected at the electrodes [245]. In addition, neither thermal annealing nor the addition of processing additives is required for achieving this high PCE.

Another very promising polycarbazole derivative for high performance OPVs is **255** (Chart 59) which has been synthesized by Suzuki cross-coupling polymerization between a diboronic ester carbazole derivative containing an octyl side chain and a DAD segment with thiophene ring as the donor and an octyloxy-substituted 2,1,3-benzothiadiazole as the acceptor unit [246]. The introduction of the octyloxy substituents onto 2,1,3-benzothiadiazole weakens the electron strength of the acceptor unit (LUMO at 3.35 eV, while the HOMO is situated at 5.21 eV) due to the electron donating ability of the octyloxy side groups as also reported before, leading to a band gap of 1.95 eV, slightly higher as compared to the structural related **248**.

Despite the relatively high band gap, a very high PCE of 5.4% with V_{oc} = 0.81 V, J_{sc} = 9.6 mA/cm^2 and FF = 0.69 was

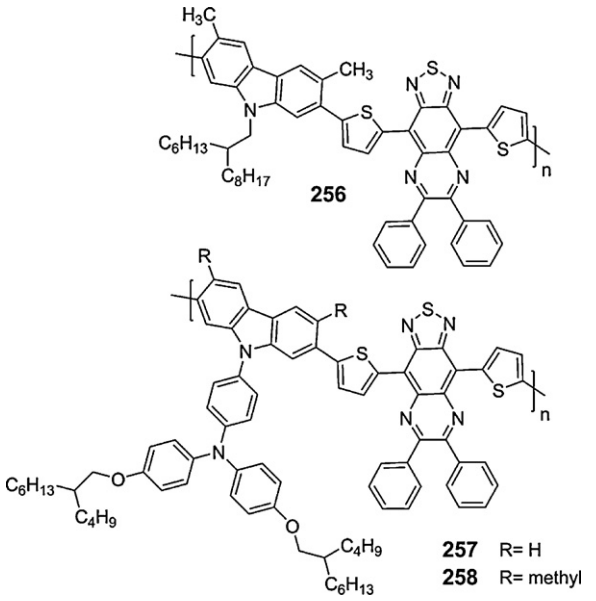

Chart 60. Chemical structures of the polycarbazole derivatives **256**–**258**.

Table 33
Optical band gaps and energy levels of **256**–**258**.

Polymers	E_g^{opt} (eV)	LUMO (eV)	HOMO (eV)
256	1.30	3.80	5.10
257	1.10	3.70	4.80
258	1.25	3.80	5.05

recorded when **255** blended with $PC_{71}BM$ in 1:2.5 (w/w) ratio [246]. The FF of 0.69 is one of the highest among all the high performance conjugated polymers for OPVs reported so far, which verifies the balanced charge transport of the **255**:$PC_{71}BM$ system (1×10^{-4} cm^2/V s for holes and 3×10^{-4} cm^2/V s for electrons in FET measurements) when deposited from a mixture of DCB:1,8-diiodooctane.

Finally, three LBG polycarbazole derivatives based on the DAD concept have been synthesized [247] by Suzuki cross-coupling polymerization and consisting of an alkyl-functionalized (**256**) or a triarylamine-functionalized carbazole unit (**257**, **258**) alternate with a thiophene-[1,2,5]thiadiazolo[3,4-*g*]quinoxaline-thiophene segment (Chart 60).

The optical band gaps and the energy levels of **256**–**258** are included in Table 33. The alternating copolymer **256** displays a low band gap of 1.30 eV, while the alternating copolymers **257**, **258** exhibit lower band gaps of 1.10 eV and 1.25 eV, respectively. Moreover, comparing the LUMO levels of the structural analogue copolymers **256** and **258** it is clearly shown that passing from the alkyl substituent on **256** to the triarylamine substituent on **258**, the LUMO levels are maintained the same (Table 33), indicating that the electron affinity of the polycarbazole derivatives **256**–**258** is adjusted by the [1,2,5]thiadiazolo[3,4-*g*]quinoxaline. On the other hand, by replacing the two methyl groups at the 3,6-positions on the carbazole unit of **258** with two hydrogen atoms on **257**, both the HOMO and LUMO levels are upshifted by 0.15 eV and 0.1 eV, respectively.

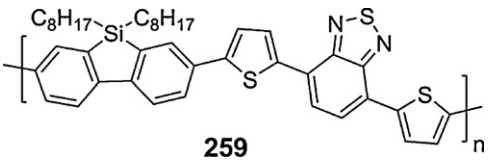

Chart 61. Chemical structure of the polydibenzosilole derivative **259**.

Furthermore, spectroscopic studies on blends consisting of either **256** or **257** or **258** as the electron donors and $PC_{61}BM$ as the electron acceptor reveal that **257**:$PC_{61}BM$ blend exhibits complete photoluminescence quenching in contrast to the partial quenching in the photoluminescence for **256**:$PC_{61}BM$ and **258**:$PC_{61}BM$ blends. These results can be explained by the fact that the LUMO of $PC_{61}BM$ is much closer in energy to those of **256** and **258**, which both have LUMO levels of 3.8 eV. However the LUMO of $PC_{61}BM$ is further offset in energy from that of **257** (3.7 eV) allowing the efficient electron transfer from **257** to $PC_{61}BM$ [247]. Based on the above observations, the photovoltaic performance of **257**:$PC_{61}BM$ in 1:1 (w/w) ratio was studied and a PCE of 0.61% with J_{sc} = 5.16 mA/cm^2, V_{oc} = 0.41 V and FF = 0.29 after thermal annealing at 150 °C for 10 min, is exhibited [247].

3.2.13.4. Dibenzosilole-based polymers. Structural related analogue to fluorene and carbazole units is dibenzosilole where the two phenylene rings are bridged with a silicon atom. It has been reported that poly(dibenzosilole) shows similar photophysical properties as PFs but with higher electroluminescent efficiency, thermal stability and hole mobility comparable to those of PFs [163]. Based on these observations and considering that TBzT based PF and polycarbazoles exhibit high PCE in BHJ solar cells, two research groups have independently reported the synthesis of the alternating copolymer **259** (Chart 61) consisting of the dioctyl substituted dibenzosilole and the TBzT segment by Suzuki cross-coupling polymerization [248,249]. The reported molecular weights of **259** are M_n = 15,000 g/mol [248] and M_n = 79,000 g/mol [249]. The optical band gap of the lower M_n derivative is 1.85 eV and that of the higher M_n is 1.82 eV, which is ~0.1 eV and ~0.05 eV lower than that of **195** and **248**, respectively. Regarding the energy levels, two different values were reported for both the HOMO and LUMO levels from the two groups. The HOMO is 5.70 eV and the LUMO is 3.81 eV for the lower M_n polymer [248], while the HOMO of the higher M_n polymer is 5.39 eV [249].

The PCE of the low M_n **259** in blends with $PC_{61}BM$ in 1:4 (w/w) is 1.6% with J_{sc} = 2.8 mA/cm^2, V_{oc} = 0.97 V and FF = 0.55 [248], while the PCE of the high M_n **259** when blended with $PC_{61}BM$ in 1:2 (w/w) ratio is remarkably high (5.4%) with J_{sc} = 9.5 mA/cm^2, V_{oc} = 0.90 V and FF = 0.51 [249]. This result indicates the effect of the molecular weight of the polymer on the overall PCE and is in accordance with the observations of Janssen et al. for the diketopyrrolo[3,4-*c*]pyrrole (DPP)-based copolymer **296** that will be reported next in the text.

3.2.13.5. Germafluorene-based polymers. Very recently Leclerc et al. reported the synthesis of a new hetero-bridged phenylene unit based on germanium (germafluorene) and

Table 34
Optical band gaps, energy levels and photovoltaic efficiency of **260**–**263**.

Polymers	E_g^{opt} (eV)	LUMO (eV)	HOMO (eV)	PCE (%)
260	2.95	2.82	5.95	–
261	1.79	3.91	5.58	2.8
262	1.63	3.70	5.38	1.5
263	1.64	3.64	5.38	1.2

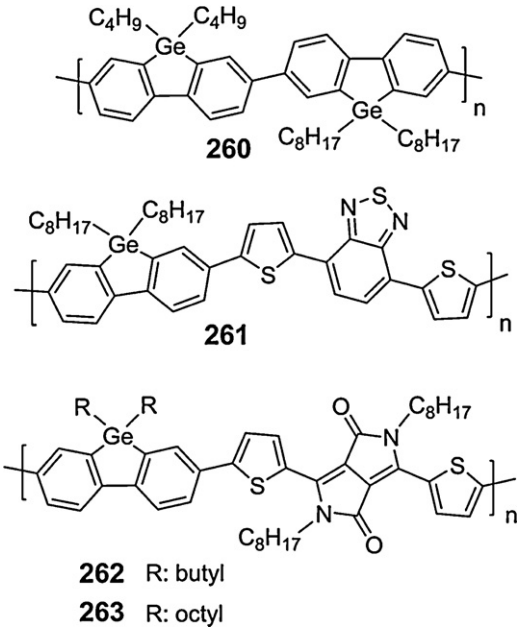

Chart 62. Chemical structures of the polygermafluorene derivatives **260**–**263**.

its related homopolymer **260** [250] and alternating copolymers **261**–**263** [250] (Chart 62). The alternating copolymers **261**–**263** are consisting of an alkyl substituted germafluorene and DAD segments with thiophene as the donor and 2,1,3-benzothiadiazole (**261**) or octyl substituted diketopyrrolo[3,4-*c*]pyrrole (DPP) (**262**, **263**) as the acceptor moiety. The polymers were synthesized by Suzuki cross-coupling polycondensation but the obtained molecular weights were moderate, ranging from M_n = 10,000 g/mol for **260** to M_n = 14,000 g/mol for **263**. The optical band gaps and the energy levels of the synthesized germafluorene copolymers are included in Table 34.

The optical band gap of **260** is very similar to that of the dioctyl substituted PF and polydibenzosilole, while the optical band gap of **261** (1.79 eV) is lower compared to those of its homologues **195**, **248** and **259**. This result indicates that the incorporation of the germafluorene unit in the polymer backbone might lead to better π–π stacking due to enhanced intermolecular interactions. Furthermore, **262** and **263** exhibit the lowest band gap among the studied polygermafluorene derivatives showing that the DPP unit facilitates better the lowering of the band gap as compared to 2,1,3-benzothiadiazole, whereas the length of the alkyl side chain attached on germafluorene does not alter significantly the band gap of **262** and **263**. Moreover, by studying the energy levels of the polymers it is observed that the electron affinity of **261** is higher (LUMO = 3.91 eV) than that of **262** (LUMO = 3.70 eV) and **263** (LUMO = 3.64). In addition, by replacing the 2,1,3-benzothiadiazole in **261** with DPP in **262** both the energy levels are upshifted by ~0.2 eV.

The photovoltaic performance of **261**–**263** was examined in blends with $PC_{71}BM$ and the results are summarized in Table 34. **261** exhibits the higher PCE even though its lower hole mobility (1.1×10^{-4} $cm^2/V s$ in FET) and the higher band gap as compared to **262** and **263**. The hole mobilities of **262** and **263** are 0.04 $cm^2/V s$ and 7.7×10^{-3} $cm^2/V s$, respectively [250]. Comparing the unoptimized PCE of **261** (2.8%) with the initial PCEs of the analogue polymers **195** (2.3%), **248** (3.6%) and the low M_n **259** (1.6%) it is expected that with further optimization on the structural characteristics (for example improving the reaction conditions towards **261** with higher molecular weights) and the processing conditions, this polymer can provide even higher PCEs.

3.2.14. Polycyclic aromatics bridged with fused aromatic rings

3.2.14.1. Ladder-type oligo-p-phenylene-based polymers. Conjugated polymers based on the indeno[1,2-*b*]fluorene moiety (a pentacene-like organic molecule using phenyl-capped ladder oligo(*p*-phenylene) derivative with two carbon bridges) are attractive alternative materials with more extended coplanar fused structure, which enables enhanced π-conjugation, π–π intermolecular interactions and improved charge carrier mobility as compared to PFs [251]. For these reasons, indeno[1,2-*b*]fluorene (IF) can serve as an efficient building block for the synthesis of LBG polymers for OPVs based on the D–A approach. Thus, new alternating poly(indeno[1,2-*b*]fluorene) (PIF)-based copolymers (**264**–**268**) consisting of an alkyl substituted IF along with various DAD segments have been synthesized by Suzuki cross-coupling polymerization (Chart 63) [252,253]. As DAD segments, thiophene ring is the fixed donor component, while different heterocycle monomers like quinoxaline (**264**) [252], 2,1,3-benzothiadiazole (**265**–**267**) [252,253] and thieno[3,4-*b*]pyrazine (TP) (**268**) [253] have been used as the electron-withdrawing units.

The optical band gaps and the energy levels of **264**–**268** are included in Table 35. The band gap of **264**–**268** lower by passing from the quinoxaline based-PIF (**264**; 2.00 eV) to 2,1,3-benzothiadiazole based-PIFs (**265**–**267**; 1.97 eV) and finally to TP-based PIF (**268**; 1.61 eV), while no difference on the band gap of **265**–**267** is detected by varying the length of the alkyl side chain. Moreover, the LUMO levels of the polymers **264**–**268** are a function of the electron-deficient unit. For example, the lowest LUMO level is presented when TP is used and then the order is as follows: 2,1,3-benzothiadiazole > quinoxaline. On the other hand,

Table 35
Optical band gaps, energy levels, hole mobility and photovoltaic efficiency of **264**–**268**.

Polymers	E_g^{opt} (eV)	LUMO (eV)	HOMO (eV)	Hole mobility ($cm^2/V\,s$)	PCE (%)
264	2.00	3.36	5.45	2.3×10^{-4}	3.04
265	1.97	3.46	5.49	1.1×10^{-3}	0.97
266	1.97	3.71	5.64	1.1×10^{-3}	1.70
267	1.97	3.44	5.47	1.8×10^{-4}	2.44
268	1.61	3.89	5.50	5.7×10^{-4}	0.45

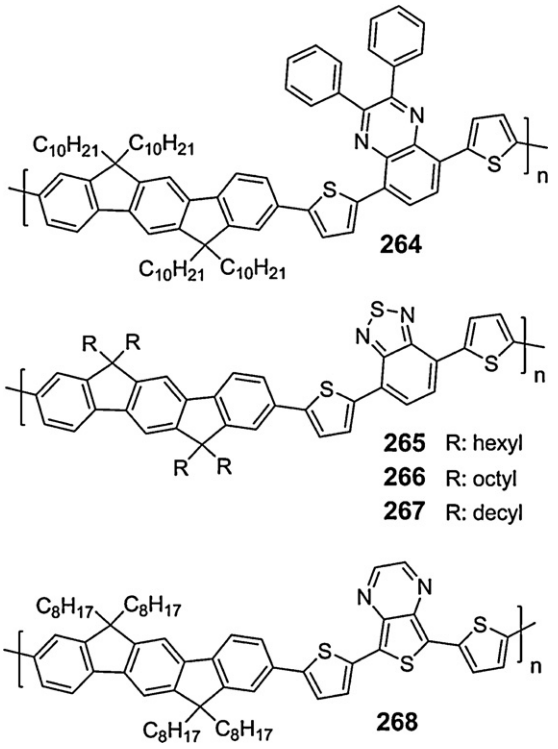

Chart 63. Chemical structures of the poly(indeno[1,2-*b*]fluorene) derivatives **264**–**268**.

the HOMO levels are situated between 5.45 and 5.64 eV confirming that all the polymers show good air stability.

Among the PIF copolymers **264**–**268**, **264** exhibits the higher PCE (3.04%) when blended with $PC_{71}BM$ in 1:3.5 (w/w) ratio with $J_{sc} = 7.57\,mA/cm^2$, $V_{oc} = 1.00\,V$ and FF = 0.40 even if it shows the higher band gap and lower hole mobility ($2.3 \times 10^{-4}\,cm^2/V\,s$ in FETs measurements) [252] than that of **265** or **266** ($1.1 \times 10^{-3}\,cm^2/V\,s$) [252,253]. Moreover, comparing the resulting hole mobilities of the structural analogue copolymers **265**–**267** with respect to their photovoltaic performance a controversial trend is detected. Despite that the hole mobility of **265**–**267** decreases with the presence of longer alkyl chains in their polymer backbone, the PCE of **265**–**267** increases as the length of the alkyl side chains is longer. This was explained on the basis of the better solubility and easy processability of **267** as compared to **265**.

Furthermore, expanding the studies on longer derivatives of the ladder-type oligo-*p*-phenylene based copolymers, a new alternating conjugated polymer consisting of a ladder-type tetra-*p*-phenylene moiety with TBzT segment

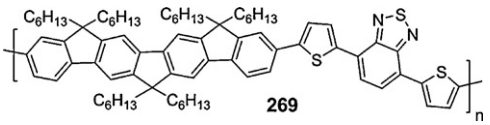

Chart 64. Chemical structure of a ladder-type tetra-*p*-phenylene based copolymer **269** consisting of TBzT segment.

(**269**) [252] has been synthesized by Suzuki cross-coupling polymerization (Chart 64).

BHJ solar cells based on **269** and $PC_{71}BM$ in 1:4 (w/w) ratio were prepared and a PCE of 4.5% was exhibited with $J_{sc} = 10.3\,mA/cm^2$, $V_{oc} = 1.04\,V$ and FF = 0.42 [252]. This PCE is the highest among **264**–**269**. Replacing the indeno[1,2-*b*]fluorene monomer, containing four hexyl side chains, by the more planar and ladder-type tetra-*p*-phenylene moiety substituted with six hexyl side chains, only a slight decrease on the band gap (1.96 eV for **269** whereas **265** has 1.97 eV) and a reduced hole mobility ($6.1 \times 10^{-4}\,cm^2/V\,s$ for **269** in FET measurements) are revealed, which cannot obviously explain the improved PCE of **269**. It seems that the number and the length of the alkyl side chains on the backbone of the ladder-type oligo-*p*-phenylene monomer play an important role on the relationship between the solubility-processability and the hole mobility of the corresponding copolymers. As mentioned before, the four hexyl side chains on the backbone of **265** provided better π–π stacking between the polymer chains, higher hole mobilities but less solubility and processability. On the other hand, the lower hole mobility of **269** indicates a lower degree of ordering of the polymer chains upon the addition of two more hexyl side chains on the backbone of **269**, but the improved solubility and the easy processability of **269**, due to the presence of six hexyl side chains per repeat unit, could lead to a difference in the nanoscale morphology of the polymer–fullerene blend, important parameter to maintain the PCE of the corresponding solar cells high. Finally, the LUMO level of **269** (3.45 eV) is similar to **265** (3.46 eV) while the HOMO level (5.45 eV) is slightly raised, but still maintained sufficiently high for preventing the material from air oxidation degradation and providing a relatively high V_{oc}.

3.2.14.2. Indeno[2,1-a]indene-based polymers. Poly(indeno[2,1-*a*]indene)s (PIIs) and its copolymers (**270**–**273**) are new class of materials having similar structure with PFs but with one more 5-member ring in the backbone [254]. The introduction of four alkyl chains to the sp^3 carbon atoms in the bridge increases the solubility of the polymers without distorting the conjugation. The subsequent copolymerization with 2,1,3-benzothiadiazole (**270**) or TBzT segment (without (**271**) or with alkyl (**272**)

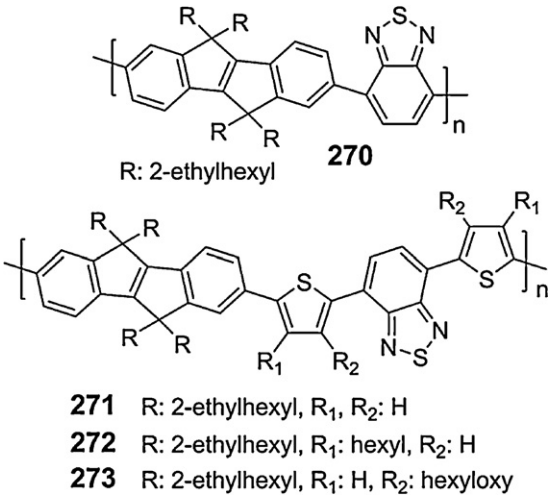

Chart 65. Chemical structures of the poly(indeno[2,1-*a*]indene) derivatives **270**–**273**.

or alkoxy (**273**) substituents) by Suzuki cross-coupling polymerization provide copolymers (Chart 65) with lower band gaps as compared to PIIs (2.48 eV) and uniform absorbance in the whole visible region [254].

The optical band gaps, the energy levels and the PCE of **270**–**273** are presented in Table 36. The alternating D–A copolymer **270** consisting of the indeno[2,1-*a*]indene unit as the donor and the 2,1,3-benzothiadiazole as the acceptor moiety exhibits a band gap above 2 eV (2.18 eV) but lower from the corresponding PII homopolymer (2.48 eV). The insertion of a thiophene ring around the benzothiadiazole core in **271**, results with the further lowering of the band gap to 1.84 eV. The anchoring of hexyl side chains at the 4-positions on the thiophene rings of the TBzT, close to the indeno[2,1-*a*]indene, for **272** increases the band gap by 0.12 eV as compared to **271**, showing that a slight steric hindrance within the polymer backbone is formed. On the other hand, when alkoxy side chains are added at the 3-positions on the thiophene rings of the TBzT (**273**), further lowering of the band gap (1.79 eV) is detected. The fact that the band gap of **273** is lower than that of **272** is attributed to the stronger electron donating ability of the alkoxy side chains similar to the results obtained for **201** and **202**.

Regarding the energy levels of **270**–**273**, the introduction of the two thiophene rings around the 2,1,3-benzothiadiazole raise the HOMO level of **271** as compared to **270** (Table 36) due to the increased electron density in the polymer backbone. The HOMO of **272** is lying lower than that of **271** due to the reduced electron delocalization as the consequence of the slight steric hindrance within the polymer backbone. Furthermore, the HOMO level of **273** is considerably raised upon substitution with the alkoxy side chains since the electron density in the polymer backbone is significantly increased due to the electron donating ability of the alkoxy groups. Finally, BHJ solar cells prepared from blends of either **271–273** with $PC_{61}BM$ in 1:3.5 (w/w) ratio exhibit PCEs of 1.88% for **271** with J_{sc} = 5.93 mA/cm^2, V_{oc} = 0.74 V and FF = 0.43 [254].

3.2.14.3. Influence of the presence of the thiophene unit around the 2,1,3-benzothiadiazole on the optical band gap of various LBG conjugated polymers. At this point it is necessary to make a comparison and summarize the effect on the optical band gap for the main LBG conjugated polymers reported up to now (Fig. 8). The most extensive and well studied D–A conjugated polymers towards high performance OPVs are those consisting of various electron donor monomers and 2,1,3-benzothiadiazole as the acceptor unit, with or without the presence of the thiophene ring around the 2,1,3-benzothiadiazole core in the polymer backbone. Based on the above mentioned results and Fig. 8, the alternating D–A LBG conjugated polymers based on the CPDT, DTS and DTP as the electron donor monomers and 2,1,3-benzothiadiazole as the electron acceptor, exhibit lower band gaps as compared to the analogue polymers with the CPDT, DTS and DTP linked with the TBzT segment. On the other hand, the band gaps of the alternating copolymers consisting of either the $B_{2134}DT$ or the fluorene or the indeno[2,1-*a*]indene as the donor units and 2,1,3-benzothiadiazole, are higher than those of the related polymers containing the same donor units alternate with the TBzT segment.

These initial results indicate that lower band gap conjugated polymers are obtained (i) when the bridged bithiophenes with 5-member fused aromatic rings in the central core are copolymerized with the 2,1,3-benzothiadiazole and (ii) when the bithiophenes with 6-member aromatic rings in the central core (for example the $B_{2134}DT$) or the bridged biphenylenes with 5-member fused aromatic rings in the central core or the polycyclic aromatics bridged with fused aromatic rings are copolymerized with the TBzT segment. However, it should always considered that the influence of additional main-chain thienylene units on the HOMO and LUMO energy levels is a complex interplay of several factors, including D–A strength, mean D–A distance and the amount of bond length alternation and aromaticity [255].

3.2.14.4. Indolo[3,2-b]carbazole-based polymers.

3.2.14.4.1. Poly(indolo[3,2-b]carbazole-alt-electron-deficient units). Structural related analogue of IF monomer is the indolo[3,2-*b*]carbazole (IC) unit which is a pentacene-like semiconducting organic material based on a phenyl-capped ladder oligo(*p*-aniline) derivative with two nitrogen bridges. Very recently some alternating D–A copolymers (Chart 66) consisting of a bulky (2-ethylhexyl) substituted-IC with various acceptor units like quinoxaline (**274**) [256], 2,1,3-benzothiadiazole (**275**) [256] and TP (**276**, **277**) [256] have been synthesized by Suzuki cross-coupling polymerization and have been explored as electron donor polymers in BHJ solar cells.

The optical band gaps, the energy levels and the PCE of **274**–**277** are presented in Table 37. As shown in Table 37, the band gaps of **274** and **275** are above 2.0 eV while only after the insertion of the TP in the polymer backbone of **276** and **277** the band gaps drop below 2.0 eV, following the order: **277** < **276** < **275** < **274**. Interestingly, the band gap of **277** is considerably lower than that of **276** due to the presence of the electron-donating alkoxyphenylene side groups on the TP moiety, which drastically raises

Table 36
Optical band gaps, energy levels and photovoltaic efficiency of **270**–**273**.

Polymers	E_g^{opt} (eV)	LUMO (eV)	HOMO (eV)	PCE (%)
270	2.18	3.42	5.60	–
271	1.84	3.61	5.45	1.88
272	1.96	3.56	5.52	1.03
273	1.79	3.33	5.12	1.28

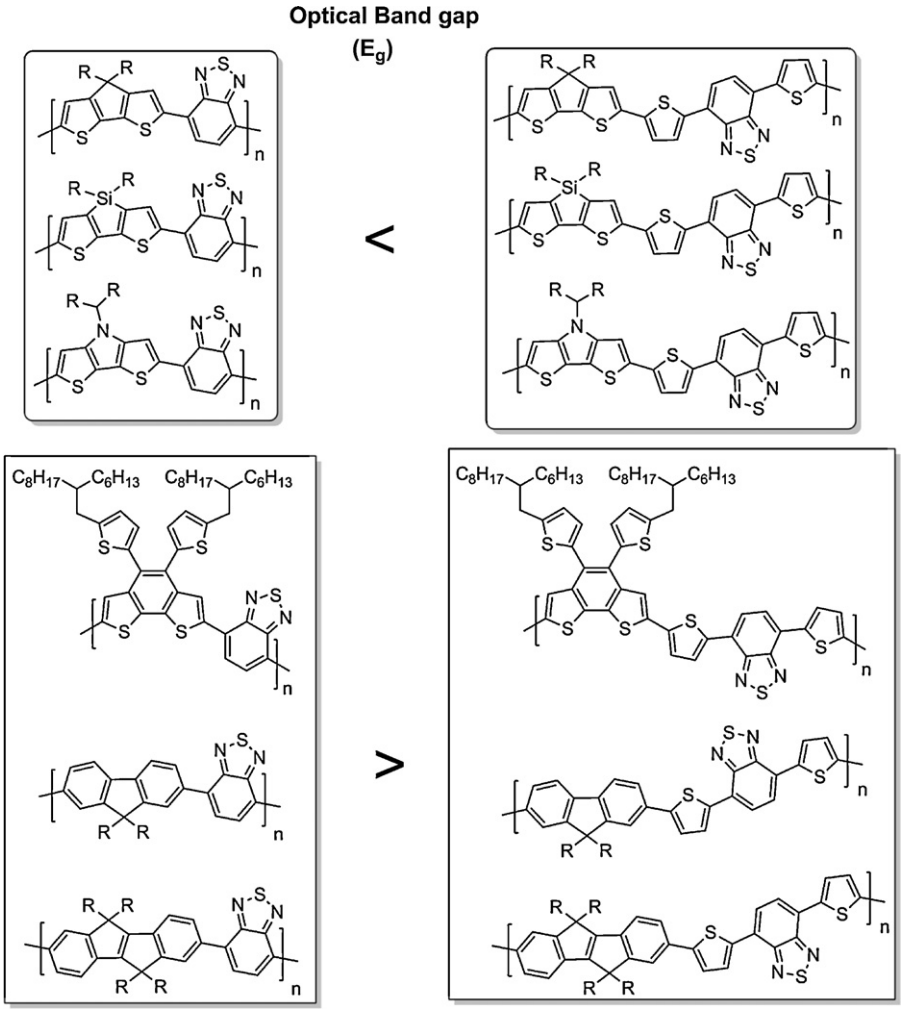

Fig. 8. Variation of the optical band gap in a series of donor–acceptor conjugated polymers.

Table 37
Optical band gaps, energy levels and photovoltaic efficiency of **274**–**277**.

Polymers	E_g^{opt} (eV)	LUMO (eV)	HOMO (eV)	PCE (%)
274	2.31	2.81	5.12	0.87[a]/1.40[b]
275	2.09	2.81	4.90	0.49[a]
276	1.89	2.99	4.88	0.22[a]
277	1.58	3.04	4.62	0.14[a]

[a] Using $PC_{61}BM$.
[b] Using $PC_{71}BM$.

the HOMO level while at the same time keeps almost similar the LUMO levels between **276** and **277**. However, the high lying HOMO levels of **275**–**277** (above 5.0 eV) indicate that are more prone to air oxidation and will prevent these polymers for achieving high V_{oc} when employed in solar cells. The photovoltaic results obtained when **274**–**277** are blended with $PC_{61}BM$ in 1:4 (w/w) ratio verified the above assumption since that the V_{oc} of

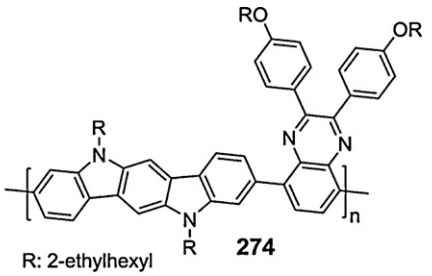

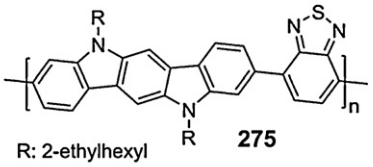

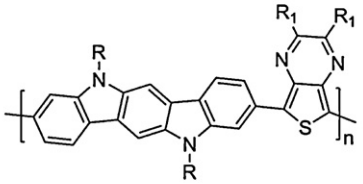

276 R: 2-ethylhexyl, R_1: dodecyl

277 R: 2-ethylhexyl, R_1: 3(2-ethylhexyloxy)phenylene

Chart 66. Chemical structures of the poly(indolo[3,2-*b*]carbazole) derivatives **274**–**277** consisting of various electron deficient units.

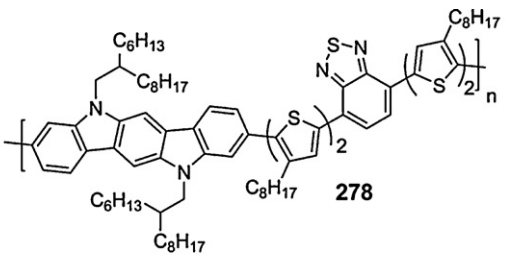

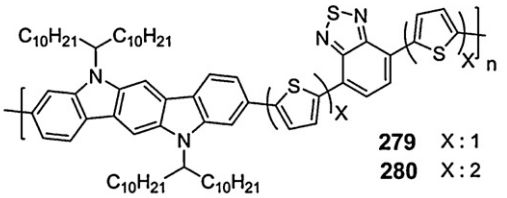

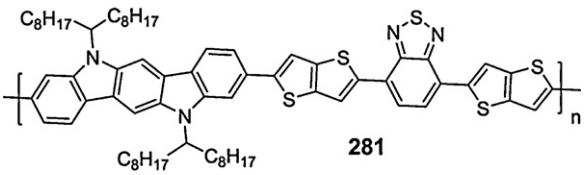

Chart 67. Chemical structures of the poly(indolo[3,2-*b*]carbazole) derivatives **278**–**281** consisting of both electron rich and deficient units.

275–**277** are decreasing (0.55 V (**275**) > 0.49 V (**276**) > 0.35 V (**277**)) following the same order as the HOMO level. Despite the very high band gap of **274** (2.31 eV), the relatively low lying HOMO level, as compared to the other copolymers, provides enhanced V_{oc} (0.66 V) and hence higher PCE (0.87% with $PC_{61}BM$ or 1.4% with $PC_{71}BM$) [256].

3.2.14.4.2. Poly(indolo[3,2-b]carbazole) derivatives with both electron-rich and electron-deficient units. Further improvement of the PCE to 3.6% for the poly(indolo[3,2-*b*]carbazole)-based copolymers has been achieved by the synthesis of **278** [257] consisting of a bulky substituted-IC unit alternate with a pentamer segment based on a dioctyl bithiophene around a 2,1,3-benzothiadiazole core (Chart 67). On the basis of this promising result, three new alternating IC-based copolymers (**279**–**281**) containing a secondary alkyl side chain substituted-IC along with either the TBzT (**279**) [258] or a pentamer segment with a bithiophene unit around the 2,1,3-benzothiadiazole (**280**) [258] or a modified TBzT segment where thiophene has been replaced by the fused thieno[3,2-*b*]thiophene (**281**) [259] have been also synthesized by Suzuki cross-coupling polymerization (Chart 67).

The optical band gaps, the energy levels and the PCE of **278**–**281** are included in Table 38. As shown in Table 38, **279** exhibits slightly higher optical band gap as compared to the other three copolymers but is somewhat lower (0.06 eV) than that of the structural related analogue **267** (1.97 eV) and 0.18 eV lower than that of **275**, similar to the observations for the indeno[2,1-*a*]indene-based copolymers **270** and **271**. Moreover, the addition of one more thiophene ring around the TBzT segment in **280** lowers the band gap by 0.06 eV due to the longer conjugation length. In addition, the substitution of the bithiophene unit around the 2,1,3-benzothiadiazole core with octyl side chains in **278** results a minor increase of the band gap as a consequence of the less efficient packing of the polymer chains. Furthermore, by replacing the thiophene ring of **279** with the fused thieno[3,2-*b*]thiophene in **281**, the band gap decreases by 0.08 eV, while as compared to **280** the band gap is maintained almost the same.

Regarding the energy levels of the IC-based copolymers **278**–**281**, it is observed that the HOMO levels of **279** and **280** are similar, a rather unexpected result since that by the addition of two more thiophene rings, which would strengthen the electron donor character of **280**, it is expected a significant raise of the HOMO level of **280**. For **281**, when the fused thieno[3,2-*b*]thiophene is incorporated in the polymer backbone, the HOMO level is raised by 0.27 eV and 0.25 eV as compared to **279** and **280**, respectively. On the contrary, the LUMO level of **280** is lower than that of **279** indicating that by increasing the conjugation length of the IC-based copolymers by the use of non fused thiophene rings, lowering of the band gap is achieved by the subsequent increase of the polymer's electron affinity. Moreover, comparing the energy levels of **279** with those of the structural analogue **267**, it is revealed that the HOMO levels of both **279** and **267** are similar, whereas the LUMO level of **279** is lower than that of **267** by 0.11 eV, indicating a higher electron effinity for the IC-based copolymer. The presence of the bridged nitrogen atoms in IC unit, which posses higher electronegativity than the bridged carbon atoms in IF unit is most likely one of the reasons for the lower LUMO level of **279**.

Table 38
Optical band gaps, energy levels and photovoltaic efficiency of **278**–**281**.

Polymers	E_g^{opt} (eV)	LUMO (eV)	HOMO (eV)	PCE (%)
278	1.89	3.15	5.17	3.60
279	1.91	3.55	5.45	1.47
280	1.85	3.62	5.43	2.07
281	1.83	3.35	5.18	2.40

Table 39
Optical band gaps, energy levels and photovoltaic efficiency of **282**–**285**.

Polymers	E_g^{opt} (eV)	LUMO (eV)	HOMO (eV)	PCE (%)
282	2.10	3.08	5.18	0.6[a]
283	2.08	3.02	5.10	2.2[a]/3.3[b]
284	2.11	3.07	5.18	1.7[a]/2.7[b]
285	2.10	3.07	5.17	1.1[a]

[a] Using $PC_{61}BM$.
[b] Using $PC_{71}BM$.

As mentioned in the beginning, **278** when is blended with $PC_{61}BM$ in 1:2 (w/w) ratio exhibits a very promising PCE of 3.6% with J_{sc} = 9.17 mA/cm^2, V_{oc} = 0.69 V and FF = 0.57 [257]. Although three new IC-based copolymers have been synthesized (**279**–**281**) which in some cases presenting more suitable energy levels and band gaps than that of **278**, the PCE obtained was not improved (Table 38). From the three new copolymers (**279**–**281**), the maximum PCE was recorded for **281** (2.4%) when blended with $PC_{71}BM$ in 1:2 (w/w) ratio with J_{sc} = 6.02 mA/cm^2, V_{oc} = 0.75 V and FF = 0.42 [259], while **279** and **280**, in blends with $PC_{61}BM$ in 1:3 (w/w) ratio, demonstrated very high V_{oc} of 0.94 V and 0.90 V, respectively [258].

3.2.14.5. Conjugated polymers with thiophene–phenylene–thiophene as building block.

3.2.14.5.1. Poly(thiophene–phenylene–thiophene) derivatives with electron-rich units. Four new conjugated polymers (**282–285**) based on the coplanar thiophene–phenylene–thiophene (TPT) building block have been designed and synthesized by Stille cross-coupling polymerization for application in OPVs (Chart 68) [260]. The TPT segment is the structural analogue of the IF where the phenylene rings at the two edges have been replaced by thiophene rings. The TPT segment presents nearly coplanar configuration which is expected to enhance the rigidity of the molecular backbone, avoiding possible "chain folding", which may limit the charge carrier mobility at higher molecular weights [261] and enhance the degree of conjugation [262]. In addition, the use of tetrahexylaryl groups, positioned as peripheral substituents of the TPT units, tailors the intermolecular interactions between the polymer chains to provide easy processability. Furthermore, the presence of the two thiophene rings instead of the phenylene rings should possibly lower the band gap of the TPT-based polymers more than the related PIF-based derivatives.

The optical band gaps, the energy levels and the PCE of **282**–**285** are included in Table 39. As expected, the band gap of TPT-homopolymer **282** is lower than that of the IF-based homopolymers (2.83 eV) [260], while upon addition of one thiophene ring in the polymer backbone slight lowering of the band gap by simultaneously raising of the HOMO level is observed for **283**. On the other hand, by the introduction of a non-functionalized bithiophene (**284**) or an alkyl substituted bithiophene (**285**) in the TPT-homopolymer backbone both the band gaps and the energy levels of the polymers remain unaltered. Moreover, even though the HOMO level of **284** is expected to raise and the band gap to be reduced in greater extent by the presence of a bithiophene unit in the polymer back-

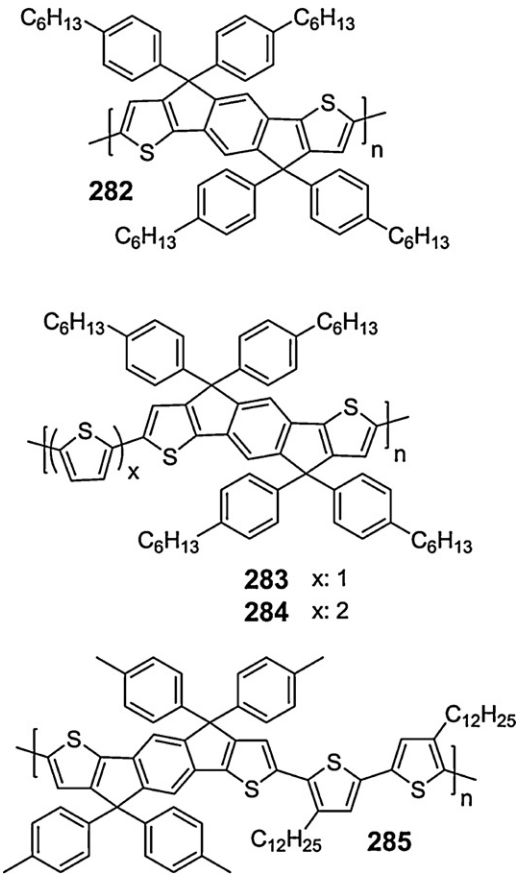

Chart 68. Chemical structures of the poly(thiophene–phenylene–thiophene) derivatives **282**–**285**.

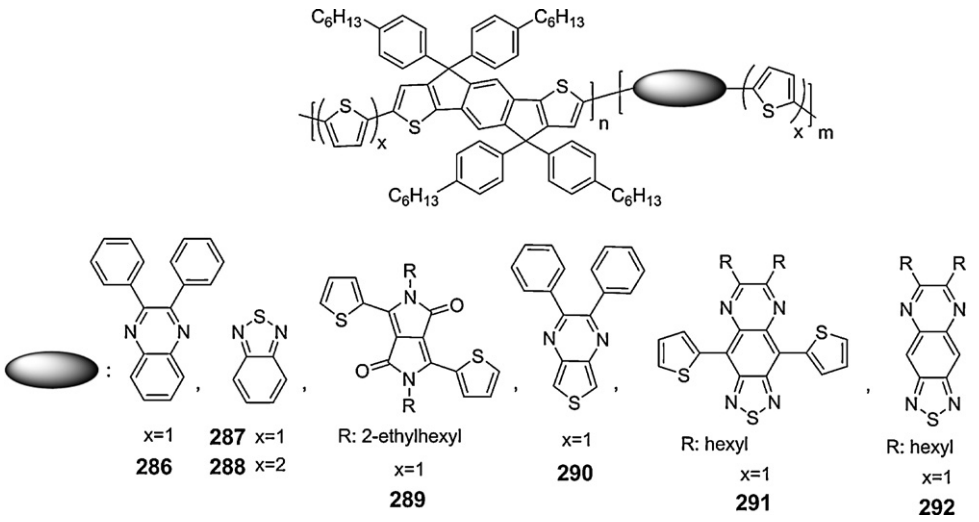

Chart 69. Chemical structures of the poly(thiophene–phenylene–thiophene) derivatives **286**–**292** consisting of both electron rich and deficient units.

bone as compared to **282**, none of these happens. On the contrary, the band gap and the HOMO level of **284** are similar to those of **282**, while as compared to **283** the band gap is higher and the HOMO is lying deeper. One of the possible reasons is that the insertion of the second thiophene ring in the backbone of **283** prevents the efficient π–π stacking of the polymer chains.

BHJ solar cells prepared based on blends of **282**–**285** using either $PC_{61}BM$ or $PC_{71}BM$ in 1:3 (w/w) ratio demonstrated PCE of 3.3% based on **283**:$PC_{71}BM$ with J_{sc} = 7.6 mA/cm^2, V_{oc} = 0.80 V and FF = 0.54, while the same polymer with the $PC_{61}BM$ revealed a PCE of 2.2% with J_{sc} = 5.3 mA/cm^2, V_{oc} = 0.77 V and FF = 0.53, even though **283** has lower hole mobility (8.3×10^{-4} cm^2/V s in FET measurements) than that of **284** (3.0×10^{-3} cm^2/V s) [260]. This high PCE is very promising especially for a polymer with a band gap above 2.0 eV, showing that TPT segment is an efficient building block for the development of a series of TPT-based conjugated polymers towards high performance solar cells.

3.2.14.5.2. Poly(thiophene–phenylene–thiophene) derivatives with both electron-rich and electron-deficient units. On the basis of these exciting results and based on the fact that the PCE of TPT-based copolymers (**282**–**285**) is limited by the insufficient absorption (band gap around 2.1 eV), further research efforts towards the synthesis of LBG TPT-based copolymers according to the D–A approach have been employed. This led to the synthesis of seven new random D–A TPT-based copolymers (Chart 69) [263,264] by Stille-cross coupling polymerization. These polymers consisting of a tetrahexylaryl-functionalized TPT moiety as donor and various electron withdrawing units including: 2,3-diphenylquinoxaline (**286**), 2,1,3-benzothiadiazole (**287**, **288**), thiophene-diketopyrrolo[3,4-*c*]pyrrole-thiophene (TDPPT) (**289**), 2,3-diphenylthieno[3,4-*b*]pyrazine (**290**), thiophene-6,7-dihexyl[1,2,5]thiadiazolo[3,4-*g*]quinoxaline-thiophene (TDTQT) (**291**), 6,7-dihexyl[1,2,5]thiadiazolo[3,4-*g*]quinoxaline (**292**).

The optical band gaps, the energy levels and the PCE of **286**–**292** are presented in Table 40. By incorporating the various electron withdrawing heterocycles, the band gaps of the resulting random TPT-based copolymers were effectively reduced following the order: **286** > **288** > **287** > **289** > **290** = **291** > **292**. Comparing the energy levels of the polymers, even though it seems to be a trend in the reduction of the LUMO level by the subsequent introduction in the polymer backbone of the 2,3-diphenylquinoxaline, 2,1,3-benzothiadiazole, TDPPT, 2,3-diphenylthieno[3,4-*b*]pyrazine, TDTQT and 6,7-dihexyl[1,2,5]thiadiazolo[3,4-*g*]quinoxaline (Table 40), the non-reproducibility of the estimated values as presented by the two different LUMO level values of **287** (Table 40) for the same molecular composition cannot easily support the above mentioned outcome. On the other hand, the band gap of **287**, regardless the two different reported energy level values, is situated at 1.70 eV.

Among the LBG TPT-based copolymers **286**–**292**, those consisting of the diphenylquinoxaline (**286**), 2,1,3-benzothiadiazole (**287**, **288**) and TDPPT segment (**289**) exhibit PCEs above 3.9% and as high as 4.3% when blended with $PC_{61}BM$ in 1:3 (w/w) (Table 40) [263,264]. **287** presents the highest PCE with J_{sc} = 10.1 mA/cm^2, V_{oc} = 0.8 V and FF = 0.53 while the PCE of **286** clearly represents one of the highest reported PCE among the known quinoxaline-based LBG polymers. The PCEs of **290**–**292** are significantly lower in comparison to the other polymers due to the lower current densities and V_{oc}, which for the latter can be attributed to their raised HOMO levels. In addition, morphological studies revealed relatively low level of roughness (<0.8 nm) and no significant aggregation for **286**, **287** and **289**, whereas **290**–**292** feature higher degrees of roughness and island-like aggregation [263,264]. Further optimization of the PCE of **287** to 5.8% was achieved by replacing the $PC_{61}BM$ with $PC_{71}BM$ by using 1,8-octanedithiol (1.25% by volume) as an additive in DCB, mainly due to the remarkable increase in the FF [265]. TEM analyses revealed that small donor and acceptor domains

Table 40
Optical band gaps, energy levels and photovoltaic efficiency of **286**–**292**.

Polymers	E_g^{opt} (eV)	LUMO (eV)	HOMO (eV)	PCE (%)
286	1.80	3.37 [263]	5.30 [263]	4.20
287	1.70	3.53 [263]/3.66 [264]	5.30 [263]/5.43 [264]	4.30 [263,264]/5.80 [265]
288	1.76	3.56 [264]	5.46 [264]	3.90
289	1.40	3.60 [263]	5.25 [263]	4.20
290	1.20	3.63 [263]	5.03 [263]	0.40
291	1.20	3.66 [263]	5.12 [263]	0.84
292	1.00	3.67 [263]	5.16 [263]	0.50

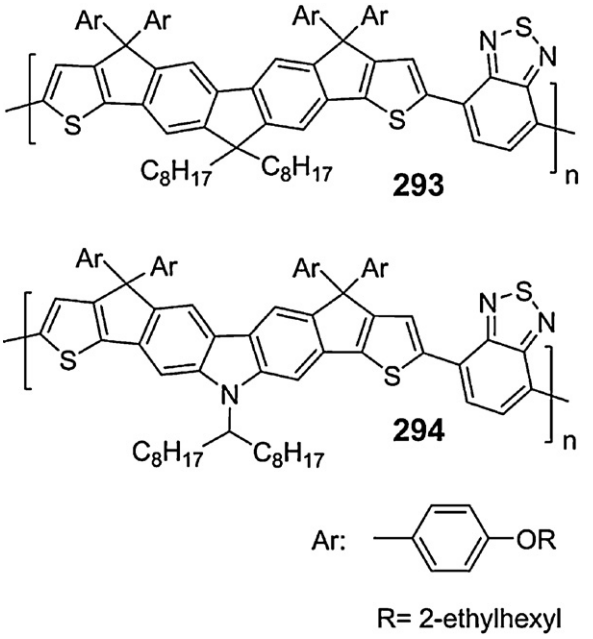

Chart 70. Chemical structures of the multifused heptacyclic based copolymers **293** and **294**.

were formed directly during the spin-coating process, thereby providing an optimal interpenetrating network and improved performance.

3.2.14.6. Conjugated polymers based on multifused heptacyclic structures. Based on the chemical structures of the well studied **195** and **248** in order to fully take advantage of their excellent properties, two new D–A copolymers poly(fluorene-dicyclopentathiophene-*alt*-benzothiadiazole) **293** [266] and poly(carbazole-dicyclopentathiophene-*alt*-benzothiadiazole) **294** [266] (Chart 70) were synthesized by Stille cross-coupling polymerization. The structural uniqueness of **293** and **294** is that the 3-positions of the two outer thiophenes are covalently tied with the 3,6-position of central fluorene or carbazole units by a carbon bridge, forming two cyclopentadienyl (CP) rings embedded in a multifused heptacyclic structure.

The optical band gaps of **293** and **294** are 1.76 eV and 1.66 eV, respectively which are lower than that of the non-fused analogues **195** and **248**. The absorption spectra profiles of **293** and **294** are essentially unchanged with slight broadening of the bands and red shift of the band edges from solution to the solid state which in combination with the no obvious thermal transition in the differential scanning calorimetry measurements confirms the amorphous nature of the polymers. This can be explained by the fact that the two 4-(2-ethylhexyloxy)phenyl moieties substituted at the carbon of cyclopentadienyl rings dilute the strong intermolecular π–π interactions between the polymer chains [266]. Moreover, comparing the energy levels of **293** and **294** (Fig. 9) it is revealed that the LUMO level of **294** is 0.06 eV lower than that of **293**, as expected since that the nitrogen atom is more electronegative than carbon, whereas the HOMO level of **293** is situated 0.06 eV higher than that of **294**. This result is in contrast with the results obtained comparing the HOMO levels of **195** and **248**. The HOMO level of **195** is 0.05 eV lower than the HOMO level of **248**, indicating that the raising of the ionization potential of the multifused heptacyclic structure formed upon chemical rigidification of the fluorene unit with the two outer thiophene rings is significantly higher. In addition, the upshift in the HOMO of **293** is higher that that of analogue carbazole-based heptacyclic structure (Fig. 9). On the other hand, the LUMO levels of both **195** and **248** remain unaltered upon their chemical rigidifications.

Preliminary photovoltaic results based on blends of either **293** or **294** with $PC_{71}BM$ in 1:2 (w/w) ratio show very promising results with PCEs of 2.8% for **293** and 3.7% for **294** with J_{sc} = 10.7 mA/cm^2, V_{oc} = 0.8 V and FF = 0.43 [266]. The reason for the moderate FF is most likely the high surface roughness as observed by AFM, rather than the hole mobilities because despite their amorphous nature, **293** and **294** show good hole transporting properties such as 2.5×10^{-4} cm^2/V s (**293**) and 1×10^{-4} cm^2/V s (**294**) as measured by the SCLC method. In addition, the hole mobilities in blends with $PC_{71}BM$ were found 5×10^{-5} cm^2/V s for **293** and 4×10^{-4} cm^2/V s for **294**.

3.2.15. Low band gap conjugated polymers based on various electron-deficient units

3.2.15.1. Diketopyrrolo[3,4-c]pyrrole-based polymers. Diketopyrrolo[3,4-*c*]pyrrole (DPP) is a versatile building block for the preparation of many LBG conjugated polymers through the D–A approach due to its high electron-withdrawing effect. Significant progress was made very recently for the DPP-based conjugated polymers in the area of OPVs by the synthesis of a LBG (1.4 eV) polythiophene derivative (**295**), containing the electron-rich quaterthiophene segments with the DPP unit (Chart 71), and shows a very promising PCE of 4.0% when blended with $PC_{71}BM$ in 1:2 (w/w) ratio with J_{sc} = 11.3 mA/cm^2, V_{oc} = 0.61 V and FF = 0.58 [267]. In addition, **295** exhibits

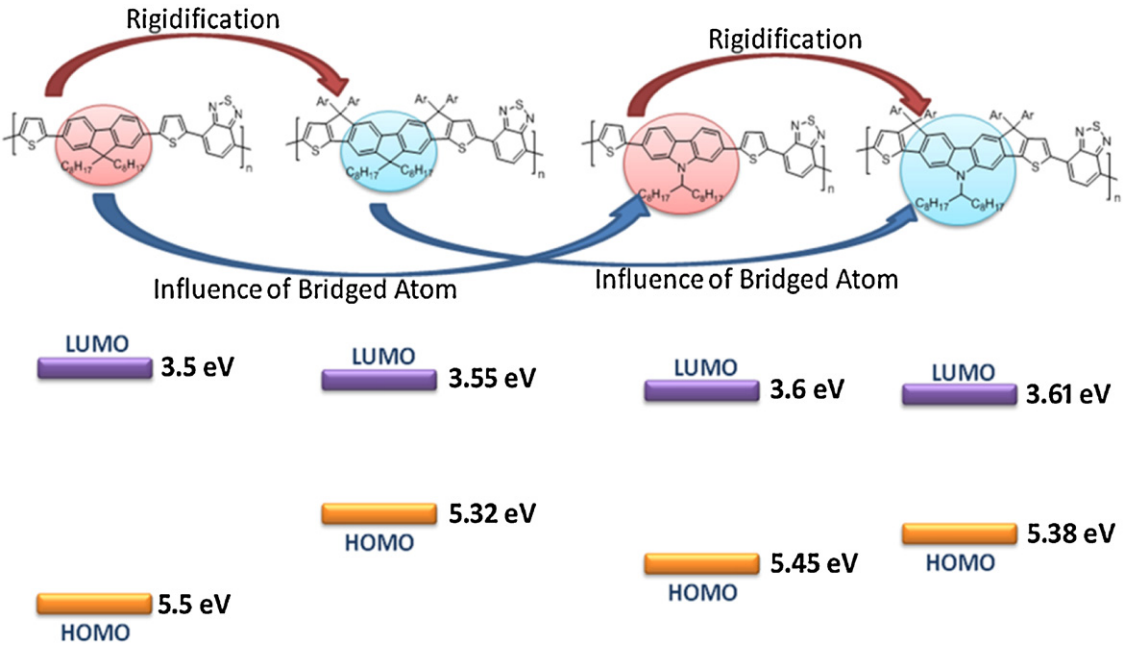

Fig. 9. Influence of the bridged atom and rigidification on the energy levels of the multifused heptacyclic copolymers **293** and **294**.

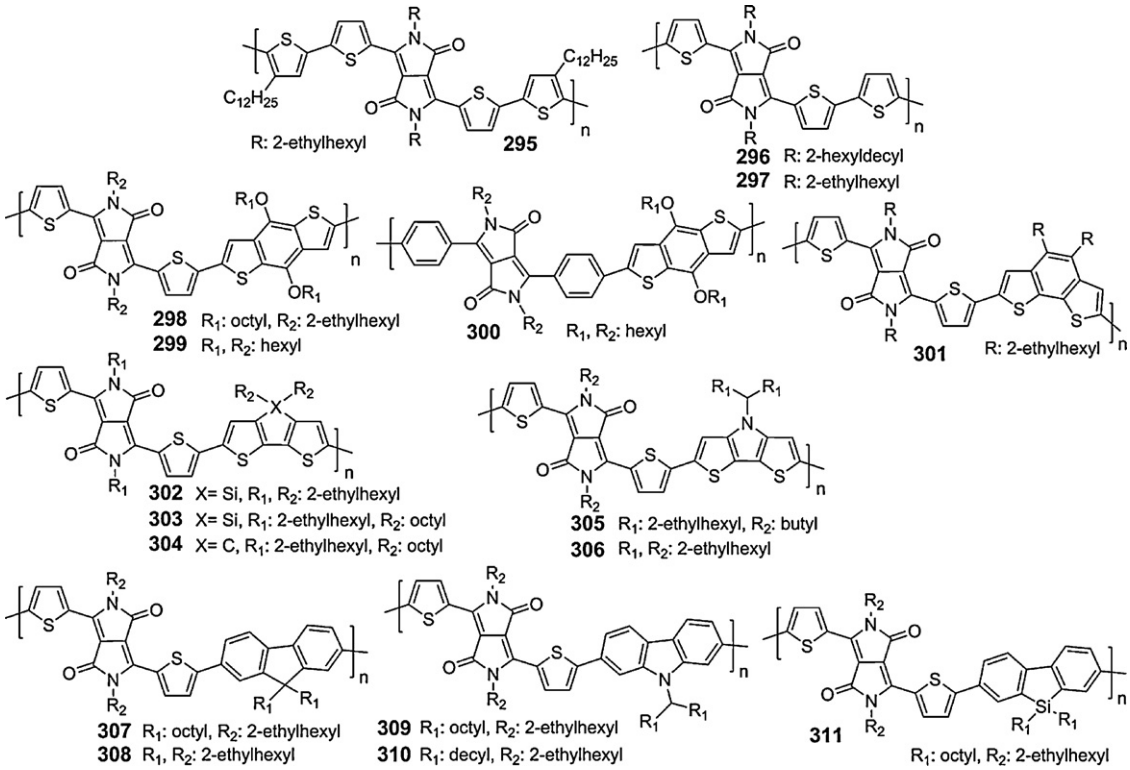

Chart 71. Chemical structures of the poly(diketopyrrolo[3,4-*c*]pyrrole) derivatives **295**–**311**.

excellent ambipolar charge transport properties (hole and electron mobilities up to 0.1 $cm^2/V\,s$) and energy levels at 4.7 eV for the HOMO and 3.0 eV for the LUMO. Finally, it was demonstrated that the selection of solvent affected the photovoltaic performance of the **295**:$PC_{61}BM$ blends [267]. For example, when CF:*o*-dichlorobenzene (ODCB) mixture or ODCB are used as solvents, higher PCE was observed compared to CF, which is related with the morphology of the as-deposit layer. The surface morphology of layers from CF:ODCB mixtures and from

ODCB dispersions displays small features (<100 nm), while films from CF present domains with dimensions of several hundreds of nanometers. The unfavourable morphology of the CF processed films cannot be improved even after the application of thermal treatment [267].

On the basis of this high PCE, a large library of DPP-based conjugated polymers has been synthesized (**296**–**311**) [268–274] from many research groups by either Suzuki or Stille cross-coupling polycondensation (Chart 71). Several typical conjugated building blocks (including: thiophene, fluorene, carbazole, dibenzosilole, CPDT, DTS, DTP, B_{1245}DT and B_{2134}DT) have been used to tune the optoelectronic properties of the DPP-based polymers. The optical band gaps, the energy levels and the PCEs of the synthesized copolymers are presented in Table 41.

As can be seen, the copolymer **296** with an unsubstituted terthiophene segment between each pair of DPP units presents enhanced PCE (4.7%) as compared to that of **295** when blended with $PC_{71}BM$ in 1:2 (w/w) [268]. Moreover, it was shown that the PCE of **296** is dependent from its molecular weight. The higher the molecular weight (M_n = 54,000 g/mol), the higher the PCE. This behaviour is attributed to the fact that the lower M_n (10,000 g/mol) of **296** presents a reduction in the photocurrent and as a sequence to the PCE (2.7% in blends with $PC_{71}BM$ in 1:2, w/w), which is in contrast to the constant FET mobility of both high and low M_n derivatives of **296** that exhibit almost the same values (10^{-2} cm^2/V s) for both electron and holes [268].

Among the other DPP-based conjugated polymers with either 5 or 6 membered fused bridged bithiophene units B_{1245}DT (**298**–**300**) [269,274], B_{2134}DT (**301**) [269], DTS (**302**, **303**) [269,272], CPDT (**304**) [273] and DTP (**305**, **306**) [270,271], **301** exhibits the highest PCE of 4.45% when blended with $PC_{71}BM$ in 1:2 (w/w) ratio with J_{sc} = 10 mA/cm^2, V_{oc} = 0.72 V and FF = 0.62 after thermal annealing at 110 °C for 30 min [269]. Then, the PCE follows the order: **299** (2.78%) [274], **305** (2.71%) [270], **298** (2.53%) [269], **304** (2.27%) [273], **302** (2.10%) [269], **300** (1.51%) [274] and **306** (1.12%) [271], which is not in accordance with the order of the band gap lowering that is as follows: **300** (1.70 eV) > **299** (1.43 eV) > **298** = **304** (1.31 eV) > **302** (1.29 eV) > **303** (1.24 eV) > **305** = **306** (1.13 eV). The higher optical band gap of **300** cannot be attributed to the B_{1245}DT unit but rather to the presence of the phenyl rings next to the DPP unit because by switching the phenyl rings with the more electron rich thiophene rings in **299**, the band gap significantly drops to 1.43 eV. The lowering of the band gap is achieved through the raising of the HOMO level since that the LUMO levels of **299** and **300** are almost similar (a small variation of 0.05 eV is detected), indicating that the LUMO level is localized at the DPP unit. The structural analogue **298** with the longer octyl side chain on the B_{1245}DT and the 2-ethylhexyl side chains on DPP exhibits lower band gap than that of **299** indicating that most probably the π–π stacking between the polymer chains is more efficient with the presence of branched alkyl chains on the DPP unit. In addition, even though the band gap of **298** is equal to **304** (1.31 eV), the replacing of the B_{1245}DT with CPDT upshifts both the energy levels of **304** by 0.2 eV. Moreover, further lowering of the band gap at 1.24 eV was achieved by changing the bridged carbon atom of **304** with silicon in **303**. Opposite to what is observed in **298** and **299**, the presence of branched alkyl side chains on the DPP unit of **302** results with slightly increased band gap as compared to **303**. Further lowering of the band gap can be achieved by switching from the DTS to the DTP. The optical band gaps of **305** and **306** are the same (1.13 eV) showing that the type of the alkyl side chains does not influence the optical band gap but rather the energy levels of the copolymers (Table 41). It is obvious that the LUMO levels of both polymers are similar, verifying that the LUMO level is localized on the DPP unit, whereas the HOMO level of **306** is situated 0.12 eV deeper than that of **305**. This can be explained by the disruption of the conjugation along the polymer chain as a result of the presence of the branched alkyl side chains. Comparing the energy levels of the structural related copolymers **302** and **306**, the lowering of the band gap by passing from the DTS to the DTP unit is achieved by the lowering of the LUMO level since that the HOMO levels of both polymers are similar (Table 41). This is the result of the presence of the more electronegative nitrogen atom of the DTP unit as compared to the silicon atom of the DTS. The PCE of **305**:$PC_{71}BM$ in 1:2 (w/w) is 2.71%, the highest recorded among copolymers that cover the whole range of the solar spectrum from 300 to 1100 nm and have a very LBG (1.13 eV) with J_{sc} = 14.87 mA/cm^2, V_{oc} = 0.38 V and FF = 0.48 [270]. The HOMO level of **305** (4.90 eV) is possibly responsible for the low V_{oc}.

Concerning the DPP-based copolymers with fluorene (**307**, **308**) [269,271,272], carbazole (**309**, **310**) [271,272] and dibenzosilole (**311**) [272], the optical band gaps of the fluorene and carbazole DPP based copolymers are influenced from the choice of the alkyl side chain (linear versus branched), as shown in Table 41. For example, **307** containing a fluorene with linear alkyl chains has a much lower band gap (1.31 eV) than the similar analogue **308** (1.75 eV) with branched alkyl chains due to the better packing of the polymer chains. This is also verified based on the energy level values of **307** and **308**. Even though their LUMO levels are similar, the presence of the branched alkyl side chains in **308** results to a deeper HOMO level. Similar observations are presented in **309** and **310** where a small increase in the length of the linear alkyl side chain of the carbazole monomer in **310** results to a small increase of the band gap (1.63 eV) as compared to **309** (1.57 eV). Interestingly, **311** containing a dibenzosilole with the same alkyl side chains in the polymer backbone as the fluorene unit of **307** exhibits an optical band gap of 1.31 eV similar to that of **307** indicating that the bridged atom of the biphenylene unit does not influence the band gap of the resulting copolymers, opposite to what is observed in the 5 member bridged bithiophene-based copolymers **303** and **304**. Finally, the photovoltaic performance of **307**–**311** has been examined and **310** exhibits the higher PCE (2.26%) in blends with $PC_{61}BM$ in 1:2 (w/w) ratio with J_{sc} = 5.35 mA/cm^2, V_{oc} = 0.76 V and FF = 0.56 [271] which is 40% increased from the related **309** (1.6%) [272]. The improved miscibility with the appearance of a rather smooth surface and intimate mixing of the **310**:$PC_{61}BM$ blend compared to the rough surface and coarse phase separation of **307** or **308**:$PC_{61}BM$ blends, as confirmed from the morphology studies based

Table 41
Optical band gaps, energy levels and photovoltaic efficiency of **295**–**311**.

Polymers	E_g^{opt} (eV)	LUMO (eV)	HOMO (eV)	PCE (%)	Polymers	E_g^{opt} (eV)	LUMO (eV)	HOMO (eV)	PCE (%)
295	1.4	3.00	4.70	4.00	**304**	1.31	3.31	4.95	2.27
296	1.3	3.61	5.17	4.70	**305**	1.13	3.63	4.90	2.71
297	1.2	3.87	5.26	–	**306**	1.13	3.64	5.02	1.12
298	1.31	3.51	5.16	2.53	**307**	1.31	3.60	5.23	0.78
299	1.43	3.69	5.15	2.78	**308**	1.75	3.64	5.42	0.88
300	1.70	3.74	5.47	1.51	**309**	1.57	3.92	5.44	1.60
301	1.34	3.63	5.21	4.45	**310**	1.63	3.66	5.35	2.26
302	1.29	3.47	5.04	2.10	**311**	1.31	3.90	5.43	–
303	1.24	3.80	5.31	–					

on AFM, explain the higher PCE of the carbazole based DPP copolymers [271].

3.2.15.2. Thieno[3,4-b]pyrazine-based polymers. One of the most well-studied electron deficient unit, except 2,1,3-benzothiadiazole, quinoxaline and DPP, used for lowering the band gap of conjugated polymers through the D–A approach is thieno[3,4-*b*]pyrazine (TP). TP moiety is an attractive building block owing to its ability to provide more planar backbone between repeating units due to the less steric hindrance of the thiophene compared to the benzene ring in 2,1,3-benzothiadiazole or quinoxaline polymers [275]. By replacing the 2,1,3-benzothiadiazole in the TBzT segment with TP, a new thiophene-thieno[3,4-*b*]pyrazine-thiophene (TTPT) segment has been synthesized, where upon its homopolymerization or copolymerization with various electron rich units, like fluorene, carbazole and thiophene (Chart 72), several TP-based copolymers were synthesized (**312**–**326**) [124,275–280] that their optoelectronic properties can be easily fine tuned.

The optoelectronic properties and the PCEs of **312**–**326** are presented in Table 42. The optical band gaps of the alternating copolymers **312**–**315** [276] are ranged between 1.68 and 1.81 eV and are significantly higher than that of the other TTPT-based homopolymers (**316**–**323**) and copolymers with thiophene units (**324**–**326**), which are between 1.20 and 1.33 eV. Regarding **312**–**315**, the optical band gaps of the carbazole alternating TTPT copolymers **314**–**315** are lower than the related fluorene analogues **312**–**313**, while the phenyl substituted TP derivatives **313** and **315** showing lower band gaps than that of the methyl substituted TP derivatives **312** and **314**. Moreover, the polymers **312**–**315** demonstrate similar HOMO levels (Table 42), while the LUMO levels of **313** and **315** are ~0.1 eV lower that the related methyl substituted **312** and **314**, indicating that the presence of aromatic substituents on the TP unit increasing the electron affinity of the resulting copolymers.

The preparation of **312** along with the above mentioned **308** allow for the reliable comparison on how the three different electron withdrawing monomers (2,1,3-benzothiadiazole, TP and DPP) influence separately the HOMO and LUMO levels and the overall optical band gap of the PF derivatives presented in Fig. 10. The selection of these PF derivatives was made on the basis to compare polymers with identical conjugated backbones and varying only the electron withdrawing unit, in order to avoid the influence of any side effects. For example, as shown

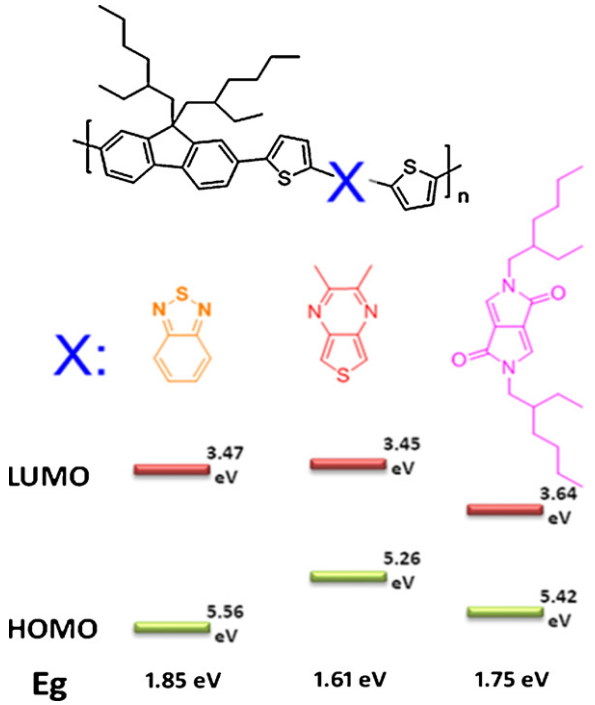

Fig. 10. Comparison of the energy levels and optical band gaps for the polyfluorene derivatives **198**, **312**, and **308**.

above in this text any differentiation on the length of the alkyl side chains affect both the energy levels and the band gap of the resulting polymers. Based on Fig. 10, the optical band gap of the PF derivatives decreases following the order 2,1,3-benzothiadiazole > DPP > TP. However, it cannot be excluded the fact that the band gap of the DPP-based PF derivative **308** is higher than that of the TP-based PF derivative **312** due to the presence of the side alkyl chains on the DPP. Moreover, comparing the energy levels of the polymers it is realized that the LUMO levels of the 2,1,3-benzothiadiazole and TP-based PF derivatives are similar [276], within the accuracy of the measurement, indicating that the electron affinity is almost the same for these two polymers and the observed variation on the band gap can mainly be attributed to the raised HOMO level of the TP-based copolymer [276]. For the DPP-based PF copolymer it is observed that the LUMO level is situated lower than that of the other two PF copolymers indicating that upon insertion of the DPP unit into the polymer backbone the

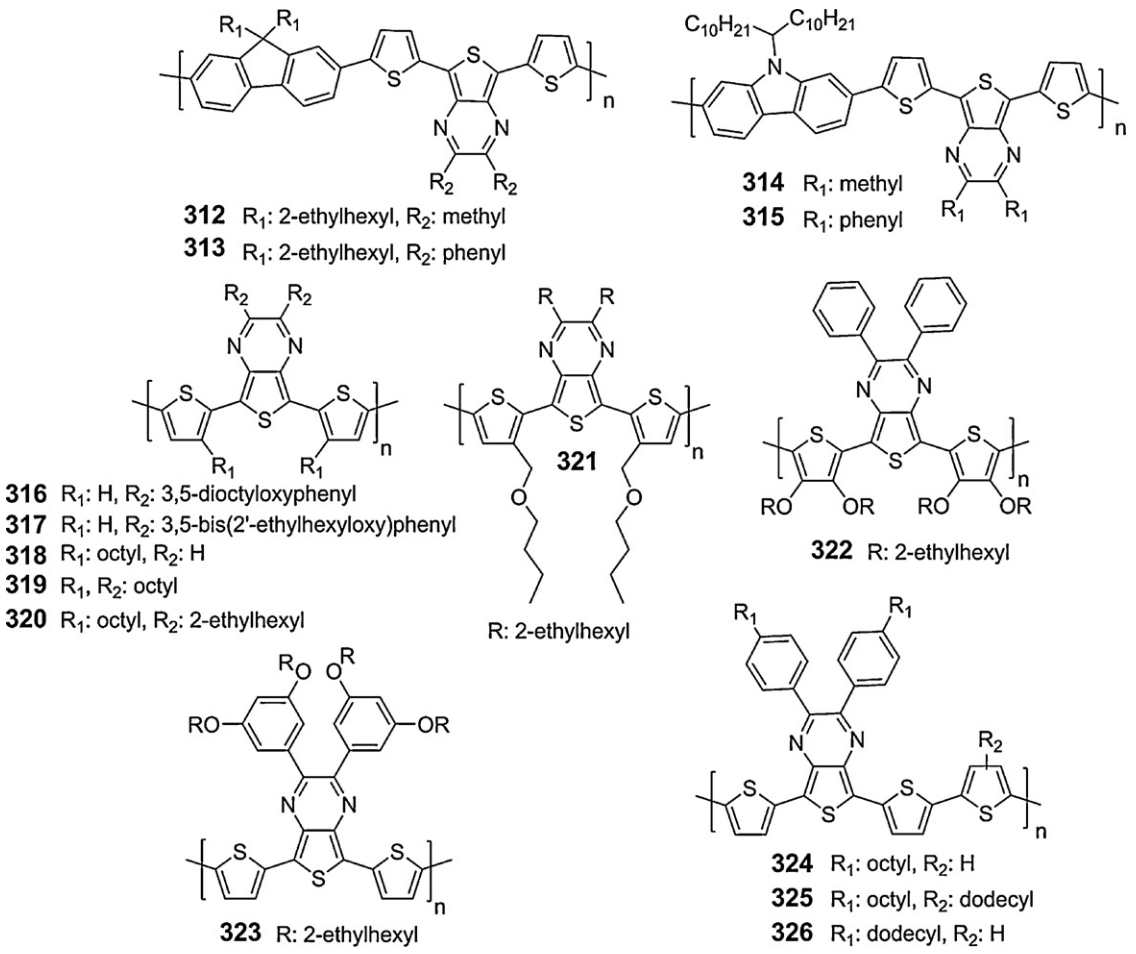

Chart 72. Chemical structures of the poly(thieno[3,4-*b*]pyrazine) derivatives **312**–**326**.

electron affinity of the resulting PF copolymer significantly increases despite the fact of the presence of the bulky alkyl chains in the sides of the DPP unit.

Moreover, studying the oxidation and reduction potential of homopolymers **318**–**321** it is shown that in **318** [277], where two octyl-substituted thiophene rings were combined with an unsubstituted-TP unit, the reduction potential is −1.68 V and the oxidation potential is +0.14 V. Upon substitution of the TP unit with linear (**319**) [278] or branched (**320**) [278] alkyl chains, the reduction potentials are identical and slightly higher than that of **318** (0.13 V and 0.15 V, respectively). On the other hand, the oxidation potential between these three polymers (**318**–**320**) presents significant variation. By passing from

Table 42
Optical band gaps, electrochemical properties and photovoltaic efficiency of **312**–**326**.

Polymers	E_g^{opt} (eV)	E_{red} (V)/LUMO (eV)	E_{ox} (V)/HOMO (eV)	PCE (%)
312	1.81	−1.35/3.45	+0.46/5.26	1.37
313	1.74	−1.27/3.53	+0.47/5.27	0.89
314	1.79	−1.35/3.45	+0.44/5.24	1.02
315	1.68	−1.25/3.55	+0.43/5.23	0.90
316	1.28	−1.47/–	−0.14/–	0.61
317	1.21	−1.40/–	−0.11/–	1.46
318	1.30	−1.65/–	+0.14/–	0.09
319	1.28	−1.78/–	−0.17/–	0.70
320	1.31	−1.80/–	−0.29/–	0.50
321	1.33	−1.79/–	−0.26/–	0.80
322	1.28	−1.65/–	−0.19/–	0.29
323	1.20	−1.47/–	−0.01/–	1.10
324	~1.30	–/–	–/–	0.22
325	~1.30	–/–	–/–	0.011
326	~1.30	–/–	–/–	0.0028

the unsubstituted-TP **318** to octyl substituted-TP **319** or to 2-ethylhexyl substituted-TP **320** subsequent lowering of the oxidation potential by 0.31 V and 0.43 V, respectively is observed indicating that introduction of alkyl side chains on the TP affects mostly the HOMO level of the polymers and less the LUMO level. In addition, the constant reduction potential of **319** and **320** points to a more localized LUMO on the TP in the polymer chain. Furthermore, the replacement of the octyl side chains from the thiophene rings of **320** with *n*-butoxymethyl chains in **321** [278] has minimum impact on the reduction potential, while the oxidation potential of **321** is slightly decreased due to an inductive effect [278].

The TTPT-based homopolymers **318**–**321** studied containing unsubstituted TP units or TP functionalized with linear or branched alkyl side chains that exhibit band gaps between 1.28 eV and 1.33 eV, while the values of their reduction potentials provide a rather high lying LUMO levels. Thus, in order to achieve further lowering of the band gap by decreasing the reduction potential, two phenyl-substituted TP homopolymers based on TTPT segment were synthesized, that carry four 2-ethylhexyloxy side chains on the thiophene rings of **322** [279] or on the outer phenyl rings in **323** [279]. As reported previously for copolymers **312**–**315**, the phenyl-substituted TP copolymers **313**–**315** exhibit at least 0.1 eV lower band gaps and 0.1 eV lower LUMO levels than alkyl-substituted TP copolymers **312**–**314**. In this case, the optical band gaps of **322** and **323** are 1.28 eV and 1.20 eV, respectively indicating better chain organization in the solid state when the alkoxy side chains are situated to the outer phenyl rings in **323**, while the band gap of **323** is ~0.1 eV lower than that of **318**–**321**. Regarding the reduction and oxidation potentials, **322** reveals a low oxidation potential at −0.19 V and a reduction potential at −1.65 V, similar to that of **318** consisting of the unsubstituted TP. Upon switching the alkoxy side chains from the thiophene rings in **322** to the outer phenyl rings in **323** both the oxidation and reduction potentials are shifted by 0.18 V (Table 42). Finally, all the thiophene-*alt*-TTPT copolymers **324**–**326** [280] present a virtually identical band gap of 1.30 eV, regardless the use or not of alkyl side chain on the thiophene ring and the length of the alkyl side chain on the phenyl rings of the TP unit.

The polymers **312**, **314** and **323** when blended with $PC_{61}BM$ in 1:3 (w/w) ratio (**312**, **314**) [276] or 1:4 (w/w) ratio (**323**) [279] and **317** in blends with $PC_{71}BM$ in 1:4 (w/w) ratio [124] present promising photovoltaic performance with PCEs above 1%. The PCE of **317** (1.46%) with J_{sc} = 5.9 mA/cm^2, V_{oc} = 0.65 V and FF = 0.38 is the highest reported for a TP-based copolymer [124]. In addition, despite the fact that **312** exhibits the higher optical band gap among the TP-based copolymers, its PCE (1.37%) with J_{sc} = 3.97 mA/cm^2, V_{oc} = 0.60 V and FF = 0.57 [276] is very close to **317**. Based on these results, it is evident that the methyl substituted TP-based PF (**312**) or polycarbazole (**314**) exhibit slightly higher PCEs than that of the phenyl-substituted TP copolymers **313** and **315**. Moreover, the positioning of the solubilizing side chains influence the PCE since that changing the position of the alkoxy side chains from the thiophene rings in **322** to the outer phenyl ring in **323** the PCE improved from 0.29% (**322**) to 1.10% (**323**) [279]. The improvement in the PCE was attributed to the more favourable morphology of the blend and higher V_{oc} due to the deeper HOMO level. In addition, the choice of the side chains (linear/branched/ether function) between the three copolymers **319**–**321** also affects the PCE of the devices. The introduction of the ether side chains (*n*-butoxymethyl) in the polymer backbone of **321** increases the solubility and as a consequence the processability, without preventing the aggregation between the polymer chains. All these lead to enhanced charge transport and PCE (Table 42) [278]. Finally, the other copolymers generally demonstrate low PCEs due to the very low V_{oc}, as a result of their high lying HOMO levels, signifying as well their poor oxidative stability.

Other examples of TP-based copolymers are those consisting of fused aromatic TP units in their polymer backbone. The presence of fused aromatic TP unit provides a flat π-electron rich face, which can promote π–π stacking between the polymeric chains. These enhanced interactions can improve the crystallinity as well as the absorption coefficiencies of the polymers in the solid state [275,280]. Therefore, several fluorene, thiophene and bithiophene copolymers containing fused phenanthrene (**327**–**331**) and acenapthalene (**332**–**335**) TP moieties were synthesized by Suzuki and Stille cross-coupling polymerization (Chart 73) [275,280].

The optical band gaps, the energy levels and the PCEs of **327**–**335** are included in Table 43. Initially, comparing the optical band gaps of **328**–**330** [280] with the structural analogue polymers **324**–**326** it is evident that by adding an extra bond between the two phenyl rings on the TP of **324**–**326**, in order to form the planar 11-thia-9,13-diazacyclopenta[*b*]triphenylene (phenanthrene) acceptor, the absorption spectra of **328**–**330** were red shifted providing a lower optical band gap around 1.2 eV. Moreover, the band gaps of **327** [275] and **331**–**335** [275] depend significantly on the fused-aromatic moiety present in the TPs, showing that the phenanthrene-containing polymers have lower band gaps than that of the acenapthalene copolymers. The phenanthrene copolymers containing the bithiophene unit exhibit the lowest band gap (1.16 eV) (Table 43). Comparing the band gaps of the structural related PF copolymers **327**, **333** or the bithiophene copolymers **331**, **335** it is shown that the band gaps of **333** and **327** are 1.62 eV and 1.40 eV, respectively whereas those of **335** and **331** are 1.43 eV and 1.16 eV, respectively. In addition, the band gap of the linear alkyl substituted acenapthalene copolymer **332** is lower than that of its corresponding branched alkyl substituted copolymer **333**, due to the better π–π stacking between the polymer chains. Similar observation is reported by studying copolymers **334** and **335**. Regarding the energy levels, the LUMO level of the phenanthrene-containing polymers is lower than that of the acenapthalene copolymers pointing out that the phenanthrene moiety has higher electron affinity than the acenapthalene unit. On the other hand, the HOMO level of the polymers is independent from the electron withdrawing unit and is primarily determined by the fluorene and the bithiophene units.

The photovoltaic properties of the acenapthalene and phenanthrene-containing polymers **327**–**335** were inves-

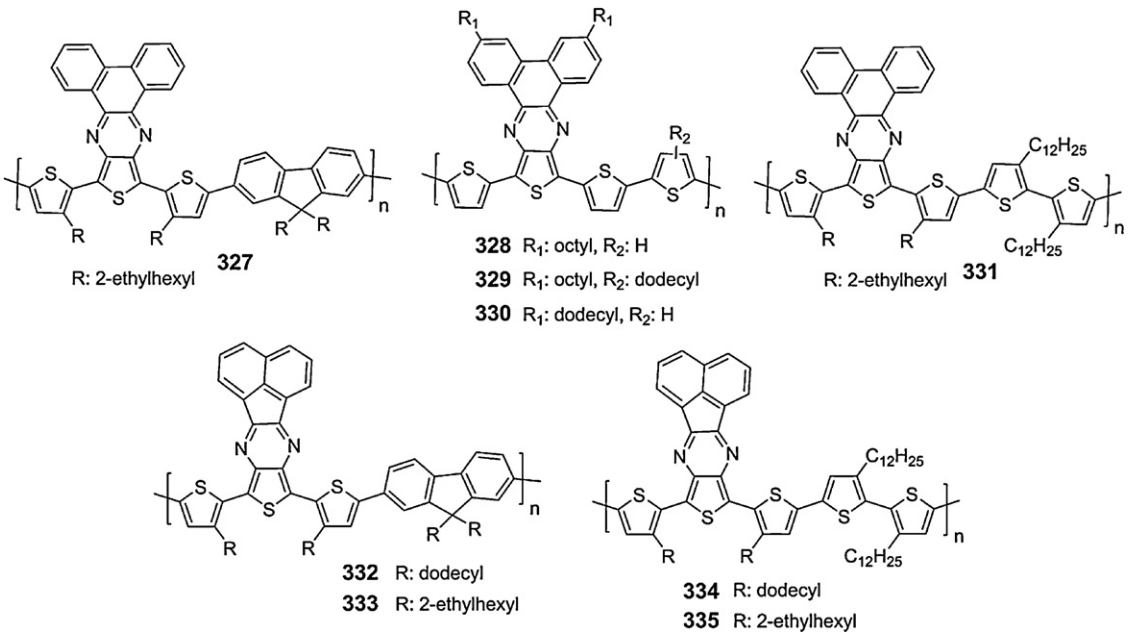

Chart 73. Chemical structures of the fused poly(thieno[3,4-*b*]pyrazine) derivatives **327**–**335**.

Table 43
Optical band gaps, energy levels and photovoltaic efficiency of **327**–**335**.

Polymers	E_g^{opt} (eV)	LUMO (eV)	HOMO (eV)	PCE (%)
327	1.40	3.53	4.93	0.57
328	~1.20	–	–	0.003
329	~1.20	–	–	0.014
330	~1.20	–	–	0.0015
331	1.16	3.79	4.95	0.14
332	1.58	3.34	4.92	0.39
333	1.62	3.38	5.00	0.70[a]/1.30[b]
334	1.33	3.44	4.77	0.13
335	1.43	3.49	4.92	0.34

[a] Using $PC_{61}BM$.
[b] Using $PC_{71}BM$.

tigated in BHJ devices using fullerene derivatives as electron acceptors. PCEs of 1.3% were achieved for **333** in blends with $PC_{71}BM$ (1:4, w/w ratio) with J_{sc} = 5.1 mA/cm^2, V_{oc} = 0.62 V and FF = 0.42 [275]. Moreover, the PF (**333**) and bithiophene (**335**) acenapthalene copolymers with the branched alkyl chains showed better PCEs as compared to their linear analogues **332** and **334** (Table 43). However, the high lying HOMO levels and the low absorption coefficiencies of these polymers are most likely responsible for the limited efficiencies.

3.2.15.3. Bithiazole-based polymers. Bithiazole (BTz) with two thiazole rings connected together is an electron acceptor unit because thiazole is a well-known electron deficient unit since it contains one electron-withdrawing nitrogen of imine in the place of the carbon atom at the 3-position of thiophene ring. Taking this into account, BTz has been used very recently for the synthesis of a series of new alternating LBG conjugated polymers through the D–A approach (Chart 74) with fluorene (**336**) [281], carbazole (**337**) [282], DTP (**338**) [282], and DTS (**339**) [282] as the electron donor moi-

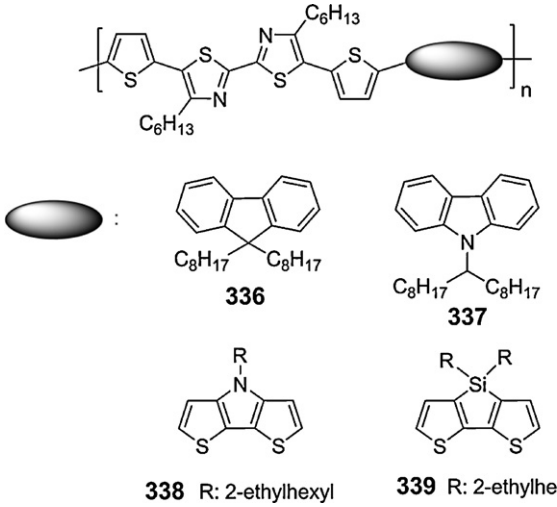

Chart 74. Chemical structures of the poly(bithiazole) derivatives **336**–**339**.

eties by Suzuki (**336**, **337**) or Stille (**338**, **339**) cross-coupling polymerization.

The optical band gap, the energy levels and the PCE of **336**–**339** are included in Table 44. **336** and **337** display higher optical band gaps (2.21 eV), **339** has a band gap of 1.85 eV and finally **338** exhibits the lowest band gap (1.68 eV). The photovoltaic performance of the four copolymers in blends with $PC_{61}BM$ (**337**–**339**) [282] or C_{60} (**336**) [281] in 1:1 (w/w) ratio was examined and **339** demonstrates the higher PCE (1.63%) with J_{sc} = 5.14 mA/cm^2, V_{oc} = 0.70 V and FF = 0.45 due to the more favourable energy levels and high hole mobility (3.07×10^{-4} cm^2/V s based on the SCLC method). The hole mobility value of **339** is one order of magnitude higher than that of **338** (5.01×10^{-5} cm^2/V s) and two order of magnitude than that of **337** (1.02×10^{-6} cm^2/V s) [282]. In addition, some other disadvantages preventing both **337** and **338** for providing higher PCEs are the low J_{sc} (1.24 mA/cm^2) of **337** due to the high optical band gap and the low V_{oc} (0.28 V) of **338** as a result of its high lying HOMO level (4.76 eV). Further optimization of **339**:$PC_{61}BM$ devices through changing the weight ratio at 1:2 (w/w) led to the slightly improvement of the PCE at 1.66% with J_{sc} = 4.49 mA/cm^2, V_{oc} = 0.73 V and FF = 0.51 [282]. The lower J_{sc} at higher $PC_{61}BM$ content could be ascribed by the reduction of the absorption of the active layer. By replacing the $PC_{61}BM$ with $PC_{71}BM$ a significant higher PCE of 2.86% was obtained from the **339**:$PC_{71}BM$ in 1:1 (w/w) ratio with J_{sc} = 7.85 mA/cm^2, V_{oc} = 0.68 V and FF = 0.54 [282]. Apparently, the J_{sc} increased significantly by using the $PC_{71}BM$ as a result of its enhanced visible absorption whereas the V_{oc} retained almost similar to the **339**:$PC_{61}BM$ device.

3.2.15.4. Pyrido[3,4-b]pyrazine-based polymers. As described previously, the pyrido[3,4-*b*]pyrazine (PP)-based polycarbazole derivative **252** display higher electron affinity relative to that of the quinoxaline-based polycarbazole derivative **251** because the former feature more electron-withdrawing nitrogen atoms in the fused ring. However, **252** exhibited a moderate PCE of 1.1% because of its low molecular weight and/or poor solubility. Therefore, four PP-containing LBG polymers (**340**–**343**) of high molecular weight and enhanced solubility in common organic solvents were synthesized by Stille cross-coupling polymerization reaction (Chart 75) [283]. The choice of $B_{1245}DT$ and CPDT as the donor monomers was based on the basis of the good performance of their derivatives when applied in OPVs, while the presence of the octyloxyphenyl groups anchored to the PP moieties increased the solubilities of the resulting copolymers. Furthermore, since that the alternating copolymers **340** and **341** absorb too little in the visible range the use of thiophene or bithiophene units in the random copolymers **342** and **343** extended their light-harvesting abilities by covering the solar spectrum from the visible to a significant portion of the NIR region.

The optical band gaps, the energy levels and the photovoltaic performance of **340**–**343** are included in Table 45. In general, the optical band gaps are tuned in the range of 1.46–1.60 eV and more specifically the PP-based copolymers with the CPDT unit (**341** and **343**) exhibit lower band gaps and elevated HOMO levels as compared to their analogues **340** and **342** (Table 45). Moreover, the LUMO levels of all copolymers are almost similar (in the range of 3.28–3.32 eV) regardless the polymeric architecture (random versus alternating) and the choice of the electron donating unit, indicating that the LUMO levels are localized in the PP monomer.

The PCE of the random copolymers **342** and **343** as estimated in BHJ solar cells with $PC_{71}BM$ in 1:4 (w/w) ratio is higher than that of the alternating copolymers **340** and **341**. The higher PCE of 3.15% is obtained for the **343**:$PC_{71}BM$ with J_{sc} = 10.85 mA/cm^2, V_{oc} = 0.63 V and FF = 0.46 [283]. One of the possible reason that the random copolymers **342** and **343** display higher PCEs than **340** and **341**, except from their broader absorption spectra, is that their morphologies in blends with $PC_{71}BM$ are more homogeneous than those of **340** and **341**. **343** exhibits the most homogeneous surface, presumably contributing to its higher carrier transport in blends with $PC_{71}BM$ (2.36×10^{-4} cm^2/V s as measured by the SCLC model) and dissociation.

3.2.15.5. Benzimidazole-based polymers. Many LBG D–A conjugated polymers with excellent efficiencies have as electron-deficient unit mainly the 2,1,3-benzothiadiazole as demonstrated previously in the text. However, very few heterocycles, that are structural analogues of the 2,1,3-benzothiadiazole, have been studied as alternative electron-withdrawing candidates. Some of these include the 2,1,3-benzooxadiazole and 2,1,3-benzoselenadiazole, where the sulphur atom of the 2,1,3-benzothiadiazole has been replaced by oxygen and selenium, respectively. Similar to 2,1,3-benzooxadiazole and 2,1,3-benzoselenadiazole, benzimidazole is another type of electron-deficient heterocycle that has compensated less attention as alternative to the 2,1,3-benzothiadiazole. In fact, only three LBG D–A conjugated polymers (Chart 76) consisting of the benzimidazole moiety along with fluorene (**344**), carbazole (**345**) and 4*H*-cyclopenta[*def*]phenanthrene (CPP) (**346**) have been synthesized very recently by Suzuki cross-coupling polymerization and have been applied as alternative electron donors in OPVs [284].

The optical band gaps, the energy levels and the PCEs of the copolymers **344**–**346** are presented in Table 46. The band gaps of **344**–**346** are estimated at 1.64 eV and 1.66 eV, which are lower as compared to the related 2,1,3-benzothiadiazole-based copolymers **198**, **248** and **355** (see next in the text). For example, the band gap of **345** is 0.24 eV lower than that of **248** while the band gap of **346** is 0.34 eV lower than that of **355**. Moreover, the LUMO levels of **344**–**346** are situated around 3.6 eV (Table 46) regardless the existence of three different electron donor units in their polymer backbones, indicating that the LUMO level is localized on the benzimidazole unit. On the other hand, the HOMO levels of the copolymers are differentiated from each other by 0.07 eV following the order: **344** > **346** > **345**. Furthermore, when comparing the energy levels of the structural related polymers **246**, **248** and **345**, it is demonstrated that the HOMO levels are similar (5.45 eV for **248** and 5.47 eV for **246**, **345**), verifying that the HOMO level of the polycarbazole derivatives consisting of benzene core-based acceptor units in the main chain

Table 44
Optical band gaps, energy levels and photovoltaic efficiency of **336**–**339**.

Polymers	E_g^{opt} (eV)	LUMO (eV)	HOMO (eV)	PCE (%)
336	2.21	2.77	5.53	0.52
337	2.21	2.91	5.44	0.30
338	1.68	2.79	4.76	0.06
339	1.85	3.09	5.18	1.66[a]/2.86[b]

[a] Using $PC_{61}BM$.
[b] Using $PC_{71}BM$.

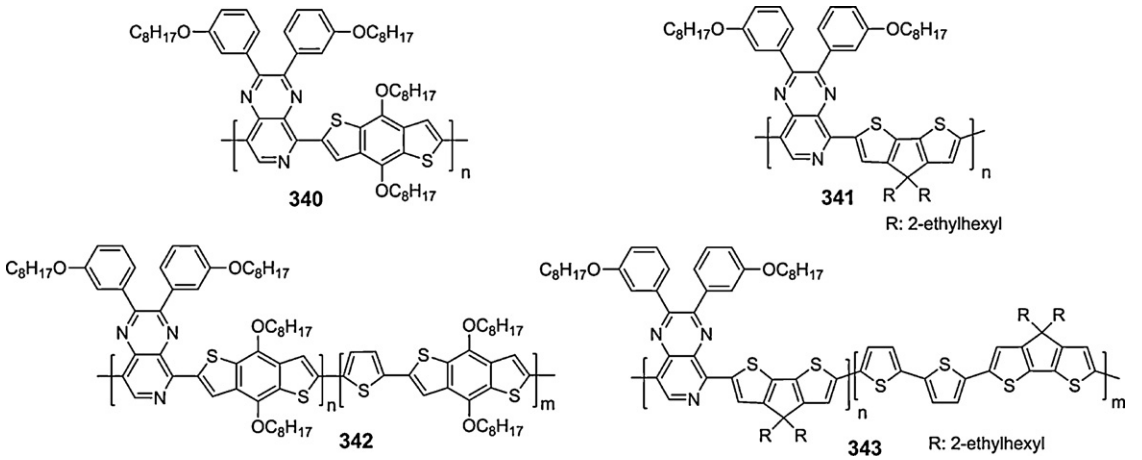

Chart 75. Chemical structures of the poly(pyrido[3,4-*b*]pyrazine) derivatives **340**–**343**.

Table 45
Optical band gaps, energy levels and photovoltaic efficiency of **340**–**343**.

Polymers	E_g^{opt} (eV)	LUMO (eV)	HOMO (eV)	PCE (%)
340	1.58	3.32	5.22	1.20
341	1.46	3.31	5.18	1.82
342	1.60	3.28	5.20	2.35
343	1.49	3.30	5.13	3.15

Table 46
Optical band gaps, energy levels and photovoltaic efficiency of **344**–**346**.

Polymers	E_g^{opt} (eV)	LUMO (eV)	HOMO (eV)	PCE (%)
344	1.64	3.63	5.61	0.42
345	1.64	3.66	5.47	3.12
346	1.66	3.61	5.54	0.67

is obtained in the range of 5.45–5.47 eV, as reported in Section 3.2.13.3.2. On the contrary, the LUMO level of **345** is similar with the LUMO level of **246** (3.65 eV) and 0.06 eV lower than that of **248** indicating that benzimidazole and 2,1,3-benzooxadiazole have similar electron accepting properties whereas both heterocycles are slightly stronger electron acceptors as compared to 2,1,3-benzothiadiazole. Similar observations are revealed by comparing the energy levels of the polymers **198** and **344**. In this case, the HOMO level of **198** is 0.1 eV raised as compared to **344**, while the LUMO level of **344** is 0.23 eV lower than that of **198**.

All the polymers were applied as donors to conventional BHJ-type OPV devices with $PC_{71}BM$ as the acceptor in 1:4 (w/w) ratio and the PCEs are included in Table 46 [284]. Even though, **345** exhibits the higher PCE (3.12%) with J_{sc} = 10.0 mA/cm^2, V_{oc} = 0.65 V and FF = 0.48, the PCE of **344** and **346** are low presumably due to their lower hole mobilities as compared to **345**. The hole mobilities of the polymers **344**–**346** as estimated in FET measurements are 7.5×10^{-6} cm^2/V s, 2.2×10^{-3} cm^2/V s and 3.9×10^{-5} cm^2/V s, respectively.

3.2.15.6. Benzotriazole-based polymers. Structural related analogue of 2,1,3-benzothiadiazole, 2,1,3-benzooxadiazole, 2,1,3-benzoselenadiazole and benzimidazole is the 1,2,3-benzotriazole heteroaromatic compound which possess strong electron accepting feature because of the two electron withdrawing imine (C=N) and the bridged nitrogen atom. Until recently, 1,2,3-benzotriazole-based homopolymers and copolymers remained relatively unexplored for solar cell applications, but the synthesis of a polymer from 1,2,3-benzotriazole and alkyl-substituted thiophenes that has shown some photovoltaic performance opened the way for the further

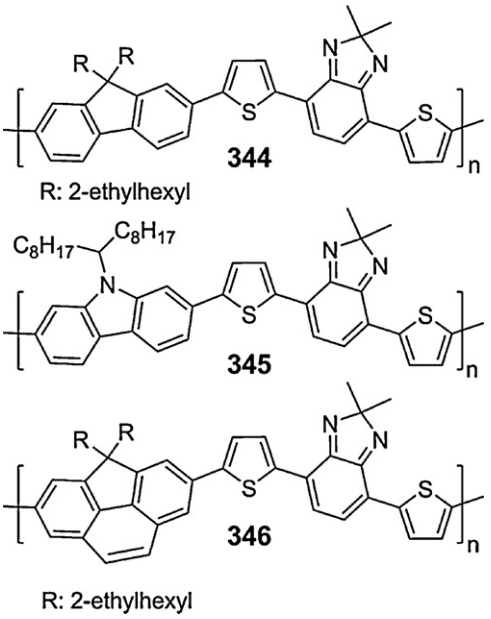

Chart 76. Chemical structures of the poly(benzimidazole) derivatives **344**–**346**.

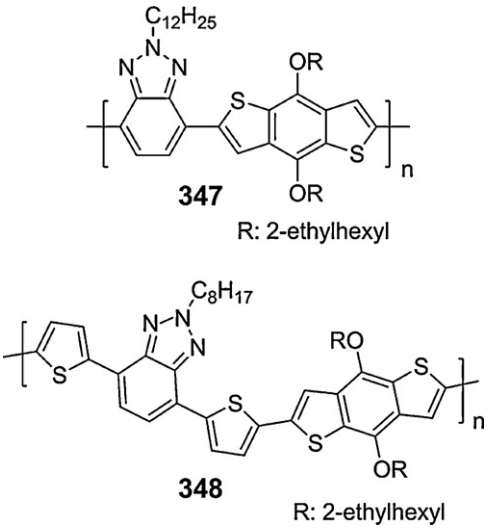

Chart 77. Chemical structures of the poly(1,2,3-benzotriazole) derivatives **347** and **348**.

exploitation of this class of materials for OPVs [285]. On this basis, two new D–A alternating 1,2,3-benzotriazole-based copolymers **347** and **348** (Chart 77) [286] consisting of B_{1245}DT as the electron donor were synthesized by Stille cross-coupling polymerization. Furthermore, the N–H bond of the 1,2,3-benzotriazole can be easily modified by various alkyl chains allowing the tuning of the structural and electronic properties as well as to enhance the processability of the resulting polymers.

The optical band gaps of **347** and **348** are 2.0 eV and 1.95 eV, respectively while their HOMO levels are similar (5.04 eV for **347** and 5.06 eV for **348**). Moreover, photovoltaic devices prepared by **347** and **348** in blends with

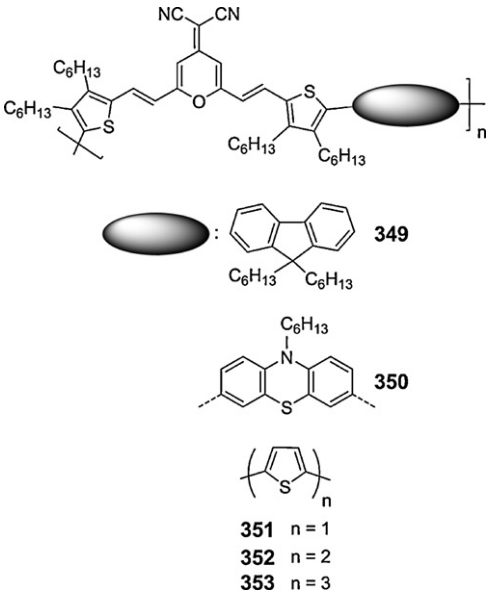

Chart 78. Chemical structures of the poly(2-pyran-4-ylidenemalononitrile) derivatives **349**–**353**.

$PC_{71}BM$ in 1:4 (w/w) ratio demonstrated moderate PCEs of 1.4% and 1.7%, respectively. The photovoltaic parameters of the **348**:$PC_{71}BM$ blend are J_{sc} = 4.5 mA/cm^2, V_{oc} = 0.61 V and FF = 0.62.

3.2.15.7. [2-Pyran-4-ylidenemalononitrile]-based polymers. Another electron-withdrawing unit that has been applied for the synthesis of LBG conjugated polymers through the D–A approach is 2-pyran-4-ylidenemalononitrile (PM). When PM is introduced between two alkyl-substituted thiophenevinyl groups, a coplanar bithiophenevinyl-2-pyran-4-ylidenemalononitrile (TVM) building block has been synthesized which upon polymerization with various electron-rich units like 9,9-dihexylfluorene (**349**) [287], 10-hexylphenothiazine (**350**) [287], thiophene (**351**) [288], bithiophene (**352**) [287,288] and terthiophene (**353**) [288] by either Suzuki or Stille cross-coupling polymerization reactions (Chart 78) provided new TVM-based copolymers with tunable optoelectronic properties as shown in Table 47.

Based on the optical band gaps included in Table 47, it is revealed that the TVM-based copolymers with the oligothiophene units (**351**–**353**) exhibit lower band gaps compared to **349** and **350**. On the other hand, no reliable conclusions can be obtained regarding the impact of the different electron-rich unit used along with TVM on the energy levels of the polymers due to the non-reproducibility of the estimated values (Table 47) for **352** (processed under identical experimental procedures) [287,288]. Even so, the values of Table 47 indicate that the HOMO level of the oligothiophene-TVM copolymers is raised as the number of the thiophene rings in the polymer backbone increases. In addition, comparing the energy levels of **349** and **350** is shown that the LUMO levels are not affected, whereas the HOMO level of **349** is situated significantly deeper than that of **350** indicating that the

Table 47
Optical band gaps, energy levels and photovoltaic efficiency of **349**–**353**.

Polymers	E_g^{opt} (eV)	LUMO (eV)	HOMO (eV)	PCE (%)
349	2.13	3.57	5.63	0.04
350	1.91	3.56	5.25	0.51
351	1.73	3.44	5.44	0.61
352	1.76	3.53 [287]/3.38 [288]	5.29 [287]/5.38 [288]	0.99
353	1.72	3.42	5.15	0.81

phenothiazine has stronger electron-donating ability than fluorene.

BHJ photovoltaic devices were prepared by using the copolymers **349**–**353** and $PC_{61}BM$ in various ratio. The highest PCE was obtained for **352** (0.99%) in 1:3 (w/w) ratio with J_{sc} = 2.39 mA/cm^2, V_{oc} = 0.90 V and FF = 0.46 [287,288]. One of the reasons for the low PCE is the unoptimized thin film morphology of the copolymers with the observation of large scale phase separation. The degree of phase separation can be controlled by adjusting the conjugation length of copolymers **351**–**353** as demonstrated by AFM and TEM studies [288].

3.2.16. Poly(aryl-2,1,3-benzothiadiazole-aryl) derivatives

3.2.16.1. Other poly(thiophene-2,1,3-benzothiadiazole-thiophene) derivatives. As repeatedly reported above, TBzT represents the most popular building block that when it is combined with various comonomers such as: oligothiophenes (**61**–**70**), thieno[3,2-*b*]thiophene (**83**–**85**), CPDT (**118**), DTS (**127**–**129**), DTP (**136** and **137**), DTT (**146**), $B_{1245}DT$ (**167**–**171**), $B_{2134}DT$ (**174**–**177**), fluorene (**194**–**202**), carbazole (**248**), dibenzosilole (**259**), germafluorene (**261**), IF (**265**–**267**), ladder-type tetra-*p*-phenylene (**269**), indeno[2,1-*a*]indene (**271**–**273**) and IC (**278**–**280**) the resulting LBG copolymers exhibit high PCEs in OPVs. Here, some other independent comonomers will be reported that were combined with TBzT segment and cannot be included in the aforementioned categories (Chart 79).

N-Dodecyl-pyrrole is one of the first electron rich unit that was combined with TBzT segment providing **354** [289], synthesized by Stille cross-coupling polymerization and exhibits an optical band gap of 1.6 eV. The energy levels of **354** are situated at 5.50 eV the HOMO and 3.73 eV the LUMO. Blends of **354** with $PC_{61}BM$ in 1:3 (w/w) ratio show a PCE of 1% with J_{sc} = 3.1 mA/cm^2, V_{oc} = 0.72 V and FF = 0.37. The low molecular weight and the unfavourable morphology within the **354**:$PC_{61}BM$ blend are two possible reasons for this moderate PCE [289].

Another monomer with rigid backbone is CPP that when copolymerized with TBzT segment by Suzuki cross-coupling polymerization, 2 new conjugated polymers (**355** and **356**) are provided [290]. The optical band gap of **356** (1.80 eV) is lower than that of **355** (2.00 eV) due to the presence of the alkoxy-substituted phenyl rings on the CPP of **356**, as compared to the alkyl side chains of **355**. In addition, the HOMO levels of **355** and **356** are 5.40 eV and 5.30 eV, respectively showing that the HOMO of **356** is slightly raised as a result of the presence of the more electron-donating substituents on its polymer backbone. BHJ solar cells based on blends of **355** and **356** with $PC_{71}BM$ in 1:4 (w/w) ratio were prepared and PCEs of 1.00% for **355** (J_{sc} = 4.70 mA/cm^2, V_{oc} = 0.71 V and FF = 0.30) and 1.12% for **356** (J_{sc} = 4.60 mA/cm^2, V_{oc} = 0.61 V and FF = 0.40) were obtained [290]. The slightly enhanced PCE of **356** is attributed to the higher FF, even though it exhibits lower V_{oc} and J_{sc}.

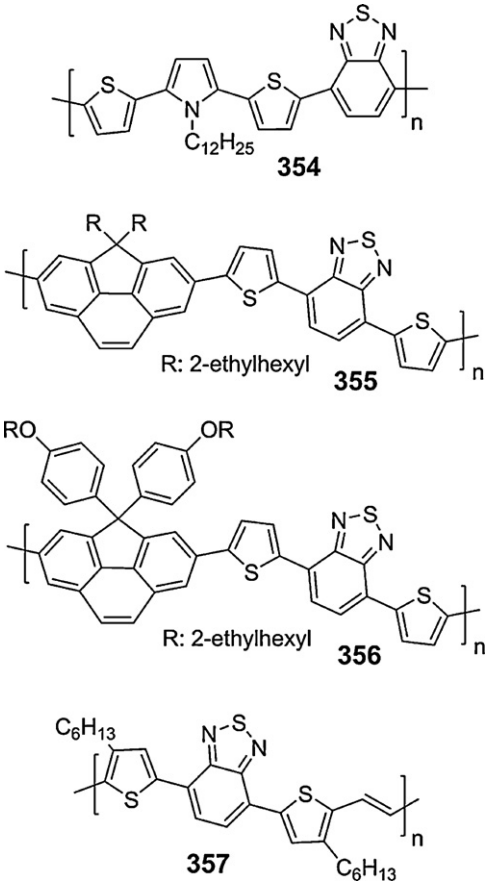

Chart 79. Chemical structures of poly(thiophene-[2,1,3]-benzothiadiazole-thiophene) derivatives **354**–**357**.

Finally, a poly(TBzT-vinylene) **357** has been synthesized by Stille cross-coupling polymerization and displays an optical band gap of 1.5 eV [291]. The HOMO and LUMO levels of **357** are 4.99 eV and 3.49 eV, respectively and a PCE of 0.51% with J_{sc} = 3.1 mA/cm^2, V_{oc} = 0.66 V and FF = 0.51 was obtained from **357**:$PC_{71}BM$ in 1:1 (w/w).

3.2.16.2. Poly(phenyl-2,1,3-benzothiadiazole-phenyl) derivatives. By switching the two thiophene rings of

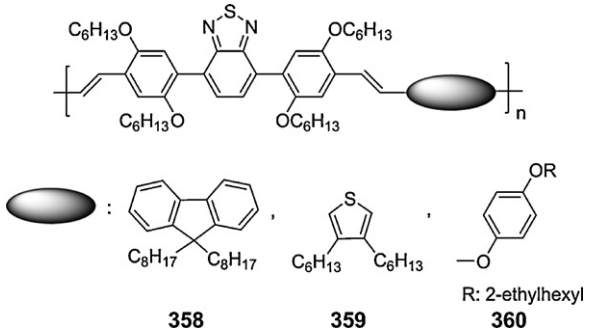

Chart 80. Chemical structures of the poly(phenylene-[2,1,3]-benzothiadiazole-phenylene) derivatives **358**–**360**.

the TBzT segment with the two less electron rich phenylene rings, the 4,7-diphenyl-2,1,3-benzothiadiazole (DPBz) is obtained which is known to be a strong fluorescent dye, with a low-lying HOMO level, finding application in many optoelectronic applications [292]. However, the band gap of DPBz is relatively large (2.8 eV), higher than that of the TBzT segment. In order to obtain LBG polymers based on the DPBz, three new vinylene-type copolymers consisting of a hexyloxy-functionalized DPBz segment alternate with dioctylfluorene (**358**) or dihexylthiophene (**359**) or dialkyloxyphenylene (**360**) were synthesized by Horner polycondensation reaction (Chart 80) [293].

The optical band gaps, the energy levels and the PCEs of **358**–**360** are included in Table 48. The optical band gaps of **358**–**360** are all above 2.0 eV which cannot be consider very LBG polymers. The decrease of the band gap follows the order: **358** > **360** > **359**. **358** and **360** exhibit low-lying HOMO levels (Table 48), whereas the HOMO level of **359** is upshifted and situated at 5.11 eV. The electron affinity follows the order **358** > **359** > **360**.

BHJ photovoltaic devices based on blends of **358**–**360** with $PC_{61}BM$ in 1:4 (w/w) ratio were prepared and PCEs of 1.62% for **360**, with J_{sc} = 3.93 mA/cm^2, V_{oc} = 0.96 V and FF = 0.43, were obtained [293]. All three copolymers demonstrated very high V_{oc}, and especially for **358**:$PC_{61}BM$ blend the V_{oc} was above 1.0 V (1.04 V), as the result of its low-lying HOMO level [293]. One of the reasons of the higher PCE of **360** is its higher hole mobility (2.4×10^{-6} cm^2/V s) as measured by the SCLC method as compared to the hole mobilities of **358** (2.4×10^{-6} cm^2/V s) and **359** (2.4×10^{-6} cm^2/V s).

3.2.17. Conjugated polymers that published after the submission of the review and act as electron donor components in organic photovoltaics

You et al. have recently reported the synthesis of alternating conjugated polymers based on alkyl functionalized on the 4-position of the thienyl groups of TBzT segment, and NDT (**361**–**366**) [294] or dithieno[3,2-*f*:2′,3′-*h*]quinoxaline (QDT) **367** [295] by Stille cross-coupling polymerization (Chart 81). It is shown that the side chains attached to the conjugated backbone of **361**–**366** affect the energy levels and significantly impact the PCE of the corresponding BHJ solar cells (Table 49). Moreover, it appears that the short and branched 2-ethylhexyl side chains, anchored through out the conjugated backbone of **366**, are the optimum side chains for the studied **361**–**366** copolymers [294]. Furthermore, comparing the two structurally related polymers **366** and **367**, it is shown that the incorporation of the electron-withdrawing nitrogen

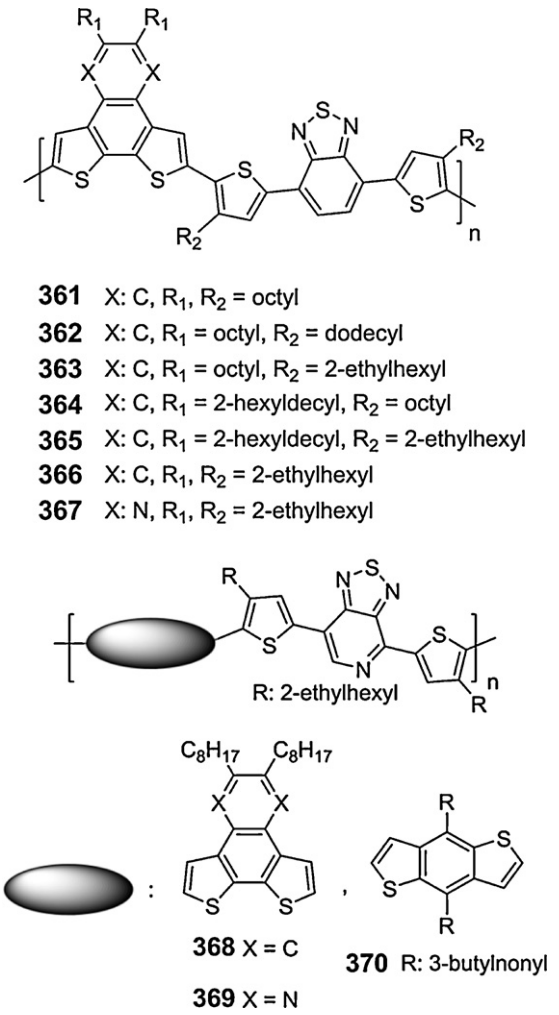

Chart 81. Chemical structures of the TBzT (**361**–**367**) and TPyT (**368**–**370**) based poly(benzodithiophene) derivatives.

Table 48
Optical band gaps, energy levels and photovoltaic efficiency of **358**–**360**.

Polymers	E_g^{opt} (eV)	LUMO (eV)	HOMO (eV)	PCE (%)
358	2.32	3.05	5.45	1.25
359	2.02	3.01	5.11	0.65
360	2.24	2.98	5.23	1.62

Table 49
Optical band gaps, energy levels and photovoltaic efficiency of **361**–**412**.

Polymers	E_g^{opt} (eV)	LUMO (eV)	HOMO (eV)	PCE (%)	Polymers	E_g^{opt} (eV)	LUMO (eV)	HOMO (eV)	PCE (%)
361	–	3.19	5.13	1.20	**387**	1.82	3.10	5.56	4.70
362	–	3.12	5.27	1.28	**388**	1.50	–	4.85	1.54
363	–	3.21	5.30	3.00	**389**	1.50	–	5.05	0.64
364	–	3.12	5.32	2.17	**390**	1.67	–	5.26	3.15
365	–	3.20	5.33	2.01	**391**[c]	–	–	–	–
366	1.61	3.29	5.34	4.30	**392**	1.84	3.70	5.49	0.95
367	1.70	3.28	5.46	5.10	**393**[c]	–	–	–	–
368	1.53	3.42	5.36	6.20	**394**	1.88	3.70	5.56	3.90
369	1.56	3.44	5.50	5.57	**395**	1.84	3.78	5.54	3.50
370	1.51	3.44	5.47	6.32	**396**	1.86	3.83	5.66	0.20
371	1.70	3.30	5.70	6.00	**397**	1.88	3.70	5.56	3.60
372	1.10	3.90	5.64	2.10	**398**	1.89	3.78	5.73	0.70
373	1.53	3.53	5.35	5.50	**399**	1.64	3.61	5.17	4.02
374	1.59	3.56	5.22	3.80	**400**	2.00	–	5.04	2.03
375	1.35	3.80	5.50	4.10	**401**	1.97	2.95	5.15	3.82
376	1.48	3.72	5.19	1.90	**402**	1.94	–	5.11	2.60
377	1.41	3.80	5.40	5.00	**403**	2.24	–	5.67	1.30
378	1.44	3.71	5.16	2.00	**404**	2.16	3.82	5.70	2.20
379	1.40	3.73	5.15	2.60	**405**	2.18	–	5.54	2.75
380	1.68	3.48	5.34	5.40	**406**	1.87	–	5.20	1.39
381	1.75	3.52	5.36	6.40	**407**	1.82	3.54	5.29	1.17
382	1.80	3.25[a]/–	5.32[a]/5.50[b]	4.30	**408**	1.75	3.56	5.26	2.34
383	1.70	–	5.25	3.64	**409**	1.75	3.57	5.28	4.05
384	1.40	3.70	5.10	1.40	**410**	1.69	3.63	5.48	2.26
385	2.17	3.52	5.42	0.73	**411**	1.56	3.20	5.00	0.42
386	1.67	3.70	5.39	1.57	**412**	1.56	3.10	5.00	2.71

[a] Using cyclic voltammetry technique.
[b] Using ambient photo electron spectroscopy (PESA).
[c] Insoluble in common organic solvents.

atoms in the NDT donor unit, leads to a deeper HOMO level and a higher band gap for **367** (Table 49) since that the LUMO levels are similar [295]. However, the PCE of **366** in blends with $PC_{61}BM$ in 1:0.8 (w/w) is higher (5.1% with J_{sc} = 14.20 mA/cm^2, V_{oc} = 0.67 V and FF = 0.54) than that of **367** (4.3% with J_{sc} = 11.38 mA/cm^2, V_{oc} = 0.83 V and FF = 0.46). The lower PCE of **367** is attributed to its slightly higher band gap and smaller absorption coefficient as compared to **366** even though its higher V_{oc} as a result of the deeper HOMO level (Table 49) [295].

The same research group also reported the synthesis of three new D–A alternating copolymers based on the thiophene–thiadiazolo[3,4-*c*]pyridine–thiophene (TPyT) functionalized on the 4-position of the thienyl groups with 2-ethylhexyl side chains as the acceptor segment and NDT (**368**), QDT (**369**) and $B_{1245}DT$ (**370**) as the donor units (Chart 81) [296]. The estimated optical band gaps and energy levels of **368**–**370** are presented in Table 49. Comparing copolymers **363** and **368**, it is demonstrated that the replacement of the 2,1,3-benzothiadiazole in the TBzT segment with the thiadiazolo[3,4-*c*]pyridine in the TPyT segment resulted with a slightly reduction of the band gap by 0.08 eV and a significant reduction of the LUMO level by approximately 0.2 eV (Table 49). On the other hand, only a small variation of the HOMO level by 0.06 eV is observed (Table 49). The lowered LUMO level is one of the reasons for the observed band gap reduction in these polymers. Moreover, the LUMO levels of all three polymers (**368**–**370**) are almost identical, independent from the donor used (Table 49), showing that are primary located in the TPyT segment [296]. BHJ solar cells prepared based on blends of **368**–**370** and $PC_{61}BM$ in 1:1 (w/w) ratio showed very high PCEs of over 5.5% for **369** and over 6% for **368** and **370** due to the simultaneously small band gaps that improves the J_{sc} values and the low lying HOMO levels that maintain the high V_{oc} values. The maximum PCE of 6.32% was obtained from **370** with J_{sc} = 12.78 mA/cm^2, V_{oc} = 0.85 V and FF = 0.58 [296].

Andersson and coworkers presented the synthesis of two new D–A alternating oligothiophene copolymers containing either quinoxaline (**371**) [297] or pyrazino[2,3-*g*]quinoxaline (**372**) [298], both substituted with octyloxy phenyl groups, as the acceptor units by Stille cross-coupling polymerization reaction (Chart 82). The optical and electrochemical properties of **371** and **372** are presented in Table 49. The optical band gap of **371** is 1.7 eV while that of **372** is 1.1 eV. Moreover, the HOMO and LUMO levels of **371** are located in suitable position matching to those of $PC_{61}BM$ but those of **372** are close to $PC_{61}BM$ (Table 49) indicating that the electron transfer between **372** and $PC_{61}BM$ is not so effective. This is verified by examining the PCE of both **371** and **372** based on photovoltaic devices (Table 49). Blends of **371** with $PC_{71}BM$ in 1:3 (w/w) showed a very high PCE of 6% with J_{sc} = 10.5 mA/cm^2, V_{oc} = 0.89 V and FF = 0.64 [297]. On the other hand, BHJ solar cells based on **372** with $PC_{71}BM$ in 1:3 (w/w) ratio showed PCE of 2.1% with a photoresponse up to 1100 nm [298].

As shown before, the copolymer **296** with an unsubstituted terthiophene segment between each pair of DPP units presents a promising PCE of 4.7% [268]. Janssen et al. have synthesized a new member of the DPP family (**373**) by introducing a phenyl ring between the two thiophene rings adjacent to the DPP unit (Chart 83) by Suzuki cross-coupling polymerization reaction [299]. The optical band

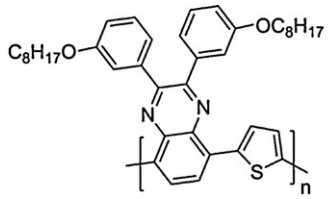

371

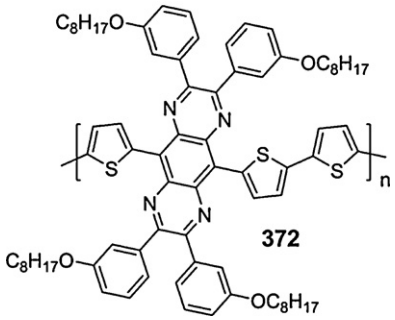

372

Chart 82. Chemical structures of the quinoxaline (**371**) and pyrazino[2,3-*g*]quinoxaline (**372**) oligothiophene copolymers.

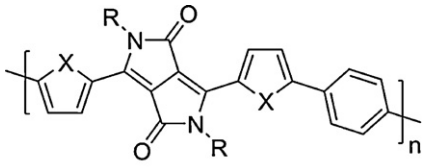

373 X: S, R: 2-hexyldecyl

374 X: O, R: 2-hexyldecyl

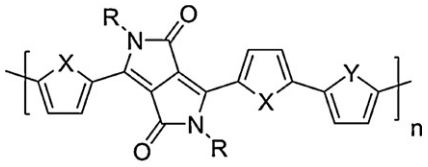

375 X: O, Y: O, R: 2-ethylhexyl

376 X: O, Y: O, R: 2-hexyldecyl

377 X: O, Y: S, R: 2-ethylhexyl

378 X: O, Y: S, R: 2-hexyldecyl

379 X: S, Y: O, R: 2-hexyldecyl

Chart 83. Chemical structure of the thiophene or furan based diketopyrrolo[3,4-*c*]pyrrole copolymers **373**–**379**.

gap of **373** is 1.53 eV, which is 0.23 eV higher than that of **296**. The HOMO level of **373** is situated at 5.35 eV and the LUMO level at 3.53 eV (Table 49). It is revealed that by replacing the thiophene ring from **296** with a phenyl ring in **373**, the HOMO level is getting deeper and the LUMO level is upshifted. These characteristics lead to photovoltaic cells with a PCE of 5.5% when **373** is blended with $PC_{71}BM$ in 1:2 (w/w) ratio with J_{sc} = 10.3 mA/cm^2, V_{oc} = 0.80 V and FF = 0.65 [299] using CF as solvent and 25 mg/mL of 1,8-diiodooctane as an additive. Moreover, the

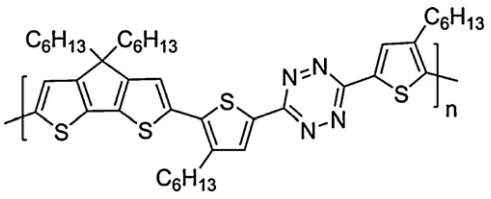

380

Chart 84. Chemical structure of the tetrazine based cyclopenta[2,1-*b*:3,4-*b*′]dithiophene copolymer **380**.

furanylene analogue of **373** has been synthesized by Suzuki cross-coupling polymerization (**374**) [300] by replacing the thiophene rings of **373** with furan rings. Comparing the optoelectronic properties of **373** and **374**, it is shown that the optical band gap of **374** is slightly higher, the LUMO level remains almost similar whereas the HOMO level is upshifted by 0.13 eV (Table 49). However, the PCE of **374** in blends with $PC_{71}BM$ in 1:2 (w/w) ratio is lower (3.8%) than that of **373**, indicating that even though the furan based derivative provides good performance in solar cells, its PCE is somewhat less than that of the corresponding thiophene derivative **373**. The reduction in the PCE was attributed to the lower molecular weight [300].

By replacing the phenyl ring from the furan based derivative **374** with either furan (**376**) or thiophene (**378**) (Chart 83) [300], lower PCEs were also obtained (Table 49), despite their lower band gaps. Comparing the energy levels of **376** and **378** with those of **374**, the HOMO levels maintain almost similar while the LUMO levels are getting deeper by ~0.15 eV (Table 49). This is in contrast of what is generally observed. For example, the lowering of the band gap is mainly attributed in the raising of the HOMO level while the LUMO level is kept almost constant. At the same time, Fréchet et al. presented the synthesis of polymers with identical conjugated backbones as **376** and **378** but with shorter and less bulkier side chains (**375** and **377**) [301]. The use of the 2-ethylhexyl instead of 2-hexyldecyl side chains resulted with the appearance of lower band gaps for **375** and **377**. However, the band gap of **375** is lower than that of **377**, opposite to the results obtained from **376** and **378** (Table 49). The LUMO levels of **375** and **377** were slightly affected (3.8 eV) but their HOMO levels were significantly altered and situated at deeper positions (5.50 eV for **375** and 5.40 eV for **377**). The simultaneously lowering of the band gap and the increased HOMO levels led to improved PCEs for the **375** and **377** (Table 49). PCEs as high as 5.0% were obtained from the **377**:$PC_{71}BM$ system in 1:3 (w/w) ratio with J_{sc} = 11.2 mA/cm^2, V_{oc} = 0.74 V and FF = 0.60 and the use of 9% by volume CN as an additive [301].

One of the newly introduced electron-withdrawing unit into the backbone of conjugated polymers for OPV applications is s-tetrazine [302]. The first solution-processable conjugated polymer with tetrazine in the main chain is **380** (Chart 84) and has been synthesized by Stille cross-coupling polymerization reaction. The optical band gap of **380** is 1.68 eV with a broad absorption profile covering the 450–700 nm region. The energy levels are situated at 5.34 eV the HOMO and 3.48 eV the LUMO (Table 49). First photovoltaic trials based on blends of **380** with $PC_{71}BM$ in

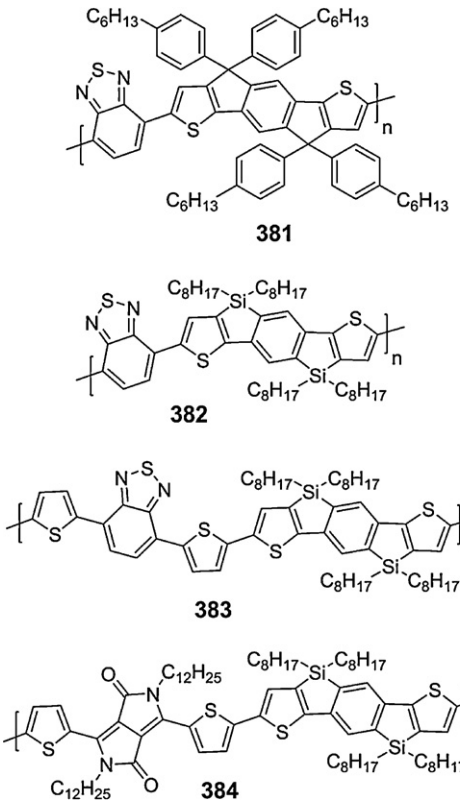

Chart 85. Chemical structures of the multifused TPT copolymer and silaindacenodithiophene derivatives **381**–**384**.

1:2 (w/w) ratio demonstrated a promising PCE of 5.4% with J_{sc} = 12.2 mA/cm^2, V_{oc} = 0.75 V and FF = 0.59 [302].

Previous studies on poly(thiophene-phenylene-thiophene) derivatives have shown efficient OPV characteristics (see Section 3.2.14.5.2). More specifically, PCE of 5.8% has been achieved from the random copolymer **287** [265]. By changing the random distribution of the selected monomers to alternating, Ting et al. have synthesized the alternating copolymer **381** (Chart 85) consisting of the TPT segment as the donor unit and 2,1,3-benzothiadiazole as the acceptor unit by Stille cross-coupling polymerization reaction [303]. The optical band gap is 1.75 eV, while the HOMO and LUMO levels are situated at 5.36 eV and 3.52 eV, respectively (Table 49). The PCE of **381** in blends with $PC_{71}BM$ was improved to 6.4% after solvent vapor annealing with J_{sc} = 11.2 mA/cm^2, V_{oc} = 0.85 V and FF = 0.67 [303].

As reported above, when the carbon atoms at the 4-position of the CPDT-based polymers are replaced by silicon atoms, enhanced interchain packing is observed, improving the crystallinity of the polymer chains, thereby the charge carrier mobility and resulting in higher PCEs [167–170]. Considering the above issues, two independent research groups [304,305] have synthesized three new alternating D–A copolymers based on the silaindacenodithiophene (SiIDT) as the donor and 2,1,3-benzothiadiazole (**382**) or TBzT (**383**) or TDPPT (**384**) as the acceptor segments (Chart 85). SiIDT is the TPT analogue where the linked carbon atoms have been replaced by silicon atoms. The

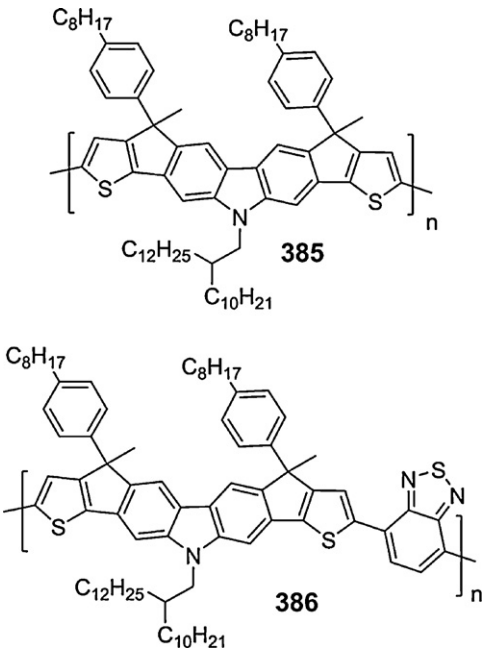

Chart 86. Chemical structures of the poly(dicyclopentathienocarbazole) derivatives **385**–**386**.

optical and electrochemical properties are presented in Table 49. It is shown that the optical band gap of **382** is 1.80 eV, while the band gap is reduced by 0.1 eV upon addition of two more thiophene units between the 2,1,3-benzothiadiazole core in **383** [304]. Moreover the presence of the TDPPT segment in **384** facilitates further the reduction of the band gap up to 1.4 eV [305]. In addition to the optical properties, the HOMO levels of **383** and **384** are upshifted as compared to **382**, whereas the SiIDT based copolymer **384** with the DPP unit exhibits the lower LUMO level. The photovoltaic properties of the SiIDT based copolymers were investigated in blends with $PC_{71}BM$ and PCEs of 4.3% were recorded for the **382**:$PC_{71}BM$ system in 1:3.5 (w/w) ratio with J_{sc} = 9.39 mA/cm^2, V_{oc} = 0.88 V and FF = 0.52 [305]. The PCE of **383** and **384** were 3.64% and 1.4%, respectively (Table 49). The lower PCE of **384** is attributed to the lower LUMO–LUMO offset energy between **384** and $PC_{71}BM$ which may be less than necessary for efficient electron transfer. Finally, two ladder-type conjugated polymers **385** and **386** [306], based on a π-excessive conjugated monomer (dicyclopentathienocarbazole (DCPTCz)) integrating the structural components of carbazole and thiophene into a single molecular entity, have been synthesized by oxidative coupling (**385**) or Suzuki cross-coupling polymerization (**386**) (Chart 86). Upon addition of the 2,1,3-benzothiadiazole in the polymer backbone of **385**, resulting polymer **386**, the band gap is significantly reduced by 0.5 eV, the HOMO level remains almost similar and the LUMO level is getting deeper by 0.18 eV (Table 49). Solar cells using the polymers **385** and **386** and $PC_{71}BM$ were prepared and PCEs of 1.57% were obtained based on the **386**:$PC_{71}BM$ system in 1:2 (w/w) ratio with J_{sc} = 4.59 mA/cm^2, V_{oc} = 0.81 V and FF = 0.42 [306].

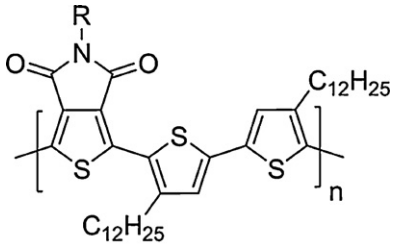

387 R: 2-ethylhexyl

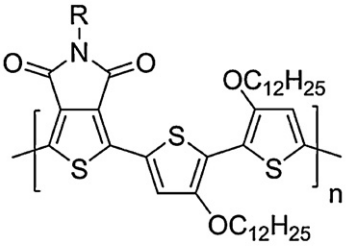

388 R: dodecyl

389 R: 2-butyloctyl

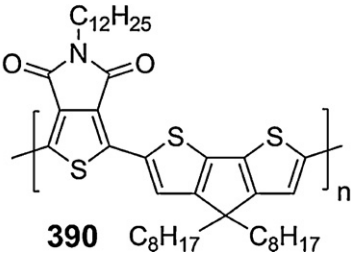

390

Chart 87. Chemical structures of the *N*-alkylthieno[3,4-*c*]pyrrole-4,6-dione based copolymers **387**–**390**.

Since that TPD moiety exhibits a symmetric, rigidly fused, coplanar structure and strong electron-withdrawing properties, two research groups have synthesized various D–A TPD based copolymers using either alkyl (**387**) or alkoxy functionalized bithiophene units (**388** and **389**) or CPDT (**390**) as the electron donor monomers (Chart 87). By combining the symmetrical bi(dodecyl)thiophene with TPD, Wei et al. presented polymer **387** [307], synthesized by Stille cross-coupling polymerization reaction. The optical band gap is 1.82 eV, while the HOMO and LUMO levels are situated at 5.56 eV and 3.10 eV, respectively. These characteristics allowed **387** to exhibit a promising PCE of 4.7% (Table 49) when blended with $PC_{61}BM$ in 1:1.5 (w/w) ratio with J_{sc} = 8.02 mA/cm^2, V_{oc} = 0.95 V and FF = 0.62. Furthermore, Watson et al. examined the properties of two conjugated polymers consisting of a dodecyloxy substituted bithiophene alternate with a TPD moiety containing two different alkyl side chains (linear (**388**) and branched (**389**)) [308]. Despite the different alkyl side chains, the band gaps of both **388** and **389** are the same. However, the HOMO level of **389** containing the bulkier side chain is shifted by 0.2 eV to deeper values. Replacing

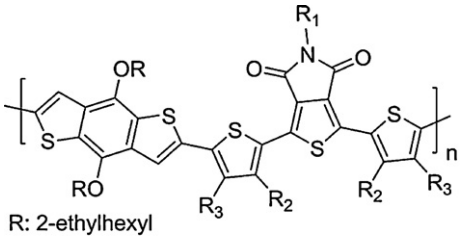

R: 2-ethylhexyl

391 R_1 = octyl, R_2, R_3 = H
392 R_1 = 2-ethylhexyl, R_2, R_3 = H
393 R_1 = dodecyl, R_2, R_3 = H
394 R_1, R_2 = octyl, R_3 = H
395 R_1 = octyl, R_2 = ethyl, R_3 = H
396 R_1, R_3 = octyl, R_2 = H
397 R_1 = dodecyl, R_2 = octyl, R_3 = H
398 R_1 = dodecyl, R_2 = H, R_3 = octyl

Chart 88. Chemical structures of the *N*-alkylthieno[3,4-*c*]pyrrole-4,6-dione based poly(benzo[1,2-*b*:4,5-*b*′]dithiophene) derivatives **391**–**398**.

the alkoxy functionalized bithiophene unit with CPDT in **390**, the band gap is higher by 0.17 eV as compared to **388**, while the HOMO level is shifted by 0.41 eV into deeper values (Table 49). BHJ solar cells based on **388**–**390** and $PC_{71}BM$ in 1:2 w/w ratio demonstrated PCEs of 3.15% for **390** with J_{sc} = 8.12 mA/cm^2, V_{oc} = 0.76 V and FF = 0.50. On the other hand, the PCEs of the **388** and **389** based solar cells was mainly hindered by the high HOMO level, poor charge transport properties and suboptimal film morphology [308].

Following the first studies on the copolymers **164**–**166** consisting of TPD alternate with $B_{1245}DT$ moieties, Leclerc et al. presented the synthesis of new copolymers based on $B_{1245}DT$ and alkylated TPD monomers (**391**–**398**), where thiophene rings were added around the TPD core in order to tune the electronic properties [309], by Stille cross-coupling polymerization (Chart 88). The optical and electrochemical properties of **391**–**398** are presented in Table 49. It is shown that neither the length nor the type of the tail chain on the TPD seems to affect the optical properties of these copolymers. The absorption spectrum of **392** in thin film form showed that the unfunctionalized thiophene rings did not modulate the optical properties and the optical band gap remains the same as **164**–**166**. Similar to the optical properties, the alkyl chain on the TPD unit did not dramatically change the HOMO and LUMO energy levels [309]. The LUMO levels are situated between 3.7 eV and 3.8 eV, while the highest variation of 0.24 eV in the HOMO levels is observed between **392** and **398**. Moreover, the copolymers with the substituted thiophene rings (alkyl chains facing the $B_{1245}DT$ unit) or unsubstituted thiophene rings tend to exhibit low PCEs (less than 1%) due to a bad morphology of the active layer, whereas the copolymers with substituted thiophene rings (alkyl chains facing TPD unit) show enhanced PCEs of 3.9% from the **394**:$PC_{61}BM$ in 1:2 (w/w) ratio with J_{sc} = 7.6 mA/cm^2, V_{oc} = 0.89 V and FF = 0.57 due to the improved morphology. However, these PCEs are still lower than that of **164**–**166**.

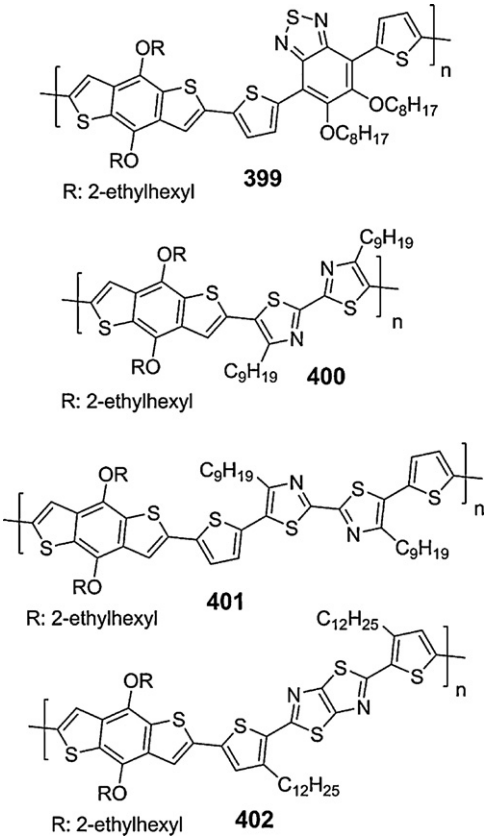

Chart 89. Chemical structures of the alternate copolymers **399**–**402**, based on the benzo[1,2-*b*:4,5-*b*′]dithiophene and various electron withdrawing units.

Other $B_{1245}DT$ based derivatives have been synthesized (Chart 89) by various research groups and consisting of either octyloxy substituted 2,1,3-benzothiadiazole (**399**) [310], or nonyl substituted bithiazole (**400** and **401**) [311,312], or thiazolothiazole (**402**) [311] by Stille cross-coupling polymerization reaction. The optical and electrochemical properties of **399**–**402** are presented in Table 49. The band gap of **399** is 1.64 eV, 0.31 eV lower than that of the related analogue **255**. The lowering of the band gap is mainly attributed to the significant lowering of the LUMO level (**399** at 3.61 eV and **255** at 3.35 eV) while the HOMO level is not affected significantly (0.04 eV). The PCE of **399** in blends with $PC_{71}BM$ in 1:2 (w/w) ratio is very promising (4.02%) with J_{sc} = 8.96 mA/cm^2, V_{oc} = 0.76 V and FF = 0.59 since that no annealing or additives were employed [310], but still lower than that of **255**.

Comparing copolymers **400** and **401** it is shown that the bands gaps are similar while the HOMO level of **401** is situated at deeper position than that of **400** (Table 49), despite the presence of two thiophene rings around the bithiazole core. BHJ solar cells were prepared based on blends of **400**:$PC_{71}BM$ in 1:2 (w/w) ratio and **401**:$PC_{71}BM$ in 1:1 (w/w) ratio and demonstrated PCEs of 3.82% for the **401**:$PC_{71}BM$ with J_{sc} = 7.84 mA/cm^2, V_{oc} = 0.86 V and FF = 0.57 [312]. In addition, the band gap and HOMO level of **402** are similar to those of **400** and **401** and a

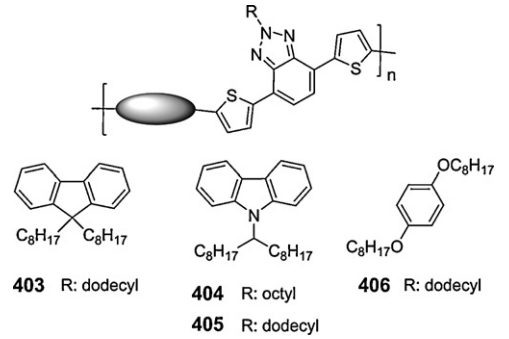

Chart 90. Chemical structures of the 1,2,3-benzotriazole based copolymers **403**–**406**.

PCE of 2.6% when blended with $PC_{71}BM$ in 1:2 (w/w) with J_{sc} = 6.68 mA/cm^2, V_{oc} = 0.77 V and FF = 0.51 is obtained [311].

New dithienyl benzotriazole based conjugated polymers with fluorene (**403**), carbazole (**404** and **405**) and alkoxy phenyl (**406**) comonomers (Chart 90) were synthesized by Suzuki cross-coupling polymerization [313,314] and their optical and electrochemical properties are presented in Table 49. It is shown that the band gaps of **403**–**405** are above 2.15 eV (Table 49) while only the band gap of **406** is below 2.00 eV (1.87 eV), which is even lower than that of the related polymer **348**. All polymers have relatively deep HOMO levels (below 5.20 eV) and the LUMO level of **404** is situated at 3.82 eV. Comparing the benzotriazole based copolymer **404** and the structural related benzimidazole based copolymer **345** it is revealed that the LUMO level of **404** is situated lower than that of **345** by 0.16 eV, indicating that the benzotriazole unit is slightly stronger electron withdrawing group than benzimidazole. On the other hand, the optical band gap of **404** is significantly higher than that of **345** by 0.52 eV, even though their electrochemical band gaps are similar (1.81 eV for **345** and 1.88 eV for **404**). The PCE of BHJ solar cells based on blends of **403**–**406** with $PC_{61}BM$ in 1:2 (w/w) ratio were as high as 2.75% for **405** with J_{sc} = 4.68 mA/cm^2, V_{oc} = 0.90 V and FF = 0.65, using an alcohol-soluble poly[(9,9-dioctyl-2,7-fluorene)-*alt*-(9,9-bis(3′-(*N*,*N*-dimethylamino)propyl)-2,7 fluorene)] (PFN) as a cathode modification [313].

A series of alternating (**407**–**409**) and random (**410**) copolymers based on 9,9-dialkyl-3,6-dialkyloxydibenzosilole and TBzT segments (Chart 91) were synthesized by Stille cross-coupling polymerization reaction. The optical and electrochemical properties of **407**–**410** are presented in Table 49. It is shown that the optical band gaps of **408** and **409** are slightly lower than that of **407** due to the unsymmetrical length of the alkyl and alkoxy side chain [315]. The energy levels of the copolymers remain almost unaffected from the length of the side chains exhibiting HOMO levels in the range of 5.26–5.28 eV and LUMO levels in the range of 3.54–3.63 eV. Moreover, PCEs in the range of 1.17–4.05% are achieved based on the alternating copolymers **407**–**409** while the PCE of the random copolymer **410** is 2.26% (Table 49). The highest PCE of **409**:$PC_{71}BM$ in 1:2.5 (w/w) ratio with J_{sc} = 11.1 mA/cm^2,

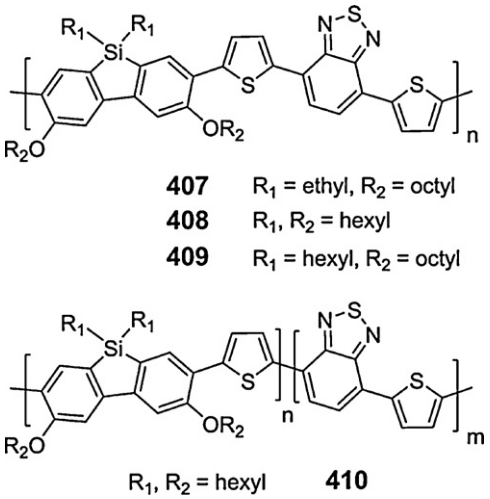

Chart 91. Chemical structures of the alternate (**407**–**409**) and random (**410**) polydibenzosilole derivatives.

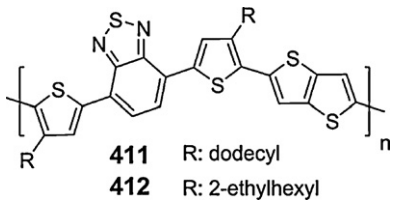

Chart 92. Chemical structures of the oligothiophene copolymers **411**–**412** consisting of both thieno[3,2-*b*]thiophene and 2,1,3-benzothiadiazole units.

V_{oc} = 0.67 V and FF = 0.54 is attributed to the longer alkoxy side chains which provided to the polymer enhanced solubility and high molecular weight [315].

Finally, Biniek et al. presented the synthesis of two new LBG oligothiophene copolymers containing both 2,1,3-benzothiadiazole and thieno[3,2-*b*]thiophene (Chart 92) and different solubilizing side chains (linear; **411** and branched; **412**) at the 4 position on the thiophene rings (β-position), by Stille cross-coupling polymerization reaction [316].

As compared to polymer **83**, containing identical conjugated backbone as **411**, **412** and linear alkyl side chains at the 3 position on the thiophene rings (α-position), the results show that the position of the side chains can have a profound impact on the optoelectronic properties. For example, **411** exhibits a lower band gap than that of **83** by 0.32 eV and the HOMO level is upshifted by 0.3 eV. Moreover, the charge carrier mobilities are a function not only of the position but of the type of the side chain as well. The hole mobility of **411** (1×10^{-5} cm^2/V s) is one order of magnitude lower than that of **83** (1×10^{-4} cm^2/V s) but the hole mobility of **412** (1×10^{-3} cm^2/V s) is one order of magnitude higher than that of **83** in FET measurements [316]. The measured average PCE obtained on devices with optimal fullerene content and **411** or **412** are summarized in Table 49. **411**:$PC_{61}BM$ in 1:4 (w/w) ratio exhibits a PCE of 0.42%, whereas the PCE of **412**:$PC_{61}BM$ in 1:1 w/w is 2.71% with J_{sc} = 7.80 mA/cm^2, V_{oc} = 0.67 V and FF = 0.52 [316]. These results indicate that using 2-ethylhexyl side chains instead of linear alkyl side chains the interaction between the polymer and the fullerene molecules is modified, leading to opposite dependences on the photovoltaic performances of the fullerene content. The latter observation supports the idea that fullerene intercalation between the side chains is at the origin of the frequently observed high optimal fullerene content in polymer:fullerene BHJ devices.

4. Conclusions and future perspectives

This review focused on how structural deviations on the backbone of conjugated polymers, for instance poly(*p*-phenylenevinylene)-substituted derivatives, polythiophene derivatives, complex (fused) structures such as bridged bithiophenes and bridged biphenylenes, polycyclic aromatics bridged with fused aromatic rings and LBG conjugated polymers based on various electron-deficient units, influence the optoelectronic properties (E_g, HOMO and LUMO levels and charge carrier mobility) and OPV performance providing to the reader a comprehensive structure–property relationship study.

Structural analysis of the conjugated polymers employed as donors in BHJ solar cells reveals that although the majority has been synthesized through the alternation of D–A moieties, the highest PCE has been obtained from the polymers synthesized by the stabilization of the quinoid structure. Another general conclusion is that the LUMO level of the D–A conjugated polymers is mainly localized on the acceptor unit. Thus, the proper selection of the acceptor unit can influence the LUMO level in these polymers. In more details, 2,1,3-benzothiadiazole and quinoxaline units appear to be the most promising acceptors even if heteroaromatic rings with different electron affinities and resonance structures are developed for the D–A type polymers. However, the electron-withdrawing ability of the acceptor in the conjugated main chain needs to be carefully adjusted to ensure efficient electron transfer to the fullerene derivatives. Taking this into account, the lowering of the band gap of a conjugated polymer cannot be the indicator for the strength of the acceptor used. Accurate estimation for the strength of an electron-deficient unit can be obtained from the LUMO level value and comparison of the electron affinities between two acceptor units should be performed for structural related polymers (similar conjugated backbone and identical side chains). Moreover, the multicyclic fused aromatic rings with enforced planarity show great promise as donor functionalities since that higher hole mobilities are usually provided, thereby accelerating charge transport, which in turn allows the preparation of thicker active layers required for increased light harvesting. We note that based on the conjugated polymers presented within this text no reliable conclusion about the proper choice of the side chain [e.g. structure (linear or branched), type (alkyl or alkoxy) and density] along the backbone can be obtained since the side chains function differently for each polymer category, especially when considering the miscibility with

the fullerene derivatives. For the design of new conjugated polymers though, the side chain positioning and density should be chosen in a configuration that is minimizing or eliminating the steric hindrance effect and maximizing the solubility of the polymer, respectively and that branched side chains usually upshift the LUMO level and drive the HOMO level to deeper values as compared with the linear analogues.

To conclude, it should be emphasized that the improvement of the PCE is a combination of parameters including optimisation of both (donor and acceptor) material properties, device architecture and processing. The above results show that the detailed structural fine-tuning of conjugated polymers is one of the major parameters to achieve the suitable properties essential for high PCE performance. More detailed studies for the role of the recently reported CT states at the interface between the D and A components would provide deeper understanding and should include studies on several LBG conjugated polymers (synthesized either through the D–A approach or the stabilization of the quinoid structure):fullerene systems. In parallel to the recent important efforts for the synthesis of LBG conjugated polymers, a better understanding of the charge separation process in polymer:fullerene blends will create design rules for new materials with the potential to further improve the PCE of BHJ solar cells.

Acknowledgements

This work performed under internal funded Cyprus University of Technology projects and the research grant "NEA Y∏OΔOMH//ΣTPATH/0308/06" funded from Cyprus Research Promotion Foundation.

References

[1] Brabec CJ, Durrant JR. Solution-processed organic solar cells. MRS Bull 2008;33:670–5.
[2] Brabec CJ, Gowrisanker S, Halls JJM, Laird D, Jia S, Williams SP. Polymer–fullerene bulk-heterojunction solar cells. Adv Mater 2010;22:3839–56.
[3] Brabec CJ, Sariciftci NS, Hummelen JC. Plastic solar cells. Adv Funct Mater 2001;11:15–26.
[4] Liang Y, Yu L. A new class of semiconducting polymers for bulk heterojunction solar cells with exceptionally high performance. Acc Chem Res 2010;43:1227–36.
[5] Günes S, Neugebauer H, Sariciftci NS. Conjugated polymer-based organic solar cells. Chem Rev 2007;107:1324–38.
[6] Heremans P, Cheyns D, Rand BP. Strategies for increasing the efficiency of heterojunction organic solar cells: material selection and device architecture. Acc Chem Res 2009;42:1740–7.
[7] Deibel C, Strobel T, Dyakonov V. Role of the charge transfer state in organic donor–acceptor solar cells. Adv Mater 2010;22: 4097–111.
[8] Cheng YJ, Yang SH, Hsu CS. Synthesis of conjugated polymers for organic solar cell applications. Chem Rev 2009;109:5868–923.
[9] Chen J, Cao Y. Development of novel conjugated donor polymers for high-efficiency bulk-heterojunction photovoltaic devices. Acc Chem Res 2009;42:1709–18.
[10] Zhan X, Zhu D. Conjugated polymers for high-efficiency organic photovoltaics. Polym Chem 2010;1:409–19.
[11] Kroon R, Lenes M, Hummelen JC, Blom PWM, de Boer B. Small bandgap polymers for organic solar cells (polymer material development in the last 5 years). Polym Rev 2008;48:531–82.
[12] Bundgaard E, Krebs FC. Low band gap polymers for organic photovoltaics. Sol Energy Mater Sol Cells 2007;91:954–85.
[13] Roncali J. Molecular bulk heterojunctions: an emerging approach to organic solar cells. Acc Chem Res 2009;42:1719–30.
[14] Brédas JL, Norton JE, Cornil J, Coropceanu V. Molecular understanding of organic solar cells: the challenges. Acc Chem Res 2009;42:1691–9.
[15] Clarke TM, Durrant JR. Charge photogeneration in organic solar cells. Chem Rev 2010;110:6736–67.
[16] Pensack RD, Asbury JB. Beyond the adiabatic limit: charge photogeneration in organic photovoltaic materials. J Phys Chem Lett 2010;1:2255–63.
[17] Veldman D, Meskers SCJ, Janssen RAJ. The energy of charge-transfer states in electron donor–acceptor blends: insight into the energy losses in organic solar cells. Adv Funct Mater 2009;19:1939–48.
[18] Schueppel R, Schmidt K, Uhrich C, Schulze K, Wynands D, Brédas JL, Brier E, Reinold E, Bu HB, Baeuerle P, Maennig B, Pfeiffer M, Leo K. Optimizing organic photovoltaics using tailored heterojunctions: a photoinduced absorption study of oligothiophenes with low band gaps. Phys Rev B 2008;77, 085311/1–14.
[19] Dyer-Smith C, Reynolds LX, Bruno A, Bradley DDC, Haque SA, Nelson J. Triplet formation in fullerene multi-adduct blends for organic solar cells and its influence on device performance. Adv Funct Mater 2010;20:2701–8.
[20] Köhler A, Bässler H. Triplet states in organic semiconductors. Mater Sci Eng R Rep 2009;66:71–109.
[21] Benson-Smith JJ, Goris L, Vandewal K, Haenen K, Manca JV, Vanderzande D, Bradley DDC, Nelson J. Formation of a ground-state charge-transfer complex in polyfluorene/[6,6]-phenyl-C_{61} butyric acid methyl ester (PCBM) blend films and its role in the function of polymer/PCBM solar cells. Adv Funct Mater 2007;17:451–7.
[22] Hallermann M, Kriegel I, Da Como E, Berger JM, von Hauff E, Feldmann J. Charge transfer excitons in polymer/fullerene blends: the role of morphology and polymer chain conformation. Adv Funct Mater 2009;19:3662–8.
[23] Vandewal K, Tvingstedt K, Gadisa A, Inganäs O, Manca JV. On the origin of the open-circuit voltage of polymer–fullerene solar cells. Nat Mater 2009;8:904–9.
[24] Vandewal K, Gadisa A, Oosterbaan WD, Bertho S, Banishoeib F, Severen IV, Lutsen L, Cleij TJ, Vanderzande D, Manca JV. The relation between open-circuit voltage and the onset of photocurrent generation by charge-transfer absorption in polymer:fullerene bulk heterojunction solar cells. Adv Funct Mater 2008;18:2064–70.
[25] Veldman D, İpek Ö, Meskers SCJ, Sweelssen J, Koetse MM, Veenstra SC, Kroon JM, van Bavel SS, Loos J, Janssen RAJ. Compositional and electric field dependence of the dissociation of charge transfer excitons in alternating polyfluorene copolymer/fullerene blends. J Am Chem Soc 2008;130:7721–35.
[26] Tvingstedt K, Vandewal K, Gadisa A, Zhang F, Manca J, Inganäs O. Electroluminescence from charge transfer states in polymer solar cells. J Am Chem Soc 2009;131:11819–24.
[27] Standard ASTM E948. Standard test method for electrical performance of non-concentrator photovoltaic cells using reference cells. In: ASTM Volume 12.02 nuclear (II), solar, and geothermal energy. West Conshocken (PA): American Society for Testing and Materials; 2011. DOI: 10.1520/E0948-09.
[28] Thompson BC, Fréchet JMJ. Polymer–fullerene composite solar cells. Angew Chem Int Ed 2007;47:58–77.
[29] Dennler G, Scharber MC, Brabec CJ. Polymer–fullerene bulk-heterojunction solar cells. Adv Mater 2009;21:1323–38.
[30] Roncali J. Synthetic principles for bandgap control in linear π-conjugated systems. Chem Rev 1997;97:173–206.
[31] Roncali J. Molecular engineering of the band gap of π-conjugated systems: facing technological applications. Macromol Rapid Commun 2007;28:1761–75.
[32] Thompson BC. Variable band gap poly(3,4-alkylenedioxythiophene)-based polymers for photovoltaic and electrochromic applications. PhD Dissertation, University of Florida; 2005. p. 1–11.
[33] McCullough RD, Ewbank PC. Head-to-tail coupled poly(3-alkylthiophene) and its derivatives. In: Skotheim TA, Elsenbaumer RL, Reynolds JR, editors. Handbook of conducting polymers. 2nd ed. New York: Marcel Dekker; 1998. p. 225–58.
[34] Salzner U, Lagowski JB, Pickup PG, Poirier RA. Comparison of geometries and electronic structures of polyacetylene, polyborole, polycyclopentadiene, polypyrrole, polyfuran, polysilole, polyphosphole, polythiophene, polyselenophene and polytellurophene. Synth Met 1998;96:177–89.
[35] Brédas JL. Relationship between band gap and bond length alternation in organic conjugated polymers. J Chem Phys 1985;82:3808–11.
[36] Havinga EE, ten Hoeve W, Wynberg H. A new class of small band gap organic polymer conductors. Polym Bull 1992;29:119–26.

[37] Brocks G, Tol A. Small band gap semiconducting polymers made from dye molecules: polysquaraines. J Phys Chem 1996;100:1838–46.
[38] Zhang W, Smith J, Watkins SE, Gysel R, McGehee M, Salleo A, Kirkpatrick J, Ashraf S, Anthopoulos T, Heeney M, McCulloch I. Indacenodithiophene semiconducting polymers for high-performance, air-stable transistors. J Am Chem Soc 2010;132:11437–9.
[39] Morana M, Koers P, Waldauf C, Koppe M, Muehlbacher D, Denk P, Scharber MD, Waller D, Brabec CJ. Organic field-effect devices as tool to characterize the bipolar transport in polymer–fullerene blends: the case of P3HT-PCBM. Adv Funct Mater 2007;17:3274–83.
[40] Caserta G, Rispoli B, Serra A. Space-charge-limited current and band structure in amorphous organic films. Phys Status Solidi B 1969;35:237–48.
[41] Reid OG, Munechika K, Ginger DS. Space charge limited current measurements on conjugated polymer films using conductive atomic force microscopy. Nano Lett 2008;8:1602–9.
[42] Mozer AJ, Sariciftci NS, Lutsen L, Vanderzande D, Osterbacka R, Westerling M, Juska G. Charge transport and recombination in bulk heterojunction solar cells studied by the photoinduced charge extraction in linearly increasing voltage technique. Appl Phys Lett 2005;86, 112104/1–3.
[43] Choulis SA, Nelson J, KimY, Poplavskyy D, Kreouzis T, Durrant JR, Bradley DDC. Investigation of transport properties in polymer/fullerene blends using time-of-flight photocurrent measurements. Appl Phys Lett 2003;83:3812–4.
[44] Shrotriya V, Wu EHE, Li G, Yao Y, Yang Y. Efficient light harvesting in multiple-device stacked structure for polymer solar cells. Appl Phys Lett 2006;88, 064104/1–3.
[45] Shaheen SE, Brabec CJ, Sariciftci NS, Padinger F, Fromherz T, Hummelen JC. 2.5% efficient organic plastic solar cells. Appl Phys Lett 2001;78:841–3.
[46] Tajima K, Suzuki Y, Hashimoto K. Polymer photovoltaic devices using fully regioregular poly[(2-methoxy-5-(3′,7′-dimethyloctyloxy))-1,4-phenylenevinylene]. J Phys Chem C 2008;112:8507–10.
[47] Arbogast JW, Foote CS. Photophysical properties of C70. J Am Chem Soc 1991;113:8886–9.
[48] Wienk M, Kroon JM, Verhees WJH, Krol J, Hummelen JC, Van Haal P, Janssen RAJ. Efficient methano[70]fullerene/MDMO-PPV bulk heterojunction photovoltaic cells. Angew Chem Int Ed 2003;42:3371–5.
[49] vanDuren JKJ, Yang X, Loos J, Bulle-Lieuwma CWT, Sieval AB, Hummelen JC, Janssen RAJ. Relating the morphology of poly(p-phenylene vinylene)/methanofullerene blends to solar-cell performance. Adv Funct Mater 2004;14:425–34.
[50] Mihailetchi VD, Koster LJA, Blom PWM, Melzer C, deBoer B, vanDuren JKJ, Janssen RAJ. Compositional dependence of the performance of poly(p-phenylene vinylene):methanofullerene bulk-heterojunction solar cells. Adv Funct Mater 2005;15:795–801.
[51] Melzer C, Koop EJ, Mihailetchi VD, Blom PWM. Hole Transport in poly(phenylene vinylene)/methanofullerene bulk-heterojunction solar cells. Adv Funct Mater 2004;14:865–70.
[52] Mayer AC, Toney MF, Scully SR, Rivnay J, Brabec CJ, Scharber M, Koppe M, Heeney M, McCulloch I, McGehee MD. Bimolecular crystals of fullerenes in conjugated polymers and the implications of molecular mixing for solar cells. Adv Funct Mater 2009;19:1173–9.
[53] Yokoyama H, Kramer EJ, Rafailovich MH, Sokolov J, Schwarz SA. Structure and diffusion of asymmetric diblock copolymers in thin films: a dynamic secondary ion mass spectrometry study. Macromolecules 1998;31:8826–30.
[54] Mihailetchi VD, vanDuren JKJ, Blom PWM, Hummelen JC, Janssen RAJ, Kroon JM, Rispens MT, Verhees WJH, Wienk MM. Electron transport in a methanofullerene. Adv Funct Mater 2003;13:43–6.
[55] Hou J, Yang C, Qiao J, Li Y. Synthesis and photovoltaic properties of the copolymers of 2-methoxy-5-(2′-ethylhexyloxy)-1,4-phenylene vinylene and 2,5-thienylene-vinylene. Synth Met 2005;150:297–304.
[56] Huo L, Hou J, He C, Han M, Li Y. Synthesis, characterization and photovoltaic properties of poly{[1′,4′-bis-(thienyl-vinyl)]-2-methoxy-5-(2′-ethylhexyloxy)-1,4-phenylene-vinylene}. Synth Met 2006;156:276–81.
[57] Colladet K, Fourier S, Cleij TJ, Lutsen L, Gelan J, Vanderzande D, Nguyen LH, Neugebauer H, Sariciftci S, Aguirre A, Janssen G, Goovaerts E. Low band gap donor–acceptor conjugated polymers toward organic solar cells applications. Macromolecules 2007;40:65–72.
[58] Thompson BC, Kim YG, McCarley TD, Reynolds JR. Soluble narrow band gap and blue propylenedioxythiophene-cyanovinylene polymers as multifunctional materials for photovoltaic and electrochromic applications. J Am Chem Soc 2006;128:12714–25.
[59] Galand EM, Kim YG, Mwaura JK, Jones AG, McCarley TD, Shrotriya V, Yang Y, Reynolds JR. Optimization of narrow band-gap propylenedioxythiophene: cyanovinylene copolymers for optoelectronic applications. Macromolecules 2006;39:9132–42.
[60] Colladet K, Nicolas M, Goris L, Lutsen L, Vanderzande D. Low-band gap polymers for photovoltaic applications. Thin Solid Films 2004;451-452:7–11.
[61] Egbe DAM, Nguyen LH, Hoppe H, Mühlbacher D, Sariciftci NS. Side chain influence on electrochemical and photovoltaic properties of yne-containing poly(phenylene vinylene)s. Macromol Rapid Commun 2005;26:1389–94.
[62] Egbe DAM, Nguyen LH, Schmidtke K, Wild A, Sieber C, Guenes S, Sariciftci NS. Combined effects of conjugation pattern and alkoxy side chains on the photovoltaic properties of thiophene-containing PPE-PPVs. J Polym Sci Part A Polym Chem 2007;45:1619–31.
[63] Egbe DAM, Türk S, Rathgeber S, Kühnlenz F, Jadhav R, Wild A, Birckner E, Adam G, Pivrikas A, Cimrova V, Knür G, Sariciftci NS, Hoppe H. Anthracene based conjugated polymers: correlation between π–π-stacking ability, photophysical properties, charge carrier mobility, and photovoltaic performance. Macromolecules 2010;43:1261–9.
[64] Egbe DAM, Adam G, Pivrikas A, Ramil AM, Birckner E, Cimrova V, Hoppe H, Sariciftci NS. Improvement in carrier mobility and photovoltaic performance through random distribution of segments of linear and branched side chains. J Mater Chem 2010;20:9726–34.
[65] Henckens A, Colladet K, Fourier S, Cleij TJ, Lutsen L, Gelan J, Vanderzande D. Synthesis of 3,4-diphenyl-substituted poly(thienylene vinylene), low-band-gap polymers via the dithiocarbamate route. Macromolecules 2005;38:19–26.
[66] Smith AP, Smith RR, Taylor BE, Durstock MF. An investigation of poly(thienylene vinylene) in organic photovoltaic devices. Chem Mater 2004;16:4687–92.
[67] Huo L, Chen TL, Zhou Y, Hou J, Chen HY, Yang Y, Li Y. Improvement of photoluminescent and photovoltaic properties of poly(thienylene vinylene) by carboxylate substitution. Macromolecules 2009;42:4377–80.
[68] Cremer J, Baïerle P, Wienk MM, Janssen RAJ. High open-circuit voltage poly(ethynylene bithienylene):fullerene solar cells. Chem Mater 2006;18:5832–4.
[69] Lu S, Yang M, Luo J, Cao Y. Photovoltaic devices based on a novel poly(phenylene ethynylene) derivative. Synth Met 2004;140:199–202.
[70] Ashraf RS, Shahid M, Klemm E, Al-Ibrahim M, Sensfuss S. Thienopyrazine-based low-bandgap poly(heteroarylene-neethynylene)s for photovoltaic devices. Macromol Rapid Commun 2006;27:1454–9.
[71] Lu S, Yang M, Luo J, Cao Y, Bai F. Novel alternating dioctyloxyphenylene vinylene-benzothiadiazole copolymer: synthesis and photovoltaic performance. Macromol Chem Phys 2005;206:664–71.
[72] Huo L, He C, Han M, Zhou E, Li Y. Alternating copolymers of electron-rich arylamine and electron-deficient 2,1,3-benzothiadiazole: synthesis, characterization and photovoltaic properties. J Polym Sci Part A Polym Chem 2007;45:3861–71.
[73] Mei J, Heston NC, Vasilyeva SV, Reynolds JR. A Facile approach to defect-free vinylene-linked benzothiadiazole–thiophene low-bandgap conjugated polymers for organic electronics. Macromolecules 2009;42:1482–7.
[74] Brabec CJ, Hauch J, Schilinsky P, Waldauf C. Production aspects of organic photovoltaics and their impact on the commercialization of devices. MRS Bull 2005;30:50–2.
[75] Li G, Shrotriya V, Huang J, Yao Y, Moriarty T, Emery K, Yang Y. High-efficiency solution processable polymer photovoltaic cells by self-organization of polymer blends. Nat Mater 2005;4:864–8.
[76] Ma W, Yang C, Gong X, Lee K, Heeger AJ. Thermally stable, efficient polymer solar cells with nanoscale control of the interpenetrating network morphology. Adv Funct Mater 2005;15:1617–22.
[77] Kim Y, Cook S, Tuladhar SM, Choulis SA, Nelson J, Durrant JR, Bradley DDC, Giles M, McCulloch I, Ha CS, Ree M. A strong regioregularity effect in self-organizing conjugated polymer films and high-efficiency polythiophene:fullerene solar cells. Nat Mater 2006;5:197–203.
[78] Irwin MD, Buchholz DB, Hains AW, Chang RPH, Marks TJ. p-Type semiconducting nickel oxide as an efficiency-enhancing anode interfacial layer in polymer bulk-heterojunction solar cells. Proc Natl Acad Sci 2008;105:2783–7.

[79] Zen A, Saphiannikova M, Neher D, Grenzer J, Grigorian S, Pietsch U, Asawapirom U, Janietz S, Scherf U, Lieberwirth I, Wegner G. Effect of molecular weight on the structure and crystallinity of poly(3-hexylthiophene). Macromolecules 2006;39:2162–71.
[80] Schilinsky P, Asawapirom U, Scherf U, Biele M, Brabec CJ. Influence of the molecular weight of poly(3-hexylthiophene) on the performance of bulk heterojunction solar cells. Chem Mater 2005;17:2175–80.
[81] Woo CH, Thompson BC, Kim BJ, Toney MF, Fréchet JMJ. The influence of poly(3-hexylthiophene) regioregularity on fullerene-composite solar cell performance. J Am Chem Soc 2008;130:16324–9.
[82] Hoth CN, Choulis SA, Schilinsky P, Brabec CJ. High photovoltaic performance of inkjet printed polymer:fullerene blends. Adv Mater 2007;19:3973–8.
[83] Padinger F, Rittberger RS, Sariciftci NS. Effects of postproduction treatment on plastic solar cells. Adv Funct Mater 2003;13:85–8.
[84] Li G, Shrotriya V, Yao Y, Huang J, Yang Y. Manipulating regioregular poly(3-hexylthiophene): [6,6]-phenyl-C61-butyric acid methyl ester blends—route towards high efficiency polymer solar cells. J Mater Chem 2007;17:3126–40.
[85] Ohkita H, Cook S, Astuti Y, Duffy W, Tierney S, Zhang W, Heeney M, McCulloch I, Nelson J, Bradley DDC, Durrant JR. Charge carrier formation in polythiophene/fullerene blend films studied by transient absorption spectroscopy. J Am Chem Soc 2008;130:3030–42.
[86] Ohkita H, Cook S, Astuti Y, Duffy W, Heeney M, Tierney S, McCulloch I, Bradley DDC, Durrant JR. Radical ion pair mediated triplet formation in polymer–fullerene blend films. Chem Commun 2006:3939–41.
[87] Hwang IW, Moses D, Heeger AJ. Photoinduced carrier generation in P3HT/PCBM bulk heterojunction materials. J Phys Chem C 2008;112:4350–4.
[88] Chen LM, Hong Z, Li G, Yang Y. Recent progress in polymer solar cells: manipulation of polymer:fullerene morphology and the formation of efficient inverted polymer solar cells. Adv Mater 2009;21:1434–49.
[89] Padinger F, Brabec CJ, Fromherz T, Hummelen JC, Sariciftci NS. Fabrication of large area photovoltaic devices containing various blends of polymer and fullerene derivatives by using the doctor blade technique. Opto-Electron Rev 2000;8:280–3.
[90] Hoth CN, Schilinsky P, Choulis SA, Brabec CJ. Printing highly efficient organic solar cells. Nano Lett 2008;8:2806–13.
[91] Kim SS, Na SI, Jo J, Tae G, Kim DY. Efficient polymer solar cells fabricated by simple brush painting. Adv Mater 2007;19:4410–5.
[92] Vak D, Kim SS, Jo J, Oh SH, Na SI, Kim J, Kim DY. Fabrication of organic bulk heterojunction solar cells by a spray deposition method for low-cost power generation. Appl Phys Lett 2007;91, 081102/1-3.
[93] Gadisa A, Oosterbaan WD, Vandewal K, Bolsée JC, Bertho S, D'Haen J, Lutsen L, Vanderzande D, Manca JV. Effect of alkyl side-chain length on photovoltaic properties of poly(3-alkylthiophene)/PCBM bulk heterojunctions. Adv Funct Mater 2009;19:3300–6.
[94] Xin H, Kim FS, Jenekhe SA. Highly efficient solar cells based on poly(3-butylthiophene) nanowires. J Am Chem Soc 2008;130:5424–5.
[95] Sivula K, Ball ZT, Watanabe N, Fréchet JMJ. Amphiphilic diblock copolymer compatibilizers and their effect on the morphology and performance of polythiophene:fullerene solar cells. Adv Mater 2006;18:206–10.
[96] Sivula K, Luscombe CK, Thompson BC, Fréchet JMJ. Enhancing the thermal stability of polythiophene:fullerene solar cells by decreasing effective polymer regioregularity. J Am Chem Soc 2006;128:13988–9.
[97] Miyanishi S, Tajima K, Hashimoto K. Morphological stabilization of polymer photovoltaic cells by using cross-linkable poly(3-(5-hexenyl)thiophene). Macromolecules 2009;42:1610–8.
[98] Koppe M, Scharber M, Brabec C, Duffy W, Heeney M, McCulloch I. Polyterthiophenes as donors for polymer solar cells. Adv Funct Mater 2007;17:1371–6.
[99] Hou J, Chen TL, Zhang S, Huo L, Sista S, Yang Y. An easy and effective method to modulate molecular energy level of poly(3-alkylthiophene) for high-voc polymer solar cells. Macromolecules 2009;42:9217–9.
[100] Wantz G, Lefevre F, Dang MT, Laliberté D, Brunner PL, Dautel OJ. Photovoltaic solar cells using poly(3,3-didodecylquaterthiophene). Sol Energy Mater Sol Cells 2008;92:558–63.
[101] Thompson BC, Kim BJ, Kavulak DF, Sivula K, Mauldin C, Fréchet JMJ. Influence of alkyl substitution pattern in thiophene copolymers on composite fullerene solar cell performance. Macromolecules 2007;40:7425–8.
[102] Ballantyne AM, Chen L, Nelson J, Bradley DDC, Astuti Y, Maurano A, Shuttle CG, Durrant JR, Heeney M, Duffy W, McCulloch I. Studies of highly regioregular poly(3-hexylselenophene) for photovoltaic applications. Adv Mater 2007;19:4544–7.
[103] Heeney M, Zhang W, Crouch D, Chabinyc ML, Gordeyev S, Hamilton R, Higgins S, McCulloch I, Skabara P, Sparrowe D, Tierney S. Regioregular poly(3-hexyl)selenophene: a low band gap organic hole transporting polymer. Chem Commun 2007:5061–3.
[104] Ballantyne AM, Ferenczi TAM, Campoy-Quiles M, Clarke TM, Maurano A, Wong KH, Zhang W, Stingelin-Stutzmann N, Kim JS, Bradley DDC, Durrant JR, McCulloch I, Heeney M, Nelson J, Tierney S, Duffy W, Mueller C, Smith P. Understanding the influence of morphology on poly(3-hexylselenothiophene):PCBM solar cells. Macromolecules 2010;43:1169–74.
[105] Chang YT, Hsu SL, Su MH, Wei KH. Soluble phenanthrenyl-imidazole-presenting regioregular poly(3-octylthiophene) copolymers having tunable bandgaps for solar cell applications. Adv Funct Mater 2007;17:3326–31.
[106] Chang YT, Hsu SL, Su MH, Wei KH. Intramolecular donor–acceptor regioregular poly(hexylphenanthrenyl-imidazole thiophene) exhibits enhanced hole mobility for heterojunction solar cell applications. Adv Mater 2009;21:2093–7.
[107] Chang YT, Hsu SL, Chen GY, Su MH, Singh TA, Diau EWG, Wei KH. Intramolecular donor–acceptor regioregular poly(3-hexylthiophene)s presenting octylphenanthrenyl-imidazole moieties exhibit enhanced charge transfer for heterojunction solar cell applications. Adv Funct Mater 2008;18:2356–65.
[108] Li Y, Zou Y. Conjugated polymer photovoltaic materials with broad absorption band and high charge carrier mobility. Adv Mater 2008;20:2952–8.
[109] Hou J, Tan Z, Yan Y, He Y, Yang C, Li Y. Synthesis and photovoltaic properties of two-dimensional conjugated polythiophenes with bi(thienylenevinylene) side chains. J Am Chem Soc 2006;128:4911–6.
[110] Zhou E, Tan Z, Huo L, He Y, Yang C, Li Y. Effect of branched conjugation structure on the optical, electrochemical, hole mobility, and photovoltaic properties of polythiophenes. J Phys Chem B 2006;110:26062–7.
[111] Hittinger E, Kokil A, Weder C. Synthesis and characterization of cross-linked conjugated polymer milli-, micro-, and nanoparticles. Angew Chem Int Ed 2004;43:1808–11.
[112] Zhou EJ, Tan ZA, Yang CH, Li YF. Linking polythiophene chains through conjugated bridges: a way to improve charge transport in polymer solar cells. Macromol Rapid Commun 2006;27:793–8.
[113] Zhou EJ, Tan ZA, Yang Y, Huo LJ, Zou YP, Yang CH, Li YF. Synthesis, hole mobility, and photovoltaic properties of cross-linked polythiophenes with vinylene–terthiophene–vinylene as conjugated bridge. Macromolecules 2007;40:1831–7.
[114] Tu G, Bilge A, Adamczyk S, Forster M, Heiderhoff R, Balk LJ, Mv̈hlbacher D, Morana M, Koppe M, Scharber MC, Choulis SA, Brabec CJ, Scherf U. The influence of interchain branches on solid state packing, hole mobility and photovoltaic properties of poly(3-hexylthiophene) (P3HT). Macromol Rapid Commun 2007;28:1781–5.
[115] Yu CY, Ko BT, Ting C, Chen CP. Two-dimensional regioregular polythiophenes with conjugated side chains for use in organic solar cells. Sol Energy Mater Sol Cells 2009;93:613–20.
[116] Tsai JH, Lee WY, Chen WC, Yu CY, Hwang GW, Ting C. New two-dimensional thiophene–acceptor conjugated copolymers for field effect transistor and photovoltaic cell applications. Chem Mater 2010;22:3290–9.
[117] Bundgaard E, Krebs FC. Low-band-gap conjugated polymers based on thiophene, benzothiadiazole, and benzobis(thiadiazole). Macromolecules 2006;39:2823–31.
[118] Yue W, Zhao Y, Tian H, Song D, Xie Z, Yan D, Geng Y, Wang F. Poly(oligothiophene-alt-benzothiadiazole)s: tuning the structures of oligothiophene units toward high-mobility "black" conjugated polymers. Macromolecules 2009;42:6510–8.
[119] Liang F, Lu J, Ding J, Movileanu R, Tao Y. Design and synthesis of alternating regioregular oligothiophenes/benzothiadiazole copolymers for organic solar cells. Macromolecules 2009;42:6107–14.
[120] Beaujuge PM, Subbiah J, Choudhury KR, Ellinger S, McCarley TD, So F, Reynolds JR. Green dioxythiophene-benzothiadiazole donor-acceptor copolymers for photovoltaic device applications. Chem Mater 2010;22:2093–106.
[121] Wienk MM, Struijk MP, Janssen RAJ. Low band gap polymer bulk heterojunction solar cells. Chem Phys Lett 2006;422:488–91.
[122] Helgesen M, Gevorgyan SA, Krebs FC, Janssen RAJ. Substituted 2,1,3-benzothiadiazole- and thiophene-based polymers for solar

cells – introducing a new thermocleavable precursor. Chem Mater 2009;21:4669–75.
[123] Xia Y, Wang L, Deng X, Li D, Zhu X, Cao Y. Photocurrent response wavelength up to 1.1 μm from photovoltaic cells based on narrow-band-gap conjugated polymer and fullerene derivative. Appl Phys Lett 2006;89, 081106/1–3.
[124] Zoombelt AP, Fonrodona M, Turbiez MGR, Wienk MM, Janssen RAJ. Synthesis and photovoltaic performance of a series of small band gap polymers. J Mater Chem 2009;19:5336–42.
[125] Xin H, Guo X, Kim FS, Ren G, Watson MD, Jenekhe SA. Efficient solar cells based on a new phthalimide-based donor–acceptor copolymer semiconductor: morphology, charge-transport, and photovoltaic properties. J Mater Chem 2009;19:5303–10.
[126] McCulloch I, Heeney M, Bailey C, Genevicius K, MacDonald I, Shkunov M, Sparrowe D, Tierney S, Wagner R, Zhang W, Chabinyc ML, Kline RJ, McGehee MD, Toney MF. Liquid-crystalline semiconducting polymers with high charge-carrier mobility. Nat Mater 2006;5:328–33.
[127] DeLongchamp DM, Kline RJ, Lin EK, Fischer DA, Richter LJ, Lucas LA, Heeney M, McCullough I, Northrup JE. High carrier mobility polythiophene thin films: structure determination by experiment and theory. Adv Mater 2007;19:833–7.
[128] Cates NC, Gysel R, Beiley Z, Miller CE, Toney MF, Heeney M, McCulloch I, McGehee MD. Tuning the properties of polymer bulk heterojunction solar cells by adjusting fullerene size to control intercalation. Nano Lett 2009;9:4153–7.
[129] Parmer JE, Mayer AC, Hardin BE, Scully SR, McGehee MD, Heeney M, McCulloch I. Organic bulk heterojunction solar cells using poly(2,5-bis(3-tetradecyllthiophen-2-yl)thieno[3,2,-b]thiophene). Appl Phys Lett 2008;92, 113309/1-3.
[130] Biniek L, Chochos CL, Leclerc N, Hadziioannou G, Kallitsis JK, Bechara R, Lévêque P, Heiser T. A [3,2-b]thienothiophene-alt-benzothiadiazole copolymer for photovoltaic applications: design, synthesis, material characterization and device performances. J Mater Chem 2009;19:4946–51.
[131] Biniek L, Chochos CL, Hadziioannou G, Leclerc N, Lévêque P, Heiser T. Electronic properties and photovoltaic performances of a series of oligothiophene copolymers incorporating both thieno[3,2-b]thiophene and 2,1,3-benzothiadiazole moieties. Macromol Rapid Commun 2010;31:651–6.
[132] Lee JY, Heo SW, Choi H, Kwon YJ, Haw JR, Moon DK. Synthesis and characterization of 2,1,3-benzothiadiazole-thieno[3,2-b]thiophene-based charge transferred-type polymers for photovoltaic application. Sol Energy Mater Sol Cells 2009;93:1932–8.
[133] Lee JY, Shin WS, Haw JR, Moon DK. Low band-gap polymers based on quinoxaline derivatives and fused thiophene as donor materials for high efficiency bulk-heterojunction photovoltaic cells. J Mater Chem 2009;19:4938–45.
[134] Wynberg H, Zwanenburg DJ. Thieno[3,4-b]thiophene. the third thiophthene. Tetrahedron Lett 1967;8:761–4.
[135] Hong SY, Marynick DS. Understanding the conformational stability and electronic structures of modified polymers based on polythiophene. Macromolecules 1992;25:4652–7.
[136] Yao Y, Liang Y, Shrotriya V, Xiao S, Yu L, Yang Y. Plastic near-infrared photodetectors utilizing low band gap polymer. Adv Mater 2007;19:3979–83.
[137] Liang Y, Xiao S, Feng D, Yu L. Control in energy levels of conjugated polymers for photovoltaic application. J Phys Chem C 2008;112:7866–71.
[138] Liang Y, Feng D, Guo J, Szarko JM, Ray C, Chen LX, Yu L. Regioregular oligomer and polymer containing thieno[3,4-b]thiophene moiety for efficient organic solar cells. Macromolecules 2009;42:1091–8.
[139] Kobayashi M, Colaneri N, Boysel M, Wudl F, Heeger AJ. The electronic and electrochemical properties of poly(isothianaphthene). J Chem Phys 1985;82:5717–23.
[140] Polec I, Lutsen L, Vanderzande D, Gelan J. Temperature dependence of the reduction of phthalic thioanhydrides by $NaBH_4$: competition between 3-hydroxythiolactone and phthalide formation. Eur J Org Chem 2002;2002:1033–6.
[141] Polec I, Henckens A, Goris L, Nicolas M, Loi MA, Adriaensens P, Lutsen L, Manca JV, Vanderzande D, Sariciftci NS. Convenient synthesis and polymerization of 5,6-disubstituted dithiophthalides toward soluble poly(isothianaphthene): an initial spectroscopic characterization of the resulting low-band-gap polymers. J Polym Sci Part A Polym Chem 2003;41:1034–45.
[142] Vangeneugden DL, Kiebooms HL, Vanderzande JM, Gelan MJV. A general synthetic route towards soluble poly(1,3-dithienylisothianaphthene) derivatives. Synth Met 1999;101:120–1.
[143] Shaheen SE, Vangeneugden D, Kiebooms R, Vanderzande D, Fromherz T, Padinger F, Brabec CJ, Sariciftci NS. Low band-gap polymeric photovoltaic devices. Synth Met 2001;121:1583–4.
[144] Qin Y, Kim JY, Frisbie CD, Hillmyer MA. Distannylated isothianaphthene: a versatile building block for low bandgap conjugated polymers. Macromolecules 2008;41:5563–70.
[145] Asawapirom U, Scherf U. Dialkylcyclopentadithiophene polymers and copolymers. Macromol Rapid Commun 2001;22:746–9.
[146] Yuan MC, Su MH, Chiu MY, Wei KH. Synthesis and characterization of donor–bridge–acceptor alternating copolymers containing perylene diimide units and their application to photovoltaic cells. J Polym Sci Part A Polym Chem 2010;48:1298–309.
[147] Lee SK, Cho NS, Cho S, Moon SJ, Lee JK, Bazan GC. Synthesis and characterization of low-bandgap cyclopentadithiophene-biselenophene copolymer and its use in field-effect transistor and polymer solar cells. J Polym Sci Part A Polym Chem 2009;47:6873–82.
[148] Xiao S, Zhou H, You W. Conjugated polymers of fused bithiophenes with enhanced π-electron delocalization for photovoltaic applications. Macromolecules 2008;41:5688–96.
[149] Zhu Z, Waller D, Gaudiana R, Morana M, Mv̈hlbacher D, Scharber M, Brabec C. Panchromatic conjugated polymers containing alternating donor/acceptor units for photovoltaic applications. Macromolecules 2007;40:1981–6.
[150] Mv̈hlbacher D, Scharber M, Morana M, Zhu Z, Waller D, Gaudiana R, Brabec C. High photovoltaic performance of a low-bandgap polymer. Adv Mater 2006;18:2884–9.
[151] Peet J, Kim JY, Coates NE, Ma WL, Moses D, Heeger AJ, Bazan GC. Efficiency enhancement in low-bandgap polymer solar cells by processing with alkane dithiols. Nat Mater 2007;6:497–500.
[152] Bijleveld JC, Shahid M, Gilot J, Wienk MM, Janssen RAJ. Copolymers of cyclopentadithiophene and electron-deficient aromatic units designed for photovoltaic applications. Adv Funct Mater 2009;19:3262–70.
[153] Hou J, Chen TL, Zhang S, Chen HY, Yang Y. Poly[4,4-bis(2-ethylhexyl)cyclopenta[2,1-b;3,4-b′]dithiophene-2,6-diyl-alt-2,1,3-benzoselenadiazole-4,7-diyl], a new low band gap polymer in polymer solar cells. J Phys Chem C 2009;113:1601–5.
[154] Jung IH, Kim H, Park MJ, Kim B, Park JH, Jeong E, Woo HY, Yoo S, Shim HK. Synthesis and characterization of cyclopentadithiophene-based low bandgap copolymers containing electron-deficient benzoselenadiazole derivatives for photovoltaic devices. J Polym Sci Part A Polym Chem 2010;48:1423–32.
[155] Jung IH, Yu J, Jeong E, Kim J, Kwon S, Kong H, Lee K, Woo HY, Shim HK. Synthesis and photovoltaic properties of cyclopentadithiophene-based low-bandgap copolymers that contain electron-withdrawing thiazole derivatives. Chem A Eur J 2010;16:3743–52.
[156] Coffin RC, Peet J, Rogers J, Bazan GC. Streamlined microwave-assisted preparation of narrow-bandgap conjugated polymers for high-performance bulk heterojunction solar cells. Nat Chem 2009;1:657–61.
[157] Hwang IW, Soci C, Moses D, Zhu Z, Waller D, Gaudiana R, Brabec CJ, Heeger AJ. Ultrafast electron transfer and decay dynamics in a small band gap bulk heterojunction material. Adv Mater 2007;19:2307–12.
[158] Lee JK, Ma WL, Brabec CJ, Yuen J, Moon JS, Kim JY, Lee K, Bazan GC, Heeger AJ. Processing additives for improved efficiency from bulk heterojunction solar cells. J Am Chem Soc 2008;130:3619–23.
[159] Nuzzo DD, Aguirre A, Shahid M, Gevaerts VS, Meskers SCJ, Janssen RAJ. Improved film morphology reduces charge carrier recombination into the triplet excited state in a small bandgap polymer–fullerene photovoltaic cell. Adv Mater 2010;22:4321–4.
[160] Li KC, Hsu YC, Lin JT, Yang CC, Wei KH, Lin HC. Soluble narrow-band-gap copolymers containing novel cyclopentadithiophene units for organic photovoltaic cell applications. J Polym Sci Part A Polym Chem 2009;47:2073–92.
[161] Moulé AJ, Tsami A, Bv̈nnagel TW, Forster M, Kronenberg NM, Scharber M, Koppe M, Morana M, Brabec CJ, Meerholz K, Scherf U. Two novel cyclopentadithiophene-based alternating copolymers as potential donor components for high-efficiency bulk-heterojunction-type solar cells. Chem Mater 2008;20:4045–50.
[162] Chen CH, Hsieh CH, Dubosc M, Cheng YJ, Hsu CS. Synthesis and characterization of bridged bithiophene-based conjugated polymers for photovoltaic applications: acceptor strength and ternary blends. Macromolecules 2010;43:697–708.

[163] Lu G, Usta H, Risko C, Wang L, Facchetti A, Ratner MA, Marks TJ. Synthesis, characterization, and transistor response of semiconducting silole polymers with substantial hole mobility and air stability. experiment and theory. J Am Chem Soc 2008;130:7670–85.
[164] Zhan XW, Risko C, Amy F, Chan C, Zhao W, Barlow S, Kahn A, Brédas JL, Marder SR. Electron affinities of 1,1-diaryl-2,3,4,5-tetraphenylsiloles: direct measurements and comparison with experimental and theoretical estimates. J Am Chem Soc 2005;127:9021–9.
[165] Risko C, Kushto GP, Kafafi ZH, Bredas JL. Electronic properties of silole-based organic semiconductors. J Chem Phys 2004;121:9031–8.
[166] Yamaguchi S, Tamao K. Theoretical study of the electronic structure of 2,2′-bisilole in comparison with 1,1′-Bi-1,3-cyclopentadiene: σ^*–π^* conjugation and a low-lying LUMO as the origin of the unusual optical properties of 3,3′,4,4′-tetraphenyl-2,2′-bisilole. Bull Chem Soc Jpn 1996;69:2327–34.
[167] Hou J, Chen HY, Zhang S, Li G, Yang Y. Synthesis, characterization, and photovoltaic properties of a low band gap polymer based on silole-containing polythiophenes and 2,1,3-benzothiadiazole. J Am Chem Soc 2008;130:16144–5.
[168] Chen HY, Hou J, Hayden AE, Yang H, Houk KN, Yang Y. Silicon atom substitution enhances interchain packing in a thiophene-based polymer system. Adv Mater 2010;22:371–5.
[169] Scharber MC, Koppe M, Gao J, Cordella F, Loi MA, Denk P, Morana M, Egelhaaf HJ, Forberich K, Dennler G, Gaudiana R, Waller D, Zhu Z, Shi X, Brabec CJ. Influence of the bridging atom on the performance of a low-bandgap bulk heterojunction solar cell. Adv Mater 2010;22:367–70.
[170] Morana M, Azimi H, Dennler G, Egelhaaf HJ, Scharber M, Forberich K, Hauch J, Gaudiana R, Waller D, Zhu Z, Hingerl K, van Bavel SS, Loos J, Brabec CJ. Nanomorphology and charge generation in bulk heterojunctions based on low-bandgap dithiophene polymers with different bridging atoms. Adv Funct Mater 2010;20:1180–8.
[171] Tong M, Cho S, Rogers JT, Schmidt K, Hsu BBY, Moses D, Coffin RC, Kramer EJ, Bazan GC, Heeger AJ. Higher molecular weight leads to improved photoresponsivity, charge transport and interfacial ordering in a narrow bandgap semiconducting polymer. Adv Funct Mater 2010;20:3959–65.
[172] Hoven CV, Dang XD, Coffin RC, Peet J, Nguyen TQ, Bazan GC. Improved performance of polymer bulk heterojunction solar cells through the reduction of phase separation via solvent additives. Adv Mater 2010;22:E63–6.
[173] Huo L, Chen HY, Hou J, Chen TL, Yang Y. Low band gap dithieno[3,2-b:2′,3′-d]silole-containing polymers, synthesis, characterization and photovoltaic application. Chem Commun 2009:5570–2.
[174] Liao L, Dai L, Smith A, Durstock M, Lu J, Ding J, Tao Y. Photovoltaic-active dithienosilole-containing polymers. Macromolecules 2007;40:9406–12.
[175] Yue W, Zhao Y, Shao S, Tian H, Xie Z, Geng Y, Wang F. Novel NIR-absorbing conjugated polymers for efficient polymer solar cells: effect of alkyl chain length on device performance. J Mater Chem 2009;19:2199–206.
[176] Zhang S, Guo Y, Fan H, Liu Y, Chen HY, Yang G, Zhan X, Liu Y, Li Y, Yang Y. Low bandgap π-conjugated copolymers based on fused thiophenes and benzothiadiazole: synthesis and structure–property relationship study. J Polym Sci Part A Polym Chem 2009;47:5498–508.
[177] Zhang X, Steckler TT, Dasari RR, Ohira S, Potscavage WJ, Tiwari SP, Coppée S, Ellinger S, Barlow S, Brédas JL, Kippelen B, Reynolds JR, Marder SR. Dithienopyrrole-based donor–acceptor copolymers: low band-gap materials for charge transport, photovoltaics and electrochromism. J Mater Chem 2010;20:123–34.
[178] Zhou E, Nakamura M, Nishizawa T, Zhang Y, Wei Q, Tajima K, Yang C, Hashimoto K. Synthesis and photovoltaic properties of a novel low band gap polymer based on n-substituted dithieno[3,2-b:2′,3′-d]pyrrole. Macromolecules 2008;41:8302–5.
[179] Millefiorini S, Kozma E, Catellani M, Luzzati S. Dithienothiophene based polymer as electron donor in plastic solar cells. Thin Solid Films 2008;516:7205–8.
[180] Zhang S, He C, Liu Y, Zhan X, Chen J. Synthesis of a soluble conjugated copolymer based on dialkyl-substituted dithienothiophene and its application in photovoltaic cells. Polymer 2009;50:3595–9.
[181] Pan H, Li Y, Wu Y, Liu P, Ong BS, Zhu S, Xu G. Low-temperature, solution-processed, high-mobility polymer semiconductors for thin-film transistors. J Am Chem Soc 2007;129:4112–3.
[182] Hou J, Park MH, Zhang S, Yao Y, Chen LM, Li JH, Yang Y. Bandgap and molecular energy level control of conjugated polymer photovoltaic materials based on benzo[1,2-b:4,5-b′]dithiophene. Macromolecules 2008;41:6012–8.
[183] Liang Y, Wu Y, Feng D, Tsai ST, Son HJ, Li G, Yu L. Development of new semiconducting polymers for high performance solar cells. J Am Chem Soc 2009;131:56–7.
[184] He Y, Zhou Y, Zhao G, Min J, Guo X, Zhang B, Zhang M, Zhang J, Li Y, Zhang F, Inganäs O. Poly(4,8-bis(2-ethylhexyloxy)benzo[1,2-b:4,5-b′]dithiophene vinylene): synthesis, optical and photovoltaic properties. J Polym Sci Part A Polym Chem 2010;48:1822–9.
[185] Liang Y, Feng D, Wu Y, Tsai ST, Li G, Ray C, Yu L. Highly efficient solar cell polymers developed via fine-tuning of structural and electronic properties. J Am Chem Soc 2009;131:7792–9.
[186] Liang Y, Xu Z, Xia J, Tsai ST, Wu Y, Li G, Ray C, Yu L. For the bright future-bulk heterojunction polymer solar cells with power conversion efficiency of 7.4%. Adv Mater 2010;22:E135–8.
[187] Guo J, Liang Y, Szarko J, Lee B, Son HJ, Rolczynski BS, Yu L, Chen LX. Structure, dynamics, and power conversion efficiency correlations in a new low bandgap polymer: PCBM solar cell. J Phys Chem B 2010;114:742–8.
[188] Hou J, Chen HY, Zhang S, Chen RI, Yang Y, Wu Y, Li G. Synthesis of a low band gap polymer and its application in highly efficient polymer solar cells. J Am Chem Soc 2009;131:15586–7.
[189] Chen HY, Hou J, Zhang S, Liang Y, Yang G, Yang Y, Yu L, Wu Y, Li G. Polymer solar cells with enhanced open-circuit voltage and efficiency. Nat Photonics 2009;3:649–53.
[190] Zou Y, Najari A, Berrouard P, Beaupré S, Aïch BR, Tao Y, Leclerc M. A thieno[3,4-c]pyrrole-4,6-dione-based copolymer for efficient solar cells. J Am Chem Soc 2010;132:5330–1.
[191] Zhang Y, Hau SK, Yip HL, Sun Y, Acton O, Jen AKY. Efficient polymer solar cells based on the copolymers of benzodithiophene and thienopyrroledione. Chem Mater 2010;22:2696–8.
[192] Piliego C, Holcombe TW, Douglas JD, Woo CH, Beaujuge PM, Fréchet JMJ. Synthetic control of structural order in N-alkylthieno[3,4-c]pyrrole-4,6-dione-based polymers for efficient solar cells. J Am Chem Soc 2010;132:7595–7.
[193] Price SC, Stuart AC, You W. Low band gap polymers based on benzo[1,2-b:4,5-b′]dithiophene: rational design of polymers leads to high photovoltaic performance. Macromolecules 2010;43:4609–12.
[194] Hou J, Chen HY, Zhang S, Yang Y. Synthesis and photovoltaic properties of two benzo[1,2-b:3,4-b′]dithiophene-based conjugated polymers. J Phys Chem C 2009;113:21202–7.
[195] Huo L, Hou J, Zhang S, Chen HY, Yang Y. A Polybenzo[1,2-b:4,5-b′]dithiophene derivative with deep homo level and its application in high-performance polymer solar cells. Angew Chem Int Ed 2010;49:1500–3.
[196] Xiao S, Stuart AC, Liu S, You W. Conjugated polymers based on benzo[2,1-b:3,4-b′]dithiophene with low-lying highest occupied molecular orbital energy levels for organic photovoltaics. ACS Appl Mater Interfaces 2009;1:1613–21.
[197] Zhou H, Yang L, Xiao S, Liu S, You W. Donor–acceptor polymers incorporating alkylated dithienylbenzothiadiazole for bulk heterojunction solar cells: pronounced effect of positioning alkyl chains. Macromolecules 2010;43:811–20.
[198] Xiao S, Stuart AC, Liu S, Zhou H, You W. Conjugated polymer based on polycyclic aromatics for bulk heterojunction organic solar cells: a case study of quadrathienonaphthalene polymers with 2% efficiency. Adv Funct Mater 2010;20:635–43.
[199] Zhou H, Yang L, Stoneking S, You W. A weak donor–strong acceptor strategy to design ideal polymers for organic solar cells. ACS Appl Mater Interfaces 2010;2:1377–83.
[200] Price SC, Stuart AC, You W. Polycyclic aromatics with flanking thiophenes: tuning energy level and band gap of conjugated polymers for bulk heterojunction photovoltaics. Macromolecules 2010;43:797–804.
[201] Beaupré S, Boudreault PLT, Leclerc M. Solar-energy production and energy-efficient lighting: photovoltaic devices and white-light-emitting diodes using poly(2,7-fluorene), poly(2,7-carbazole), and poly(2,7-dibenzosilole) derivatives. Adv Mater 2010;22:E6–27.
[202] Inganäs O, Zhang F, Tvingstedt K, Andersson LM, Hellström S, Andersson MR. Polymer photovoltaics with alternating copolymer/fullerene blends and novel device architectures. Adv Mater 2010;22:E100–16.
[203] Zhao B, Liu D, Peng L, Li H, Shen P, Xiang N, Liu Y, Tan S. Effect of oxadiazole side chains based on alternating fluorene–thiophene copolymers for photovoltaic cells. Eur Polym J 2009;45:2079–86.
[204] Schulz GL, Chen X, Holdcroft S. High band gap poly(9,9-dihexylfluorene-alt-bithiophene) blended with [6,6]-phenyl C61

butyric acid methyl ester for use in efficient photovoltaic devices. Appl Phys Lett 2009;94, 023302/1-3.
[205] Huang JH, Yang CY, Ho ZY, Kekuda D, Wu MC, Chien FC, Chen P, Chu CW, Ho KC. Annealing effect of polymer bulk heterojunction solar cells based on polyfluorene and fullerene blend. Org Electron 2009;10:27–33.
[206] Tang W, Ke L, Tan L, Lin T, Kietzke T, Chen ZK. Conjugated copolymers based on fluorene–thieno[3,2-b]thiophene for light-emitting diodes and photovoltaic cells. Macromolecules 2007;40:6164–71.
[207] Wang F, Luo J, Yang K, Chen J, Huang F, Cao Y. Conjugated fluorene and silole copolymers: synthesis, characterization, electronic transition, light emission, photovoltaic cell, and field effect hole mobility. Macromolecules 2005;38:2253–60.
[208] Okamoto T, Jiang Y, Qu F, Mayer AC, Parmer JE, McGehee MD, Bao Z. Synthesis and characterization of pentacene– and anthradithiophene–fluorene conjugated copolymers synthesized by Suzuki reactions. Macromolecules 2008;41:6977–80.
[209] Inganäs O, Svensson M, Zhang F, Gadisa A, Persson NK, Wang X, Andersson MR. Low bandgap alternating polyfluorene copolymers in plastic photodiodes and solar cells. Appl Phys A 2004;79:31–5.
[210] Slooff LH, Veenstra SC, Kroon JM, Moet DJD, Sweelssen J, Koetse MM. Determining the internal quantum efficiency of highly efficient polymer solar cells through optical modeling. Appl Phys Lett 2007;90, 143506/1-3.
[211] Chen MH, Hou J, Hong Z, Yang G, Sista S, Chen LM, Yang Y. Efficient polymer solar cells with thin active layers based on alternating polyfluorene copolymer/fullerene bulk heterojunctions. Adv Mater 2009;21:4238–42.
[212] McNeill CR, Abrusci A, Zaumseil J, Wilson R, McKiernan MJ, Burroughes JH, Halls JJM, Greenham NC, Friend RH. Dual electron donor/electron acceptor character of a conjugated polymer in efficient photovoltaic diodes. Appl Phys Lett 2007;90, 193506/1–3.
[213] Li W, Qin R, Zhou Y, Andersson M, Li F, Zhang C, Li B, Liu Z, Bo Z, Zhang F. Tailoring side chains of low band gap polymers for high efficiency polymer solar cells. Polymer 2010;51:3031–8.
[214] Shi C, Yao Y, Yang Y, Pei Q. Regioregular copolymers of 3-alkoxythiophene and their photovoltaic application. J Am Chem Soc 2006;128:8980–6.
[215] Hsu SLC, Lin YC, Lee RF, Sivakumar C, Chen JS, Chou WY. Synthesis and characterization of new low bandgap polyfluorene copolymers for bulk heterojunction solar cells. J Polym Sci Part A Polym Chem 2009;47:5336–43.
[216] Park JS, Ryu TI, Song M, Yoon KJ, Lee MJ, Shin IA, Lee GD, Lee JW, Gal YS, Jin SH. Synthesis and characterization of fluorene-based low-band gap copolymers containing propylenedioxythiophene and benzothiadiazole derivatives for bulk heterojunction photovoltaic cell applications. J Polym Sci Part A Polym Chem 2008;46:6175–84.
[217] Yang R, Tian R, Yan J, Zhang Y, Yang J, Hou Q, Yang W, Zhang C, Cao Y. Deep-red electroluminescent polymers: synthesis and characterization of new low-band-gap conjugated copolymers for light-emitting diodes and photovoltaic devices. Macromolecules 2005;38:244–53.
[218] Zhang F, Perzon E, Wang X, Mammo W, Andersson MR, Inganäs O. Polymer solar cells based on a low-bandgap fluorene copolymer and a fullerene derivative with photocurrent extended to 850 nm. Adv Funct Mater 2005;15:745–50.
[219] Mammo W, Admassie S, Gadisa A, Zhang F, Inganäs O, Andersson MR. New low band gap alternating polyfluorene copolymer-based photovoltaic cells. Sol Energy Mater Sol Cells 2007;91:1010–8.
[220] Zhang F, Mammo W, Andersson LM, Admassie S, Andersson MR, Inganäs O. Low-bandgap alternating fluorene copolymer/methanofullerene heterojunctions in efficient near-infrared polymer solar cells. Adv Mater 2006;18:2169–73.
[221] Kmínek I, Výprachtický D, Kříž J, Dybal J, Cimrová V. Low-band gap copolymers containing thienothiadiazole units: synthesis, optical, and electrochemical properties. J Polym Sci Part A Polym Chem 2010;48:2743–56.
[222] Perzon E, Wang X, Admassie S, Inganäs O, Andersson MR. An alternating low band-gap polyfluorene for optoelectronic devices. Polymer 2006;47:4261–8.
[223] Wang X, Perzon E, Mammo W, Oswald F, Admassie S, Persson NK, Langa F, Andersson MR, Inganäs O. Polymer solar cells with low-bandgap polymers blended with C70-derivative give photocurrent at 1 μm. Thin Solid Films 2006;511–512:576–80.
[224] Wang X, Perzon E, Oswald F, Langa F, Admassie S, Andersson MR, Inganäs O. Enhanced photocurrent spectral response in low-bandgap polyfluorene and C_{70}-derivative-based solar cells. Adv Funct Mater 2005;15:1665–70.
[225] Wang X, Perzon E, Delgado JL, de la Cruz P, Zhang F, Langa F, Andersson M, Inganäs O. Infrared photocurrent spectral response from plastic solar cell with low-band-gap polyfluorene and fullerene derivative. Appl Phys Lett 2004;85:5081–3.
[226] Kitazawa D, Watanabe N, Yamamoto S, Tsukamoto J. Quinoxaline-based π-conjugated donor polymer for highly efficient organic thin-film solar cells. Appl Phys Lett 2009;95, 053701/1–3.
[227] Lindgren LJ, Zhang F, Andersson M, Barrau S, Hellström S, Mammo W, Perzon E, Inganäs O, Andersson MR. Synthesis, characterization, and devices of a series of alternating copolymers for solar cells. Chem Mater 2009;21:3491–502.
[228] Gadisa A, Mammo A, Andersson LM, Admassie S, Zhang F, Andersson MR, Inganäs O. A new donor–acceptor–donor polyfluorene copolymer with balanced electron and hole mobility. Adv Funct Mater 2007;17:3836–42.
[229] Gedefaw D, Zhou Y, Hellström S, Lindgren L, Andersson LM, Zhang F, Mammo W, Inganäs O, Andersson MR. Alternating copolymers of fluorene and donor–acceptor–donor segments designed for miscibility in bulk heterojunction photovoltaics. J Mater Chem 2009;19:5359–63.
[230] Zhang F, Bijleveld J, Perzon E, Tvingstedt K, Barrau S, Inganäs O, Andersson MR. High photovoltage achieved in low band gap polymer solar cells by adjusting energy levels of a polymer with the LUMOs of fullerene derivatives. J Mater Chem 2008;18:5468–74.
[231] Lee SK, Cho NS, Kwak JH, Lim KS, Shim HK, Hwang DH, Brabec CJ. New low band-gap alternating polyfluorene derivatives for photovoltaic cells. Thin Solid Films 2006;511–512:157–62.
[232] Svensson M, Zhang F, Veenstra SC, Verhees WJH, Hummelen JC, Kroon JM, Inganäs O, Andersson MR. High-performance polymer solar cells of an alternating polyfluorene copolymer and a fullerene derivative. Adv Mater 2003;15:988–91.
[233] Tvingstedt K, Andersson V, Zhang F, Inganäs O. Folded reflective tandem polymer solar cell doubles efficiency. Appl Phys Lett 2007;91, 123514/1-3.
[234] Wang E, Wang M, Wang L, Duan C, Zhang J, Cai W, He C, Wu H, Cao Y. Donor polymers containing benzothiadiazole and four thiophene rings in their repeating units with improved photovoltaic performance. Macromolecules 2009;42:4410–5.
[235] Zhang ZG, Zhang KL, Liu G, Zhu CX, Neoh KG, Kang ET. Triphenylamine–fluorene alternating conjugated copolymers with pendant acceptor groups: synthesis, structure–property relationship, and photovoltaic application. Macromolecules 2009;42:3104–11.
[236] Huang F, Chen KS, Yip HL, Hau SK, Acton O, Zhang Y, Luo J, Jen AKY. Development of new conjugated polymers with donor–π-bridge–acceptor side chains for high performance solar cells. J Am Chem Soc 2009;131:13886–7.
[237] Duan C, Cai W, Huang F, Zhang J, Wang M, Yang T, Zhong C, Gong X, Cao Y. Novel silafluorene-based conjugated polymers with pendant acceptor groups for high performance solar cells. Macromolecules 2010;43:5262–8.
[238] Perzon E, Zhang F, Andersson M, Mammo W, Inganäs O, Andersson MR. A conjugated polymer for near infrared optoelectronic applications. Adv Mater 2007;19:3308–11.
[239] Blouin N, Leclerc M. Poly(2,7-carbazole)s: structure–property relationships. Acc Chem Res 2008;41:1110–9.
[240] Leclerc N, Michaud A, Sirois K, Morin JF, Leclerc M. Synthesis of 2,7-carbazolenevinylene-based copolymers and characterization of their photovoltaic properties. Adv Funct Mater 2006;16:1694–704.
[241] Blouin N, Michaud A, Gendron D, Wakim S, Blair E, Neagu-Plesu R, Belletête M, Durocher G, Tao Y, Leclerc M. Toward a rational design of poly(2,7-carbazole) derivatives for solar cells. J Am Chem Soc 2008;130:732–42.
[242] Gendron D, Morin PO, Najari A, Leclerc M. Synthesis of new pyridazine-based monomers and related polymers for photovoltaic applications. Macromol Rapid Commun 2010;31:1090–4.
[243] Blouin N, Michaud A, Leclerc M. A low-bandgap poly(2,7-carbazole) derivative for use in high-performance solar cells. Adv Mater 2007;19:2295–300.
[244] Wakim S, Beaupré S, Blouin N, Aich BR, Rodman S, Gaudiana R, Tao Y, Leclerc M. Highly efficient organic solar cells based on a poly(2,7-carbazole) derivative. J Mater Chem 2009;19:5351–8.
[245] Park SH, Roy A, Beaupré S, Cho S, Coates N, Moon JS, Moses D, Leclerc M, Lee K, Heeger AJ. Bulk heterojunction solar cells with internal quantum efficiency approaching 100%. Nat Photonics 2009;3:297–302.
[246] Qin R, Li W, Li C, Du C, Veit C, Schleiermacher HF, Andersson M, Bo Z, Liu Z, Inganäs O, Wuerfel U, Zhang F. A planar copolymer

for high efficiency polymer solar cells. J Am Chem Soc 2009;131:14612–3.
[247] Yi H, Johnson RG, Iraqi A, Mohamad D, Royce R, Lidzey DG. Narrow energy gap polymers with absorptions up to 1200 nm and their photovoltaic properties. Macromol Rapid Commun 2008;29:1804–9.
[248] Boudreault PLT, Michaud A, Leclerc M. A new poly(2,7-dibenzosilole) derivative in polymer solar cells. Macromol Rapid Commun 2007;28:2176–9.
[249] Wang E, Wang L, Lan L, Luo C, Zhuang W, Peng J, Cao Y. High-performance polymer heterojunction solar cells of a polysilafluorene derivative. Appl Phys Lett 2008;92, 033307/1–3.
[250] Allard N, Aïch RB, Gendron D, Boudreault PLT, Tessier C, Alem S, Tse SC, Tao Y, Leclerc M. Germafluorenes: new heterocycles for plastic electronics. Macromolecules 2010;43:2328–33.
[251] Vak D, Lim B, Lee SH, Kim DY. Synthesis of a double spiro-polyindenofluorene with a stable blue emission. Org Lett 2005;7:4229–32.
[252] Zheng Q, Jung BJ, Sun J, Katz HE. Ladder-type oligo-p-phenylene-containing copolymers with high open-circuit voltages and ambient photovoltaic activity. J Am Chem Soc 2010;132:5394–404.
[253] Kim J, Kim SH, Jung IH, Jeong E, Xia Y, Cho S, Hwang IW, Lee K, Suh H, Shim HK, Woo HY. Synthesis and characterization of indeno[1,2-b]fluorene-based low bandgap copolymers for photovoltaic cells. J Mater Chem 2010;20:1577–86.
[254] Song S, Jin Y, Kim SH, Moon J, Kim K, Kim JY, Park SH, Lee K, Suh H. Stabilized polymers with novel indenoindene backbone against photodegradation for LEDs and solar cells. Macromolecules 2008;41:7296–305.
[255] Tsami A, Bünnagel TW, Farrell T, Scharber M, Choulis SA, Brabec CJ, Scherf U. Alternating quinoxaline/oligothiophene copolymers-synthesis and unexpected absorption properties. J Mater Chem 2007;17:1353–5.
[256] Tsai JH, Chueh CC, Lai MH, Wang CF, Chen WC, Ko BT, Ting C. Synthesis of new indolocarbazole-acceptor alternating conjugated copolymers and their applications to thin film transistors and photovoltaic cells. Macromolecules 2009;42:1897–905.
[257] Lu J, Liang F, Drolet N, Ding J, Tao Y, Movileanu R. Crystalline low band-gap alternating indolocarbazole and benzothiadiazole-cored oligothiophene copolymer for organic solar cell applications. Chem Commun 2008:5315–7.
[258] Zhou E, Yamakawa S, Zhang Y, Tajima K, Yang C, Hashimoto K. Indolo[3,2-b]carbazole-based alternating donor–acceptor copolymers: synthesis, properties and photovoltaic application. J Mater Chem 2009;19:7730–7.
[259] Xia Y, Su X, He Z, Ren X, Wu H, Cao Y, Fan D. An alternating copolymer derived from indolo[3,2-b]carbazole and 4,7-di(thieno[3,2-b]thien-2-yl)-2,1,3-benzothiadiazole for photovoltaic cells. Macromol Rapid Commun 2010;31:1287–92.
[260] Chan SH, Chen CP, Chao TC, Ting C, Lin CS, Ko BT. Synthesis, characterization, and photovoltaic properties of novel semiconducting polymers with thiophene–phenylene–thiophene (TPT) as coplanar units. Macromolecules 2008;41:5519–26.
[261] Wong KT, Chao TC, Chi LC, Chu YY, Balaiah A, Chiu SF, Liu YH, Wang Y. Syntheses and structures of novel heteroarene-fused coplanar π-conjugated chromophores. Org Lett 2006;8:5033–6.
[262] Ando S, Nishida J, Tada H, Inoue Y, Tokito S, Yamashita Y. High performance n-type organic field-effect transistors based on π-electronic systems with trifluoromethylphenyl groups. J Am Chem Soc 2005;127:5336–7.
[263] Yu CY, Chen CP, Chan SH, Hwang GW, Ting C. Thiophene/phenylene/thiophene-based low-bandgap conjugated polymers for efficient near-infrared photovoltaic applications. Chem Mater 2009;21:3262–9.
[264] Chen CP, Chan SH, Chao TC, Ting C, Ko BT. Low-bandgap poly(thiophene–phenylene–thiophene) derivatives with broaden absorption spectra for use in high-performance bulk-heterojunction polymer solar cells. J Am Chem Soc 2008;130:12828–33.
[265] Chan SH, Hsiao YS, Hung LI, Hwang GW, Chen HL, Ting C, Chen CP. Morphology evolution of spin-coated films of poly(thiophene–phenylene–thiophene) and [6,6]-phenyl-C71-butyric acid methyl ester by solvent effect. Macromolecules 2010;43:3399–405.
[266] Wu JS, Cheng YJ, Dubosc M, Hsieh CH, Chang CY, Hsu CS. Donor–acceptor polymers based on multi-fused heptacyclic structures: synthesis, characterization and photovoltaic applications. Chem Commun 2010;46:3259–61.
[267] Wienk MM, Turbiez M, Gilot J, Janssen RAJ. Narrow-bandgap diketo-pyrrolo-pyrrole polymer solar cells: the effect of processing on the performance. Adv Mater 2008;20:2556–60.
[268] Bijleveld JC, Zoombelt AP, Mathijssen SGJ, Wienk MM, Turbiez M, de Leeuw DM, Janssen RAJ. Poly(diketopyrrolopyrrole–terthiophene) for ambipolar logic and photovoltaics. J Am Chem Soc 2009;131:16616–7.
[269] Huo L, Hou J, Chen HY, Zhang S, Jiang Y, Chen TL, Yang Y. Bandgap and molecular level control of the low-bandgap polymers based on 3,6-dithiophen-2-yl-2,5-dihydropyrrolo[3,4-c]pyrrole-1,4-dione toward highly efficient polymer solar cells. Macromolecules 2009;42:6564–71.
[270] Zhou E, Wei Q, Yamakawa S, Zhang Y, Tajima K, Yang C, Hashimoto K. Diketopyrrolopyrrole-based semiconducting polymer for photovoltaic device with photocurrent response wavelengths up to 1.1 μm. Macromolecules 2010;43:821–6.
[271] Zhou E, Yamakawa S, Tajima K, Yang C, Hashimoto K. Synthesis and photovoltaic properties of diketopyrrolopyrrole-based donor–acceptor copolymers. Chem Mater 2009;21:4055–61.
[272] Zou Y, Gendron D, Neagu-Plesu R, Leclerc M. Synthesis and characterization of new low-bandgap diketopyrrolopyrrole-based copolymers. Macromolecules 2009;42:6361–5.
[273] Chen GY, Chiang CM, Kekuda D, Lan SC, Chu CW, Wei KH. Synthesis and characterization of a narrow-bandgap polymer containing alternating cyclopentadithiophene and diketo-pyrrolopyrrole units for solar cell applications. J Polym Sci Part A Polym Chem 2010;48:1669–75.
[274] Kanimozhi C, Balraju P, Sharma GD, Patil S. Synthesis of diketopyrrolopyrrole containing copolymers: a study of their optical and photovoltaic properties. J Phys Chem B 2010;114:3095–103.
[275] Mondal R, Miyaki N, Becerril HA, Norton JE, Parmer J, Mayer AC, Tang ML, Brédas JL, McGehee MD, Bao Z. Synthesis of acenaphthyl and phenanthrene based fused-aromatic thienopyrazine co-polymers for photovoltaic and thin film transistor applications. Chem Mater 2009;21:3618–28.
[276] Zhou E, Cong J, Yamakawa S, Wei Q, Nakamura M, Tajima K, Yang C, Hashimoto K. Synthesis of thieno[3,4-b]pyrazine-based and 2,1,3-benzothiadiazole-based donor–acceptor copolymers and their application in photovoltaic devices. Macromolecules 2010;43:2873–9.
[277] Campos LM, Tontcheva A, Günes S, Sonmez G, Neugebauer H, Sariciftci NS, Wudl F. Extended photocurrent spectrum of a low band gap polymer in a bulk heterojunction solar cell. Chem Mater 2005;17:4031–3.
[278] Zoombelt AP, Leenen MAM, Fonrodona M, Nicolas Y, Wienk MM, Janssen RAJ. The influence of side chains on solubility and photovoltaic performance of dithiophene–thienopyrazine small band gap copolymers. Polymer 2009;50:4564–70.
[279] Wienk MM, Turbiez MGR, Struijk MP, Fonrodona M, Janssen RAJ. Low-band gap poly(di-2-thienylthienopyrazine):fullerene solar cells. Appl Phys Lett 2006;88, 153511/1-3.
[280] Petersen MH, Hagemann O, Nielsen KT, Jørgensen M, Krebs FC. Low band gap poly-thienopyrazines for solar cells—introducing the 11-thia-9,13-diaza-cyclopenta[b]triphenylenes. Sol Energy Mater Sol Cells 2007;91:996–1009.
[281] Lee J, Jung BJ, Lee SK, Lee JI, Cho HJ, Shim HK. Fluorene-based alternating polymers containing electron-withdrawing bithiazole units: preparation and device applications. J Polym Sci Part A Polym Chem 2005;43:1845–57.
[282] Zhang M, Fan H, Guo X, He Y, Zhang Z, Min J, Zhang J, Zhao G, Zhan X, Li Y. Synthesis and photovoltaic properties of bithiazole-based donor–acceptor copolymers. Macromolecules 2010;43:5706–12.
[283] Yuan MC, Chiu MY, Chiang CM, Wei KH. Synthesis and characterization of pyrido[3,4-b]pyrazine-based low-bandgap copolymers for bulk heterojunction solar cells. Macromolecules 2010;43:6270–7.
[284] Song S, Jin Y, Park SH, Cho S, Kim I, Lee K, Heeger AJ, Suh H. A low-bandgap alternating copolymer containing the dimethylbenzimidazole moiety. J Mater Chem 2010;20:6517–23.
[285] Baran D, Balan A, Celebi S, Esteban BM, Neugebauer H, Sariciftci NS, Toppare L. Processable multipurpose conjugated polymer for electrochromic and photovoltaic applications. Chem Mater 2010;22:2978–87.
[286] Zhang Z, Peng B, Liu B, Pan C, Li Y, He Y, Zhou K, Zou Y. Copolymers from benzodithiophene and benzotriazole: synthesis and photovoltaic applications. Polym Chem 2010;1:1441–7.
[287] Li Y, Xue L, Li H, Li Z, Xu B, Wen S, Tian W. Energy level and molecular structure engineering of conjugated donor–acceptor copolymers for photovoltaic applications. Macromolecules 2009;42:4491–9.

[288] Li Y, Li Z, Wang C, Li H, Lu H, Xu B, Tian W. Novel low-bandgap oligothiophene-based donor-acceptor alternating conjugated copolymers: synthesis, properties, and photovoltaic applications. J Polym Sci Part A Polym Chem 2010;48:2765–76.
[289] Brabec CJ, Winder C, Sariciftci NS, Hummelen JC, Dhanabalan A, van Hal PA, Janssen RAJ. A low-bandgap semiconducting polymer for photovoltaic devices and infrared emitting diodes. Adv Funct Mater 2002;12:709–12.
[290] Kim J, Park SH, Cho S, Jin Y, Kim J, Kim I, Lee JS, Kim JH, Woo HY, Lee K, Suh H. Low-bandgap poly(4H-cyclopenta[def]phenanthrene) derivatives with 4,7-dithienyl-2,1,3-benzothiadiazole unit for photovoltaic cells. Polymer 2010;51:390–6.
[291] He Y, Zhao G, Min J, Zhang M, Li Y. Poly(thienylene-benzothiadiazole-thienylene-vinylene): a narrow bandgap polymer with broad absorption from visible to infrared region. Polymer 2009;50:5055–8.
[292] Kato SI, Matsumoto T, Shigeiwa M, Gorohmaru H, Maeda S, Ishi-i T, Mataka S. Novel 2,1,3-benzothiadiazole-based red-fluorescent dyes with enhanced two-photon absorption cross-sections. Chem A Eur J 2006;12:2303–17.
[293] Wen S, Pei J, Zhou Y, Li P, Xue L, Li Y, Xu B, Tian W. Synthesis of 4,7-diphenyl-2,1,3-benzothiadiazole-based copolymers and their photovoltaic applications. Macromolecules 2009;42:4977–84.
[294] Yang L, Zhou H, You W. Quantitatively analyzing the influence of side chains on photovoltaic properties of polymer–fullerene solar cells. J Phys Chem C 2010;114:16793–800.
[295] Zhou H, Yang L, Liu S, You W. A tale of current and voltage: interplay of band gap and energy levels of conjugated polymers in bulk heterojunction solar cells. Macromolecules 2010;43:10390–6.
[296] Zhou H, Yang L, Price SC, Knight KJ, You W. Enhanced photovoltaic performance of low-bandgap polymers with deep LUMO levels. Angew Chem Int Ed 2010;49:7992–5.
[297] Wang E, Hou L, Wang Z, Hellström S, Zhang F, Inganäs O, Andersson MR. An easily synthesized blue polymer for high-performance polymer solar cells. Adv Mater 2010;22:5240–4.
[298] Wang E, Hou L, Wang Z, Hellström S, Mammo W, Zhang F, Inganäs O, Andersson MR. Small band gap polymers synthesized via a modified nitration of 4,7-dibromo-2,1,3-benzothiadiazole. Org Lett 2010;12:4470–3.
[299] Bijleveld JC, Gevaerts VS, Nuzzo DD, Turbiez M, Mathijssen SGJ, de Leeuw DM, Wienk MM, Janssen RAJ. Efficient solar cells based on an easily accessible diketopyrrolopyrrole polymer. Adv Mater 2010;22:E242–6.
[300] Bijleveld JC, Karsten BP, Mathijssen SGJ, Wienk MM, de Leeuw DM, Janssen RAJ. Small band gap copolymers based on furan and diketopyrrolopyrrole for field-effect transistors and photovoltaic cells. J Mater Chem 2011;21:1600–6.
[301] Woo CH, Beaujuge PM, Holcombe TW, Lee OP, Fréchet JMJ. Incorporation of furan into low band-gap polymers for efficient solar cells. J Am Chem Soc 2010;132:15547–9.
[302] Li Z, Ding J, Song N, Lu J, Tao Y. Development of a new s-tetrazine-based copolymer for efficient solar cells. J Am Chem Soc 2010;132:13160–1.
[303] Chen Y-C, Yu C-Y, Fan Y-L, Hung L-I, Chen C-P, Ting C. Low-bandgap conjugated polymer for high efficient photovoltaic applications. Chem Commun 2010;46:6503–5.
[304] Wang J-Y, Hau SK, Yip H-L, Davies JA, Chen K-S, Zhang Y, Sun Y, Jen AK-Y. Benzobis(silolothiophene)-based low bandgap polymers for efficient polymer solar cells. Chem Mater; in press.
[305] Ashraf RS, Chen Z, Leem DS, Bronstein H, Zhang W, Schroeder B, Geerts Y, Smith J, Watkins S, Anthopoulos TD, Sirringhaus H, de Mello JC, Heeney M, McCulloch I. Silaindacenodithiophene semiconducting polymers for efficient solar cells and high-mobility ambipolar transistors. Chem Mater; in press.
[306] Cheedarala RK, Kim G-H, Cho S, Lee J, Kim J, Song H-K, Kim JY, Yang C. Ladder-type heteroacene polymers bearing carbazole and thiophene ring units and their use in field-effect transistors and photovoltaic cells. J Mater Chem 2011;21:843–50.
[307] Yuan M-C, Chiu M-Y, Liu S-P, Chen C-M, Wei K-H. A thieno[3,4-c]pyrrole-4,6-dione-based donor-acceptor polymer exhibiting high crystallinity for photovoltaic applications. Macromolecules 2010;43:6936–8.
[308] Guo X, Xin H, Kim FS, Liyanage ADT, Jenekhe SA, Watson MD. Thieno[3,4-c]pyrrole-4,6-dione-based donor-acceptor conjugated polymers for solar cells. Macromolecules 2011;44:269–77.
[309] Najari A, Beaupré S, Berrouard P, Zou Y, Pouliot J-R, Lepage-Pérusse C, Leclerc M. Synthesis and characterization of new thieno[3,4-c]pyrrole-4,6-dione derivatives for photovoltaic applications. Adv Funct Mater; in press.
[310] Ding P, Chu C-C, Liu B, Peng B, Zou Y, He Y, Zhou K, Hsu C-S. A high-mobility low-bandgap copolymer for efficient solar cells. Macromol Chem Phys 2010;211:2555–61.
[311] Yang M, Peng B, Liu B, Zou Y, Zhou K, He Y, Pan C, Li Y. Synthesis and photovoltaic properties of copolymers from benzodithiophene and thiazole. J Phys Chem C 2010;114:17989–94.
[312] Zhang M, Fan H, Guo X, He Y, Zhang Z-G, Min J, Zhang J, Zhao G, Zhan X, Li Y. Synthesis and photovoltaic properties of a copolymer of benzo[1,2-b:4,5-b′]dithiophene and bithiazole. Macromolecules 2010;43:8714–7.
[313] Zhang L, He C, Chen J, Yuan P, Huang L, Zhang C, Cai W, Liu Z, Cao Y. Bulk-heterojunction solar cells with benzotriazole-based copolymers as electron donors: largely improved photovoltaic parameters by using PFN/Al bilayer cathode. Macromolecules 2010;43:9771–8.
[314] Peng B, Najari A, Liu B, Berrouard P, Gendron D, He Y, Zhou K, Zou Y, Leclerc M. A new dithienylbenzotriazole-based poly(2,7-carbazole) for efficient photovoltaics. Macromol Chem Phys 2010;211:2026–33.
[315] Jin J-K, Choi J-K, Kim B-J, Kang H-B, Yoon S-C, You H, Jung H-T. Synthesis and photovoltaic performance of low-bandgap polymers on the basis of 9,9-dialkyl-3,6-dialkyloxysilafluorene. macromolecules; in press.
[316] Biniek L, Fall S, Chochos CL, Anokhin DV, Ivanov DA, Leclerc N, Lévêque P, Heiser T. Impact of the alkyl side chains on the opto-electronic properties of a series of photovoltaic low-band-gap copolymers. Macromolecules 2010;43:9779–86.